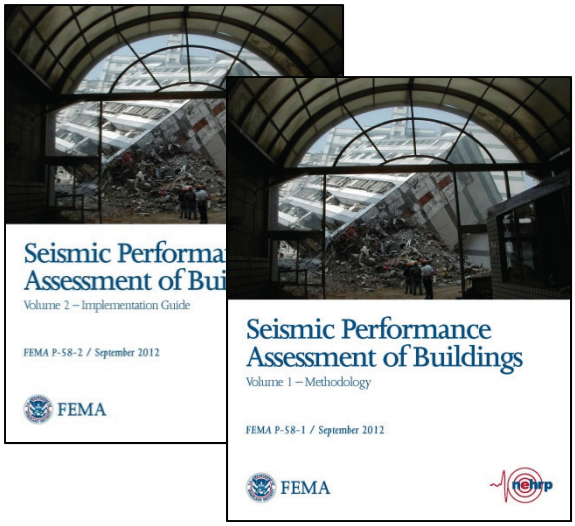

Background Document

FEMA P-58/BD-3.8.5

Damage States and Fragility Functions for W-Shape Steel Link Beams in Eccentrically Braced Frames

Prepared by

C. Kerem Gulec, Bruce Gibbons, and Albert Chen
Thornton Tomasetti Inc, Los Angeles, California

Andrew Whittaker
University at Buffalo, New York, Buffalo, New York

Submitted to

APPLIED TECHNOLOGY COUNCIL
201 Redwood Shores Parkway, Suite 240
Redwood City, California 94065
www.ATCouncil.org

Prepared for

FEDERAL EMERGENCY MANAGEMENT AGENCY
U.S. Department of Homeland Security
500 C Street, SW
Washington, D.C. 20472

July 4, 2010

nehrp

FEMA

Background Documentation

FEMA P-58 Background Documents are a series of reports documenting the technical background and source information for key aspects of the FEMA P-58 methodology and its implementation. These reports were developed over the course of the 10-year ATC-58/ATC-58-1 Projects funded under FEMA Contracts EMW-2001-RP-0056 and HSFEHQ-06-D-1105.

Background Documents were developed by consultants, serving at various levels within the project hierarchy, reporting the results of: (1) decisions on technical development protocols; (2) focused studies on the development of key aspects of the methodology; (3) documentation of recommended procedures; and (4) collection of available data for the development of structural and nonstructural fragilities. They were initially intended to serve as a record of the technical state-of-knowledge at the time they were produced, and as resources for the development of the eventual project reports. As such, they represent a snapshot in time, and may, or may not, match the technical content, recommended procedures, or data incorporated into the final methodology and its implementation.

This Background Document is intended for the purpose of providing supplemental knowledge to users of the FEMA P-58 methodology. Information contained herein has not been independently verified for accuracy as a stand-alone document, and may have been superseded in its final implementation within the methodology. Users of information in this document assume all liability arising from such use.

Notice

Cover illustration – Primary resource documents for the FEMA P-58 *Seismic Performance Assessment of Buildings, Methodology and Implementation* series of products: FEMA P-58-1, *Volume 1 – Methodology*, and FEMA P-58-2, *Volume 2 – Implementation Guide*.

DAMAGE STATES AND FRAGILITY FUNCTIONS FOR W-SHAPE STEEL LINK BEAMS IN ECCENTRICALLY BRACED FRAMES

Prepared for the Applied Technology Council

Project ATC-58

Prepared by

C. Kerem Gulec, Ph.D., Senior Engineer
Bruce Gibbons, P.E., S.E., Senior Principal
Albert Chen, P.E., S.E., Vice President
Thornton Tomasetti Inc, Los Angeles

Andrew Whittaker, Ph.D., S.E., Professor
University at Buffalo, New York

July 04, 2010

Table of Contents

Acknowledgements

Professor Michael Engelhardt of the University of Texas at Austin and Professor Ahmad Itani of the University of Nevada at Reno transmitted information and data on tests of link beams in eccentrically braced frames. Mr. Patrick Hassett of Hassett Engineering provided information on heat straightening repair of steel components. Professor Gregory Deierlein of Stanford University reviewed two drafts of the report. The authors gratefully acknowledge these important contributions to the study described herein.

1 Introduction

Eccentrically Braced Frames (EBFs) are steel frames used in buildings and infrastructure constructed in regions of moderate to high seismic hazard. EBFs are an alternative to Moment Resisting frames (MRFs) if high elastic stiffness is needed to control drift and an alternative to Concentrically Braced Frames (CBFs) if deformation demands are relatively great.

In a well-designed EBF, the majority or all of the inelastic action occurs in the link beams (termed *links* hereafter). Other components of the frame are proportioned using capacity-design based procedures to remain essentially elastic for the maximum strength of the links. The seismic performance of a building with EBFs is therefore related directly to the inelastic performance of the links.

AISC 341-05 [AISC (2005)] defines three modes of response for links in EBFs using a normalized link length, ρ, which is defined in Equations 1-1 through 1-3 below: 1) for ρ less than 1.6, the response is governed by shear yielding (*shear links*), 2) for ρ greater than 2.6, the response is governed by flexural yielding (*flexural links*), and 3) for ρ between 1.6 and 2.6, the response is a function of the coexisting shearing force and moment (*intermediate links*).

$$\rho = \frac{e}{M_p / V_p} \tag{1-1}$$

$$V_p = 0.6 F_y \left(d - 2t_f \right) t_w \tag{1-2}$$

$$M_p = F_y Z \tag{1-3}$$

In these equations, V_p is the plastic shear strength, M_p is the plastic moment strength, F_y is the yield stress for steel, e is the link length, d is the link depth, t_w is the web thickness, t_f is the flange thickness, and Z is plastic modulus of the cross-section.

A general framework for the next generation seismic performance assessment and loss computations is provided in the 50% draft of the ATC-58, *Guidelines for Seismic Performance Assessment of Buildings* [ATC (2008)]. A key component of the framework is fragility functions for components and elements of seismic framing systems. Fragility functions relate the probability of exceeding one or more damage thresholds (described using damage states and repair measures) to a demand parameter such as story drift or component plastic deformation. Damage states for steel components are characterized typically using descriptors such as yielding, local buckling, fracture, and global buckling. To compute dollar losses and estimates of building downtime after an earthquake, damage states must be characterized by measures (or scopes) of repair.

This report summarizes the development of fragility curves for steel link beams in EBFs. Information from experiments on link beams in EBFs reported in the literature is used to generate damage data as a function of an efficient component-level demand parameter. The lognormal distribution is used to characterize the damage data. Goodness-of-fit testing is performed to evaluate the utility of the fitted distributions.

2 Summary of Experimental Data

Early research on EBF links in US was conducted at the University of California at Berkeley between the late 1970s and early 1990s [Roeder and Popov (1977), Hjelmstad and Popov (1983), Malley and Popov (1983), Kasai and Popov (1986), Ricles and Popov (1987), Engelhardt and Popov (1989)]. Details of a pseudo-dynamic testing of a full-scale 6-story dual structure (EBF-MRF) was reported by Foutch et al. (1987) and Roeder et al. (1987). Whittaker et al. (1987) examined the earthquake response of EBFs by performing earthquake simulator tests on a 0.3-scale model of a 6-story building including these frames. Other tests on EBF links have been conducted at the University of Nevada at Reno [Itani (1997), Dusicka (2004)], University of California at San Diego [McDaniel et al. (2002)], and University of Texas at Austin [Arce (2002), Galvez (2004), Okazaki (2004), Ryu (2005)].

A database was assembled that includes test results for 110 steel link beams reported in the literature. The properties of the test specimens are summarized (chronologically) in Table 2-1. Measured rather than nominal (specified) material and geometric properties are used to calculate the normalized link length ρ because the researchers often reported different values of yield strength for the flanges and the web. More detailed information on the geometric and material properties of the links of the database are presented in Appendix A together with the damage data used to develop fragility functions. Appendix B presents the test fixture used by each researcher. Appendix C presents the load-deformation relationships, and Appendix D presents the damage pictures, for the EBF links presented in Appendix A.

Table 2-1 Summary of experimental data on EBF links

No	Reference	Specimen ID	Section	Loading	ρ	AISC classification
1	Hjelmstad and Popov (1983)	1	W18x40	Cyclic	1.26	shear
2		2	W18x40	Cyclic	1.26	shear
3		3	W18x40	Cyclic	1.26	shear
4		4	W18x40	Cyclic	1.26	shear
5		5	W18x40	Cyclic	1.26	shear
6		6	W18x40	Cyclic	1.26	shear
8		7	W18x35	Cyclic	1.60	shear
7		8	W18x60	Cyclic	1.41	shear
9		9	W18x40	Cyclic	1.63	intermediate
10		10	W16x26	Cyclic	1.87	intermediate
11		11	W18x35	Cyclic	2.06	intermediate
12		12	W12x22	Cyclic	2.77	flexure
13		13	W16x26	Cyclic	1.87	intermediate
14		14	W18x35	Cyclic	2.06	intermediate
15		15	W12x22	Cyclic	2.77	flexure
16	Malley and Popov (1983)	16	W18x60	Cyclic	1.24	shear
17		17	W18x40	Cyclic	1.48	shear
18		18	W18x60	Cyclic	1.24	shear
19		20	W18x40	Cyclic	1.48	shear
20		21	W18x40	Cyclic	1.48	shear
21		22	W18x40	Cyclic	1.48	shear
22		23	W18x40	Cyclic	1.48	shear
23		25	W18x40	Cyclic	1.48	shear
24		26	W18x40	Cyclic	1.48	shear
25		27	W18x40	Cyclic	1.48	shear
26		28	W18x40	Cyclic	1.48	shear
27		24	W18x40	Monotonic	1.48	shear
28	Kasai and Popov (1986)	1	W8x10	Monotonic	1.40	shear
29		2	W8x10	Cyclic	1.40	shear
30		3	W8x10	Cyclic	1.40	shear
31		4	W8x10	Cyclic	1.40	shear
32		5	W8x10	Cyclic	1.70	shear
33		6	W8x10	Cyclic	1.70	intermediate
34		7	W8x10	Cyclic	1.11	intermediate
35	Ricles and Popov (1987)	A1	W12x19	Cyclic	1.43	shear
36		A2	W12x19	Cyclic	1.43	shear
37		B1	W12x19	Cyclic	1.43	shear
38		B2	W12x19	Cyclic	1.43	shear
39		C1	W12x19	Cyclic	1.43	shear
40		C2	W12x19	Cyclic	1.43	shear

Table 2-1 Summary of experimental data on EBF links (cont'd)

No	Reference	Specimen ID	Section	Loading	ρ	AISC classification
41	Ricles and Popov (1987) (cont'd)	D1	W12x19	Cyclic	1.43	shear
42		D2	W12x19	Cyclic	1.43	shear
43	Engelhardt and Popov (1989)	1	W12x16	Cyclic	2.36	intermediate
44		2	W12x16	Cyclic	2.36	intermediate
45		3	W12x22	Cyclic	2.36	intermediate
46		4	W12x22	Cyclic	2.30	intermediate
47		5	W12x16	Cyclic	3.71	flexure
48		6	W12x16	Cyclic	3.70	flexure
49		7	W12x16	Cyclic	2.45	intermediate
50		8	W12x22	Cyclic	2.37	intermediate
51		9	W12x22	Cyclic	1.34	shear
52		10	W12x16	Cyclic	1.77	intermediate
53		11	W12x22	Cyclic	1.81	intermediate
54		12	W12x22	Cyclic	3.95	flexure
55	Itani (1997)	BU30	Built-up	Cyclic	1.39	shear
56		BU16	Built-up	Cyclic	1.40	shear
57	McDaniel et al. (2002)	Type 1	Built-up	Cyclic	0.79	shear
58		Type 3	Built-up	Cyclic	0.57	shear
59	Arce (2002)	1c	W10x19	Cyclic	1.77	intermediate
60		2	W10x19	Cyclic	2.31	intermediate
61		3	W10x19	Cyclic	3.70	flexure
62		4a	W10x33	Cyclic	1.04	shear
63		4b	W10x33	Cyclic	1.04	shear
64		4c	W10x33	Cyclic	1.04	shear
65		5	W10x33	Cyclic	1.65	intermediate
66		6b	W10x33	Cyclic	2.17	intermediate
67		7	W10x33	Cyclic	3.29	flexure
68		8	W16x36	Cyclic	1.39	shear
69		9	W16x36	Cyclic	1.82	intermediate
70		10	W10x68	Cyclic	1.25	shear
71		11	W10x68	Cyclic	1.64	intermediate
72	Galvez (2004)	1 (A)	W10x33	Cyclic	1.00	shear
73		2 (B)	W10x33	Cyclic	1.02	shear
74		3 (C)	W10x33	Cyclic	0.97	shear
75		4 (B)	W10x33	Cyclic	1.02	shear
76		5 (B)	W10x33	Cyclic	1.02	shear
77		6 (B)	W10x33	Cyclic	1.02	shear
78		7 (B)	W10x33	Cyclic	1.02	shear
79		8 (B)	W10x33	Cyclic	1.02	shear
80		9 (B)	W10x33	Cyclic	1.02	shear
81		10 (B)	W10x33	Cyclic	1.02	shear

Table 2-1 Summary of experimental data on EBF links (cont'd)

No	Reference	Specimen ID	Section	Loading	ρ	AISC classification
82	Dusicka (2004)	C345a	Built-up	Cyclic	0.80	shear
83		C345b	Built-up	Cyclic	0.58	shear
84		H485	Built-up	Cyclic	0.82	shear
85	Okazaki (2004)	FFS	W18x40	Cyclic	0.90	shear
86		FFS-RLP	W18x40	Cyclic	0.90	shear
87		MWS	W18x40	Cyclic	1.13	shear
88		NAS	W18x40	Cyclic	1.13	shear
89		NAS-RLP	W18x40	Cyclic	1.13	shear
90		PNS	W18x40	Cyclic	1.13	shear
91		PNI	W18x40	Cyclic	2.26	intermediate
92		PNM	W18x40	Cyclic	3.39	flexure
93		MWI	W18x40	Cyclic	2.26	intermediate
94		MWM	W18x40	Cyclic	3.39	flexure
95		FFI	W18x40	Cyclic	2.26	intermediate
96		FFM	W18x40	Cyclic	3.39	flexure
97		FFSL-RLP	W18x40	Cyclic	1.75	intermediate
98		NAI	W18x40	Cyclic	2.26	intermediate
99		NAM	W18x40	Cyclic	3.39	flexure
100		NASL-RLP	W18x40	Cyclic	1.75	intermediate
101	Ryu (2005)	4A-RLP	W10x33	Cyclic	1.04	shear
102		4C-RLP	W10x33	Cyclic	1.04	shear
103		8-RLP	W16x36	Cyclic	1.39	shear
104		10-RLP	W10x68	Cyclic	1.25	shear
105		12-RLP	W18x40	Cyclic	1.02	shear
106		12-AISC	W18x40	Cyclic	1.02	shear
107		12-SEV	W18x40	Cyclic	1.02	shear
108		12-RAN	W18x40	Cyclic	1.02	shear
109		12-MON	W18x40	Monotonic	1.02	shear
110		11-RLP	W10x68	Cyclic	1.64	intermediate

Of the 110 specimens presented in Table 2-1, 3 were subjected to monotonic loading and 107 were subjected to reversed cyclic loading. Load was applied quasi-statically in all cases. Two of the 110 specimens were tested with large axial forces in the link. In all other tests, axial forces were reported to be insignificant. Based on the AISC 341-05 [AISC (2005)] classification, the behavior of 71 of the 110 specimens are governed by shear, 11 are governed by flexure, and 28 are governed by a combination of shear and flexure. The normalized link length (ρ) ranged between 0.57 and 3.95. The test assembly for the Ricles and Popov (1987) and Whittaker et al. (1987) experiments included concrete slabs on metal decking but all other tests were performed on bare steel links. Except for 7 tests of built-up link members, the specimens (103 of 110) were constructed using standard wide-flange rolled sections. Table 2-2 and Table 2-3 summarize the geometric and material properties of the EBF links. In these tables, e is the link length, d is the link depth, t_w is the web thickness, t_f is the flange thickness, b is the flange width, F_{yw} is the yield strength of web, F_{yf} is the yield strength of flange, F_{uw} is the ultimate strength of web, and F_{uf} is the ultimate strength of flange. For shear-critical links, the table differentiates between links of hot rolled W-shapes and links constructed from steel plate (or built up) because of the substantial differences in the size of the test specimens. The influence of link construction and size is investigated in Section 5.5.

Table 2-2 Statistical summary of the shear-critical links

		e	d	t_w	b	t_f	F_{yw}	F_{yf}	F_{uw} [a]	F_{uf} [a]
		(in)	(in)	(in)	(in)	(in)	(ksi)	(ksi)	(ksi)	(ksi)
Rolled W-	Min	11.5	8.0	0.17	4.0	0.21	39.5	35.0	60.1	58.5
	Median	23.0	16.1	0.31	6.0	0.49	54.5	51.0	73.0	70.7
	Max	36.6	18.3	0.45	10.3	0.77	62.3	58.6	79.9	79.7
Built-up	Min	19.7	16.0	0.38	9.4	0.75	51.3	53.4	72.1	77.2
	Median	39.4	18.7	0.55	14.0	1.50	54.0	53.7	76.3	80.5
	Max	144.0	37.4	1.10	23.6	1.77	73.0	73.0	80.5	83.7

a. The data provided by Dusicka Dusicka (2004), which constitute 3 of the 7 built-up sections, did not include measured ultimate strengths for steel.

Table 2-3 Statistical summary of the intermediate and flexure-critical links

		e	d	t_w	b	t_f	F_{yw}	F_{yf}	F_{uw} [a]	F_{uf} [a]
		(in)	(in)	(in)	(in)	(in)	(ksi)	(ksi)	(ksi)	(ksi)
Int.	Min	17.5	8.0	0.17	4.0	0.21	39.5	35.0	60.1	58.5
	Median	36.0	12.3	0.28	5.7	0.43	57.0	49.7	73.0	69.5
	Max	50.0	17.9	0.45	10.3	0.77	61.0	56.3	79.9	79.7
Flexure critical	Min	36.0	9.7	0.22	4.0	0.27	47.0	42.4	64.0	60.0
	Median	60.0	12.3	0.27	4.0	0.43	57.0	51.0	73.0	72.4
	Max	75.0	17.8	0.32	8.0	0.50	61.0	55.3	77.0	73.8

3 Demand Parameter

The experimental data described in Section 2 was mined to prepare fragility curves. The fragility curves are presented as a function of plastic (or inelastic) link rotation, which is the most appropriate component-level demand parameter to characterize the behavior of EBF links. Importantly, plastic link rotation is an efficient demand parameter because it is computed for each test identified in Section 2 and is a product of nonlinear response-history analysis of eccentrically braced frames.

Plastic link rotation (γ_p) is calculated as:

$$\gamma_p = \gamma_T - \gamma_E \tag{3-1}$$

where γ_T is the total rotation that is equal to ratio of the relative total displacement of the ends of the link to the length of the link, and γ_E is the elastic rotation. In some studies, measured elastic stiffness was used to calculate the elastic rotation of the links and the data was presented in terms of shear force-plastic link rotation. In this case, the reported shear force-plastic link rotation data are used to identify the fragility data. In some experiments, the reported data was presented in terms of the shear force-relative end displacement or shear force-total rotation. For these specimens, the elastic rotations are calculated using the Timoshenko beam theory Equations 3-2 through 3-5 [e.g., Malley and Popov (1983)].

$$\gamma_E = \frac{V}{eK_e} \tag{3-2}$$

$$K_e = \frac{12EI}{e^3\left(1+2\beta\right)} \tag{3-3}$$

$$\beta = \frac{6EI}{GA_w e^2} \tag{3-4}$$

$$A_w = dt_w \tag{3-5}$$

In Equations 3-2 through 3-5, V is the shear force, e is the link length, K_e is the elastic stiffness per Timoshenko beam theory, E is the modulus of elasticity of steel, I is the moment of inertia of the cross-section, G is the shear modulus for steel, and A_w is the web area equal to the product of the link depth (d) and web thickness (t_w).

4 Damage States and Methods of Repair for EBF Links

4.1 Introduction

Damage states (DS) define threshold levels of damage sustained by structural components under earthquake loading. A family of damage states, which is listed in Table 4-1, was assembled for EBF links following analysis of test data and review of the literature. Each state is related directly to visible damage. The scope of repair for each damage state is substantially different from those of the adjacent damage states. In Table 4-1, damage states are presented for shear, flexural and intermediate links. Although the methods of repair are the same for all three types of links, the damage states slightly differ. In shear links, buckling is mainly in the form of web buckling whereas in flexural links buckling is mainly symmetric or asymmetric flange local buckling at each end of the link. Shear-critical links generally experience web fracture whereas flexure-critical links generally experience flange fracture. Lateral-torsional buckling was not seen in the shear link experiments. Intermediate links may be susceptible to damage states associated with either shear-critical links or flexure-critical links.

The authors considered other damage states for EBF links, including a) residual vertical floor displacement in the immediate vicinity of the link, and b) residual horizontal floor displacement. The calculation of residual component deformation, residual floor displacement, and residual story drift requires the use of component models that accommodate deterioration of strength and stiffness. The values of residual deformation, displacement and drift are highly dependant on the characteristics of the ground motion

record(s) used for the nonlinear response-history analysis and the nonlinear mechanical properties of the soil column through which the ground motion record(s) is(are) propagated.

Table 4-1 Damage states and corresponding methods of repair

ID	Damage States	Applicable link type			Method of Repair (MoR)
DS0.1	Web yielding	Shear	Int.	Flexural	Cosmetic repair (MoR-0)
DS0.2	Flange yielding	Shear	Int.	Flexural	
DS0.3	Yielding in intermediate stiffeners	Shear	Int.	Flexural	
DS1.1	Damage to concrete slab above the link	Shear	Int.	Flexural	Concrete replacement (MoR-1)
DS2.1	Web local buckling	Shear	Int.		Heat straightening (MoR-2)
DS2.2	Flange local buckling	Shear	Int.	Flexural	
DS3.1	Web fracture	Shear	Int.		Link replacement (MoR-3)
DS3.2	Flange fracture	Shear	Int.	Flexural	
DS3.3	Lateral torsional buckling		Int.	Flexural	

Section 4.3 addresses residual vertical floor displacement. A short discussion on residual horizontal floor displacement (story drift) is presented in Section 4.6.

Expert opinion was used to link the damage states with the Methods of Repair (MoR) listed in Table 4-1. The following subsections present information on each method of repair and the corresponding damage states.

4.2 MoR-0, Cosmetic Repair

Damage states DS0.1 through DS0.3 of Table 4-1 are associated with the onset of significant yielding in the web, flange, or intermediate stiffeners of the EBF link. Structural repair to restore the pre-earthquake strength and stiffness is unnecessary. Repair of the architectural enclosure and finishes in the vicinity of the link may be required. Cosmetic repair has no

impact on structural performance but is included herein for completeness. An example of damage state 0.1 is presented in Figure 4-1.

Figure 4-1 Web yielding on EBF link 2 tested by Galvez (2004)

4.3 MoR-1, Concrete Replacement

EBF link rotations cause vertical deflections in the slab immediately above the link. Such slabs are typically concrete fill on metal deck. An example of damage state 1.1 is presented in Figure 4-2. Damage state DS1.1 requires either injection of cracks in the concrete slab or replacement of the damaged concrete slab. Given that there is likely less construction work associated with replacement of concrete over the length and width of the link, this method of repair was assumed for MoR-1.

There is limited test information in the literature on damage to concrete slabs in eccentrically braced frames because tests on link beams were generally performed on bare steel shapes. Ricles and Popov (1987) tested 6 EBF link beams constructed with composite slabs.

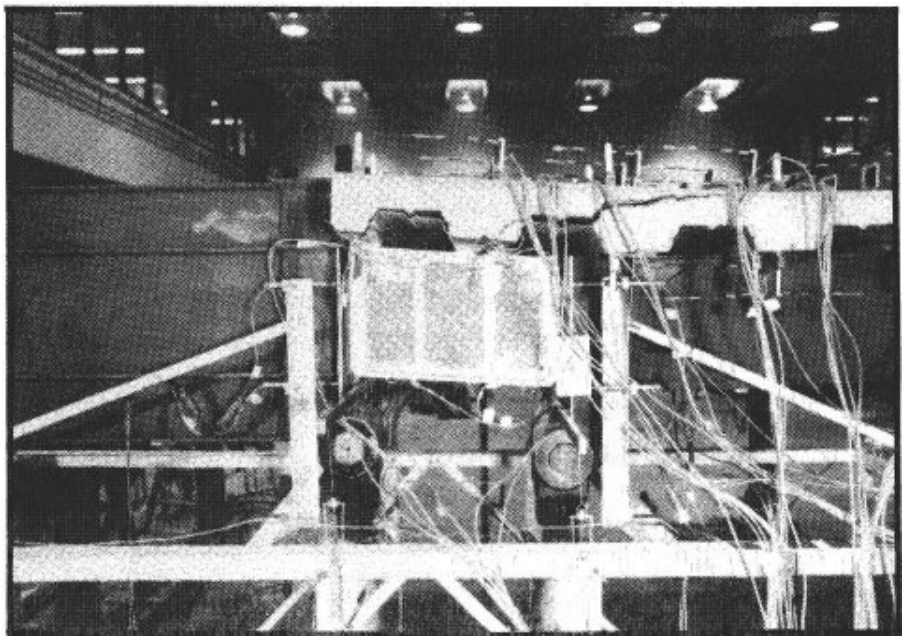

Figure 4-2 Concrete slab damage on EBF link C-2 tested by Ricles and Popov (1987)

Whittaker et al. (1987) studied the earthquake response of a 0.3-scale model of a 6-story, 2-bay by 2-bay eccentrically braced steel frame structure, which was constructed with composite slabs and shear-critical links. The information provided by these authors was used to develop the fragility curve for this method of repair.

Residual vertical displacement in shear links will produce residual displacement in the supported slab and thus an uneven floor plate. Replacement of the concrete immediately above the link beam would accommodate large residual vertical displacements of the link beam because only the top surface of the slab need be at the same level of the surrounding slab.

4.4 MoR-2, Heat Straightening

Damage states DS2.1 and DS2.2, minor local buckling of web and flanges, respectively, can be repaired using heat straightening. An example of damage state DS2.1, which is linked to MoR-2, is presented in Figure 4-3. Descriptions of the *onset* of flange and web local

buckling, as reported by the authors of the test reports, were used to identify the values of the inelastic rotation associated with web and flange local buckling.

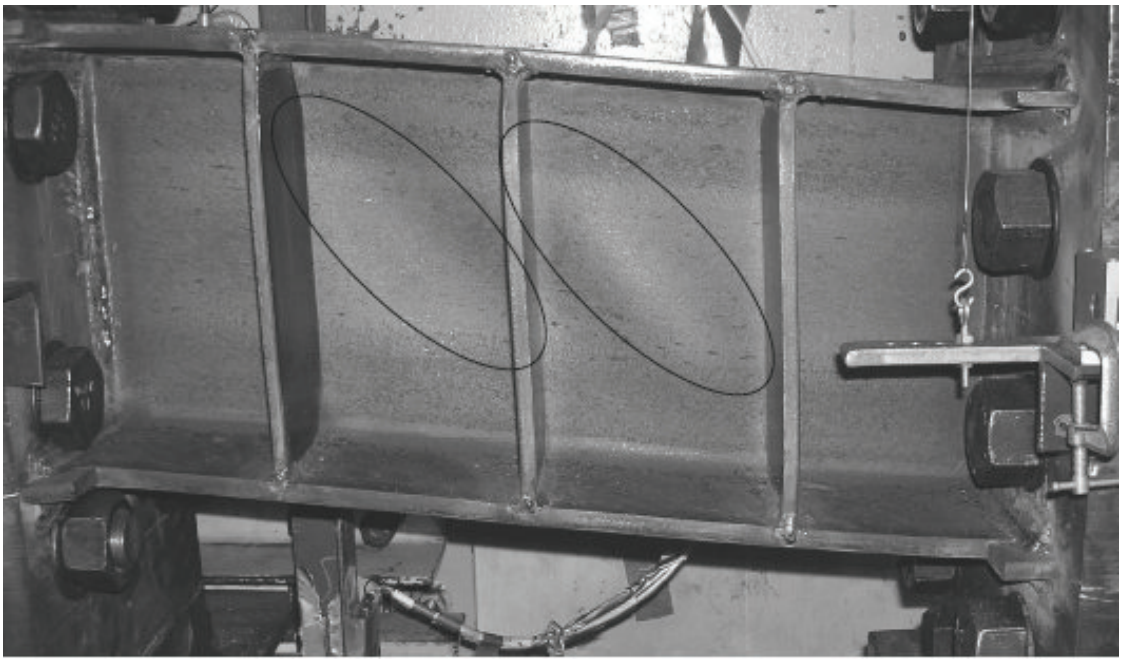

Figure 4-3 Web buckling on EBF link 8 tested by Galvez (2004)

4.5 MoR-3, Link Replacement

Damage states DS3.1 and DS3.3 of Table 4-1 are associated with replacement of the link. Lateral torsional buckling, web fracture, and flange fracture each result in irrecoverable loss of strength in a link. The images and descriptions of damage presented in the test reports were used to identify the value of the inelastic rotation associated with link replacement. An example of damage state DS3.1 is presented in Figure 4-4.

4.6 Residual Displacement in Eccentrically Braced Frames

Large residual displacements in eccentrically braced frames with shear-critical links are possible because the hysteretic response of such links is bilinear and stable; deterioration in response is unlikely up to the point of fracture. However, the magnitude of calculated residual displacements is highly dependant on the characteristics (e.g., frequency content,

duration) of the ground motion and the soil column used for nonlinear response-history analysis.

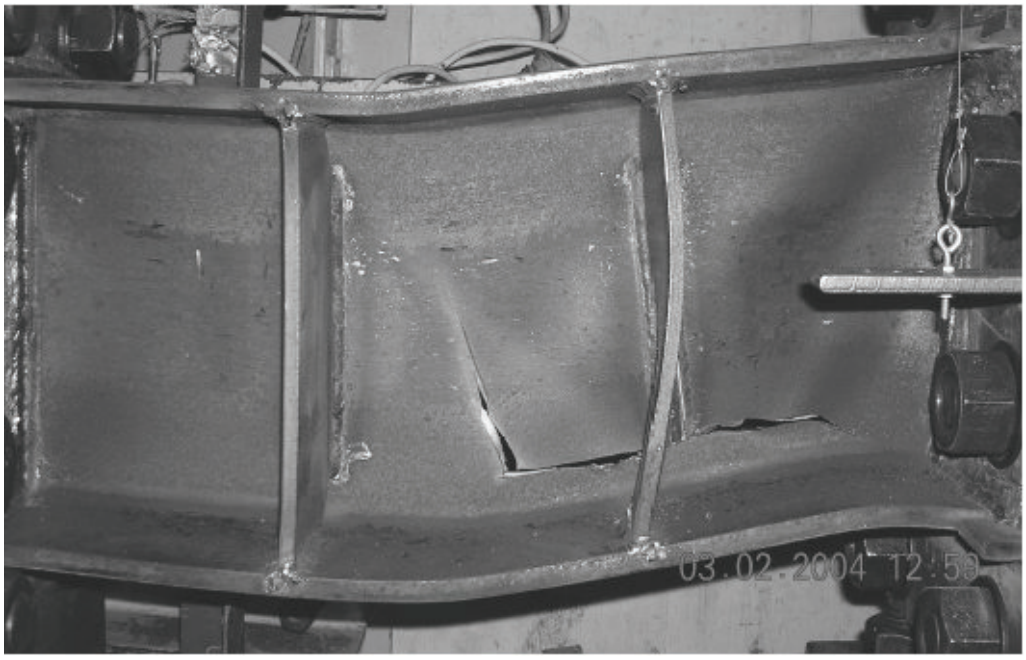

Figure 4-4 Web fracture on EBF link 10 tested by Galvez (2004)

Whittaker et al. (1987) tested a 0.3-scale model of a 6-story eccentrically braced steel building, which included a split-K eccentrically braced frame (i.e., links in the middle of the span of the floor beam) and a steel moment-resisting frame of significant lateral strength and stiffness. This model was subjected to a series of collapse-level simulations [see Table 7.1 in Whittaker et al. (1987)] that resulted in a maximum first story drift angle of 1.28% for the Taft-66 test, a maximum second floor link rotation of 0.092 rad, and residual second floor link rotation of approximately 0.01 rad. The residual floor displacements and story drifts for the Taft-66 test were negligible [see Figures 8.52 and 8.53 in Whittaker et al. (1987)].

For a single-story building frame composed of a split-K eccentrically braced frame and columns with pinned connections, the residual story drift (or floor displacement in this instance) could be estimated as

$$\gamma_r = \frac{L}{e}\frac{\delta_r}{h} \tag{4-1}$$

where δ_r is the residual story drift, γ_r is the residual link rotation angle, L is the length of the bay, e is the link length, and h is the height of the braced bay. The ratio δ_r/h is the residual story drift angle. For a ratio of beam span-to-link length in the range of 7 to 10, a residual link rotation angle of between 0.01 and 0.02 rad would result in a residual story drift angle of between 0.001 (0.1%) and 0.003 (0.3%).

5 Fragility Analysis for Shear-Critical Links

5.1 Introduction

Fragility functions are developed to characterize the probability that a specific MoR will be required as a function of inelastic link rotation. The data that links inelastic link rotation to damage states, and thus repair, is presented using a continuous probability distribution. For specimens with multiple damage data per MoR (e.g., plastic link rotation at initiation of web buckling, plastic link rotation at initiation of flange buckling), all data are used to develop the fragility functions.

5.2 Probability Distribution

Fragility functions are developed using the lognormal distribution, which requires positive values of the random variable (demand parameter). This distribution is widely used for fragility studies [ATC (2008)]. The two parameters that define lognormal distribution, namely, the median θ and dispersion β, are presented below.

The method of maximum likelihood [Benjamin and Cornell (1970), Soong (2004)] is used for finding point estimations of distribution parameters for sample data and is used herein to estimate the parameters for the lognormal distribution. To quantify the quality of the lognormal distributions, the Lilliefors goodness-of-fit test is performed on each fit. This test is a variant of the Kolmogorov-Smirnov test and is used when the distribution parameters are unknown Lilliefors (1967). More information on the lognormal distribution, method of maximum likelihood and goodness-of-fit testing is presented in the following sub-sections.

5.2.1 Lognormal Distribution

The lognormal distribution is a one-sided probability distribution of a random variable whose logarithm is normally distributed. This distribution is widely used for fragility studies because the demand parameter (drift, acceleration, rotation) must be positive and its relationship with the normal or Gaussian distribution. Equation 5-1 presents the probability density function (pdf) for the lognormal distribution.

$$f_X(x) = \begin{cases} \dfrac{1}{x\sigma_{\ln x}\sqrt{2\pi}} \exp\left[-\dfrac{\left(\ln(x) - \mu_{\ln x}\right)^2}{2\sigma_{\ln x}^2} \right] & \text{for } x \geq 0 \\ 0, \quad \text{elsewhere} \end{cases} \tag{5-1}$$

In Equation 5-1, $\mu_{\ln x}$ and $\sigma_{\ln x}$ are the mean and standard deviation of the natural logs of the demand parameter. The standard deviation of the natural log of the data, $\sigma_{\ln x}$, is termed dispersion in the ATC-58 project [ATC (2008)] and is denoted β. The median (θ), mean (μ) and standard deviation (σ) for a lognormally distributed demand parameter (x) are presented in Equations 5-2 through 5-4.

$$\theta = \exp(\mu_{\ln x}) \tag{5-2}$$

$$\mu = \theta \exp\left(\frac{\sigma_{\ln x}^2}{2} \right) \tag{5-3}$$

$$\sigma = \mu \sqrt{\exp\left(\sigma_{\ln x}^2\right) - 1} \tag{5-4}$$

5.2.2 Method of Maximum Likelihood

The method of maximum likelihood is the most widely used rule for finding point estimations of distribution parameters for sample data and is used below to estimate the

parameters for the aforementioned distributions. This method makes use of the sample likelihood function that is presented below for completeness.

First, let $f(x;\theta)$ be the probability density function of the population where θ is(are) the parameter(s) of the distribution X. The joint density function of a sample $X_1, X_2, \ldots, X_n$ has the form:

$$f_{X_1,X_2,\ldots,X_n}(x_1,x_2,\ldots,x_n|\theta) = f_{X_1}(x_1)f_{X_2}(x_2)\cdots f_{X_n}(x_n) = \Pi f_X(x_i|\theta) \quad (5\text{-}5)$$

where Π denotes product.

The *likelihood function* $L(\theta)$ of a set of n sample values is

$$L(\theta|x_1,x_2,\ldots x_n) = \prod_{i=1}^{n} f_X(x_i|\theta) \quad (5\text{-}6)$$

which gives the *relative likelihood* of having observed this particular sample ($X_1 = x_1$, $X_2 = x_2, \ldots, X_n = x_n$) as a function of θ [Benjamin and Cornell (1970)].

The *maximum likelihood estimate* (MLE) of θ is the value that maximizes the *likelihood function* $L(\theta)$. Per Benjamin and Cornell, maximum likelihood estimators possess the following desirable properties

- *Asymptotical unbiasedness*: means are asymptotically ($n \to \infty$) equal to the true parameter value(s), θ
- *Efficiency*: minimum expected squared error among all possible unbiased estimators.
- *Consistency*: be close to the true parameter values as the sample size increases with increasingly high probability
- *Sufficiency*: make maximum use of the information contained in the data.

5.2.3 Goodness-of-Fit Testing

To quantify the utility of the distributions, goodness-of-fit tests were performed on each fit. The Kolmogorov-Smirnov test (denoted hereafter as the K-S test) is a general test that is applicable to any distribution. The Lilliefors test is a special case of Kolmogorov-Smirnov test that can assess normality only.

Kolmogorov-Smirnov test (K-S test)

Given a set of sample values x_1, x_2, …, x_n observed from a population X, the test parameter for the K-S test (D) is calculated as:

$$D = \max_{i=1}^{n} \left\{ \left| F_X(x_i) - S_X(x_i) \right| \right\} \tag{5-7}$$

In Equation 5-7, $F_X(x_i)$ and $S_X(x_i)$ are the theoretical and empirical CDFs, respectively, calculated at the i^{th} observation. Thus, the test parameter (D) of the K-S test corresponds to the maximum of the absolute values of n (sample size) differences between the empirical CDF and the hypothesized CDF evaluated for the observed samples. The distribution of D is independent of the hypothesized distribution and is a function of n only [Benjamin and Cornell (1970)].

The null hypothesis, H_0, for the K-S test is that the population X comes from the hypothesized probability distribution. At a specified significance level (α), if D is less than or equal to D_{crit}, the null hypothesis is accepted.

$$P(D \le D_{crit}) = 1 - \alpha \tag{5-8}$$

Values for D_{crit} have been tabulated [e.g., Soong (2004)] as a function of the sample size (n) and significance level (α).

The advantage of the K-S test is that it is applicable to all sample sizes and uses data in unaltered form (does not require arbitrary grouping of the sample data) unlike the chi-square goodness-of-fit test. However, the K-S test is valid strictly for continuous distributions and values for D_{crit} are based on a completely specified hypothesized distribution (parameters known). This is not the case herein since the distribution parameters are unknown and must be estimated from the data. Using the K-S test with estimated distribution parameters may result in an unconservative acceptance of the null hypothesis [Benjamin and Cornell (1970)].

Lilliefors test

The Lilliefors test evaluates the normality of a given data. The test is used in this study to assess the acceptability of the lognormal distribution by testing the logarithm of the available data. This test is a variant of the K-S test to account for computation of the distribution parameters from the sample data [Lilliefors (1967)]. The test statistic for the Lilliefors test is calculated in a similar manner to that for the K-S test; the difference is in the calculation of D_{crit}. The Lilliefors test accounts for the unknown sample mean and variance and uses Monte Carlo simulation to determine approximate values of D_{crit}. The Lilliefors test is valid for small sample sizes but is also appropriate when the distribution parameters are unknown [Lilliefors (1967)], which is the case in this study.

5.3 Data Reduction

Seventy-one of the 110 EBF link specimens presented in Table 2-1 are governed by shear (or shear-critical). Four of the 71 shear-critical EBF links are set aside for the fragility analysis performed in Section 5.4 because of a) loading protocol (3 specimens excluded), and b) steel

type (1 specimen excluded). Two limits on stiffener spacing were considered for analysis, which further reduced the size of the dataset.

5.3.1 Loading Protocol

The damage data for three specimens, which were tested using monotonically increasing loading (27, 28, and 109 per Table 2-1) are excluded from the fragility analysis since these specimens achieved significantly higher inelastic link rotations than the other specimens, which were tested under cyclic loading (see Figure 5-1). The effect of different cyclic loading protocols on the performance of shear links is not considered.

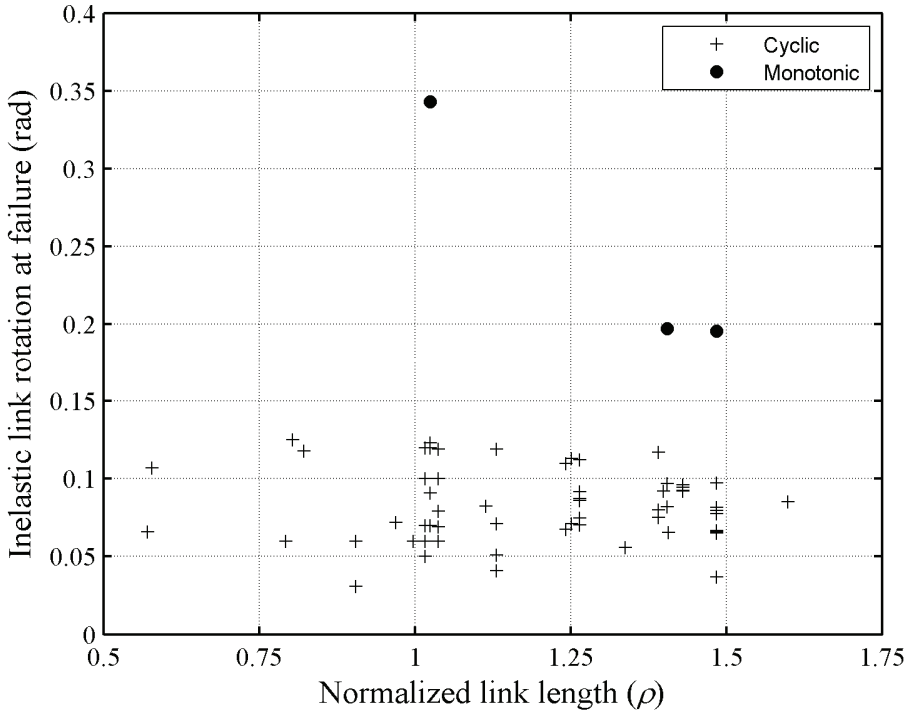

Figure 5-1 Variation of inelastic link rotation at failure with normalized link length

5.3.2 Steel Type

The damage data for one specimen (84 per Table 2-1), constructed using a high-strength H485 steel, is excluded from the fragility analysis.

5.3.3 Stiffener Spacing

For shear-critical EBF links ($\rho \leq 1.6$), AISC 341-05 [AISC (2005)] requires that the stiffener spacing be no less than $52t_w - d/5$ to achieve an inelastic link rotation of 0.02 rad and $30t_w - d/5$ to achieve an inelastic link rotation of 0.08 rad. Interpolation on stiffener spacing is used to compute values of inelastic rotation between 0.02 rad and 0.08 rad. Herein, fragility curves are developed for links that comply with the stiffener requirements of ASCE 341-05 [AISC (2005)] to achieve a minimum inelastic rotation of a) 0.05 rad and b) 0.08 rad. Eleven specimens per Table 2-1 do not meet the stiffener requirements for a) and 31 specimens do not meet the requirements for b). The data associated with these specimens are not included in the corresponding fragility analyses.

5.4 Fragility Functions

Fragility functions that define the probability that a certain method of repair will be required conditional on inelastic link rotation are developed in this section. The damage-state descriptions are used as the basis for collecting and sorting the damage data.

There is a limited amount of test data associated with MoR-1. A formal statistical analysis of such a small dataset is inappropriate. The data developed by Ricles and Popov (1987) and Whittaker et al. (1987) is used to identify the median value for this method of repair. Ricles and Popov (1987) reported initial cracking in the concrete slab at a link rotation amplitude of 0.02 rad and substantial cracking and separation of the concrete from the metal deck at a link rotation angle greater than 0.04 rad. Whittaker et al. (1987) reported substantial damage to concrete slab at higher link rotation angles (0.05 to 0.06 rad). Based on these data, a lognormal distribution with a median inelastic link rotation of 0.04 rad is considered

appropriate for MoR-1. A logarithmic standard deviation of 0.30, which is similar to dispersions reported later for other MoR, is not inappropriate for MoR-1. In all tests with composite slabs, most of the damage to the concrete slab was in the immediate vicinity of the link.

The fragility functions for MoR-2 and MoR-3 are developed for the following four datasets and shear-critical links:

Dataset 1: Links that comply with the stiffener requirements of ASCE 341-05 [AISC (2005)] to achieve a minimum inelastic rotation of 0.05 rad.

Dataset 2: Links that comply with the stiffener requirements of ASCE 341-05 [AISC (2005)] to achieve a minimum inelastic rotation of 0.08 rad.

Dataset 3: Similar to Dataset 1 but excluding those shear-critical links in D-braced EBFs [Bruneau et al. (1998)] that *fractured* at the link-to-column joint. (In a D-braced EBF, the link is joined to the column flange and the moment demand at the column face is larger than the moment demand at the breace-link connection.) These fractures are premature in the sense that they prevent the link beam from developing its full capacity. There are five such fractures in Dataset 1: specimens 51, 85, 86, 87, and 90 in Table 2-1. At fracture, these link beams developed plastic link rotations of 0.056, 0.060, 0.031, 0.051, and 0.041 rad, respectively. A photograph of a fractured test specimen, MWS tested by Okazaki (2004), is shown in Figure 5-2.

Dataset 4: A subset of Dataset 1 that excludes all shear-critical links connected at one end to a column (D-braced EBF). The link beams in the split-K-braced configuration [Bruneau et al. (1998)] are generally continuous and subjected to similar moment demands at both ends of

the link beam. This dataset is assembled to investigate the effect of EBF configuration on the fragility data.

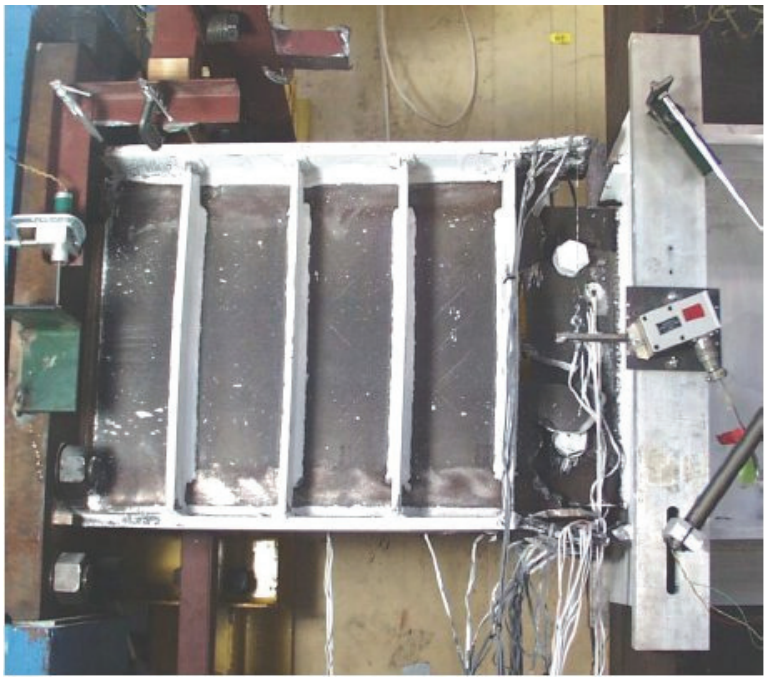

Figure 5-2 Flange fracture at the link-to-column connection, specimen MWS [Okazaki (2004)]

The parameters and the Lilliefors test results for the lognormal distribution and all four datasets are presented in Table 5-1 for MoR-2 and MoR-3. The goodness-of-fit tests of Table 5-1 are conducted at the 5% significance level.

The data presented in Table 5-1 include the Lilliefors test parameter (D), decision on the null hypothesis that the data comes from the hypothesized probability distribution (A = Accept, R = Reject), p value of the test and the critical test parameter (D_{crit}). As noted previously, if $D \le D_{crit}$, the null hypothesis (H_0) is accepted. As seen in the table, the null hypothesis is accepted for all MoRs and datasets. The distributions pass the Lilliefors goodness-of-fit test in all cases.

Table 5-1 Distribution parameters and Lilliefors test results for lognormal distribution

Dataset No	MoR	lognormal		Lilliefors test results			
		θ	β	D_{crit}	p	H_0	D
1	**2**	0.060	0.30	0.14	0.41	A	0.10
	3	0.079	0.32	0.12	0.24	A	0.10
2	**2**	0.056	0.30	0.21	0.50	A	0.08
	3	0.076	0.34	0.15	0.50	A	0.10
3	**2**	0.060	0.30	0.14	0.41	A	0.10
	3	0.083	0.27	0.13	0.33	A	0.10
4	**2**	0.062	0.28	0.19	0.24	A	0.15
	3	0.083	0.26	0.20	0.16	A	0.17

As seen in Table 5-1, the medians calculated using Dataset 1 are 0.60 and 0.79 for MoR-2 and MoR-3, respectively. The corresponding values for Dataset 2 are slightly lower although this dataset includes links with closer-on-average stiffener spacing (i.e., target plastic rotation = 0.08 rad and not 0.05 rad per Dataset 1). This observation suggests that the stiffener-spacing requirements for shear-critical EBF links may be unnecessarily conservative.

The fragility data associated with Dataset 3, which excludes the damage data from link beams that failed prematurely due to fracture of the link at the column face, is identical to that of Dataset 1 for MoR-2 and very similar for MoR-3. The parameters for Dataset 4 are similar to those of Dataset 3, which suggests that similar performance should be expected for links in split-K- and D-braced EBFs if premature link fracture at the column face is prevented in the latter. Of all the datasets studied, Dataset 4 yielded the smallest logarithmic standard deviations for the MoR-2 and MoR-2 fragility curves. However, the differences in the standard deviations are small and a value of 0.30 is reasonable for both MoRs. Figure 5-3 presents the empirical and theoretical fragility functions developed using the lognormal distribution and Dataset 1. The dispersions should not be increased due to epistemic

uncertainty because the dataset used to construct the fragility curves involves a range of specimen sizes, a large number of specimens, and number of testing laboratories.

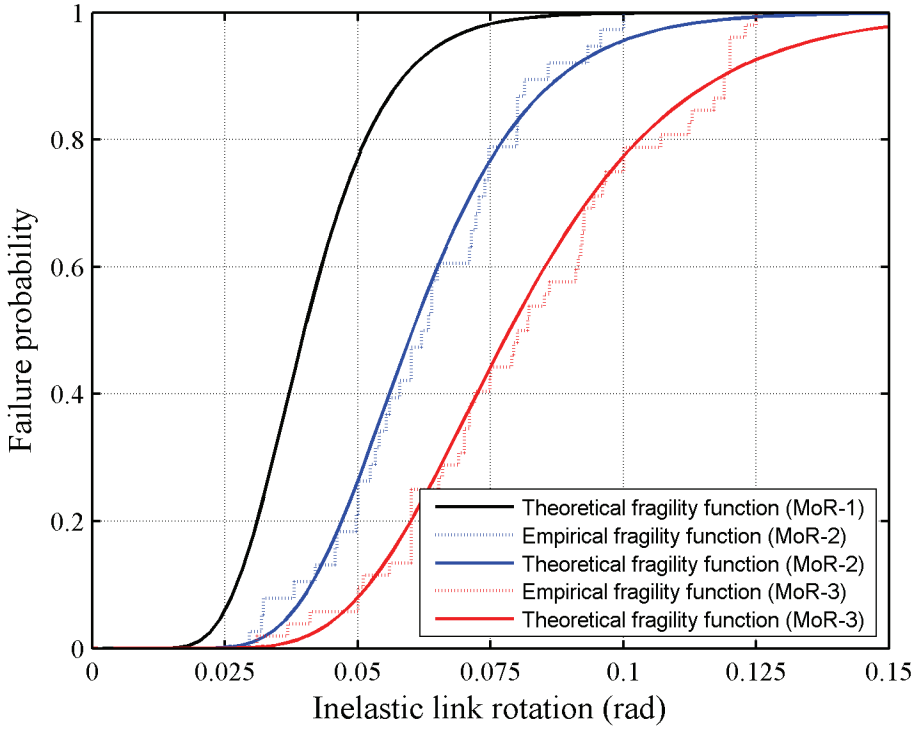

Figure 5-3 Fragility functions for shear-critical EBF links

5.5 Effect of Link Parameters on Fragility Data

In this section, scatter plots are presented for MoR-2 and MoR-3 as a function of selected link parameters to identify possible relationships between link and distribution parameters. Figure 5-4, Figure 5-5, Figure 5-6 and Figure 5-7 present damage data as a function of link depth (d), ratio of link depth to link length (d/e), the ratio of link depth to link web thickness (d/t_w), and normalized link length (ρ) respectively. There is no strong correlation between the damage data and these link parameters. However, limited experimental data is available for link beams with deep cross-sections. As seen in Figure 5-4, the database used to develop the fragility functions includes 3 link beams deeper than 30 in.

Figure 5-8 presents damage data as a function of target inelastic rotation per ASCE 341-05 [AISC (2005)]. Figure 5-8a shows that reducing the stiffener spacing (or increasing the target rotation) delays the initiation of buckling in shear-critical links. Figure 5-8b shows that delaying the initiation of buckling (or increasing the target rotation) does not necessarily increase the plastic rotation capacity of the link. In this figure, some links with target inelastic link rotations of between 0.02 and 0.03 develop inelastic rotations in experiments between 0.06 and 0.10 radian. Most of this data is from the early tests conducted at UC Berkeley. This data should be reviewed carefully since these experiments utilized a different loading protocol than the recently conducted tests. Galvez (2004) and Ryu (2005) have shown that link performance may be affected by the choice of loading protocol.

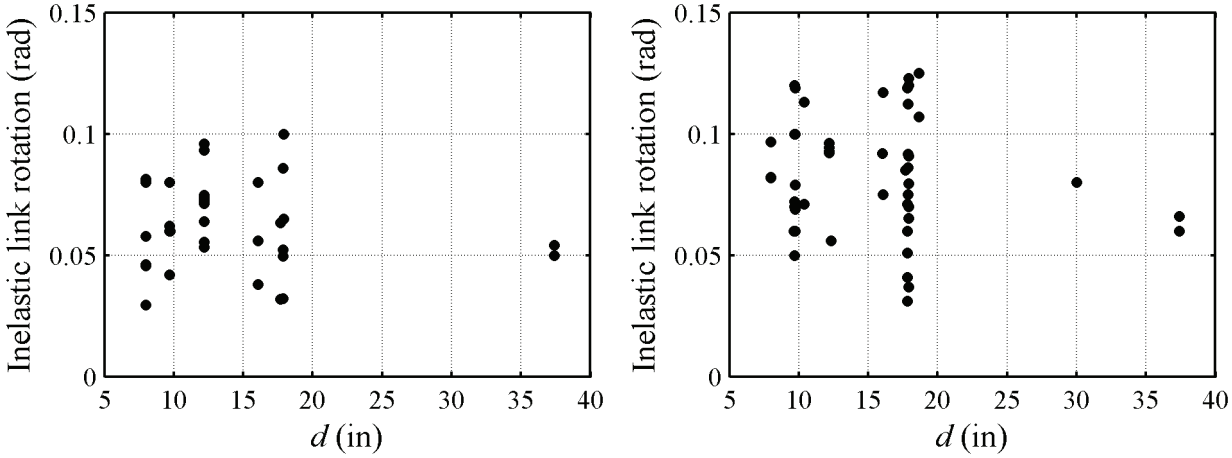

a) MoR-2 **b) MoR-3**

Figure 5-4 Variation of inelastic link rotation with d (Dataset 1)

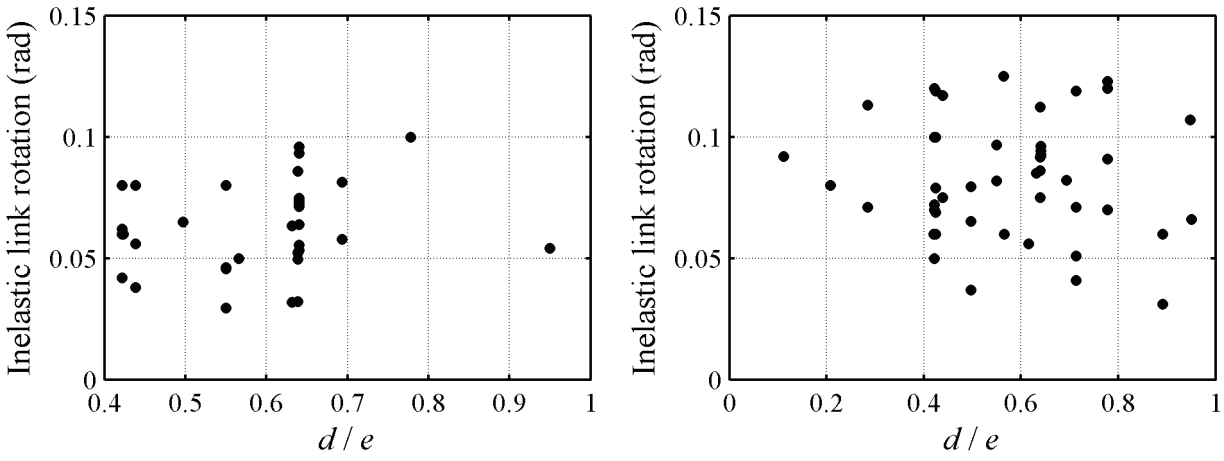

a) MoR-2 **b) MoR-3**

Figure 5-5 Variation of inelastic link rotation with d / e (Dataset 1)

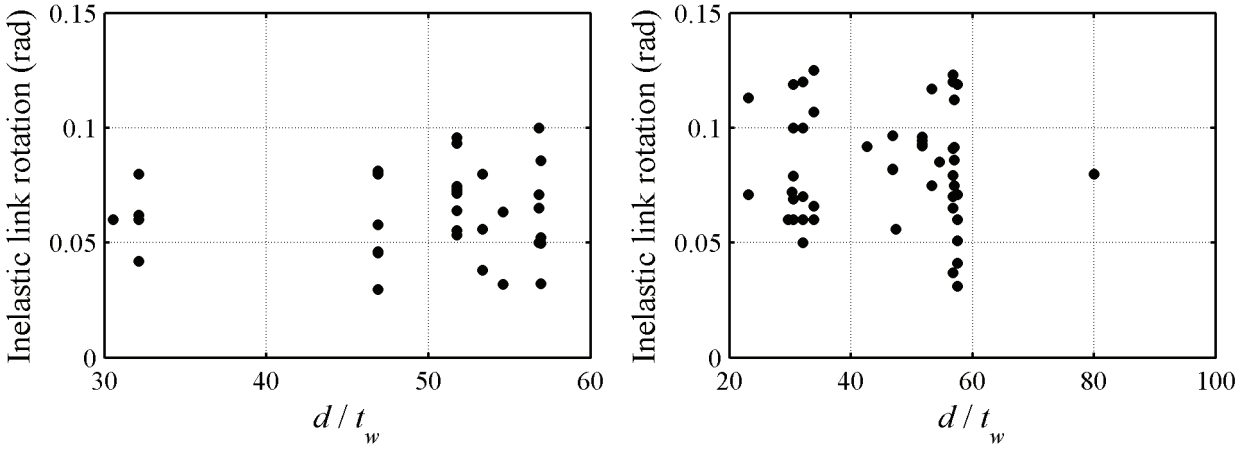

a) MoR-2 **b) MoR-3**

Figure 5-6 Variation of inelastic link rotation with d / t_w (Dataset 1)

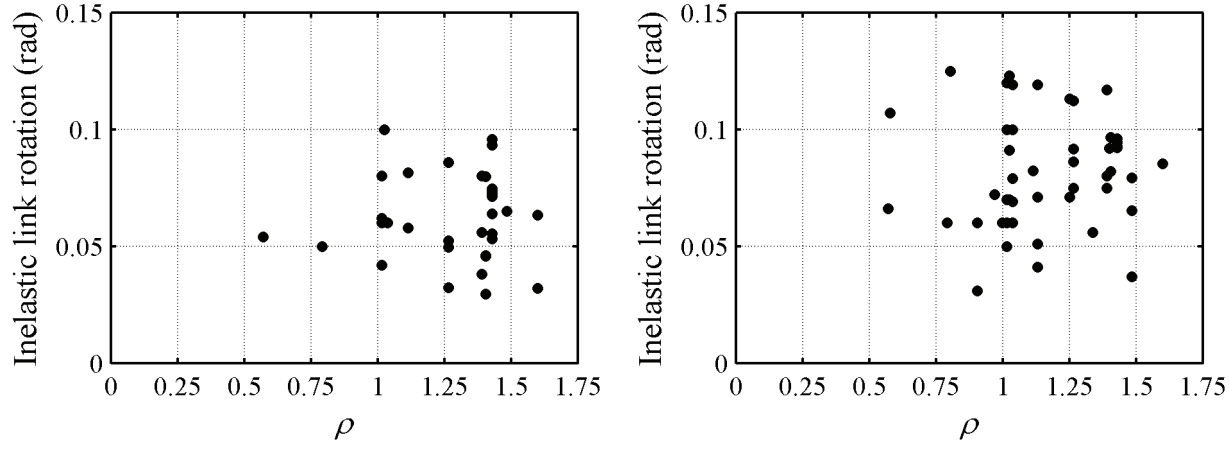

a) MoR-2 **b) MoR-3**

Figure 5-7 Variation of inelastic link rotation with ρ (Dataset 1)

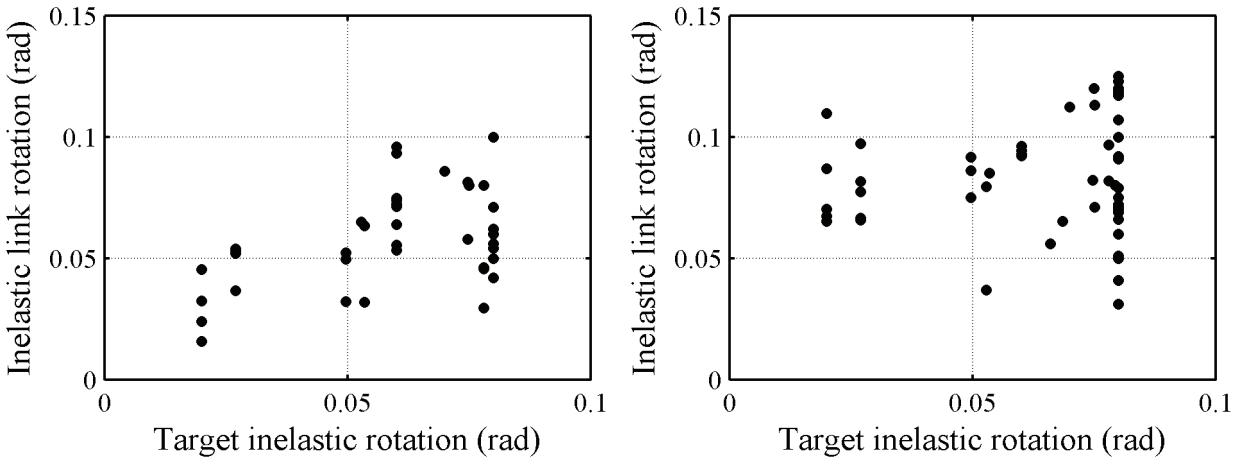

a) MoR-2 **b) MoR-3**

Figure 5-8 Variation of inelastic link rotation with target inelastic rotation per AISC (all shear –critical links)

6 Fragility Functions for Flexure-Critical Links

6.1 Introduction

The response of flexure-critical links in EBFs is dominated by inelastic flexural deformations concentrated at the link ends. The failure of such links is generally initiated by flange buckling at the link ends and/or lateral torsional buckling [Engelhardt and Popov (1989)].

Based on the AISC 341-05 [AISC (2005)] classification, 11 of the 110 specimens presented in Table 2-1 are flexure-critical links (ρ>2.6) and 28 of the 110 are intermediate links (1.6< ρ <2.6). The damage data used to develop fragility functions for flexure-critical links is presented in Table 6-1. As seen in this table, the specimens tested by Hjelmstad and Popov (1983) developed significantly greater inelastic link rotation than the other flexural links in the dataset. The Hjelmstad links differed from the others in two aspects 1) a cantilever test setup was used, and 2) the loading history was significantly different (less demanding in terms of cumulative deformation). The data for these two specimens was not used to develop fragility functions for flexure-critical links.

6.2 Damage States and Methods of Repair

Damage States and Methods of Repair for flexure-critical and intermediate links are presented in Section 4. Fragility functions are developed for MoR-2 (heat straightening) and MoR-3 (link replacement) cases only. Functions are not developed for MoR-1 because there are no data for tests of flexure-critical links constructed with composite slabs. Similar to shear-critical EBF links, local buckling damage in flexure-critical links can be repaired by

heat straightening. Flange fracture and lateral-torsional buckling damage require link replacement.

Table 6-1 Damage data for flexure-critical links

Researcher	Specimen	ρ	γ_{exp}	
			Flange buckling	Flange fracture
Hjelmstad and Popov (1983)	12	2.77	0.037	0.067
	15	2.77	0.037	0.050
Engelhardt and Popov (1989)	5	3.71	0.007	0.010
	6	3.70	0.004	0.021
	12	3.95	0.014	0.021
Okazaki (2004)	PNM	3.39	None	0.008
	MWM	3.39	None	0.018
	FFM	3.39	None	0.016
	NAM	3.39	None	0.017
Arce (2002)	3	3.70	0.019	0.039
	7	3.29	0.015	0.035

6.3 Fragility Functions

The fragility functions for flexure–critical links are developed following a similar approach to that outlined in Sections 5.1 and 5.2. The parameters and the Lilliefors test results for the lognormal distribution are presented in Table 6-2 for MoR-2 and MoR-3.

Table 6-2 Distribution parameters and Lilliefors test results for lognormal distribution

MoR	**lognormal**		**Lilliefors test results**			
	θ	β	D_{crit}	p	H_0	D
2	0.010	0.58	0.34	0.21	A	0.29
3	0.018	0.48	0.27	0.50	A	0.17

The response of an intermediate link is influenced by both shearing force and bending moment and is dependent on the normalized link length. Figure 6-1 presents the variation of inelastic link rotation at failure with normalized link length for shear-critical, flexure-critical and intermediate links. The figure shows a trend of decreasing inelastic link rotation decreasing with increasing normalized link length as expected. Explicit, normalized-link-length-dependent fraglity functions for intermediate links are not proposed. Rather, the parameters can be interpolated on the basis of normalized link length using the data of Table 5-1 ($\rho \leq 1.6$) and Table 6-2 ($\rho \geq 2.6$). For example, a fragility function for a link with a normalized length of 2.1 and MoR-3 could be defined with a median of (0.079+0.018)/2 = 0.0485, and dispersion of (0.048+0.032)/2 = 0.040, assuming that the variable is lognormally distributed.

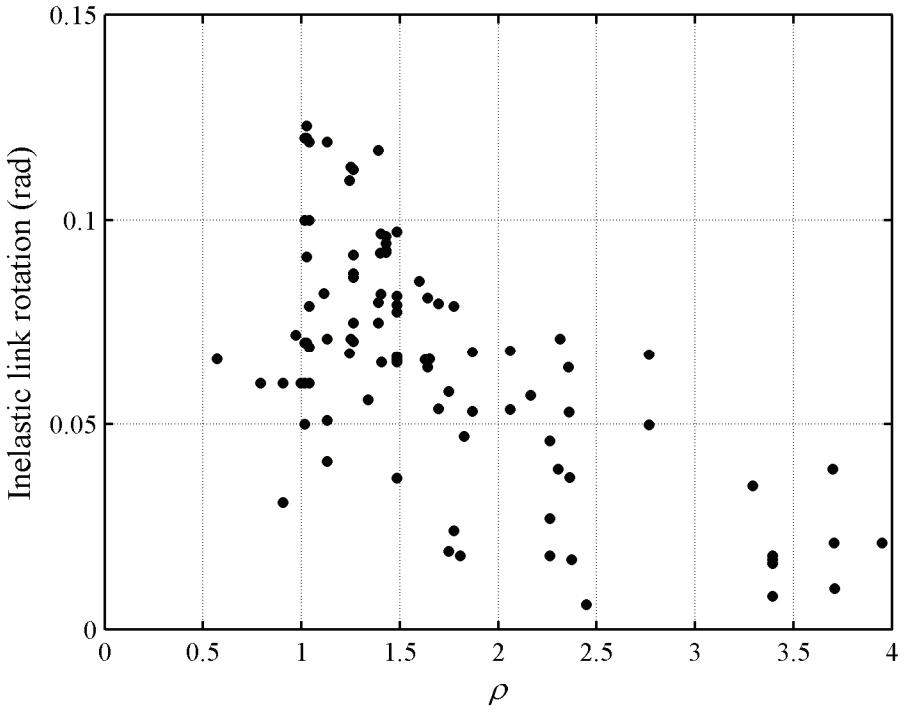

Figure 6-1 Inelastic link rotation at failure for shear, flexural and intermediate links (3 monotonically tested specimens not included)

7 Scopes of Repair for Earthquake-damaged EBF Links

7.1 Introduction

To establish consequence functions and costs of repair, a list of repair activities is assigned to each method of repair.

No repair method is proposed herein for excessive residual horizontal displacements because the scope and strategy will depend on the amount of residual deformation in adjacent link beams, both horizontal and vertical. The scope could involve a combination of heat straightening of damaged links (MoR-2) and link replacement (MoR-3).

7.2 MoR-0, Cosmetic Repair

Depending on the specific circumstances, cosmetic repair may involve one or more of the following measures: repaint structural steel; replace spray-on thermal fire protection; and remove and replace of architectural enclosure. No structural repair is required.

7.3 MoR-1, Concrete Replacement

The replacement of damaged concrete will involve the following steps: 1) remove the concrete in the immediate vicinity of the link, assumed to be the length of the link plus 2 feet and a width equal to the flange of the link plus 2 feet; and 2) recast the composite slab.

7.4 MoR-2, Heat Straightening

The method of repair associated with heat straightening involves the following steps: 1) shore the floor framing in the immediate vicinity of the damaged link; 2) remove of concrete in the immediate vicinity of the link beam, assumed to be the length of the link plus 2 feet

and a width equal to the flange of the link plus 2 feet; 3) heat-straighten the steel in the immediate vicinity of the web and flange local buckles; and 4) recast the composite slab.

7.5 MoR-3, Link Replacement

The method of repair associated with link replacement is a function of the construction details used for the link and the adjacent structural framing.

For traditional EBF construction, where the link and the beam framing outside the link are continuous, link replacement will involve the following tasks: 1) shore and remove the composite floor slab above the damaged link beam, and shore and disconnect any floor framing members that are connected to the link; 2) remove by flame cutting the link beam and a 5-foot section of beam on either side of the link (assuming a split-K braced EBF) from the supporting braces and adjacent framing; depending on the connection details, short sections of braces attached to the link beam may also need to be removed; 3) weld a new beam/link section to replace the section removed in step 3; and 4) re-attach the floor framing perpendicular to the line of the link beam and recast the composite floor removed in step 1.

8 Conclusions

Fragility functions for shear-critical links and flexure-critical links in Eccentrically Braced Frames were developed by review and statistical evaluation of data from tests of 82 links. Fragility functions for intermediate links can be established by interpolation between the functions for shear-critical and flexure-critical links. Damage to links is associated with one of four methods of repair (cosmetic, concrete replacement, heat straightening, and link replacement). Fragility functions are presented for each method of repair using the lognormal distribution and plastic link rotation as the demand parameter. The scope of each method of repair is established by analysis of photographs of damaged specimens to enable the development of consequence functions and computation of repair cost and loss due to business interruption.

9 References

AISC, 2005, "Seismic Provisions for Structural Steel Buildings (ANSI/AISC 341-05)," American Institute of Steel Construction, Inc., Chicago, IL, 309 pp.

Arce, G., 2002, "Impact of Higher Strength Steels on Local Buckling and Overstrength of Links in Eccentrically Braced Frames," MS Thesis, Department of Civil, Architectural and Environmental Engineering, The University of Texas at Austin, Austin, TX.

ATC, 2008, "Guidelines for Seismic Performance Assessment of Buildings (ATC-58)," Applied Technology Council, <http://www.atcouncil.org/atc-58.shtml>.

Benjamin, J. R., and Cornell, C. A., 1970, *Probability, Statistics, and Decision for Civil Engineers*, McGraw-Hill, New York, 684 pp.

Bruneau, M., Uang, C.-M., and Whittaker, A. S., 1998, *Ductile Design of Steel Structures*, McGraw-Hill.

Dusicka, P., 2004, "Built-up Shear Links as Energy Dissipators for Seismic Protection of Bridges," PhD Dissertation, Department of Civil and Environmental Engineering, University of Nevada, Reno, NV, 349 pp.

Engelhardt, M. D., and Popov, E. P., 1989, "Behavior of Long Links in Eccentrically Braced Frames," *Report* No. UCB/EERC-89/01, Earthquake Engineering Research Institute, Berkeley, CA.

Foutch, D. A., Goel, S. C., and Roeder, C. W., 1987, "Seismic Testing of Full-Scale Steel Building - Part I," *Journal of Structural Engineering*, ASCE, Vol. 113, No. 11, pp. 2111-2129.

Galvez, P., 2004, "Investigation of Factors Affecting Web Fractures in Shear Links," MS Thesis, Department of Civil, Architectural and Environmental Engineering, The University of Texas at Austin, Austin, TX.

Hjelmstad, K. D., and Popov, E. P., 1983, "Seismic Behavior of Active Beam Links in Eccentrically Braced Frames," *Report* No. UCB/EERC-83/15, Earthquake Engineering Research Institute, Berkeley, CA.

Itani, A. M., 1997, "Cyclic Behavior of Richmond-San Rafael Tower Links," *Report* No. CCEER 97-4, Center for Civil Engineering Earthquake Research, University of Nevada at Reno, Reno, NV.

Kasai, K., and Popov, E. P., 1986, "A Study of Seismically Resistant Eccentrically Braced Frame Systems," *Report* No. UCB/EERC-86/01, Earthquake Engineering Research Institute, Berkeley, CA.

Lilliefors, H. W., 1967, "On the K-S Test for Normality with Mean and Variance Unknown," *Journal of American Statistical Association*, Vol. 62, June, pp. 399-402.

Malley, J. O., and Popov, E. P., 1983, "Design Considerations for Shear Links in Eccentrically Braced Frames," *Report* No. UCB/EERC-83/24, Earthquake Engineering Research Institute, Berkeley, CA.

McDaniel, C. C., Uang, C.-M., and Seible, F., 2002, "Cyclic Testing of Suspension Tower Shear Links of the San Franciso - Oakland Bay Bridge," *Report* No. SSRP-2001/14, Department of Structural Engineering, University of California, San Diego, CA.

Okazaki, T., 2004, "Seismic Performance of Link-to-Column Connections in Steel Eccentrically Braced Frames," PhD Dissertation, Department of Civil, Architectural and Environmental Engineering, The University of Texas at Austin, Austin, TX, 621 pp.

Ricles, J. M., and Popov, E. P., 1987, "Experiments on Eccentrically Braced Frames with Composite Floors," *Report* No. UCB/EERC-87/06, Earthquake Engineering Research Institute, Berkeley, CA.

Roeder, C. W., and Popov, E. P., 1977, "Inelastic Behavior of Eccentrically Braced Steel Frames Under Cyclic Loadings," *Report* No. UCB/EERC-77/18, Earthquake Engineering Research Center, Berkeley, CA.

Roeder, C. W., Foutch, D. A., and Goel, S. C., 1987, "Seismic Testing of Full-Scale Steel Building - Part II," *Journal of Structural Engineering*, ASCE, Vol. 113, No. 11, pp. 2130-2145.

Ryu, H.-C., 2005, "Effects of Loading History on the Behavior of Links in Seismic-Resistant Eccentrically Braced Frames," MS Thesis, Department of Civil, Architectural and Environmental Engineering, The University of Texas at Austin, Austin, TX, 124 pp.

Soong, T. T., 2004, *Fundamentals of Probability and Statistics for Engineers*, John Wiley & Sons, Chichester, England, 391 pp.

Whittaker, A. S., Uang, C.-M., and Bertero, V. V., 1987, "Earthquake Simulation Tests and Associated Studies of a 0.3-Scale Model of a Six-Story Eccentrically Braced Steel Structure," *Report* No. UCB/EERC-87/02, Earthquake Engineering Research Center, University of California, Berkeley, CA.

Appendix A – Summary of Tests on EBF Links

Table A-1 General information on the tests of EBF links

No	Reference	Specimen ID	Link Behavior[1]	Section	Loading	ρ	Axial force	Steel Type	F_{yw}[2] (ksi)	F_{yf}[3] (ksi)
1	Hjelmstad and Popov (1983)	1	S	W18x40	Cyclic	1.26	No	A36	39.5	35.0
2		2	S	W18x40	Cyclic	1.26	No	A36	39.5	35.0
3		3	S	W18x40	Cyclic	1.26	No	A36	39.5	35.0
4		4	S	W18x40	Cyclic	1.26	No	A36	39.5	35.0
5		5	S	W18x40	Cyclic	1.26	No	A36	39.5	35.0
6		6	S	W18x40	Cyclic	1.26	No	A36	39.5	35.0
7		7	S	W18x35	Cyclic	1.60	No	A36	46.7	41.4
8		8	S	W18x60	Cyclic	1.41	No	A36	44.4	38.9
9	Malley and Popov (1983)	16	S	W18x60	Cyclic	1.24	No	A36	44.0	44.0
10		17	S	W18x40	Cyclic	1.48	No	A36	48.0	48.0
11		18	S	W18x60	Cyclic	1.24	No	A36	44.0	44.0
12		20	S	W18x40	Cyclic	1.48	No	A36	48.0	48.0
13		21	S	W18x40	Cyclic	1.48	No	A36	48.0	48.0
14		22	S	W18x40	Cyclic	1.48	No	A36	48.0	48.0
15		23	S	W18x40	Cyclic	1.48	No	A36	48.0	48.0
16		24	S	W18x40	Monotonic	1.48	No	A36	48.0	48.0
17		25	S	W18x40	Cyclic	1.48	No	A36	48.0	48.0
18		26	S	W18x40	Cyclic	1.48	No	A36	48.0	48.0
19		27	S	W18x40	Cyclic	1.48	No	A36	48.0	48.0
20		28	S	W18x40	Cyclic	1.48	No	A36	48.0	48.0
21	Kasai and Popov (1986)	1	S	W8x10	Monotonic	1.40	No	A36	60.6	52.4
22		2	S	W8x10	Cyclic	1.40	No	A36	60.6	52.4
23		3	S	W8x10	Cyclic	1.40	No	A36	60.6	52.4
24		4	S	W8x10	Cyclic	1.40	Yes	A36	60.6	52.4
25		7	S	W8x10	Cyclic	1.11	No	A36	60.6	52.4
26	Ricles and Popov (1987)	A1	S	W12x19	Cyclic	1.43	No	A36	54.3	45.1
27		A2	S	W12x19	Cyclic	1.43	No	A36	54.3	45.1
28		B1	S	W12x19	Cyclic	1.43	No	A36	54.3	45.1
29		B2	S	W12x19	Cyclic	1.43	No	A36	54.3	45.1
30		C1	S	W12x19	Cyclic	1.43	No	A36	54.3	45.1
31		C2	S	W12x19	Cyclic	1.43	No	A36	54.3	45.1
32		D1	S	W12x19	Cyclic	1.43	No	A36	54.3	45.1
33		D2	S	W12x19	Cyclic	1.43	No	A36	54.3	45.1

1. S = Shear-critical, I = Intermediate, F = Flexure-critical per ASCE 341-05 [AISC (2005)]
2. Yield stress measured at the web of the section.
3. Yield stress measured at the flanges of the section.

Table A-1 General information on the tests of EBF links (cont'd)

No	Reference	Specimen ID	Link Behavior[1]	Section	Loading	ρ	Axial force	Steel Type	F_{yw}[2] (ksi)	F_{yf}[3] (ksi)
34	Engelhardt and Popov (1989)	9	S	W12x22	Cyclic	1.34	No	A36	47.0	42.0
35	Itani (1997)	BU30	S	Built-up	Cyclic	1.39	No	A572	57.3	53.7
36		BU16	S	Built-up	Cyclic	1.40	No	A572	57.3	53.7
37	McDaniel et al. (2002)	Type 1	S	Built-up	Cyclic	0.79	No	A709	51.3	53.4
38		Type 3	S	Built-up	Cyclic	0.57	No	A709	51.3	53.4
39	Arce (2002)	4a	S	W10x33	Cyclic	1.04	No	A992	57.7	55.3
40		4b	S	W10x33	Cyclic	1.04	No	A992	57.7	55.3
41		4c	S	W10x33	Cyclic	1.04	No	A992	57.7	55.3
42		8	S	W16x36	Cyclic	1.39	No	A992	54.5	56.3
43		10	S	W10x68	Cyclic	1.25	No	A992	61.0	48.7
44	Galvez (2004)	1 (A)	S	W10x33	Cyclic	1.00	No	A992	54.5	58.2
45		2 (B)	S	W10x33	Cyclic	1.02	No	A992	62.3	58.6
46		3 (C)	S	W10x33	Cyclic	0.97	No	A992	54.2	58.1
47		4 (B)	S	W10x33	Cyclic	1.02	No	A992	62.3	58.6
48		5 (B)	S	W10x33	Cyclic	1.02	No	A992	62.3	58.6
49		6 (B)	S	W10x33	Cyclic	1.02	No	A992	62.3	58.6
50		7 (B)	S	W10x33	Cyclic	1.02	No	A992	62.3	58.6
51		8 (B)	S	W10x33	Cyclic	1.02	No	A992	62.3	58.6
52		9 (B)	S	W10x33	Cyclic	1.02	No	A992	62.3	58.6
53		10 (B)	S	W10x33	Cyclic	1.02	No	A992	62.3	58.6
54	Dusicka (2004)	C345a	S	Built-up	Cyclic	0.80	No	A709	54.0	56.6
55		C345b	S	Built-up	Cyclic	0.58	No	A709	54.0	56.6
56		H485	S	Built-up	Cyclic	0.82	No	A709 HPS	73.0	73.0
57	Okazaki (2004)	FFS	S	W18x40	Cyclic	0.90	No	A992	57.0	51.0
58		FFS-RLP	S	W18x40	Cyclic	0.90	No	A992	57.0	51.0
59		MWS	S	W18x40	Cyclic	1.13	No	A992	57.0	51.0
60		NAS	S	W18x40	Cyclic	1.13	No	A992	57.0	51.0
61		NAS-RLP	S	W18x40	Cyclic	1.13	No	A992	57.0	51.0
62		PNS	S	W18x40	Cyclic	1.13	No	A992	57.0	51.0
63	Ryu (2005)	4A-RLP	S	W10x33	Cyclic	1.04	No	A992	57.7	55.3
64		4C-RLP	S	W10x33	Cyclic	1.04	No	A992	57.7	55.3
65		8-RLP	S	W16x36	Cyclic	1.39	No	A992	54.5	56.3
66		10-RLP	S	W10x68	Cyclic	1.25	No	A992	61.0	48.7
67		12-RLP	S	W18x40	Cyclic	1.02	No	A992	57.0	51.0
68		12-AISC	S	W18x40	Cyclic	1.02	No	A992	57.0	51.0
69		12-SEV	S	W18x40	Cyclic	1.02	No	A992	57.0	51.0
70		12-RAN	S	W18x40	Cyclic	1.02	No	A992	57.0	51.0
71		12-MON	S	W18x40	Monotonic	1.02	No	A992	57.0	51.0

Table A-1 General information on the tests of EBF links (cont'd)

No	Reference	Specimen ID	Link Behavior[1]	Section	Loading	ρ	Axial force	Steel Type	F_{yw}[2] (ksi)	F_{yf}[3] (ksi)
72	Kasai and Popov (1986)	5	I	W8x10	Cyclic	1.70	No	A36	60.6	52.4
73		6	I	W8x10	Cyclic	1.70	Yes	A36	60.6	52.4
74	Hjelmstad and Popov (1983)	9	I	W18x40	Cyclic	1.63	No	A36	39.5	35.0
75		10	I	W16x26	Cyclic	1.87	No	A36	48.3	49.7
76		11	I	W18x35	Cyclic	2.06	No	A36	46.7	41.4
77		12	F	W12x22	Cyclic	2.77	No	A36	55.5	42.4
78		13	I	W16x26	Cyclic	1.87	No	A36	48.3	49.7
79		14	I	W18x35	Cyclic	2.06	No	A36	46.7	41.4
80		15	F	W12x22	Cyclic	2.77	No	A36	55.5	42.4
81	Engelhardt and Popov (1989)	1	I	W12x16	Cyclic	2.36	No	A36	53.0	46.0
82		2	I	W12x16	Cyclic	2.36	No	A36	52.0	45.0
83		3	I	W12x22	Cyclic	2.36	No	A36	57.0	46.0
84		4	I	W12x22	Cyclic	2.30	No	A36	56.0	47.0
85		5	F	W12x16	Cyclic	3.71	No	A36	52.0	45.0
86		6	F	W12x16	Cyclic	3.70	No	A36	60.0	52.0
87		7	I	W12x16	Cyclic	2.45	No	A36	51.0	44.0
88		8	I	W12x22	Cyclic	2.37	No	A36	46.0	42.0
89		10	I	W12x16	Cyclic	1.77	No	A36	51.0	44.0
90		11	I	W12x22	Cyclic	1.81	No	A36	48.0	44.0
91		12	F	W12x22	Cyclic	3.95	No	A36	47.0	43.0
92	Okazaki (2004)	PNI	I	W18x40	Cyclic	2.26	No	A992	57.0	51.0
93		PNM	F	W18x40	Cyclic	3.39	No	A992	57.0	51.0
94		MWI	I	W18x40	Cyclic	2.26	No	A992	57.0	51.0
95		MWM	F	W18x40	Cyclic	3.39	No	A992	57.0	51.0
96		FFI	I	W18x40	Cyclic	2.26	No	A992	57.0	51.0
97		FFM	F	W18x40	Cyclic	3.39	No	A992	57.0	51.0
98		FFSL-	I	W18x40	Cyclic	1.75	No	A992	57.0	51.0
99		NAI	I	W18x40	Cyclic	2.26	No	A992	57.0	51.0
100		NAM	F	W18x40	Cyclic	3.39	No	A992	57.0	51.0
101		NASL-	I	W18x40	Cyclic	1.75	No	A992	57.0	51.0
102	Arce (2002)	1c	I	W10x19	Cyclic	1.77	No	A992	61.0	54.8
103		2	I	W10x19	Cyclic	2.31	No	A992	61.0	54.8
104		3	F	W10x19	Cyclic	3.70	No	A992	61.0	54.8
105		5	I	W10x33	Cyclic	1.65	No	A992	57.7	55.3
106		6b	I	W10x33	Cyclic	2.17	No	A992	57.7	55.3
107		7	F	W10x33	Cyclic	3.29	No	A992	57.7	55.3
108		9	I	W16x36	Cyclic	1.82	No	A992	54.5	56.3
109		11	I	W10x68	Cyclic	1.64	No	A992	61.0	48.7
110	Ryu (2005)	11-RLP	I	W10x68	Cyclic	1.64	No	A992	61.0	48.7

Table A-2 Geometric properties of the EBF links

No	Reference	Specimen ID	Link Behavior[1]	e (in)	d (in)	t_w (in)	b (in)	t_f (in)
1	Hjelmstad and Popov (1983)	1	S	28.0	17.88	0.314	5.99	0.521
2		2	S	28.0	17.88	0.314	5.99	0.521
3		3	S	28.0	17.88	0.314	5.99	0.521
4		4	S	28.0	17.88	0.314	5.99	0.521
5		5	S	28.0	17.88	0.314	5.99	0.521
6		6	S	28.0	17.88	0.314	5.99	0.521
7		7	S	28.0	17.69	0.324	5.91	0.378
8		8	S	36.0	18.28	0.422	7.56	0.681
9	Malley and Popov (1983)	16	S	36.0	18.24	0.415	7.56	0.695
10		17	S	36.0	17.90	0.315	6.02	0.525
11		18	S	36.0	18.24	0.415	7.56	0.695
12		20	S	36.0	17.90	0.315	6.02	0.525
13		21	S	36.0	17.90	0.315	6.02	0.525
14		22	S	36.0	17.90	0.315	6.02	0.525
15		23	S	36.0	17.90	0.315	6.02	0.525
16		24	S	36.0	17.90	0.315	6.02	0.525
17		25	S	36.0	17.90	0.315	6.02	0.525
18		26	S	36.0	17.90	0.315	6.02	0.525
19		27	S	36.0	17.90	0.315	6.02	0.525
20		28	S	36.0	17.90	0.315	6.02	0.525
21	Kasai and Popov (1986)	1	S	14.5	7.97	0.170	3.96	0.208
22		2	S	14.5	7.97	0.170	3.96	0.208
23		3	S	14.5	7.97	0.170	3.96	0.208
24		4	S	14.5	7.97	0.170	3.96	0.208
25		7	S	11.5	7.97	0.170	3.96	0.208
26	Ricles and Popov (1987)	A1	S	19.0	12.16	0.235	4.01	0.350
27		A2	S	19.0	12.16	0.235	4.01	0.350
28		B1	S	19.0	12.16	0.235	4.01	0.350
29		B2	S	19.0	12.16	0.235	4.01	0.350
30		C1	S	19.0	12.16	0.235	4.01	0.350
31		C2	S	19.0	12.16	0.235	4.01	0.350
32		D1	S	19.0	12.16	0.235	4.01	0.350
33		D2	S	19.0	12.16	0.235	4.01	0.350
34	Engelhardt and Popov (1989)	9	S	20.0	12.31	0.260	4.03	0.425
35	Itani (1997)	BU30	S	72.0	30.00	0.400	14.00	1.500
36		BU16	S	72.0	16.00	0.400	14.00	1.500
37	McDaniel et al. (2002)	Type 1	S	66.1	37.40	1.102	23.62	1.772
38		Type 3	S	39.4	37.40	1.102	18.70	1.772

1. S = Shear-critical, I = Intermediate, F = Flexure-critical per ASCE 341-05 [AISC (2005)]

Table A-2 Geometric properties of the EBF links (cont'd)

No	Reference	Specimen ID	Link Behavior[1]	e (in)	d (in)	t_w (in)	b (in)	t_f (in)
39	Arce (2002)	4a	S	23.0	9.74	0.319	8.05	0.437
40		4b	S	23.0	9.74	0.319	8.05	0.437
41		4c	S	23.0	9.74	0.319	8.05	0.437
42		8	S	36.6	16.06	0.301	6.96	0.487
43		10	S	36.6	10.40	0.449	10.26	0.773
44	Galvez (2004)	1 (A)	S	23.0	9.65	0.325	8.05	0.420
45		2 (B)	S	23.0	9.70	0.302	8.00	0.435
46		3 (C)	S	23.0	9.70	0.320	8.10	0.423
47		4 (B)	S	23.0	9.70	0.302	8.00	0.435
48		5 (B)	S	23.0	9.70	0.302	8.00	0.435
49		6 (B)	S	23.0	9.70	0.302	8.00	0.435
50		7 (B)	S	23.0	9.70	0.302	8.00	0.435
51		8 (B)	S	23.0	9.70	0.302	8.00	0.435
52		9 (B)	S	23.0	9.70	0.302	8.00	0.435
53		10 (B)	S	23.0	9.70	0.302	8.00	0.435
54	Dusicka (2004)	C345a	S	33.1	18.66	0.551	11.81	0.866
55		C345b	S	19.7	18.66	0.551	9.37	0.866
56		H485	S	33.1	18.43	0.394	10.04	0.748
57	Okazaki (2004)	FFS	S	20.0	17.82	0.310	6.09	0.500
58		FFS-RLP	S	20.0	17.82	0.310	6.09	0.500
59		MWS	S	25.0	17.82	0.310	6.09	0.500
60		NAS	S	25.0	17.82	0.310	6.09	0.500
61		NAS-RLP	S	25.0	17.82	0.310	6.09	0.500
62		PNS	S	25.0	17.82	0.310	6.09	0.500
63	Ryu (2005)	4A-RLP	S	23.0	9.74	0.319	8.05	0.437
64		4C-RLP	S	23.0	9.74	0.319	8.05	0.437
65		8-RLP	S	36.6	16.06	0.301	6.96	0.487
66		10-RLP	S	36.6	10.40	0.449	10.26	0.773
67		12-RLP	S	23.0	17.90	0.315	6.02	0.525
68		12-AISC	S	23.0	17.90	0.315	6.02	0.525
69		12-SEV	S	23.0	17.90	0.315	6.02	0.525
70		12-RAN	S	23.0	17.90	0.315	6.02	0.525
71		12-MON	S	23.0	17.90	0.315	6.02	0.525

Table A-2 Geometric properties of the EBF links (cont'd)

No	Reference	Specimen ID	Link Behavior[1]	e (in)	d (in)	t_w (in)	b (in)	t_f (in)
72	Kasai and Popov (1986)	5	I	17.5	7.97	0.17	3.96	0.21
73		6	I	17.5	7.97	0.17	3.96	0.21
74	Hjelmstad and Popov (1983)	9	I	36.0	17.88	0.31	5.99	0.52
75		10	I	36.0	15.70	0.26	5.48	0.36
76		11	I	36.0	17.69	0.32	5.91	0.38
77		12	F	36.0	12.31	0.27	4.00	0.42
78		13	I	36.0	15.70	0.26	5.48	0.36
79		14	I	36.0	17.69	0.32	5.91	0.38
80		15	F	36.0	12.31	0.27	4.00	0.42
81	Engelhardt and Popov (1989)	1	I	28.0	11.99	0.22	3.99	0.27
82		2	I	28.0	11.99	0.22	3.99	0.27
83		3	I	33.0	12.31	0.26	4.03	0.43
84		4	I	33.0	12.31	0.26	4.03	0.43
85		5	F	44.0	11.99	0.22	3.99	0.27
86		6	F	44.0	11.99	0.22	3.99	0.27
87		7	I	29.0	11.99	0.22	3.99	0.27
88		8	I	36.0	12.31	0.26	4.03	0.43
89		10	I	21.0	11.99	0.22	3.99	0.27
90		11	I	27.5	12.31	0.26	4.03	0.43
91		12	F	60.0	12.31	0.26	4.03	0.43
92	Okazaki (2004)	PNI	I	50.0	17.82	0.31	6.09	0.50
93		PNM	F	75.0	17.82	0.31	6.09	0.50
94		MWI	I	50.0	17.82	0.31	6.09	0.50
95		MWM	F	75.0	17.82	0.31	6.09	0.50
96		FFI	I	50.0	17.82	0.31	6.09	0.50
97		FFM	F	75.0	17.82	0.31	6.09	0.50
98		FFSL-RLP	I	38.6	17.82	0.31	6.09	0.50
99		NAI	I	50.0	17.82	0.31	6.09	0.50
100		NAM	F	75.0	17.82	0.31	6.09	0.50
101		NASL-	I	38.6	17.82	0.31	6.09	0.50
102	Arce (2002)	1c	I	23.0	10.30	0.27	4.00	0.38
103		2	I	30.0	10.30	0.27	4.00	0.38
104		3	F	48.0	10.30	0.27	4.00	0.38
105		5	I	36.6	9.74	0.32	8.05	0.44
106		6b	I	48.0	9.74	0.32	8.05	0.44
107		7	F	73.0	9.74	0.32	8.05	0.44
108		9	I	48.0	16.06	0.30	6.96	0.49
109		11	I	48.0	10.40	0.45	10.26	0.77
110	Ryu (2005)	11-RLP	I	48.0	10.40	0.45	10.26	0.77

Table A-3 Performance data for the EBF shear links

No	Reference	Specimen ID	ρ [1]	l_s [2] (in)	γ_{tar} [3] (rad)	γ_{wb} [4] (rad)	γ_{fb} [5] (rad)	γ_{frac} [6] (rad)
1	Hjelmstad and Popov (1983)	1	1.26	N/A	N/A	0.016	N/A	0.070
2		2	1.26	14.0	<0.02	0.032	N/A	0.087
3		3	1.26	9.3	0.050	0.052	N/A	0.075
4		4	1.26	7.0	0.070	0.086	N/A	0.112
5		5	1.26	9.3[7]	0.050	0.032	N/A	0.092
6		6	1.26	9.3[7]	0.050	0.050	N/A	0.086
7		7	1.60	9.3	0.053	0.063	0.032	0.085
8		8	1.41	N/A	N/A	0.024	N/A	0.065
9	Malley and Popov (1983)	16	1.24	N/A	N/A	0.045	N/A	0.067
10		17	1.48	12.0	0.027	0.053	N/A	0.067
11		18	1.24	N/A	N/A	NR	N/A	0.110
12		20	1.48	12.0	0.027	0.037	N/A	0.097
13		21	1.48	12.0	0.027	0.052	N/A	0.078
14		22	1.48	12.0	0.027	0.054	N/A	0.066
15		23	1.48	12.0	0.027	NR	N/A	0.066
16		24	1.48	12.0	0.027	0.100	NR	0.195
17		25	1.48	12.0	0.027	NR	N/A	0.082
18		26	1.48	9.0	0.053	0.065	N/A	0.079
19		27	1.48	7.2	0.068	NR	N/A	0.065
20		28	1.48	9.0	0.053	NR	N/A	0.037
21	Kasai and Popov (1986)	1	1.40	3.6	0.078	0.167	N/A	0.203
22		2	1.40	3.6	0.078	N/A	N/A	N/A
23		3	1.40	3.6	0.078	0.080	0.046	0.097
24		4	1.40	3.6	0.078	0.046	0.030	0.082
25		7	1.11	3.8	0.075	0.081	0.058	0.082
26	Ricles and Popov (1987)	A1	1.43	6.3	0.060	0.093	N/A	N/A
27		A2	1.43	3.2	>0.080	N/A	0.073	N/A
28		B1	1.43	6.3	0.060	0.064	0.064	0.092
29		B2	1.43	6.3	0.060	0.074	N/A	0.094
30		C1	1.43	6.3	0.060	0.075	0.055	N/A
31		C2	1.43	6.3	0.060	0.072	0.053	0.093
32		D1	1.43	6.3	0.060	0.075	N/A	0.093
33		D2	1.43	6.3	0.060	0.071	0.096	0.096

1. Damage data for flexure-critical specimens is presented in Section 6.
2. Stiffener spacing.
3. Achievable inelastic rotation capacity per ASCE 341-05 [AISC (2005)].
4. Measured inelastic rotation at web buckling damage state.
5. Measured inelastic rotation at flange buckling damage state.
6. Measured inelastic rotation at fracture.
7. Stiffener spacing not uniform.

Table A-3 Performance data for the EBF shear links (cont'd)

No	Reference	Specimen ID	ρ	l_s (in)	γ_{tar} (rad)	γ_{wb} (rad)	γ_{fb} (rad)	γ_{frac} (rad)
34	Engelhardt and Popov (1989)	9	1.34	6.7	0.066	N/A	N/A	0.056
35	Itani (1997)	BU30	1.39	5.3	>0.08	N/A	N/A	0.080
36		BU16	1.40	8.0	>0.08	N/A	N/A	0.092
37	McDaniel et al. (2002)	Type 1	0.79	22.0	>0.08	0.050	N/A	0.060
38		Type 3	0.57	19.7	>0.08	0.054	N/A	0.066
39	Arce (2002)	4a	1.04	5.8	>0.08	N/A	N/A	0.060
40		4b	1.04	5.8	>0.08	N/A	N/A	0.069
41		4c	1.04	5.8	>0.08	0.060	N/A	0.079
42		8	1.39	5.2	>0.08	0.056	0.038	0.075
43		10	1.25	12.2	0.075	N/A	N/A	0.071
44	Galvez (2004)	1 (A)	1.00	5.8	>0.08	N/A	N/A	0.060
45		2 (B)	1.02	5.8	>0.08	N/A	N/A	0.060
46		3 (C)	0.97	5.8	>0.08	N/A	N/A	0.072
47		4 (B)	1.02	5.8	>0.08	N/A	N/A	0.060
48		5 (B)	1.02	5.8	>0.08	0.060	N/A	0.070
49		6 (B)	1.02	5.8	>0.08	N/A	N/A	0.050
50		7 (B)	1.02	5.8	>0.08	0.042	N/A	0.050
51		8 (B)	1.02	5.8	>0.08	0.062	N/A	0.130
52		9 (B)	1.02	5.8	>0.08	N/A	N/A	0.100
53		10 (B)	1.02	7.7	0.075	0.080	N/A	0.120
54	Dusicka (2004)	C345a	0.80	11.0	>0.08	N/A	N/A	0.125
55		C345b	0.58	9.8	>0.08	N/A	N/A	0.107
56		H485	0.82	6.6	>0.08	N/A	N/A	0.118
57	Okazaki (2004)	FFS	0.90	5.0	>0.08	N/A	N/A	0.060
58		FFS-RLP	0.90	5.0	>0.08	N/A	N/A	0.031
59		MWS	1.13	5.0	>0.08	N/A	N/A	0.051
60		NAS	1.13	5.0	>0.08	N/A	N/A	0.071
61		NAS-RLP	1.13	5.0	>0.08	N/A	N/A	0.119
62		PNS	1.13	5.0	>0.08	N/A	N/A	0.041
63	Ryu (2005)	4A-RLP	1.04	5.8	>0.08	N/A	N/A	0.100
64		4C-RLP	1.04	5.8	>0.08	N/A	N/A	0.119
65		8-RLP	1.39	5.2	>0.08	N/A	N/A	0.117
66		10-RLP	1.25	12.2	0.075	N/A	N/A	0.113
67		12-RLP	1.02	5.8	>0.08	0.100	N/A	0.120
68		12-AISC	1.02	5.8	>0.08	0.071	N/A	0.091
69		12-SEV	1.02	5.8	>0.08	0.050	N/A	0.070
70		12-RAN	1.02	5.8	>0.08	N/A	N/A	0.123
71		12-MON	1.20	5.8	>0.08	0.198	N/A	0.343

Appendix B – Test Setups for the EBF Link Experiments

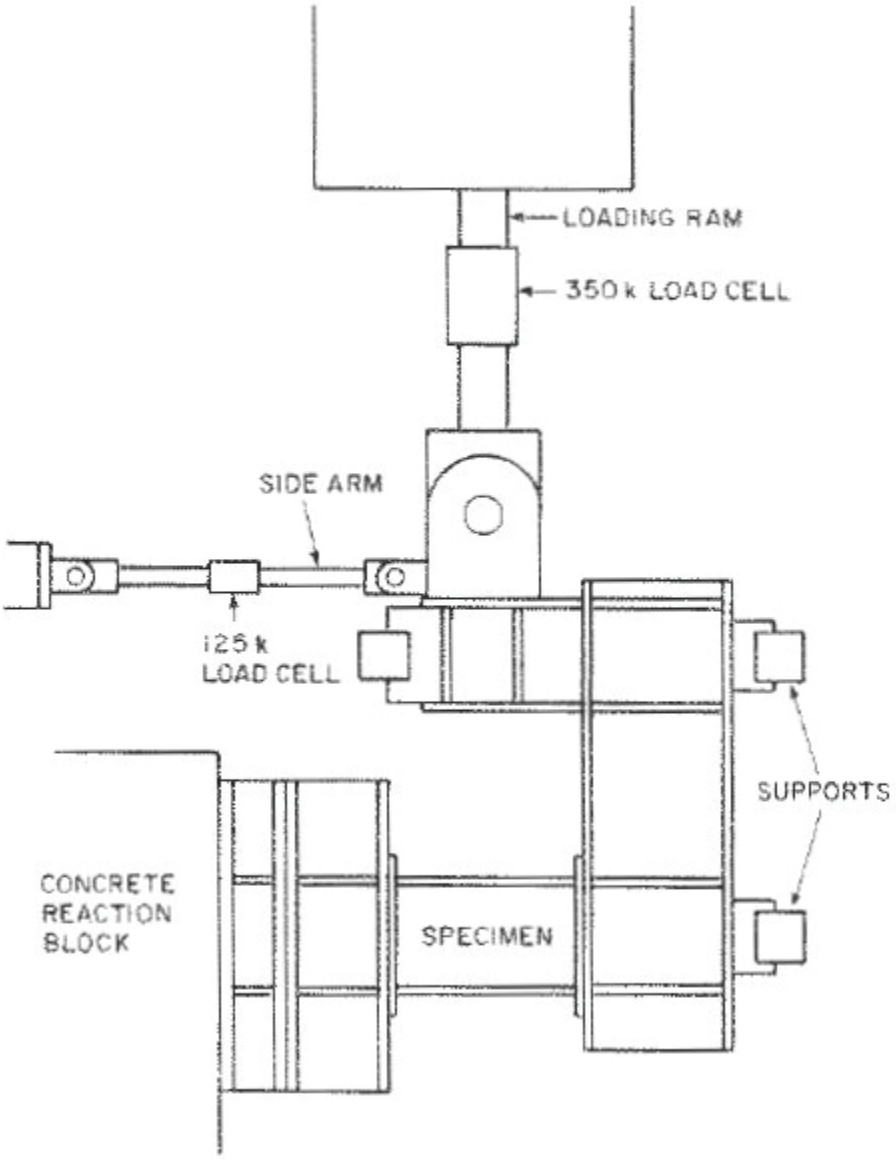

Figure B-1 Loading scheme for Hjelmstad and Popov (1983) and Malley and Popov (1983) tests

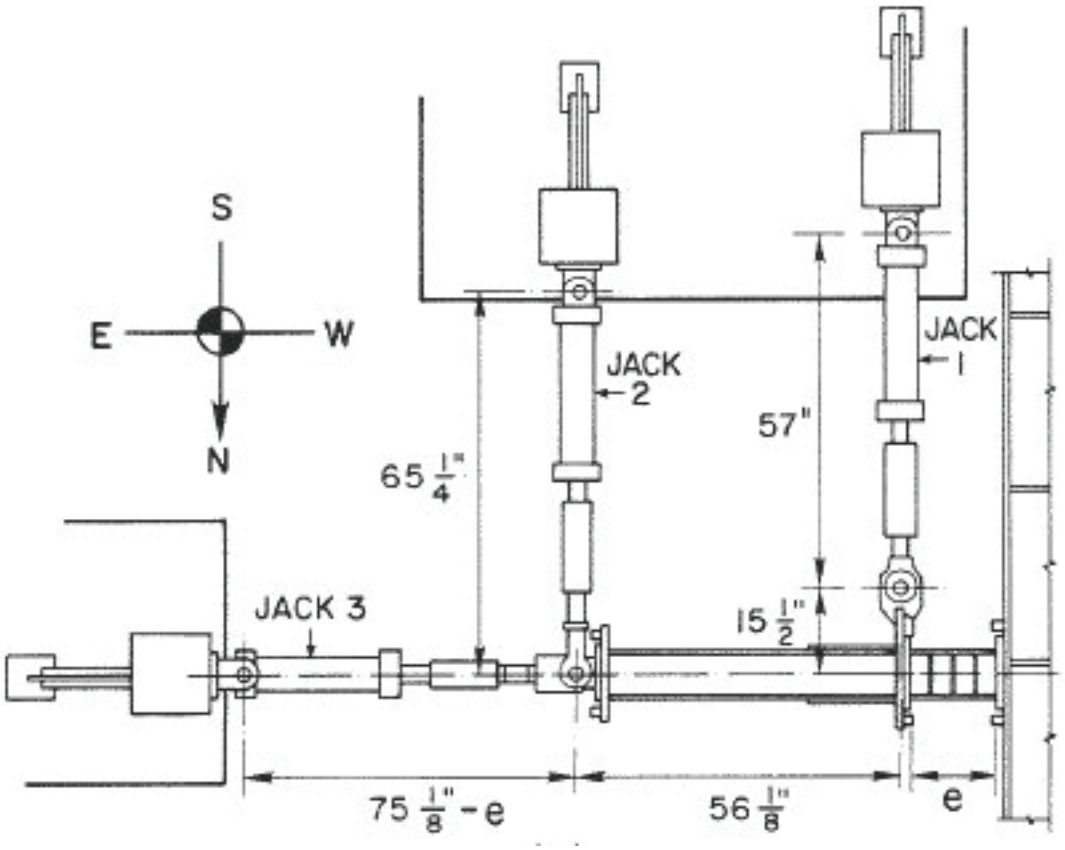

Figure B-2 Loading scheme for Kasai and Popov (1986) tests

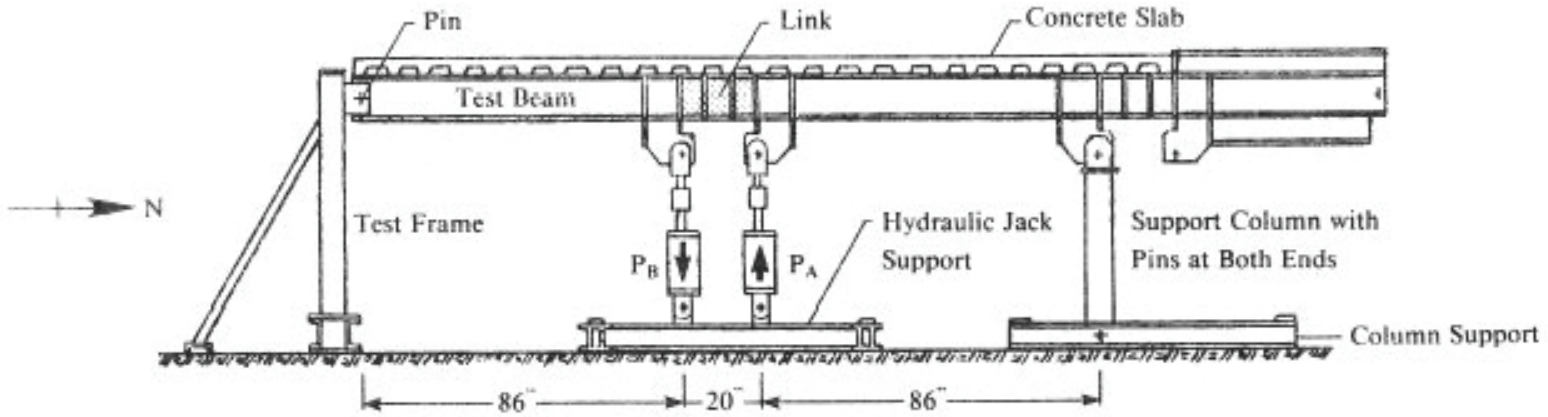

(a) K-Braced EBF Subassembly, Test Series I

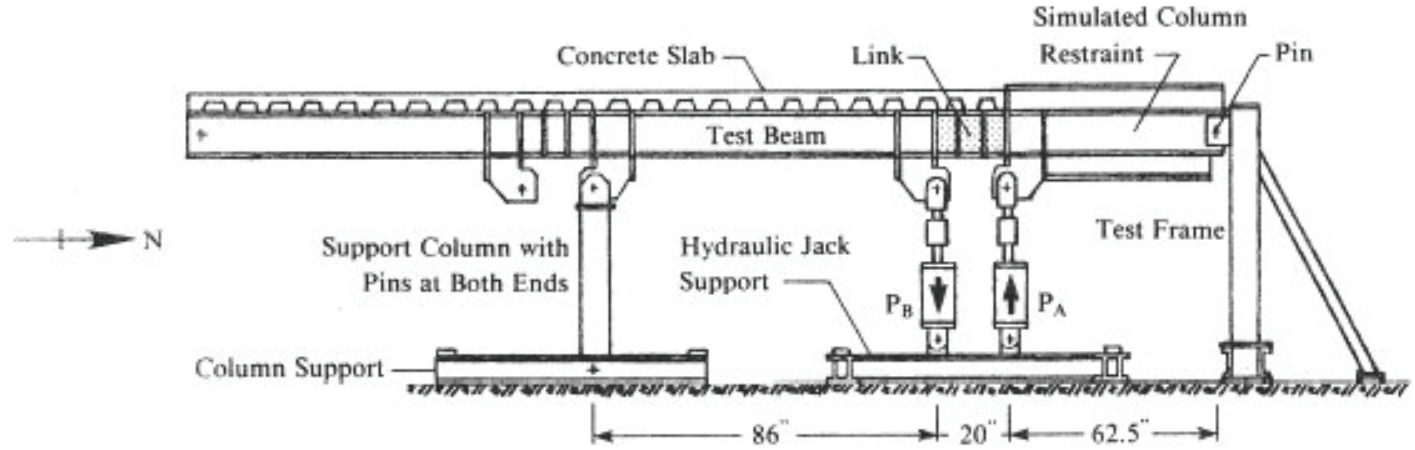

(b) V-Braced EBF Subassembly, Test Series II

Figure B-3 Loading scheme for Ricles and Popov (1987) tests

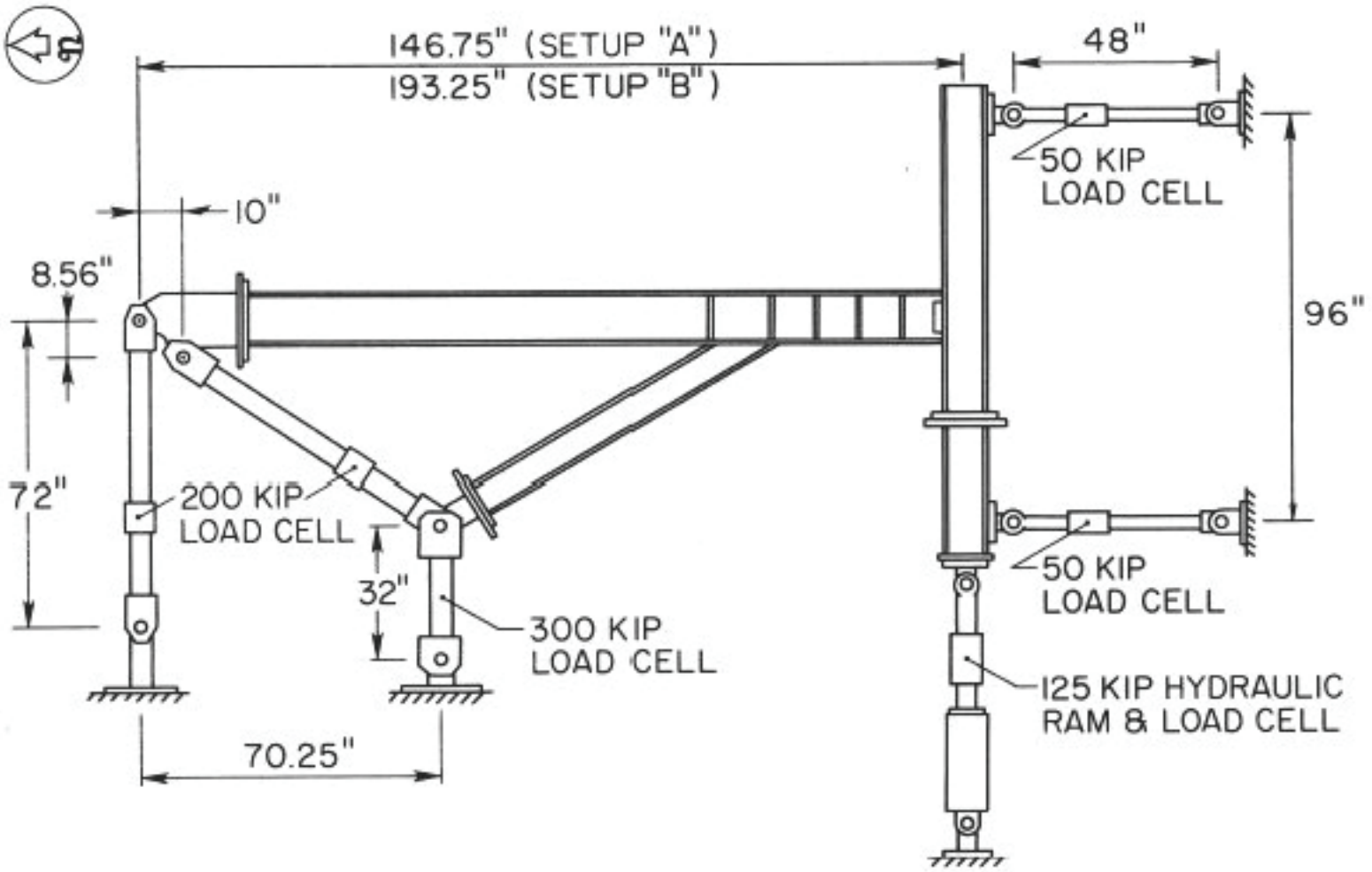

Figure B-4 Loading scheme for Engelhardt and Popov (1989) tests

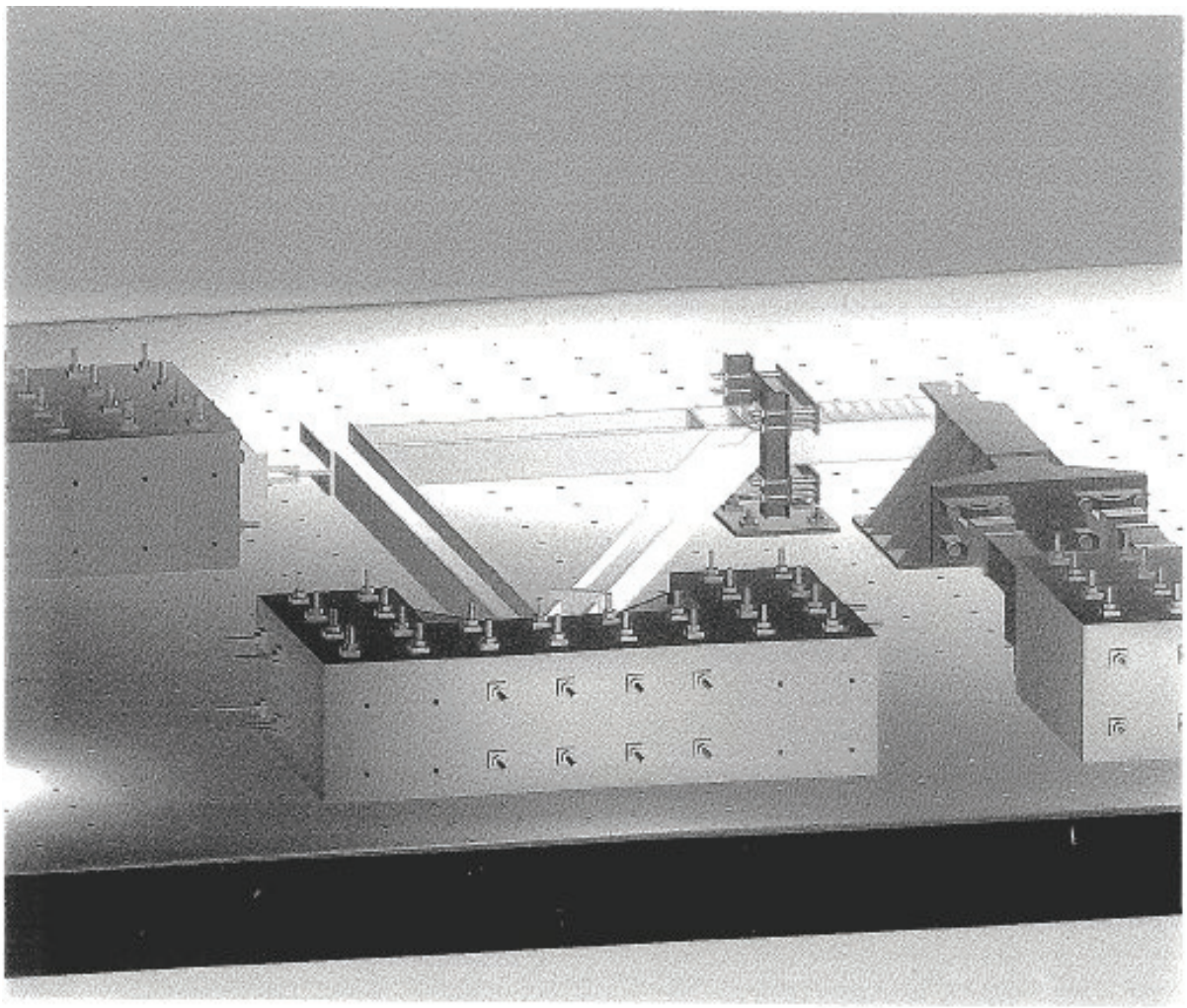

Figure B-5 Loading scheme for Itani (1997) tests

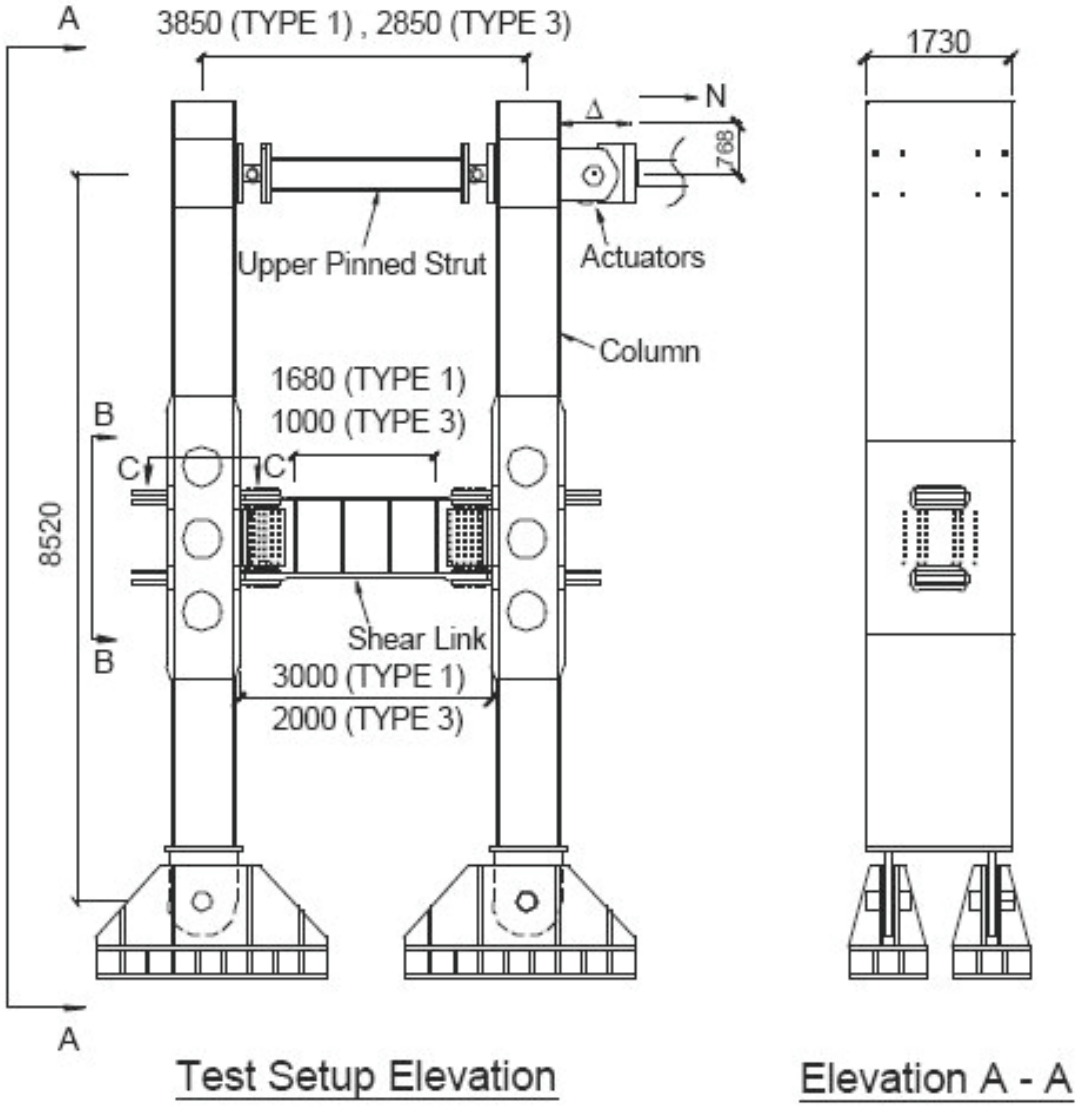

Figure B-6 Loading scheme for McDaniel et al. (2002) tests

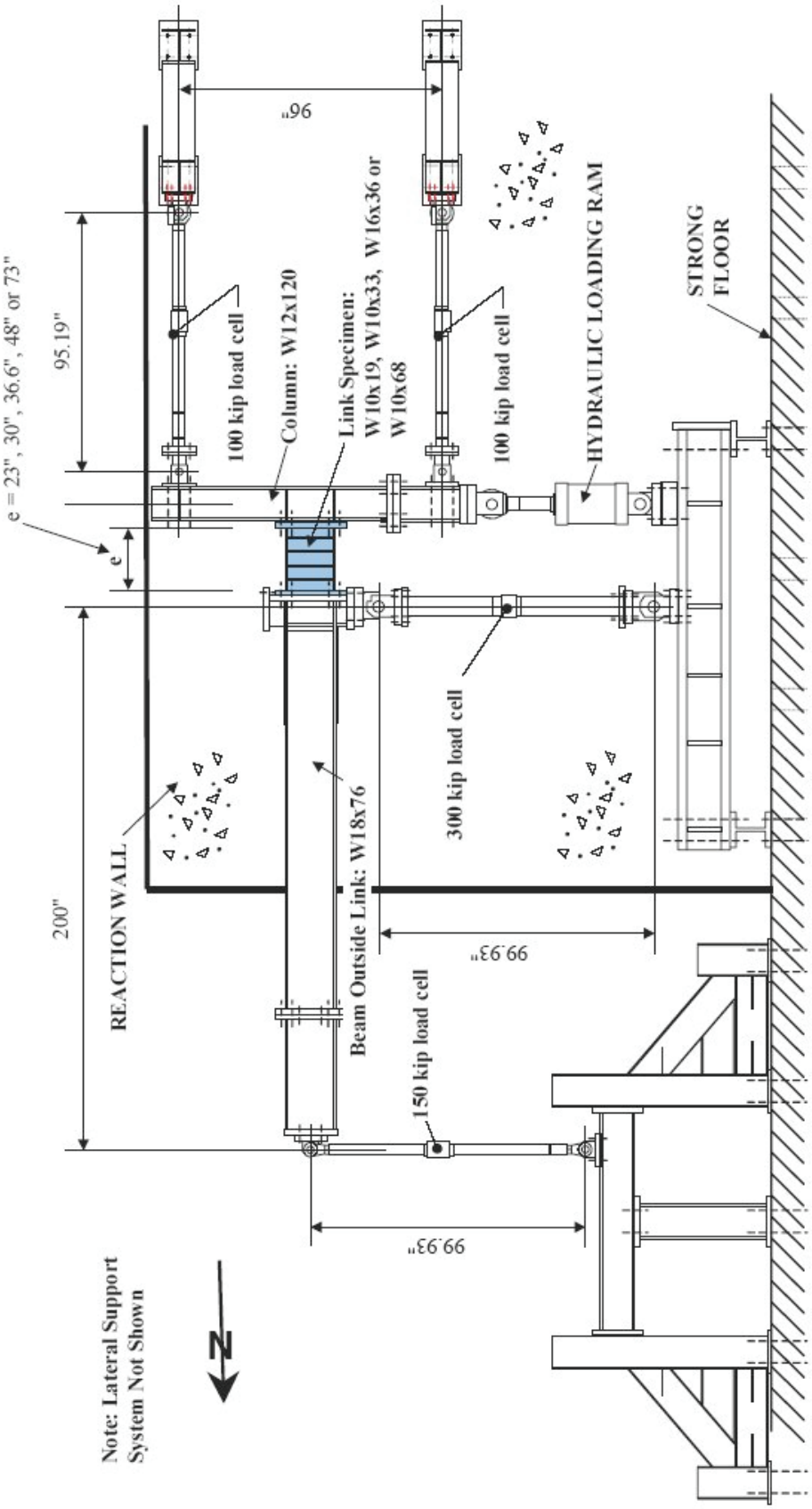

Figure B-7 Loading scheme for Arce (2002) tests

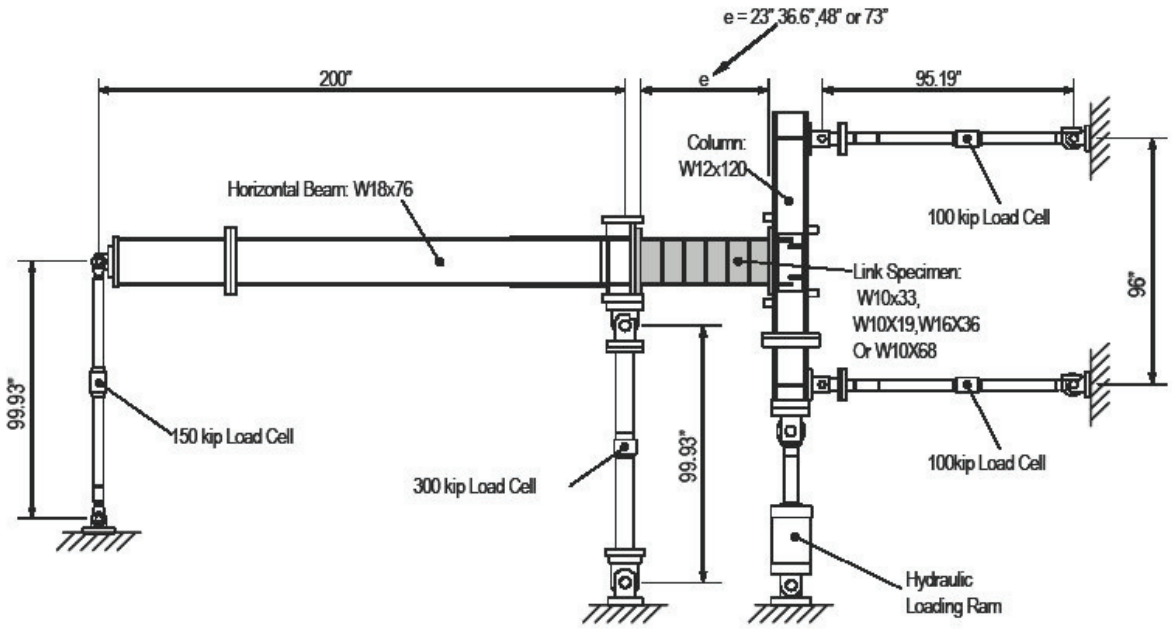

Figure B-8 Loading scheme for Galvez (2004) tests

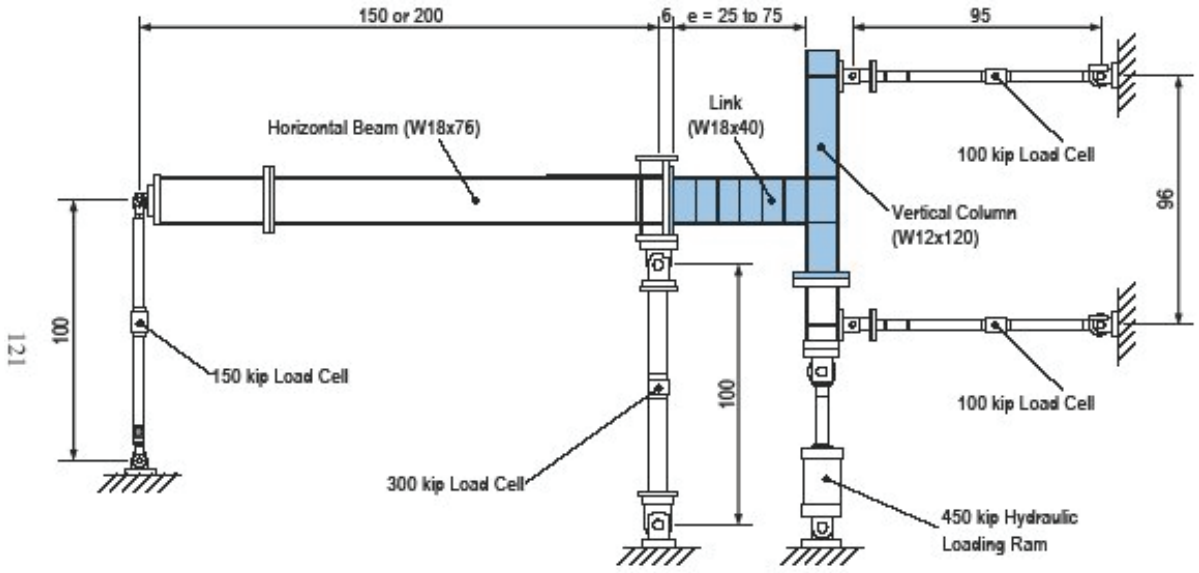

Figure B-9 Loading scheme for Okazaki (2004) tests

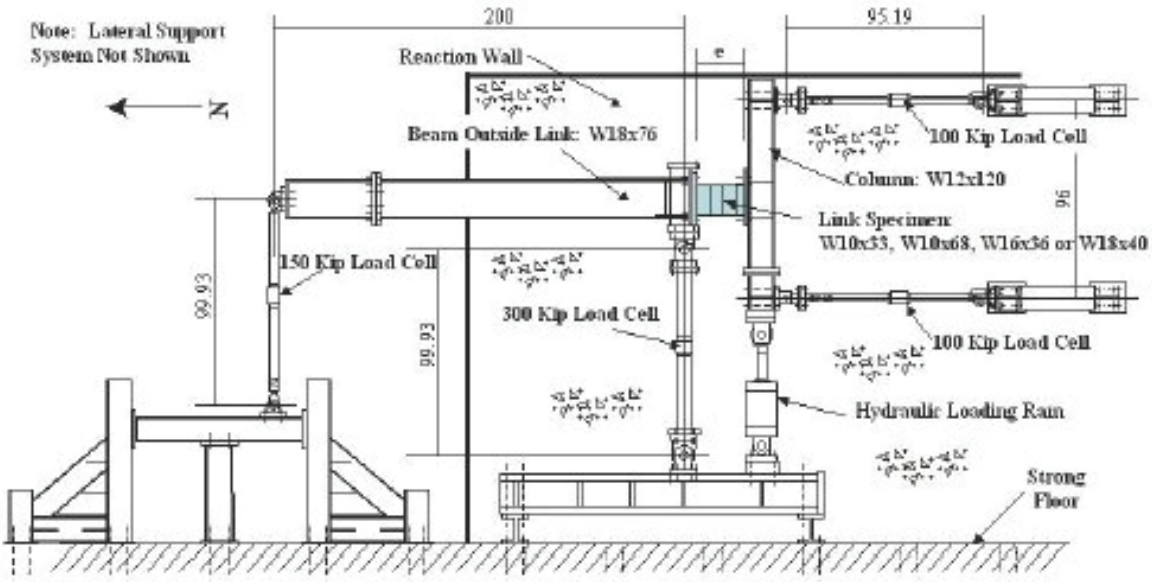

Figure B-10 Loading scheme for Ryu (2005) tests

Appendix C – Force-Deformation Relationships

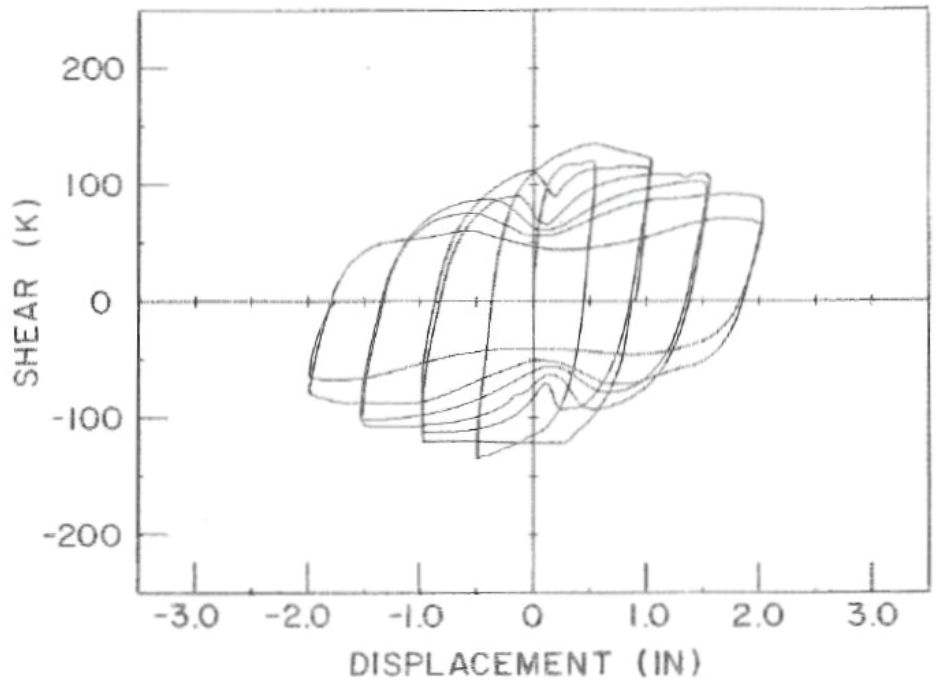

Figure C-1 Force-displacement relationship for link 1 tested by Hjelmstad and Popov (1983)

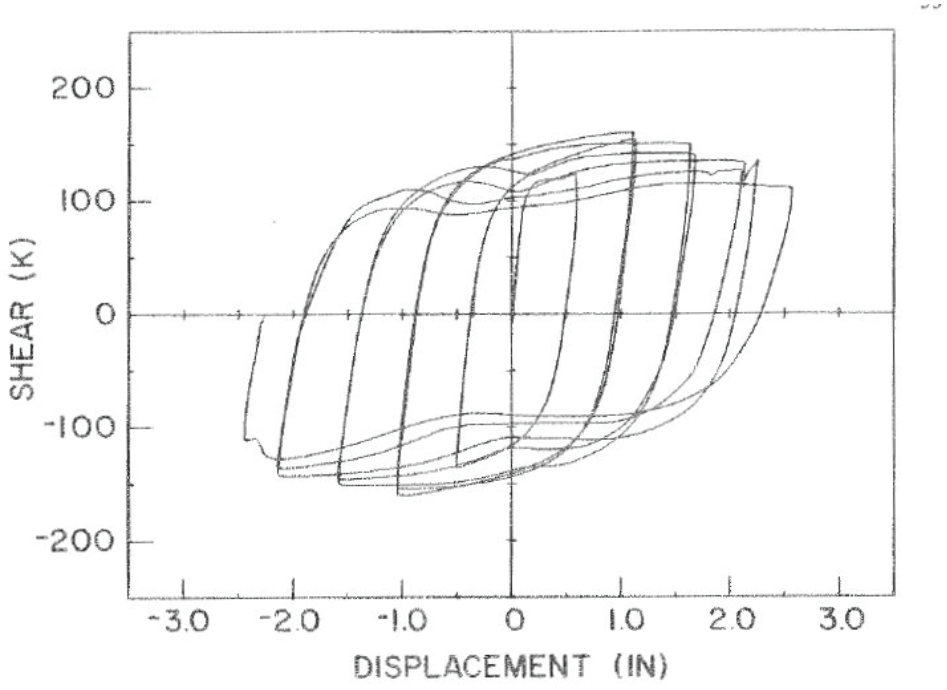

Figure C-2 Force-displacement relationship for link 2 tested by Hjelmstad and Popov (1983)

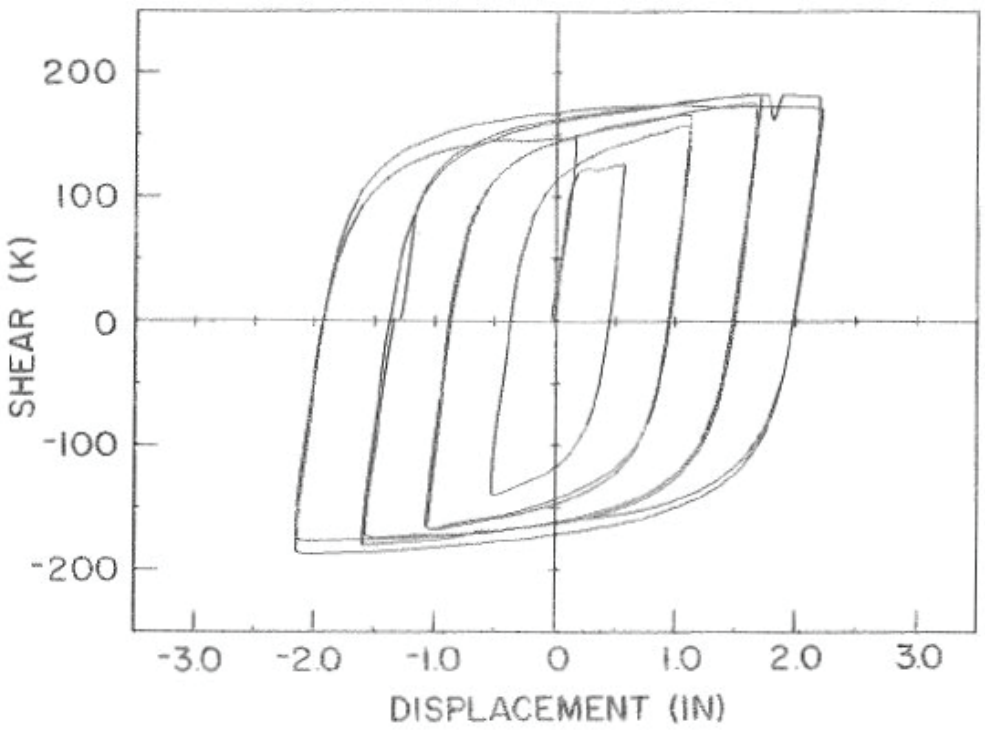

Figure C-3 Force-displacement relationship for link 3 tested by Hjelmstad and Popov (1983)

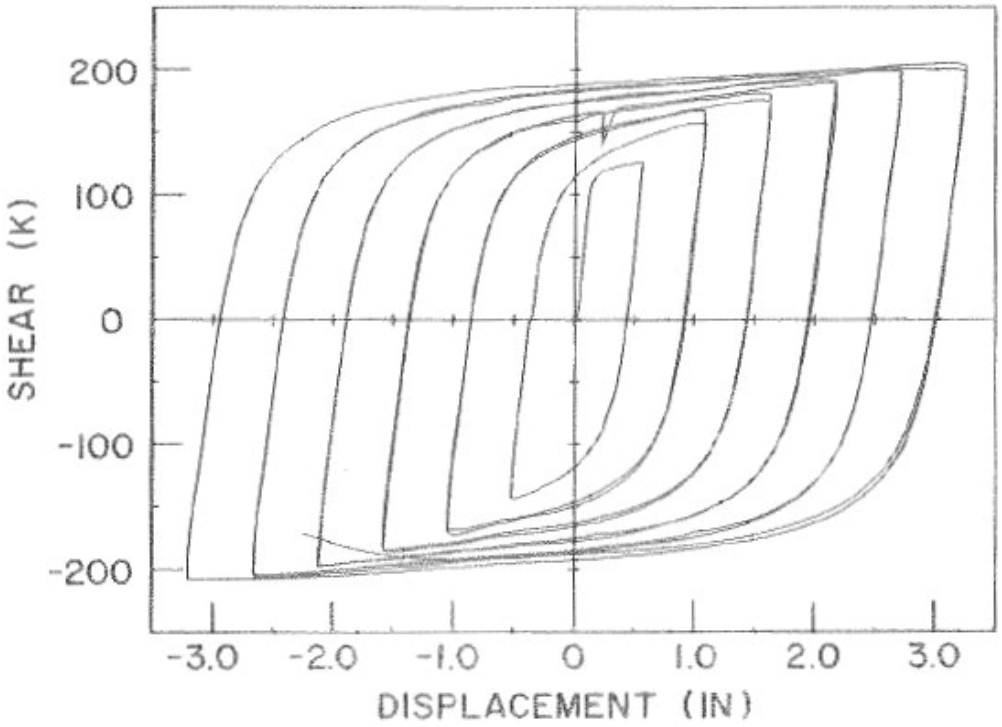

Figure C-4 Force-displacement relationship for link 4 tested by Hjelmstad and Popov (1983)

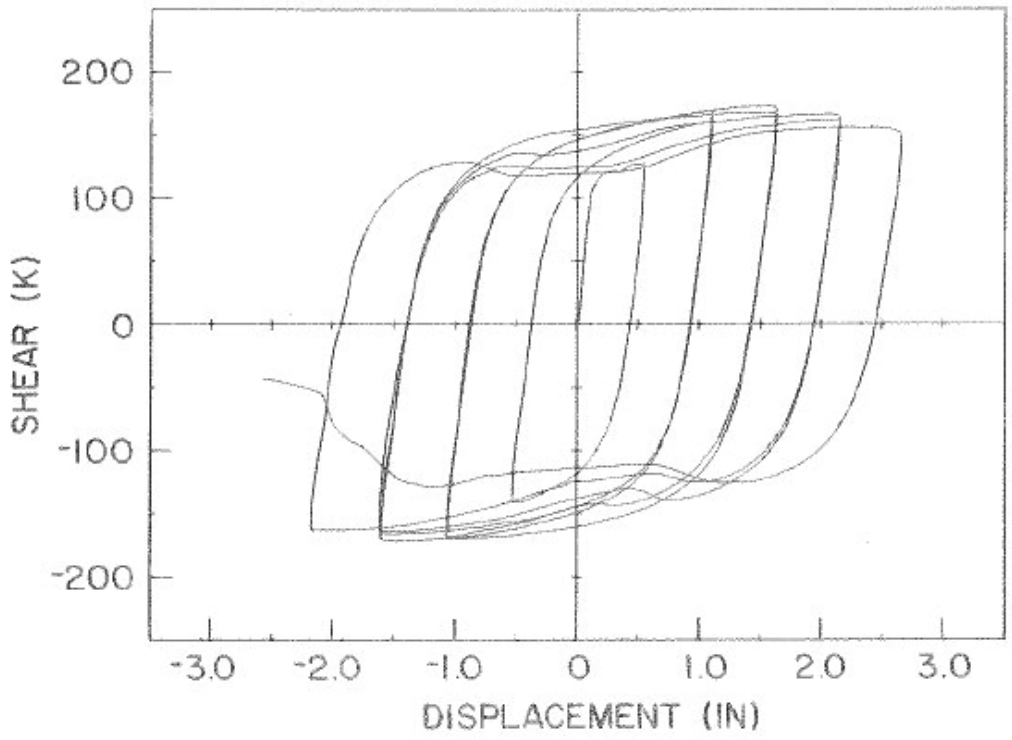

Figure C-5 Force-displacement relationship for link 5 tested by Hjelmstad and Popov (1983)

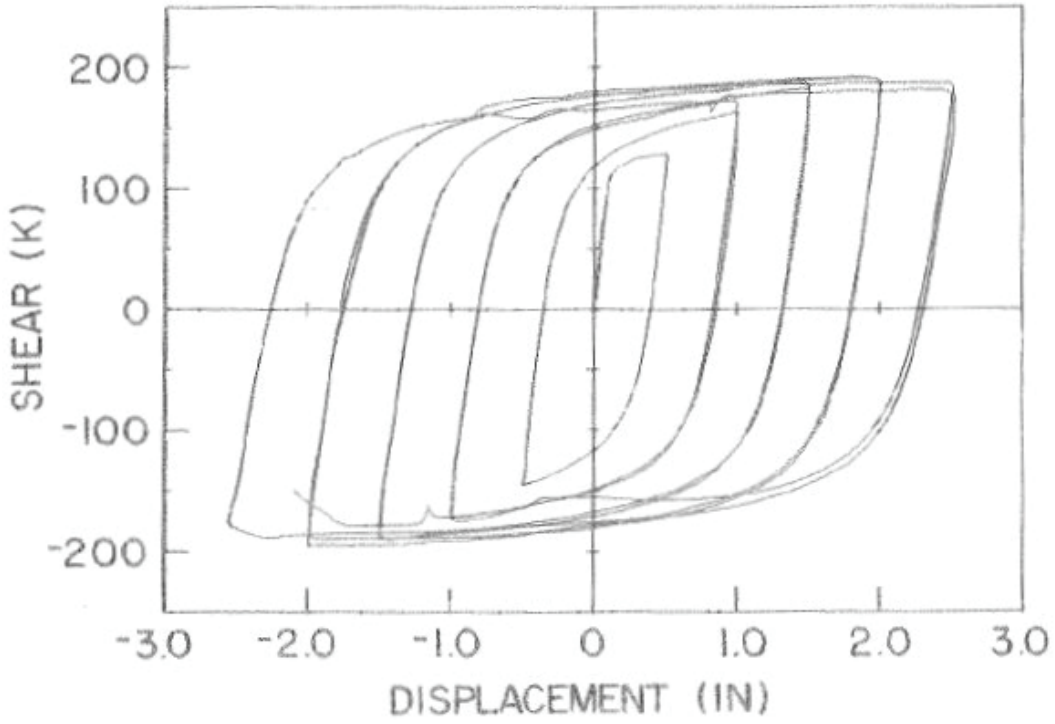

Figure C-6 Force-displacement relationship for link 6 tested by Hjelmstad and Popov (1983)

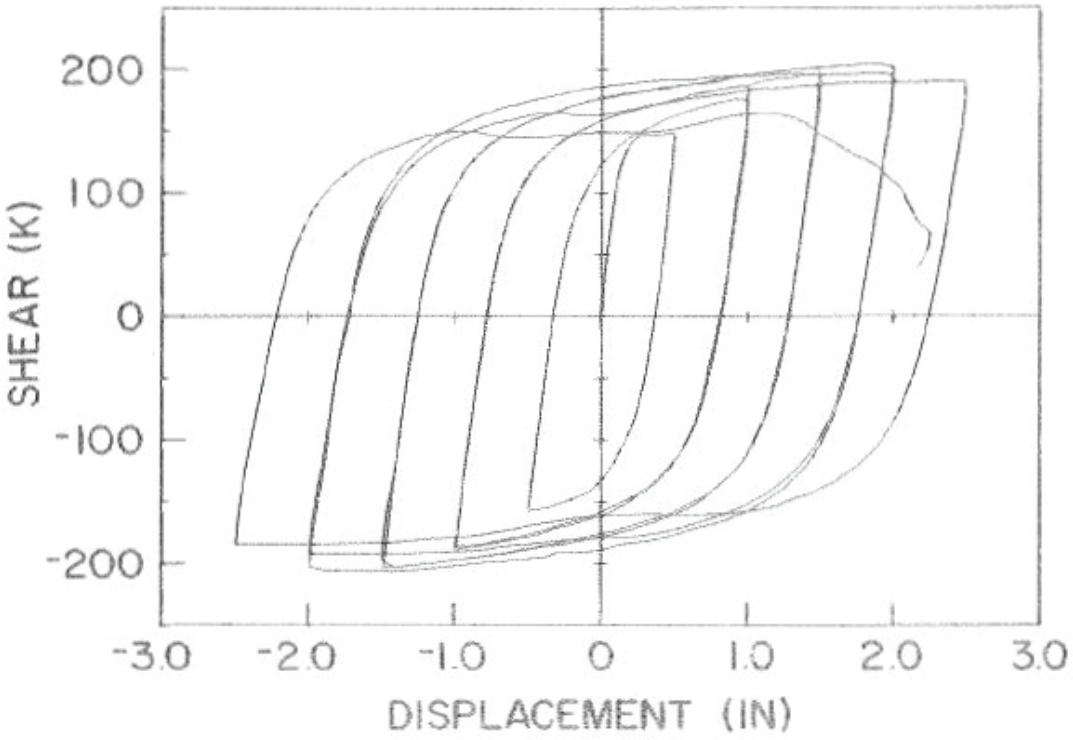

Figure C-7 Force-displacement relationship for link 7 tested by Hjelmstad and Popov (1983)

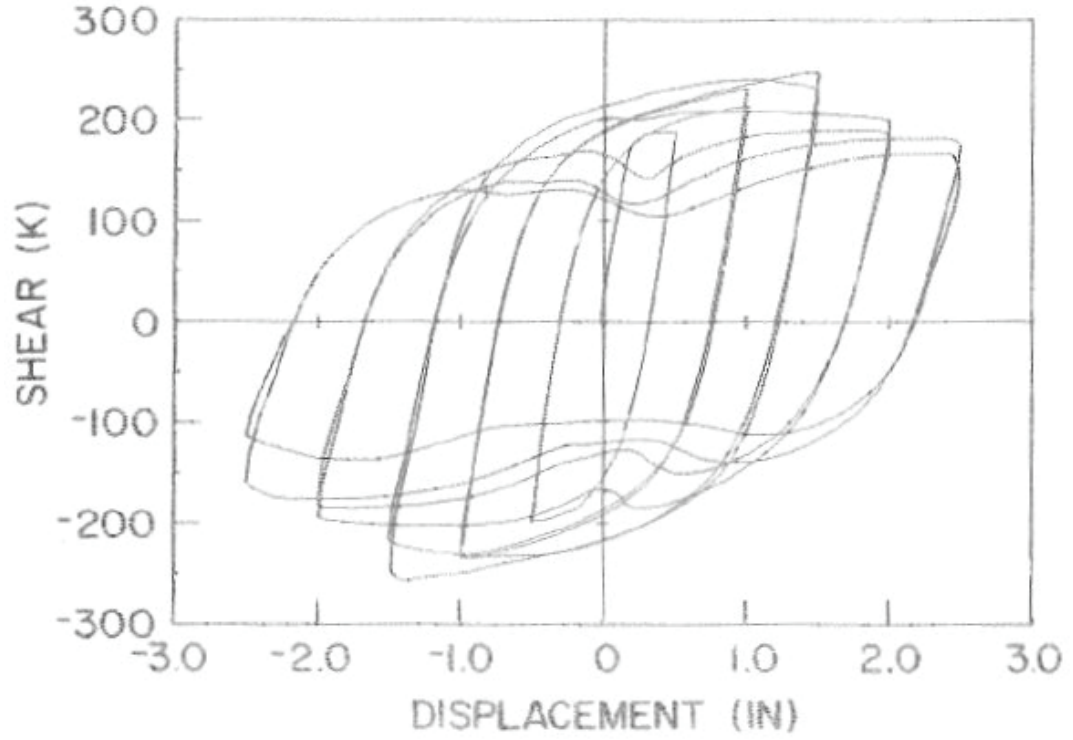

Figure C-8 Force-displacement relationship for link 8 tested by Hjelmstad and Popov (1983)

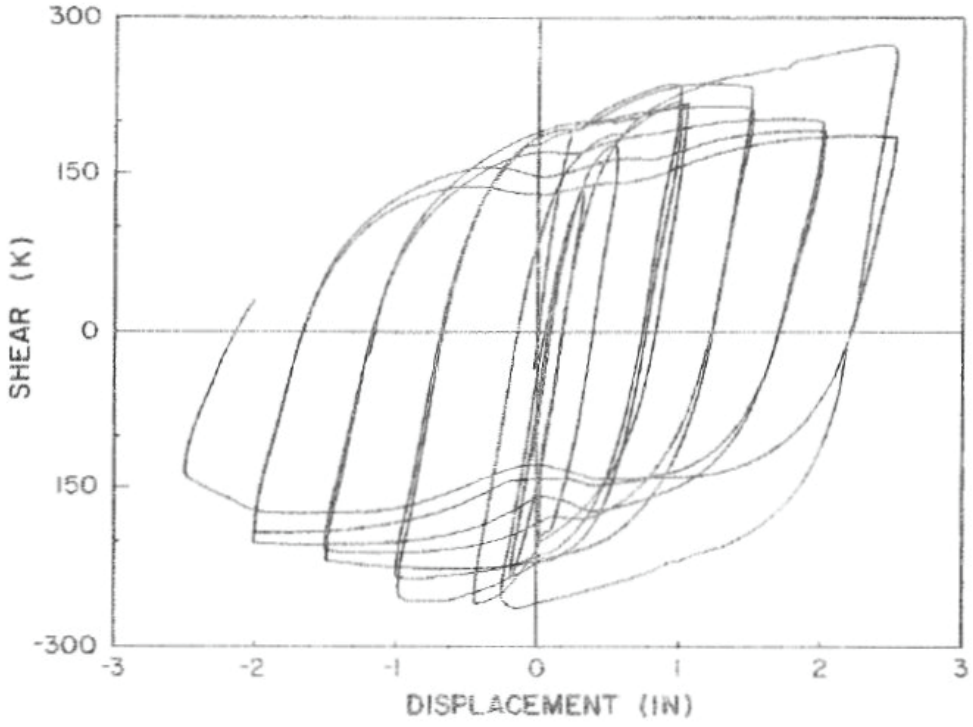

Figure C-9 Force-displacement relationship for link B16 tested by Malley and Popov (1983)

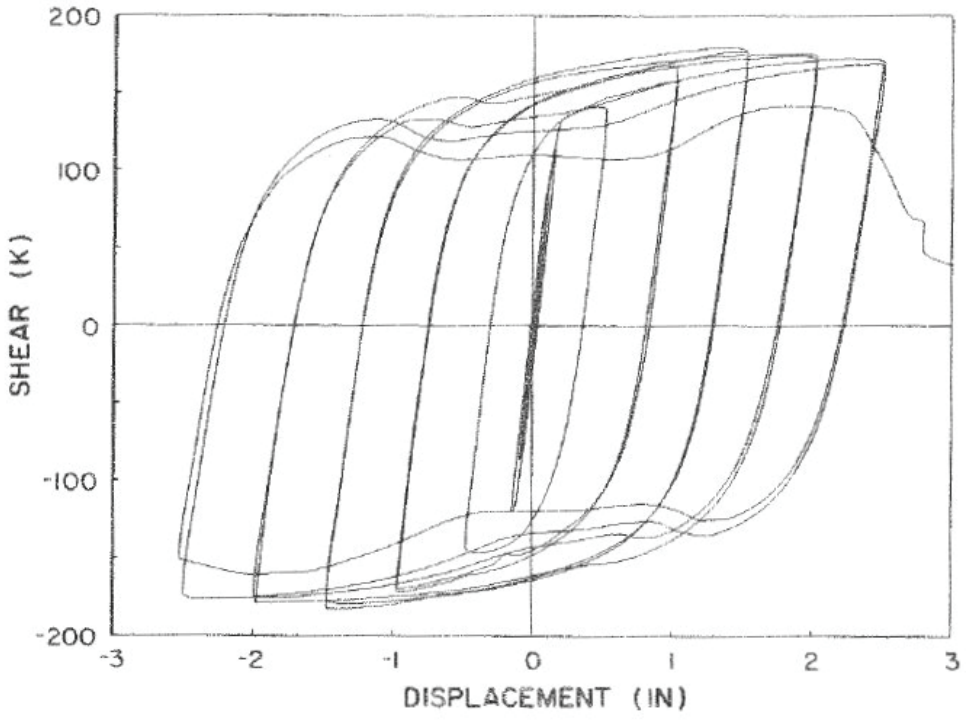

Figure C-10 Force-displacement relationship for link B17 tested by Malley and Popov (1983)

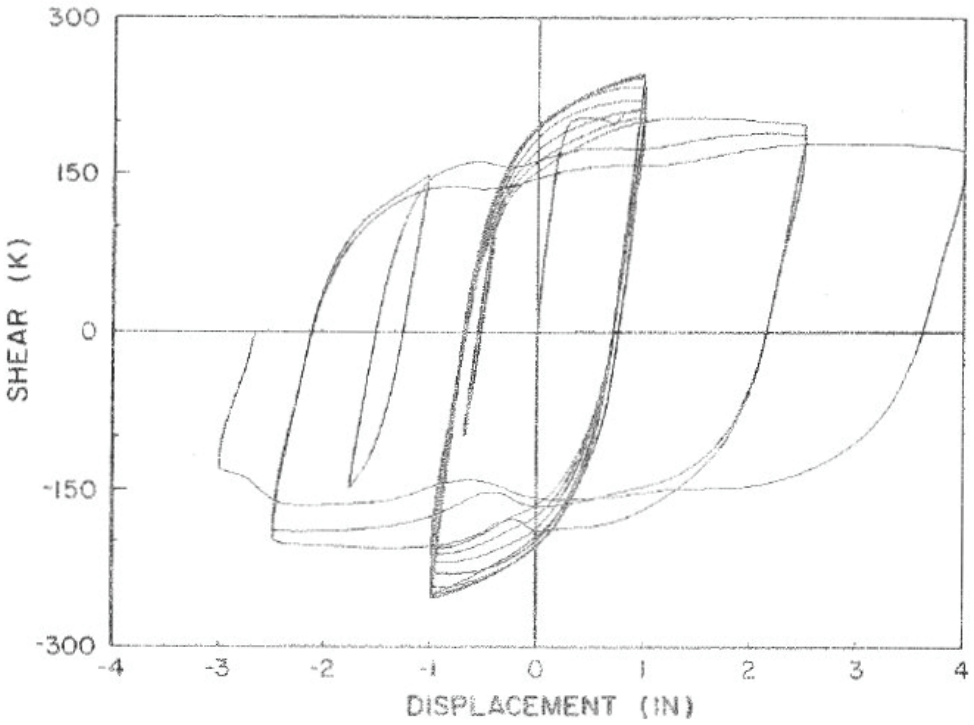

Figure C-11 Force-displacement relationship for link B18 tested by Malley and Popov (1983)

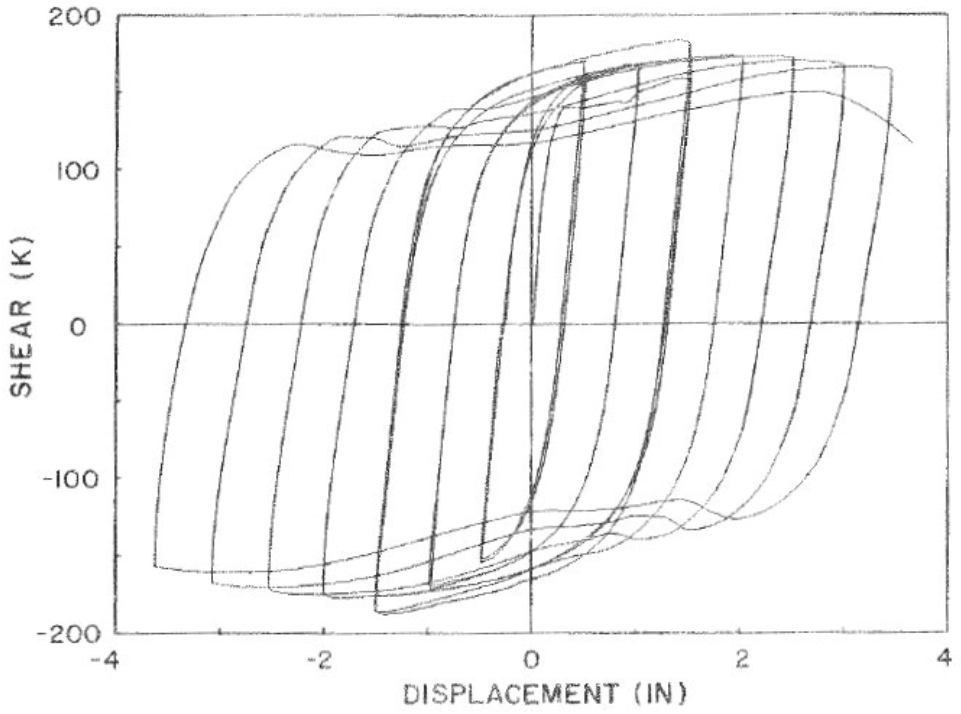

Figure C-12 Force-displacement relationship for link B20 tested by Malley and Popov (1983)

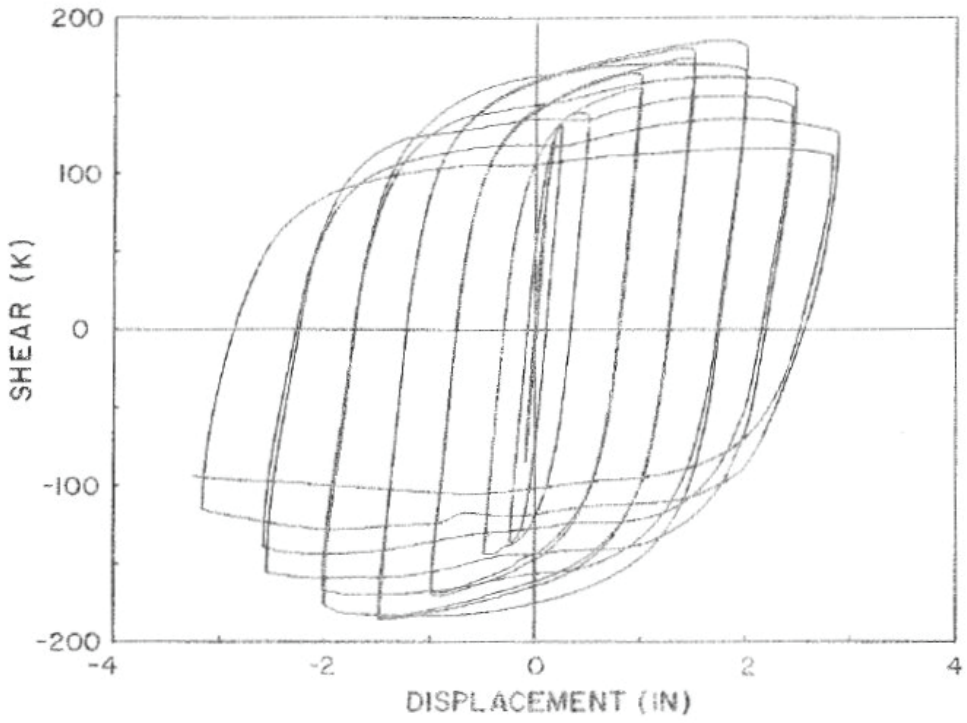

Figure C-13 Force-displacement relationship for link B21 tested by Malley and Popov (1983)

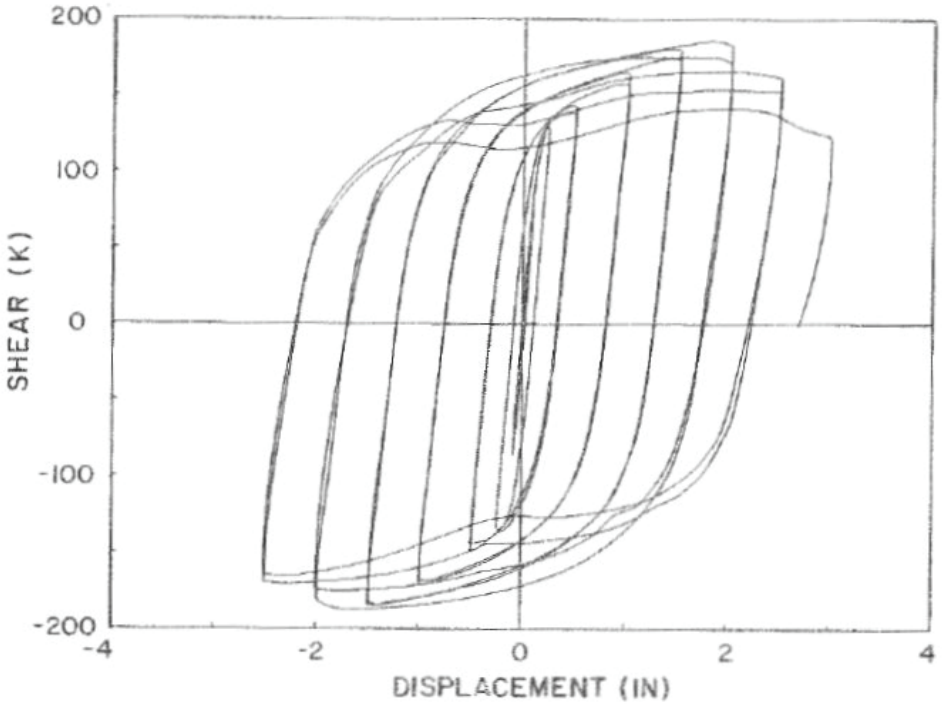

Figure C-14 Force-displacement relationship for link B22 tested by Malley and Popov (1983)

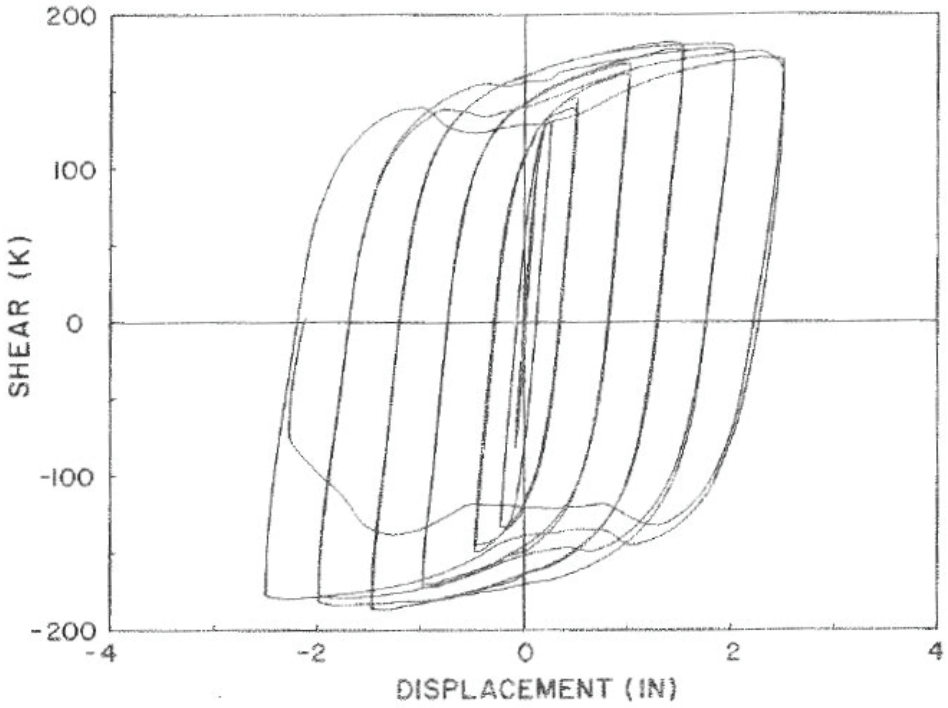

Figure C-15 Force-displacement relationship for link B23 tested by Malley and Popov (1983)

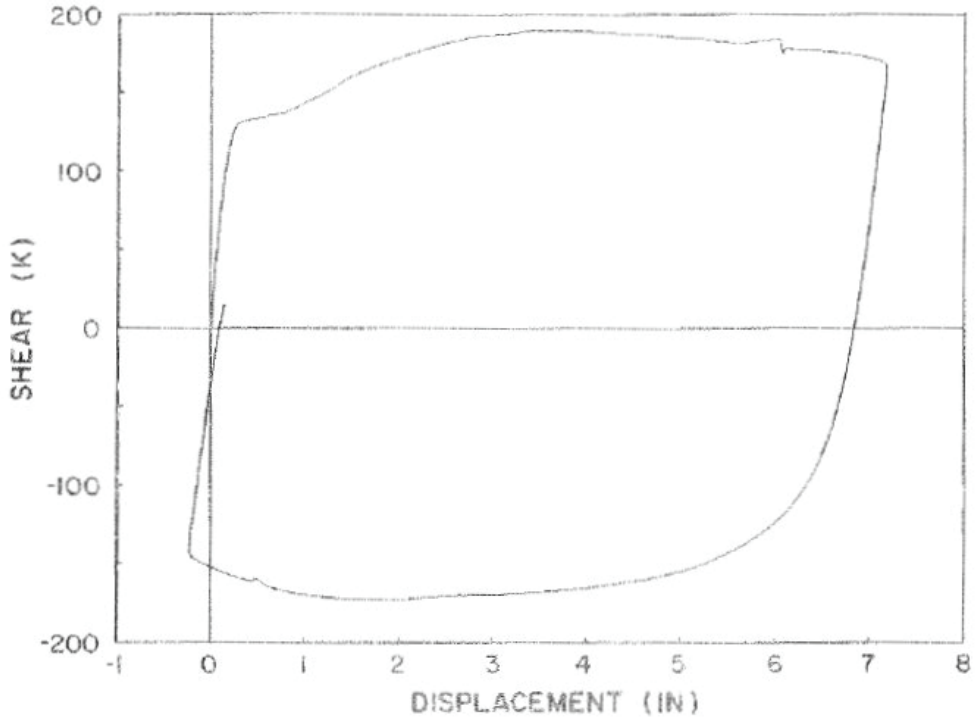

Figure C-16 Force-displacement relationship for link B24 tested by Malley and Popov (1983)

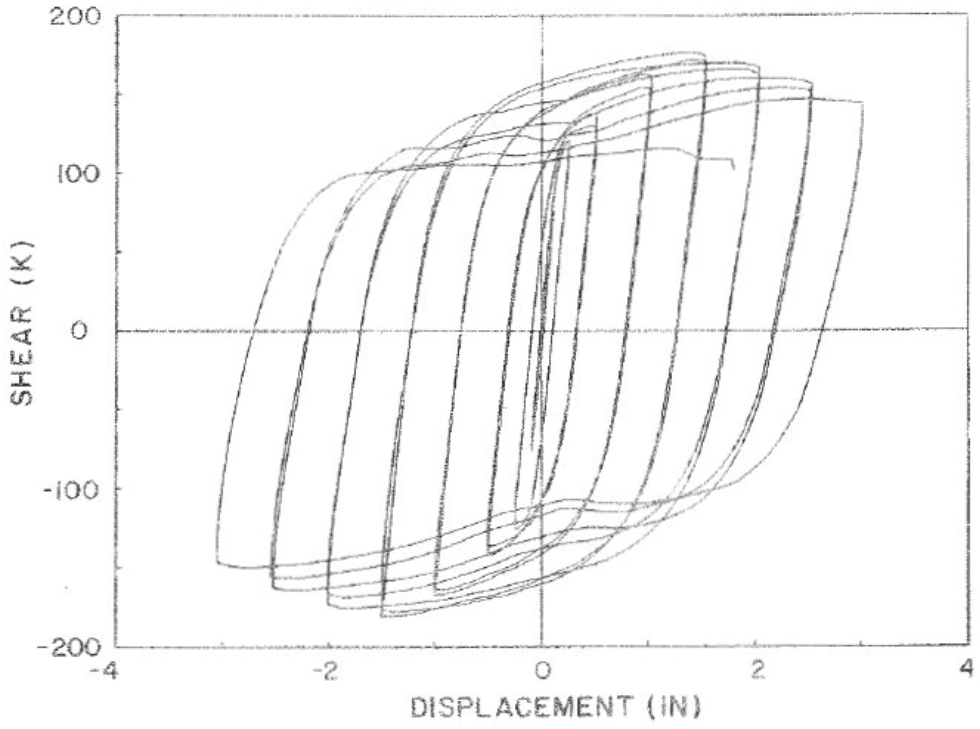

Figure C-17 Force-displacement relationship for link B25 tested by Malley and Popov (1983)

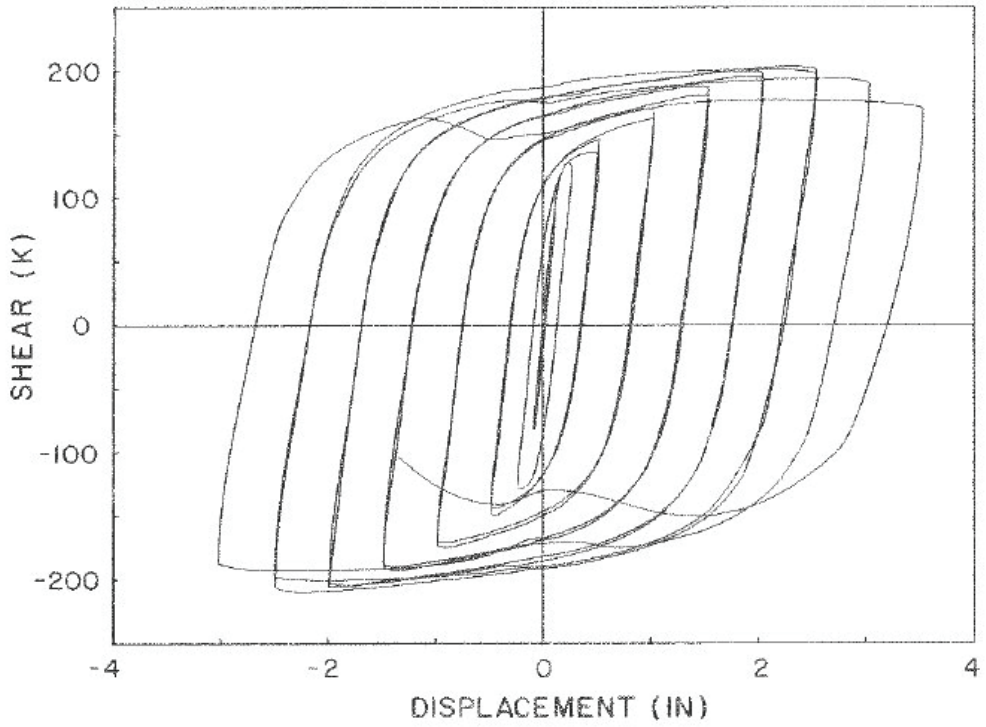

Figure C-18 Force-displacement relationship for link B26 tested by Malley and Popov (1983)

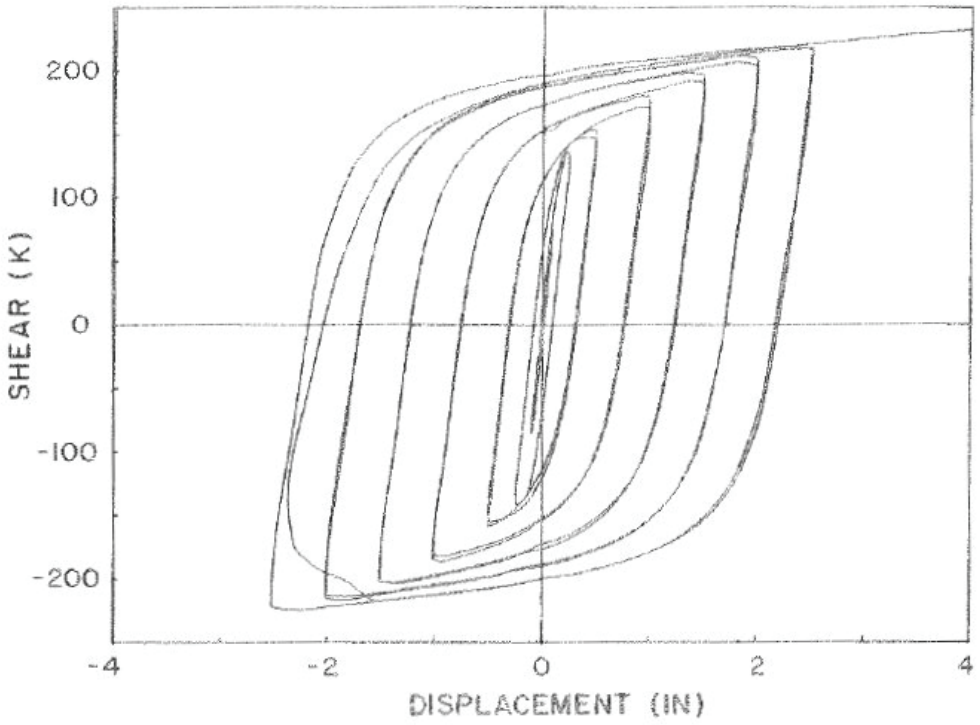

Figure C-19 Force-displacement relationship for link B27 tested by Malley and Popov (1983)

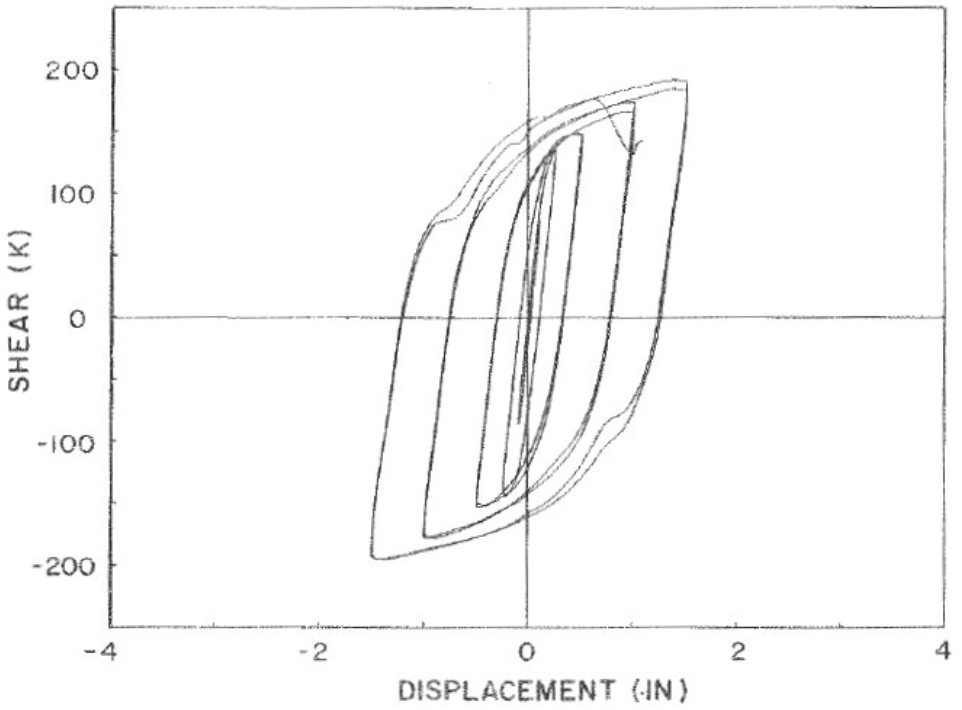

Figure C-20 Force-displacement relationship for link B28 tested by Malley and Popov (1983)

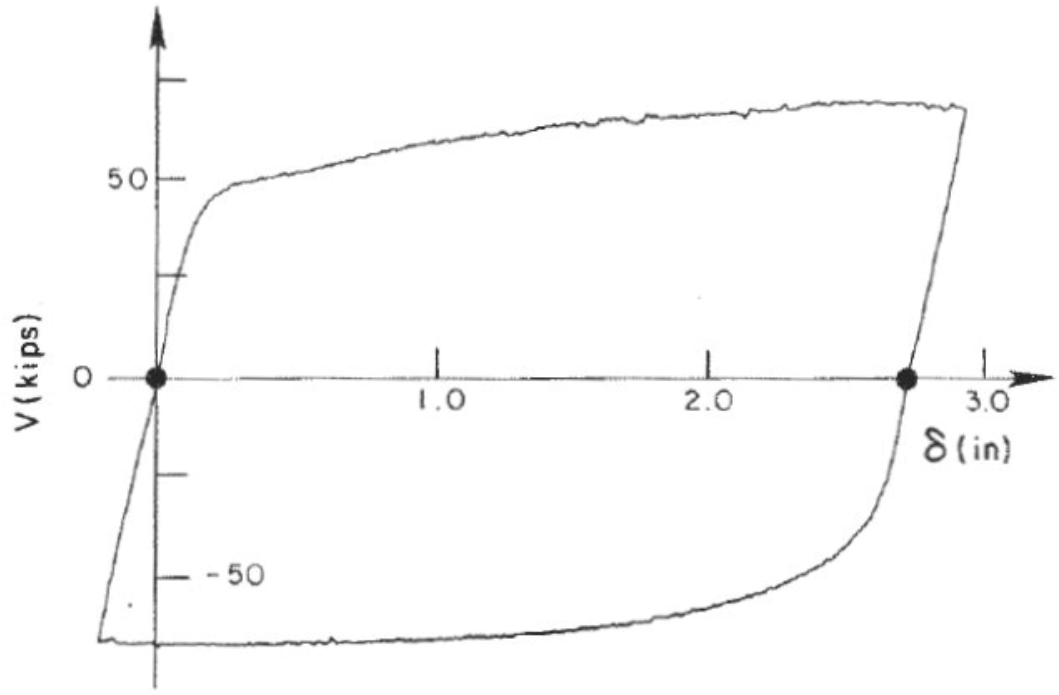

Figure C-21 Force-displacement relationship for link C1 tested by Kasai and Popov (1986)

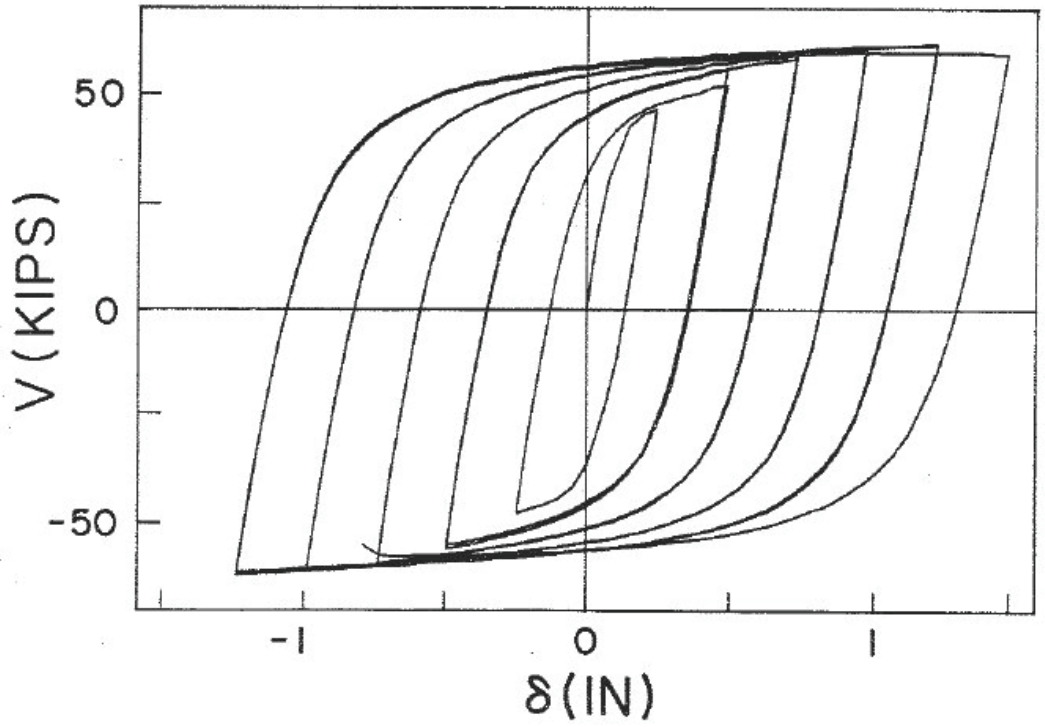

Figure C-22 Force-displacement relationship for link C3 tested by Kasai and Popov (1986)

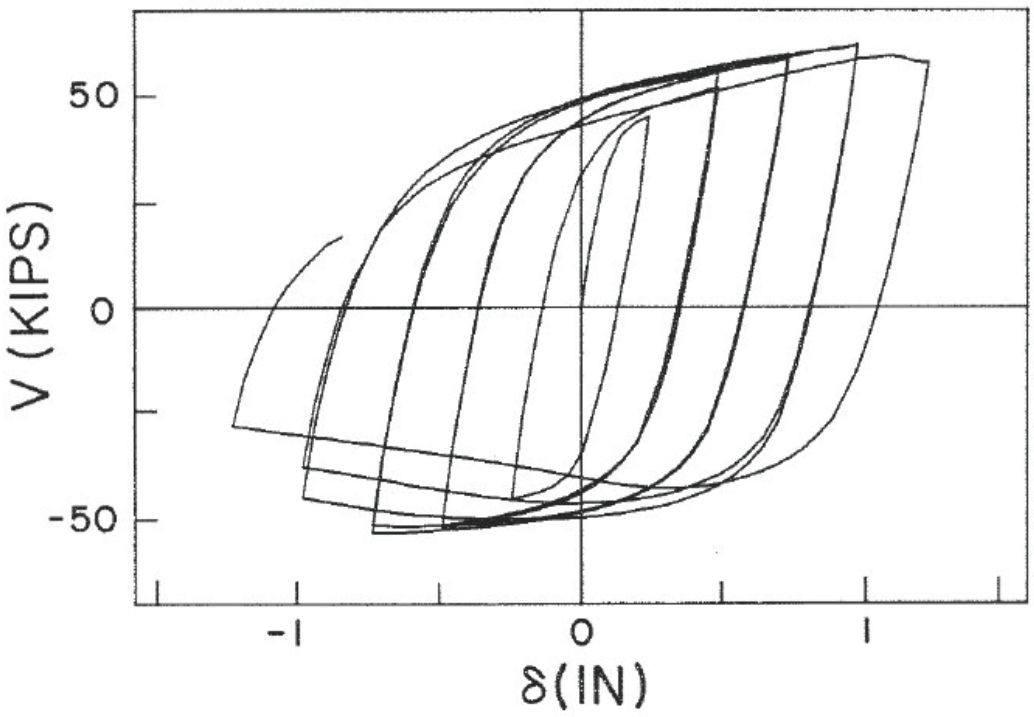

Figure C-23 Force-displacement relationship for link C4 tested by Kasai and Popov (1986)

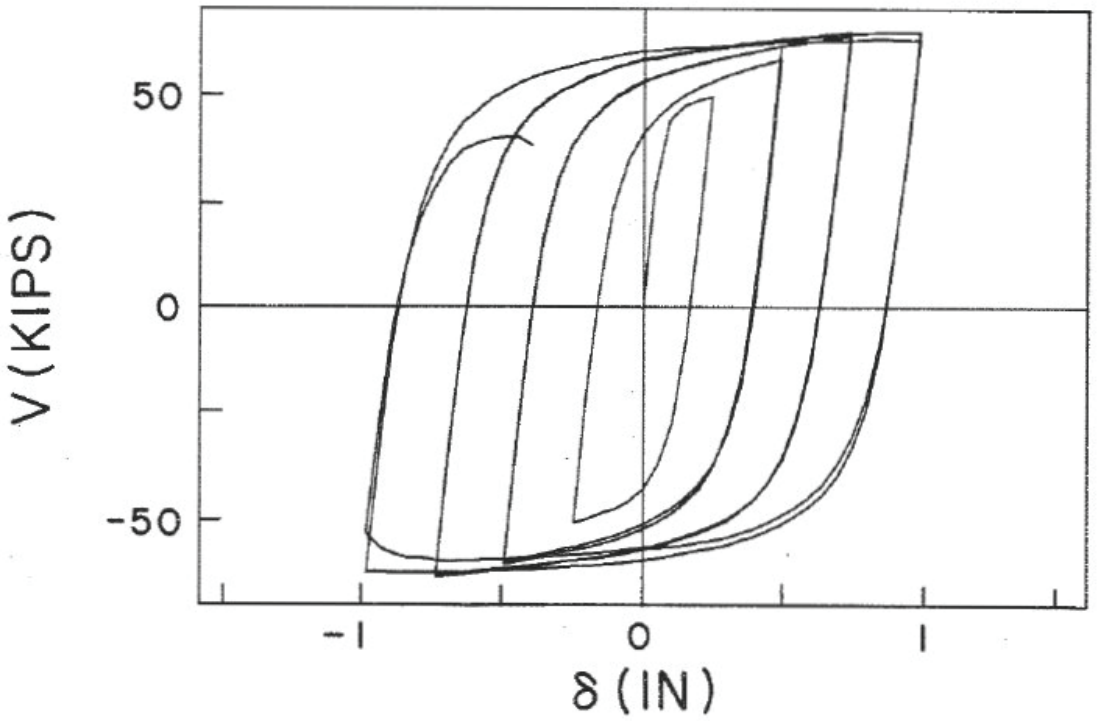

Figure C-24 Force-displacement relationship for link C7 tested by Kasai and Popov (1986)

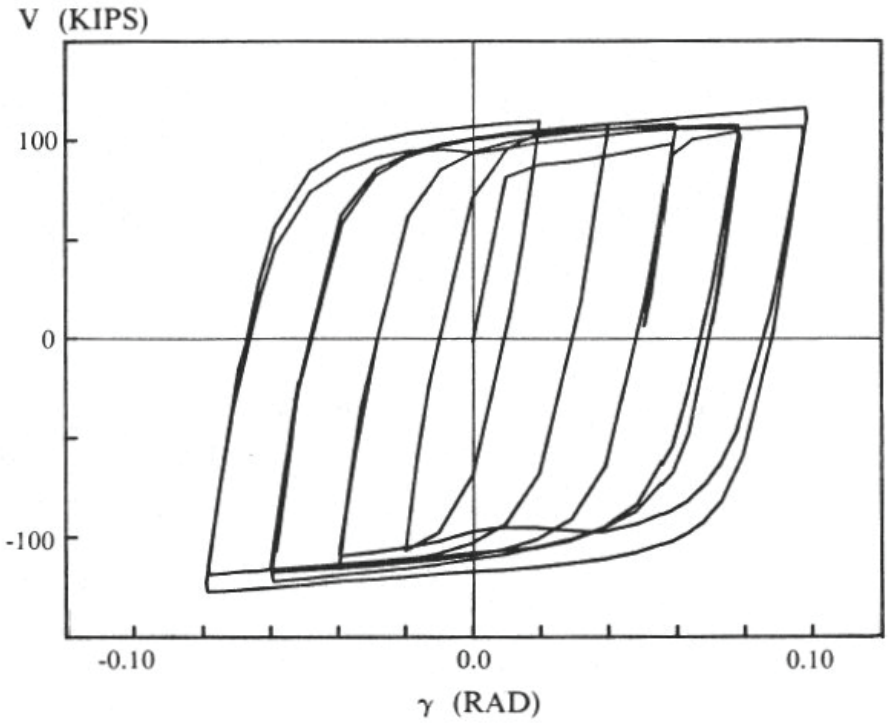

Figure C-25 Force-total rotation relationship for link A1 tested by Ricles and Popov (1987)

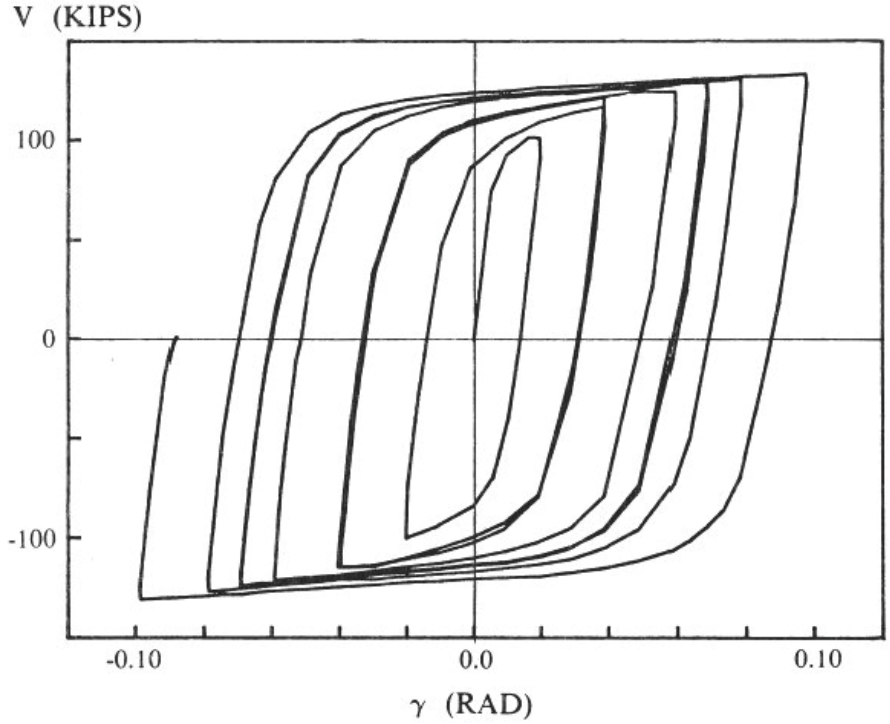

Figure C-26 Force-total rotation relationship for link A2 tested by Ricles and Popov (1987)

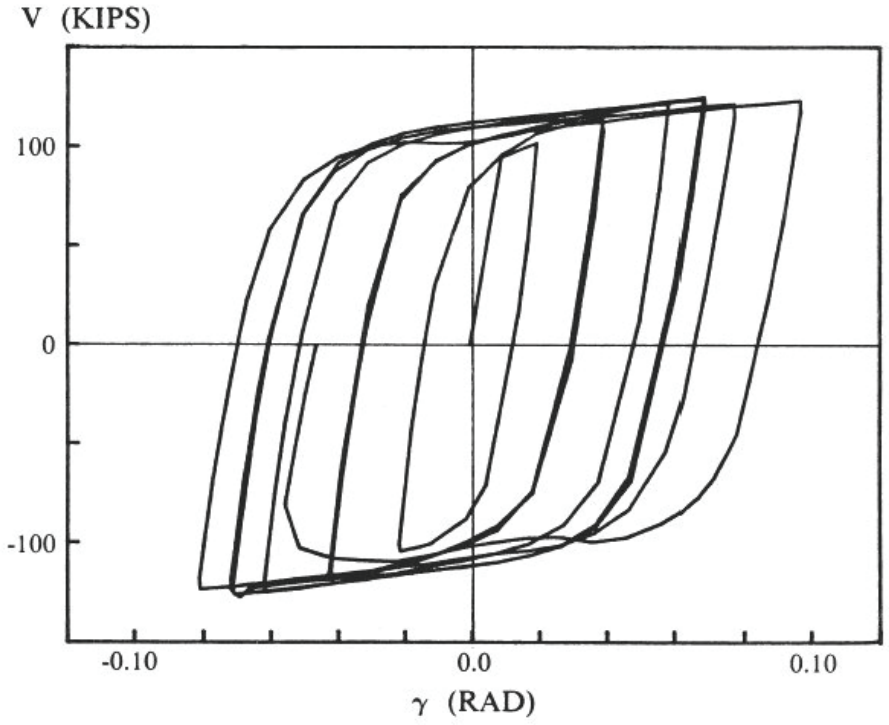

Figure C-27 Force-total rotation relationship for link B1 tested by Ricles and Popov (1987)

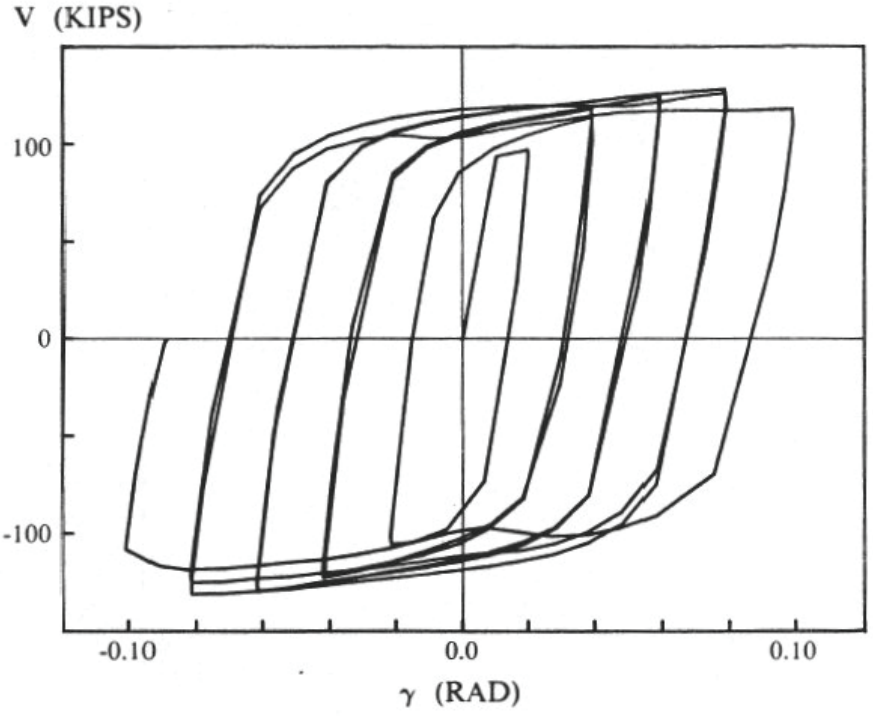

Figure C-28 Force-total rotation relationship for link B2 tested by Ricles and Popov (1987)

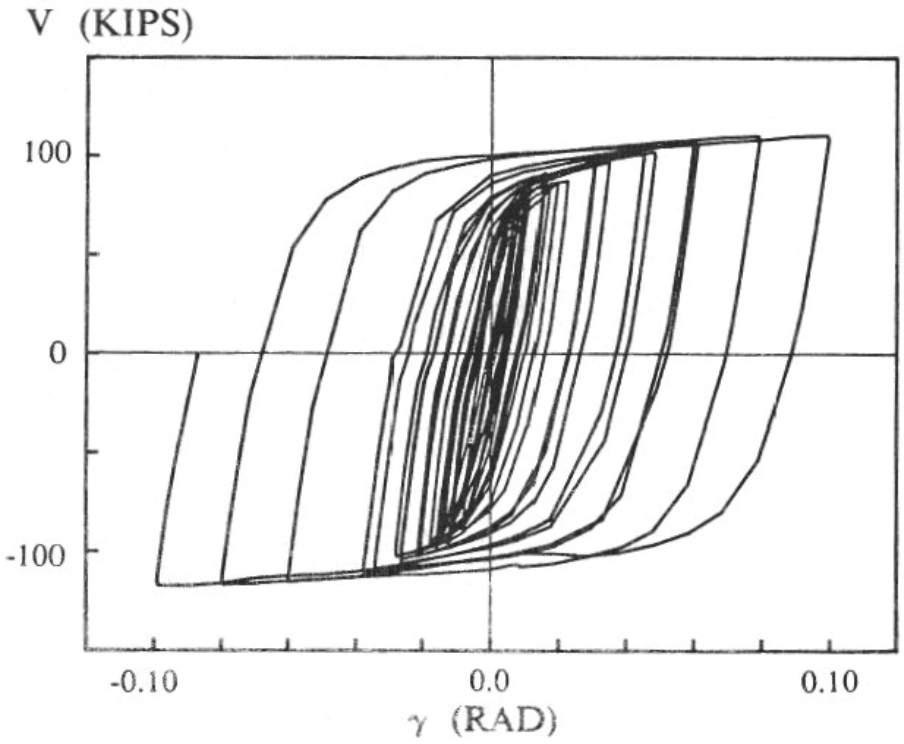

Figure C-29 Force-total rotation relationship for link C1 tested by Ricles and Popov (1987)

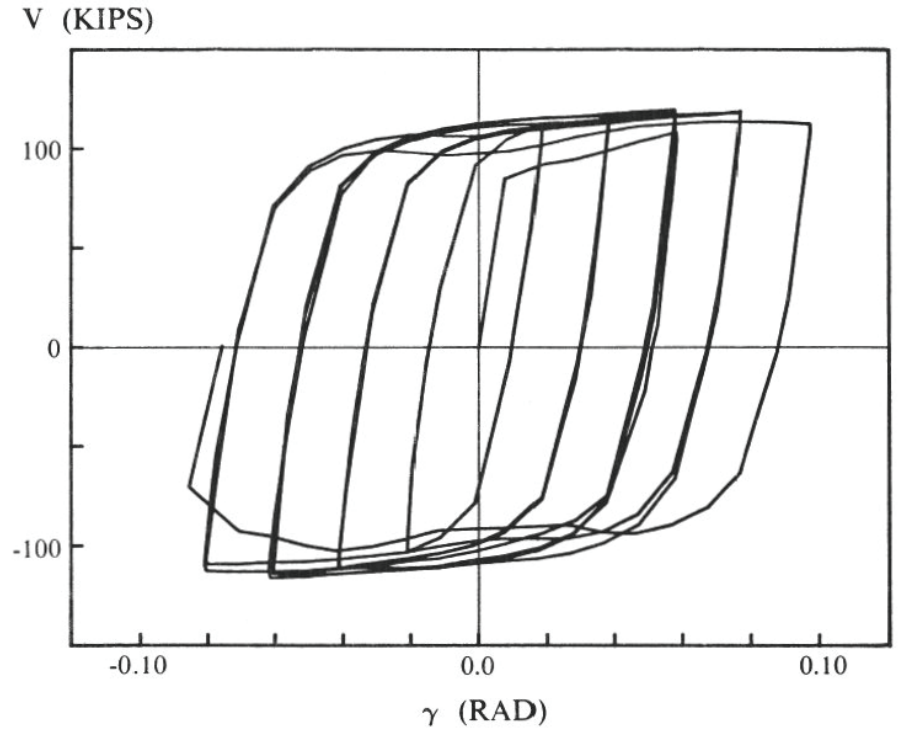

Figure C-30 Force-total rotation relationship for link C2 tested by Ricles and Popov (1987)

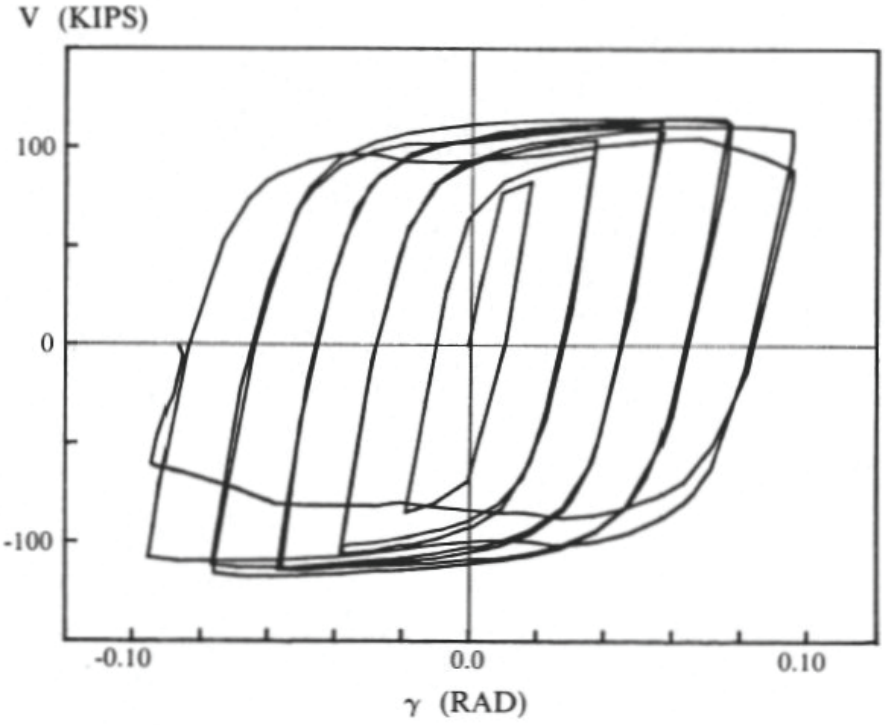

Figure C-31 Force-total rotation relationship for link D1 tested by Ricles and Popov (1987)

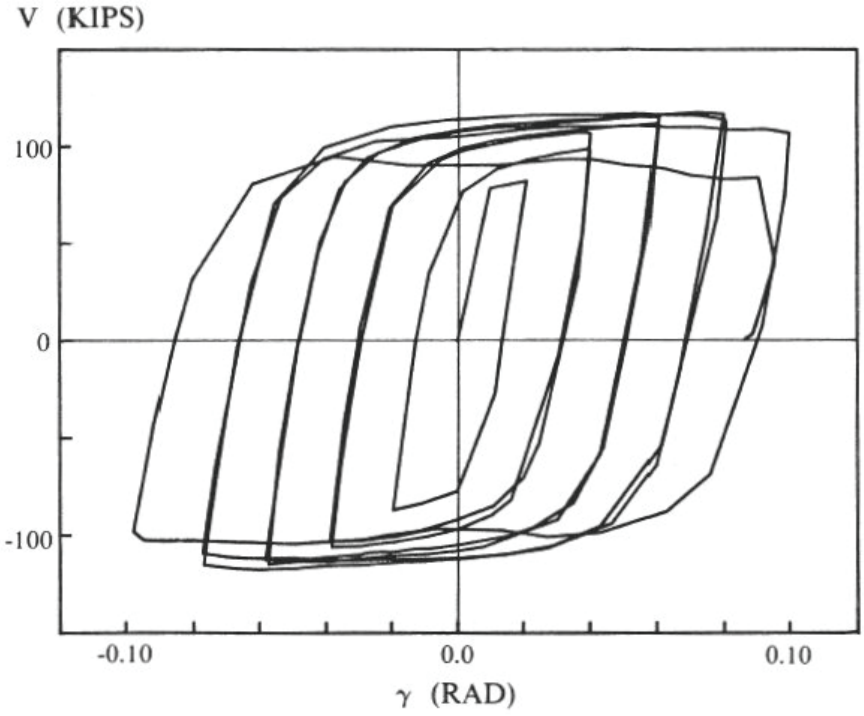

Figure C-32 Force-total rotation relationship for link D2 tested by Ricles and Popov (1987)

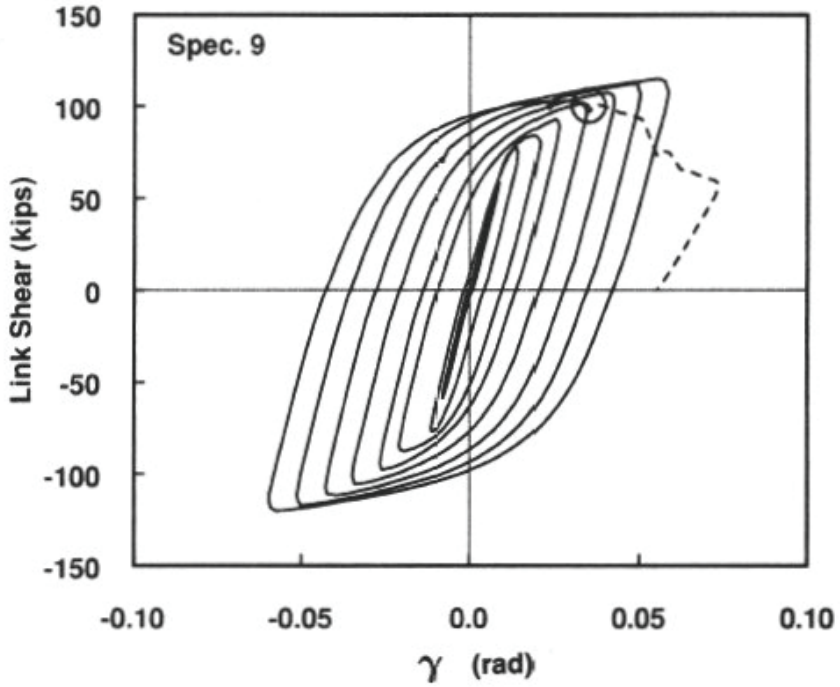

Figure C-33 Force-total rotation relationship for link 9 tested by Engelhardt and Popov (1989)

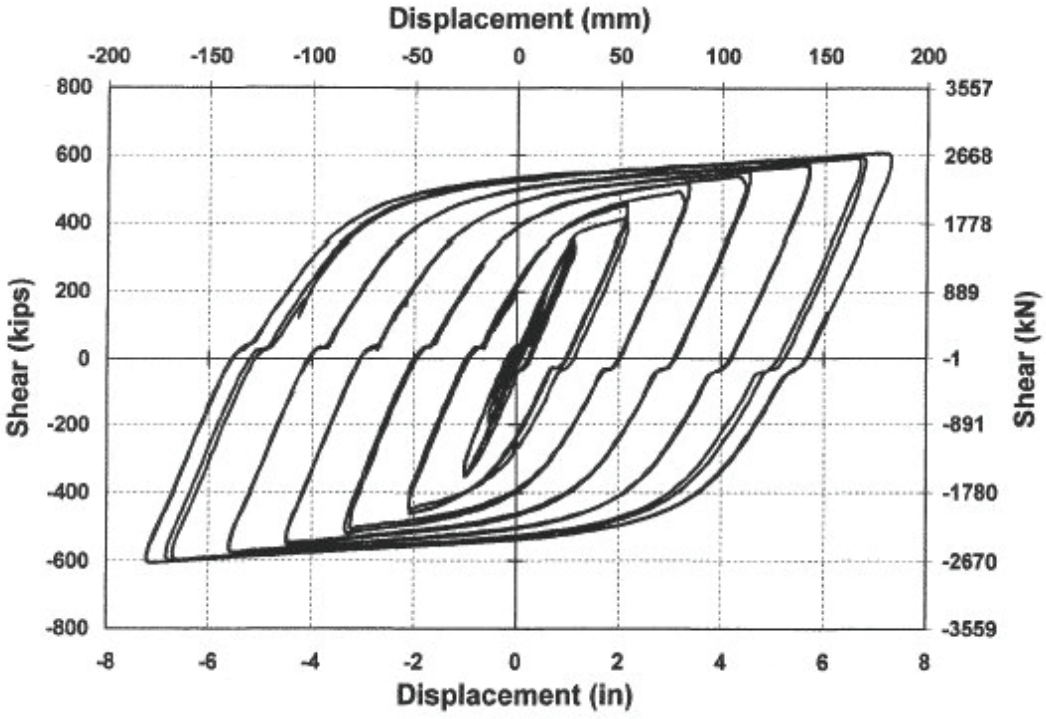

Figure C-34 Force-displacement relationship for link BU30 tested by Itani (1997)

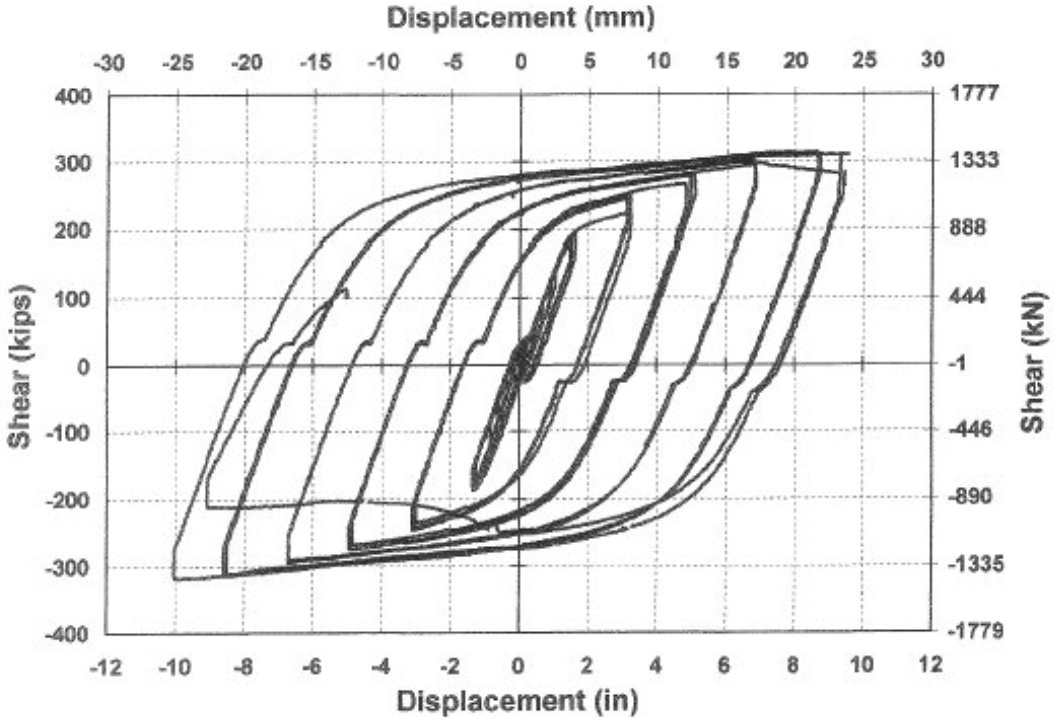

Figure C-35 Force-displacement relationship for link BU16 tested by Itani (1997)

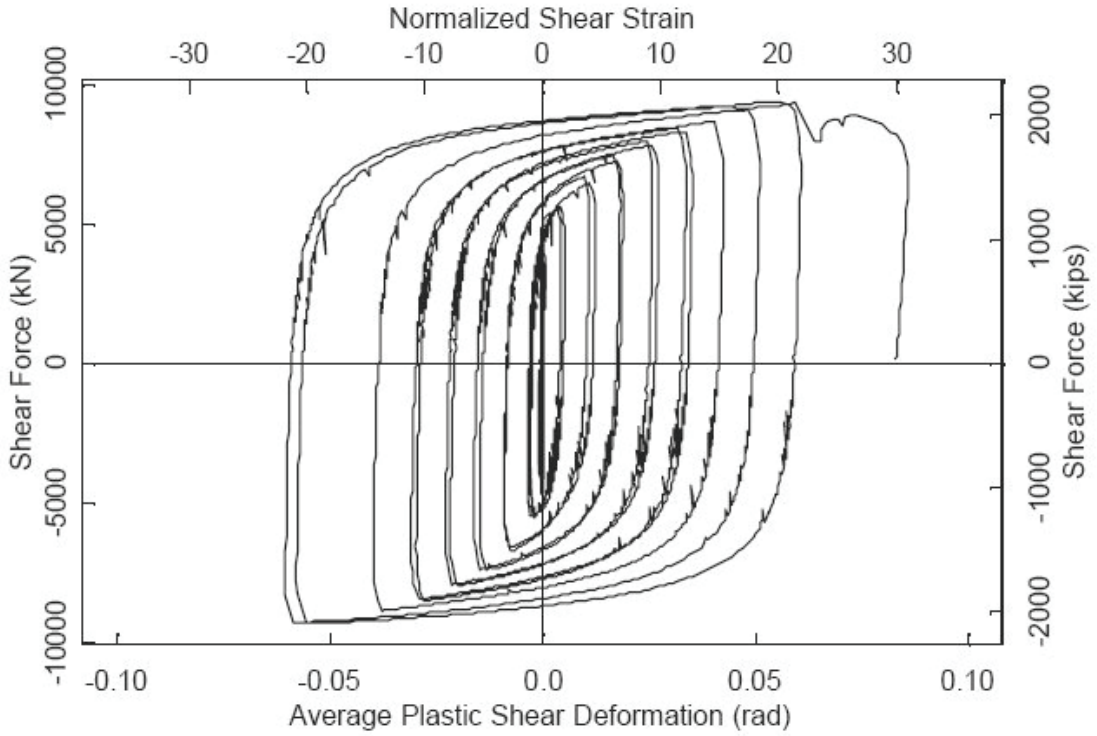

Figure C-36 Force-plastic rotation relationship for link Type1 tested by McDaniel et al. (2002)

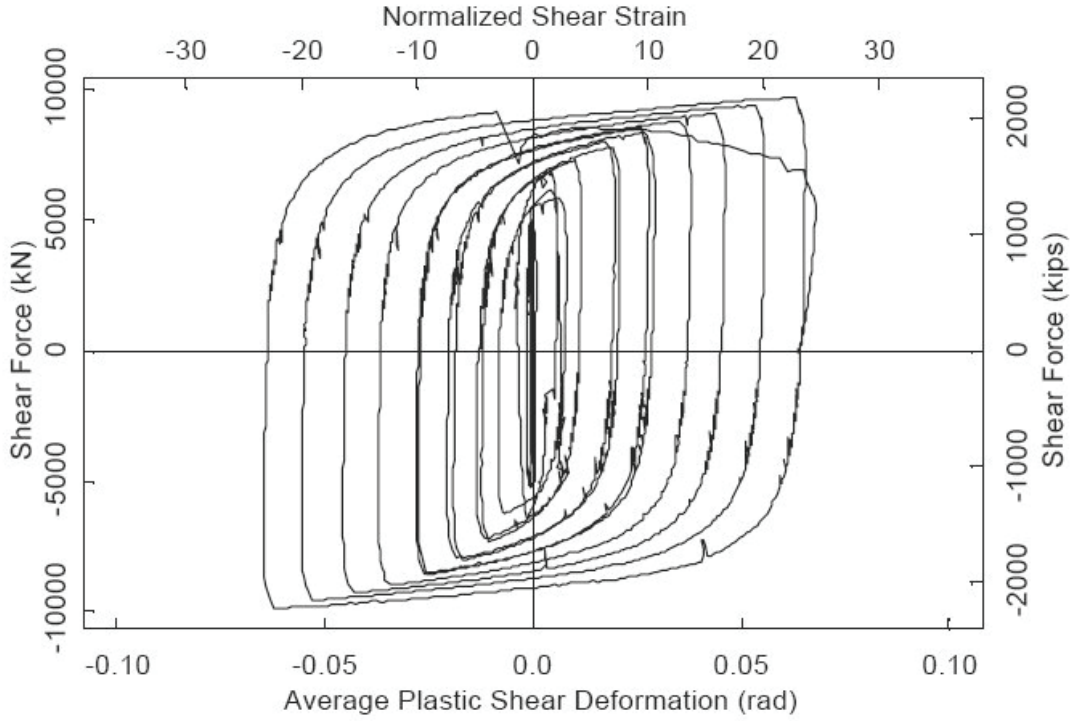

Figure C-37 Force-plastic rotation relationship for link Type3 tested by McDaniel et al. (2002)

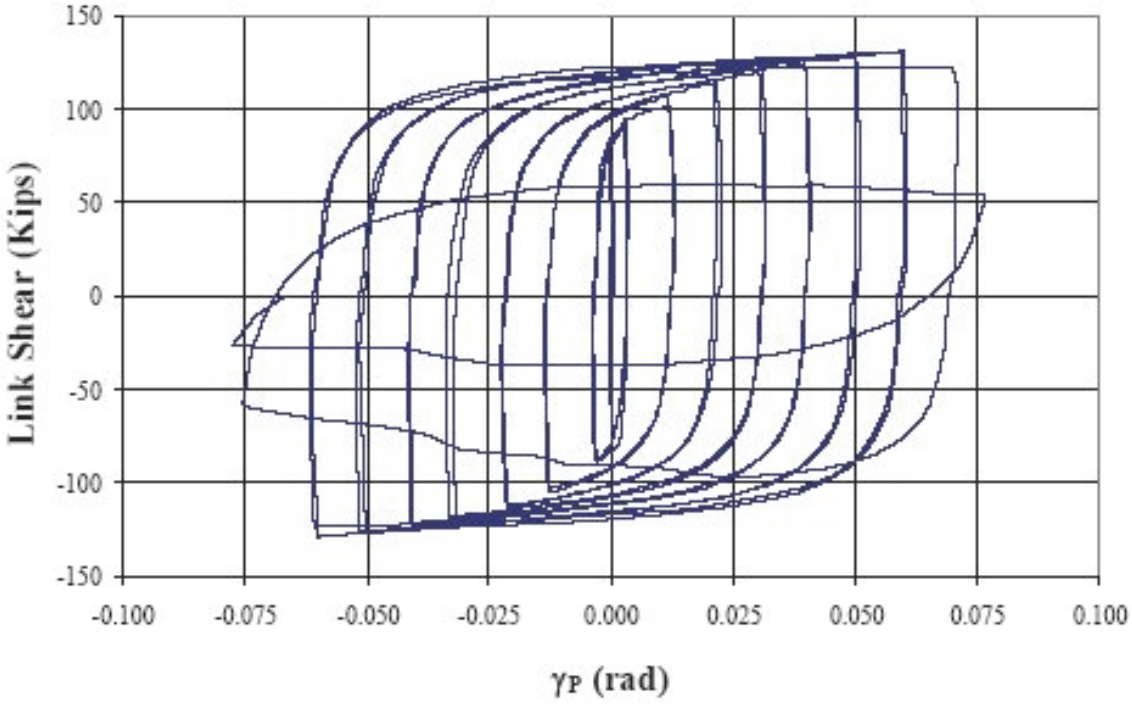

Figure C-38 Force-plastic rotation relationship for link 4A tested by Arce (2002)

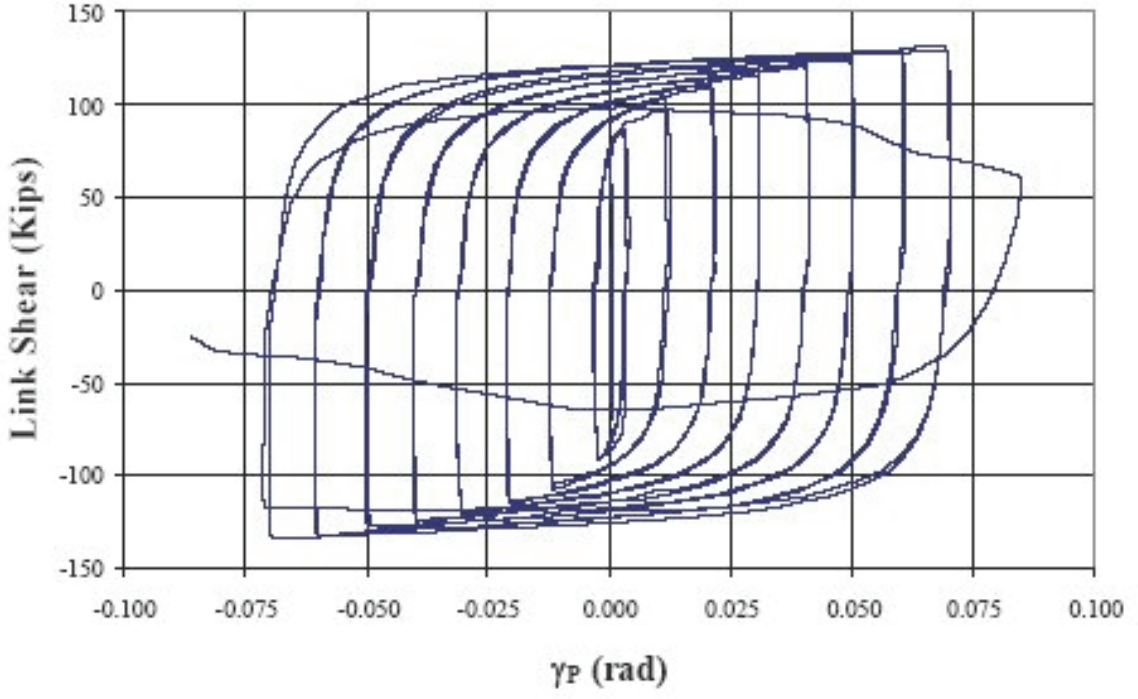

Figure C-39 Force-plastic rotation relationship for link 4B tested by Arce (2002)

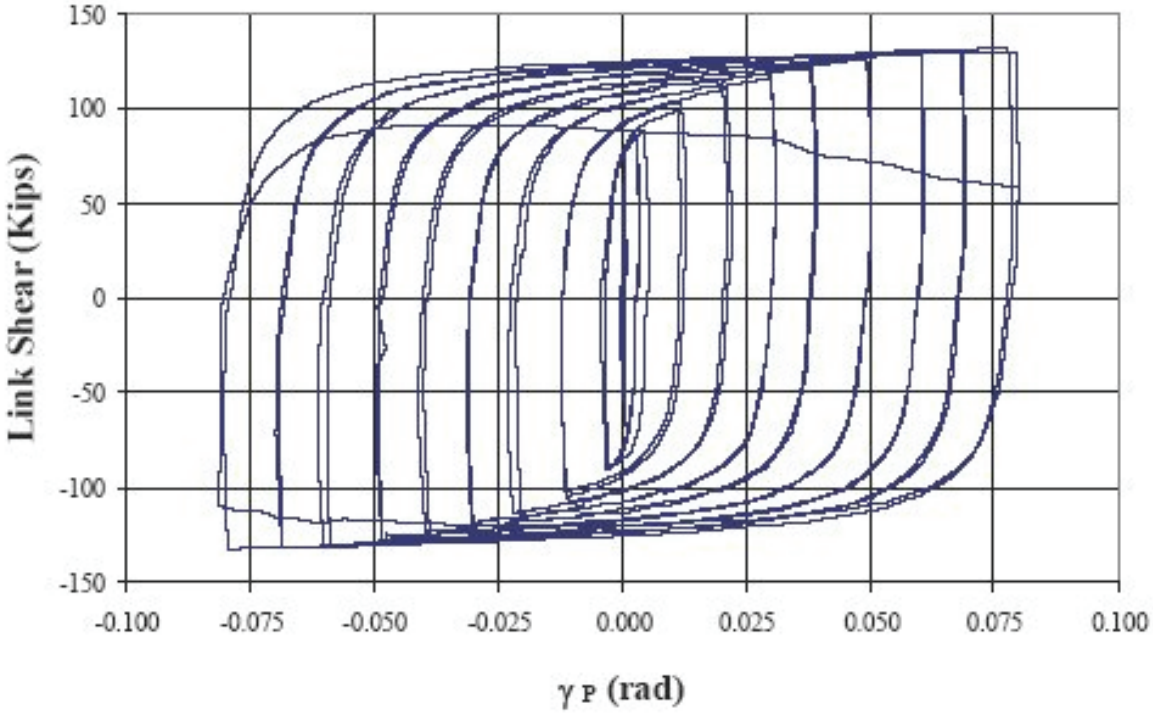

Figure C-40 Force-plastic rotation relationship for link 4C tested by Arce (2002)

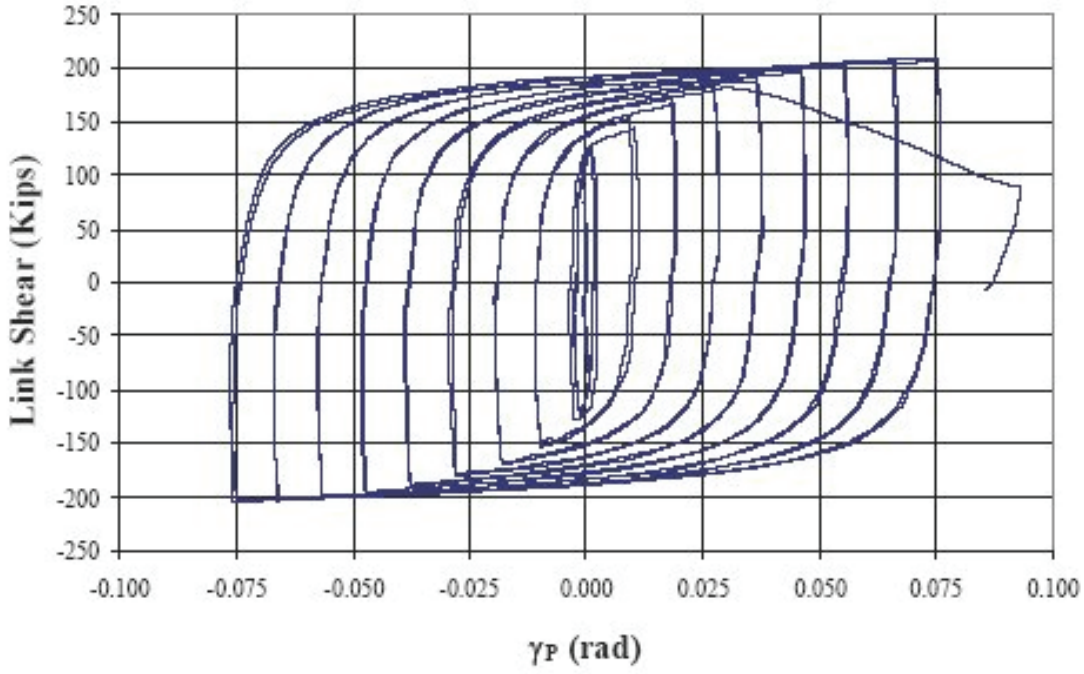

Figure C-41 Force-plastic rotation relationship for link 8 tested by Arce (2002)

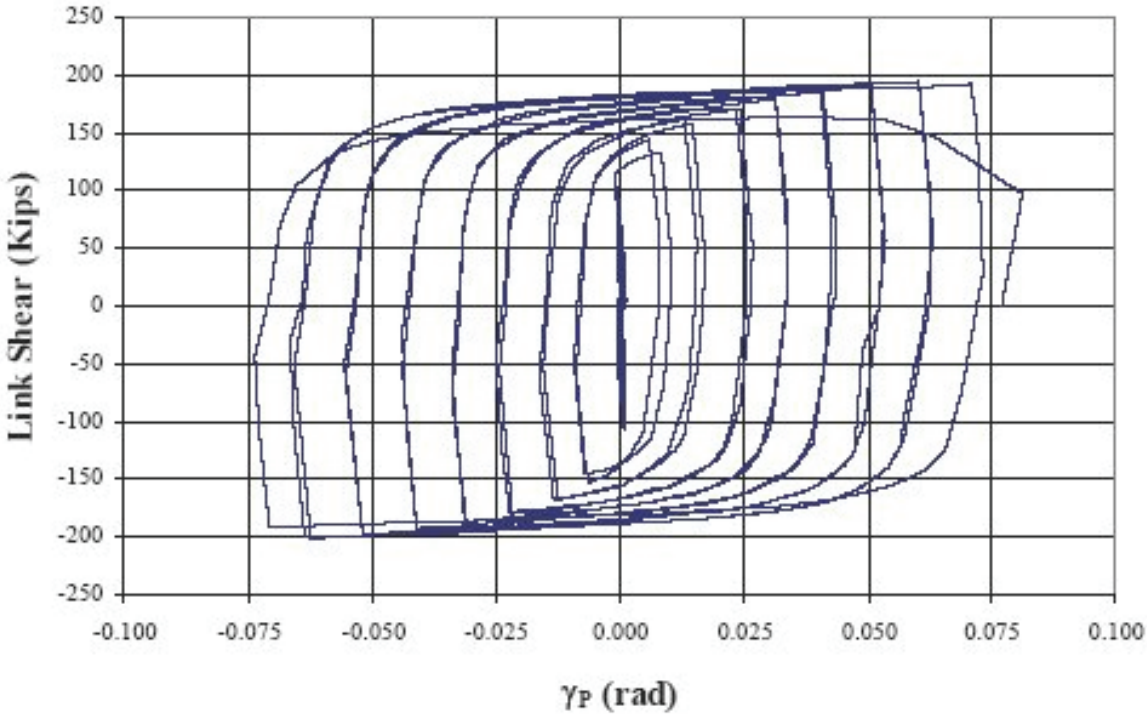

Figure C-42 Force-plastic rotation relationship for link 4A tested by Arce (2002)

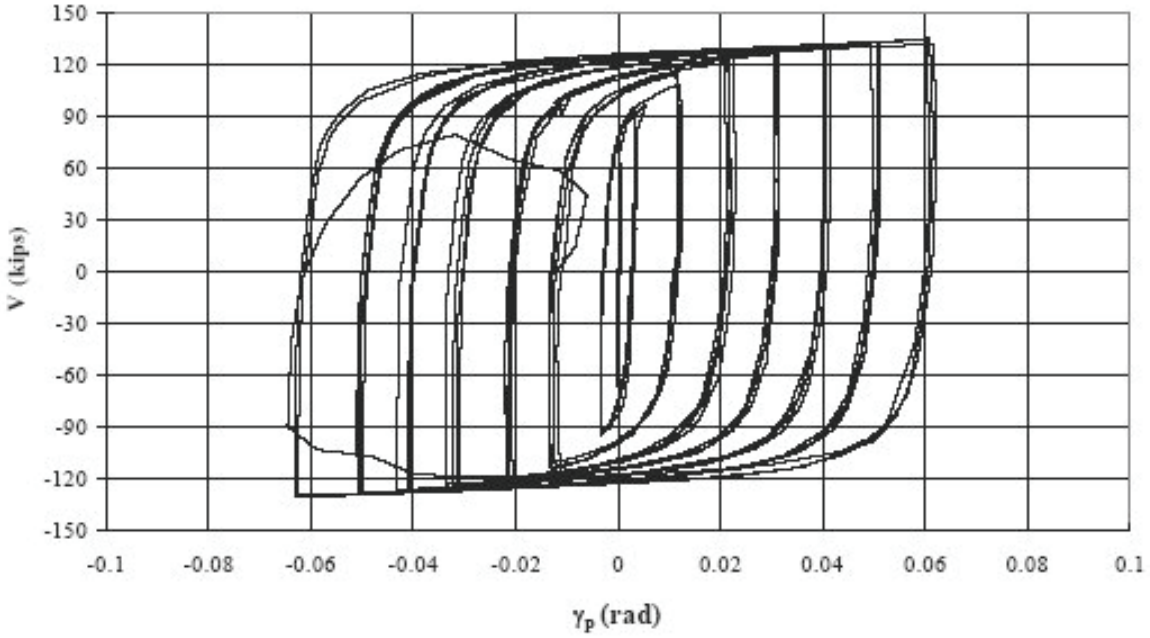

Figure C-43 Force-plastic rotation relationship for link 1 tested by Galvez (2004)

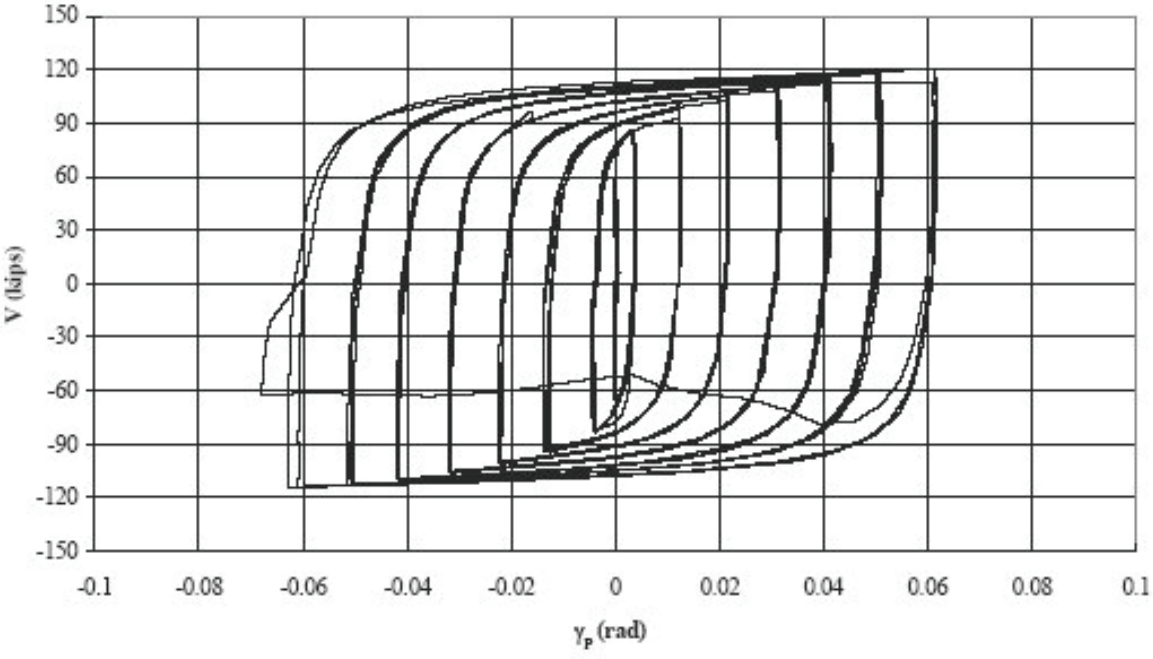

Figure C-44 Force-plastic rotation relationship for link 2 tested by Galvez (2004)

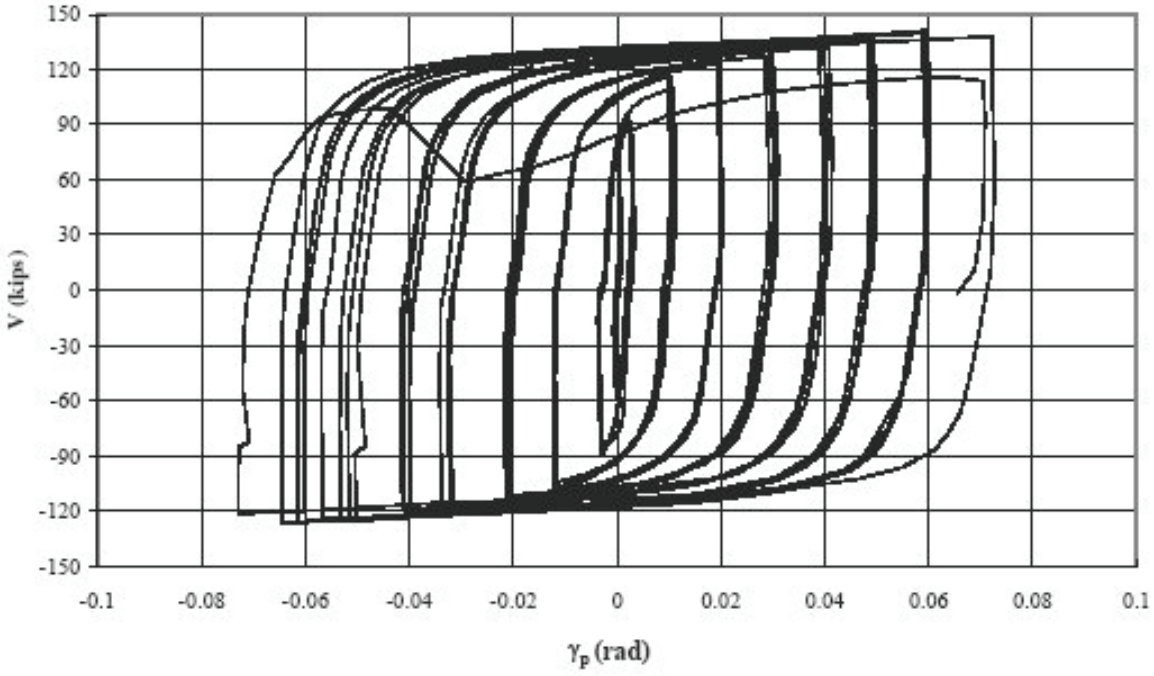

Figure C-45 Force-plastic rotation relationship for link 3 tested by Galvez (2004)

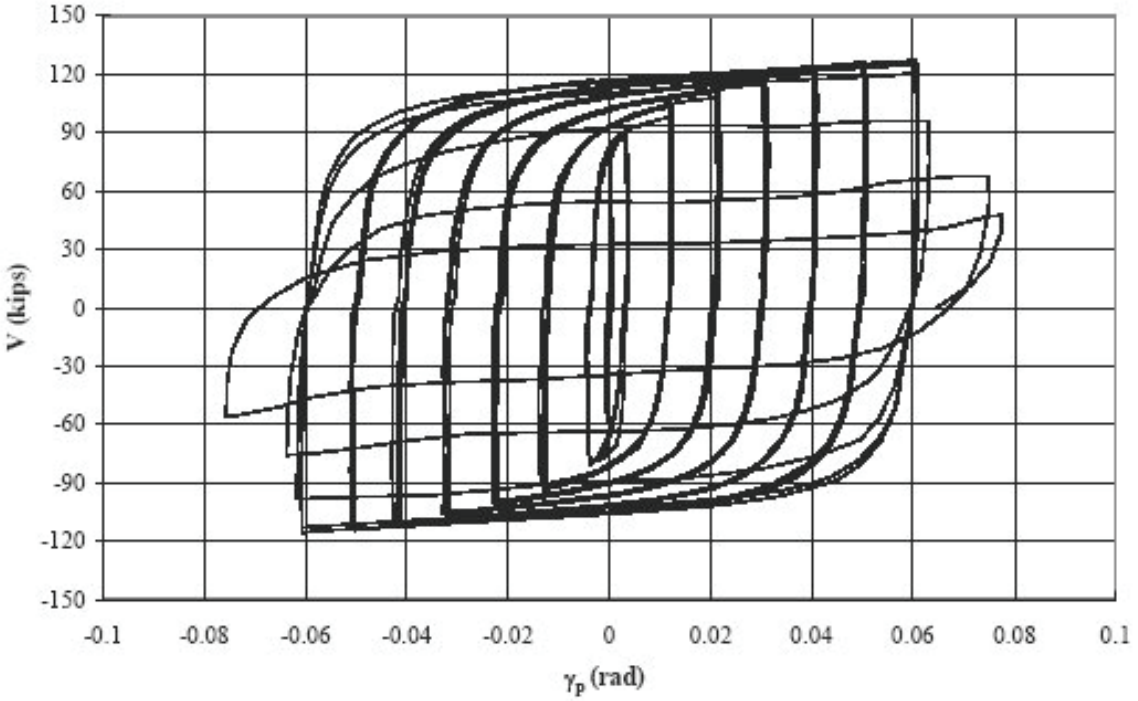

Figure C-46 Force-plastic rotation relationship for link 4 tested by Galvez (2004)

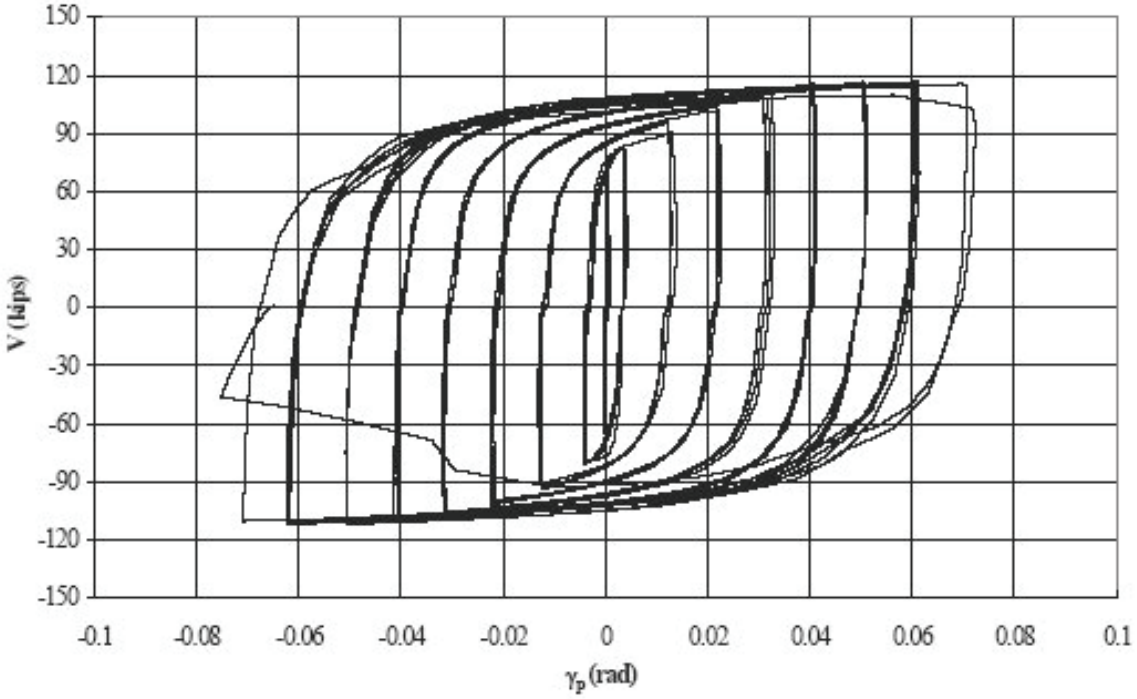

Figure C-47 Force-plastic rotation relationship for link 5 tested by Galvez (2004)

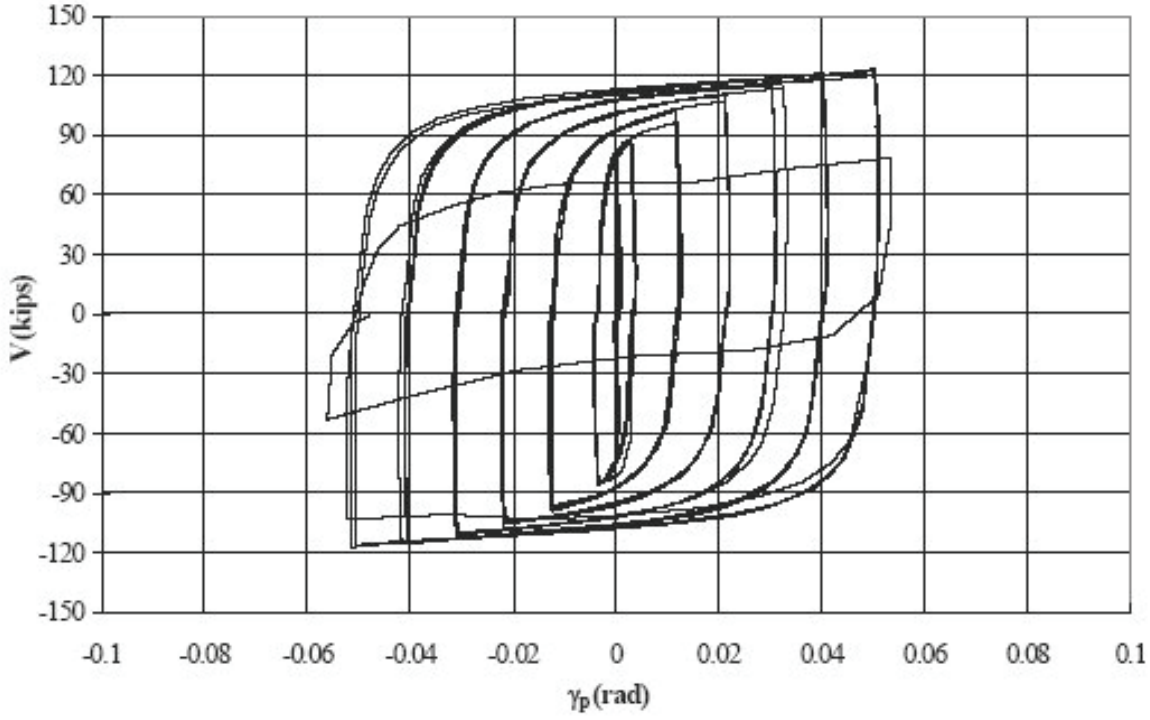

Figure C-48 Force-plastic rotation relationship for link 6 tested by Galvez (2004)

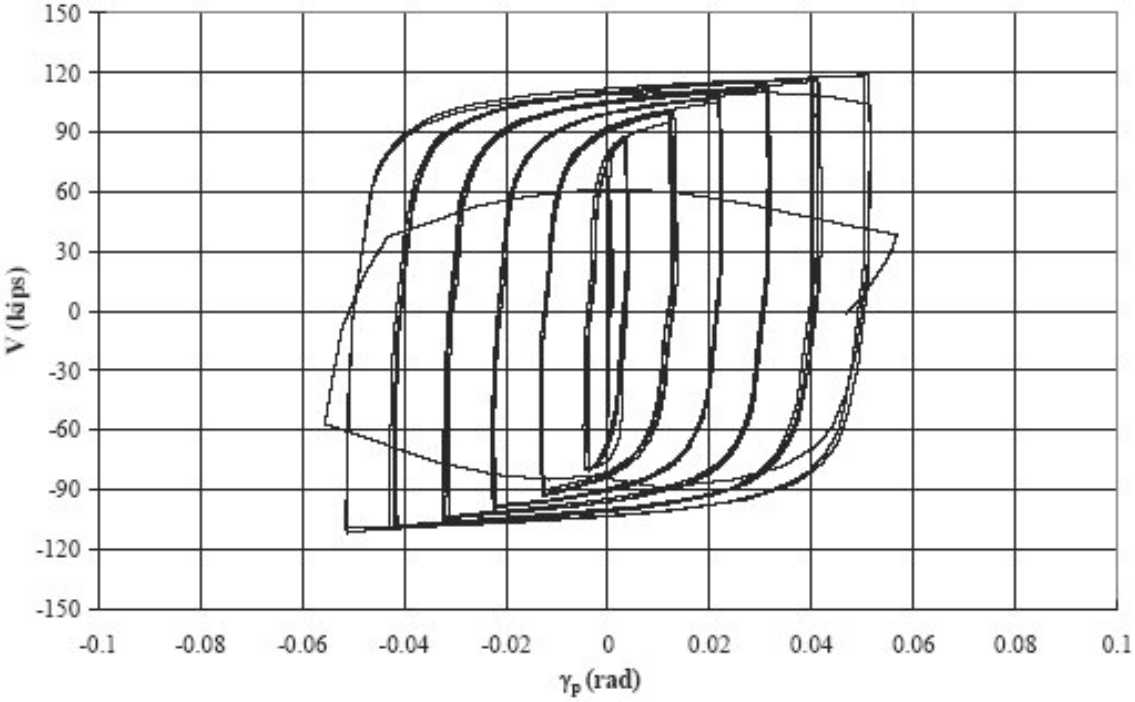

Figure C-49 Force-plastic rotation relationship for link 7 tested by Galvez (2004)

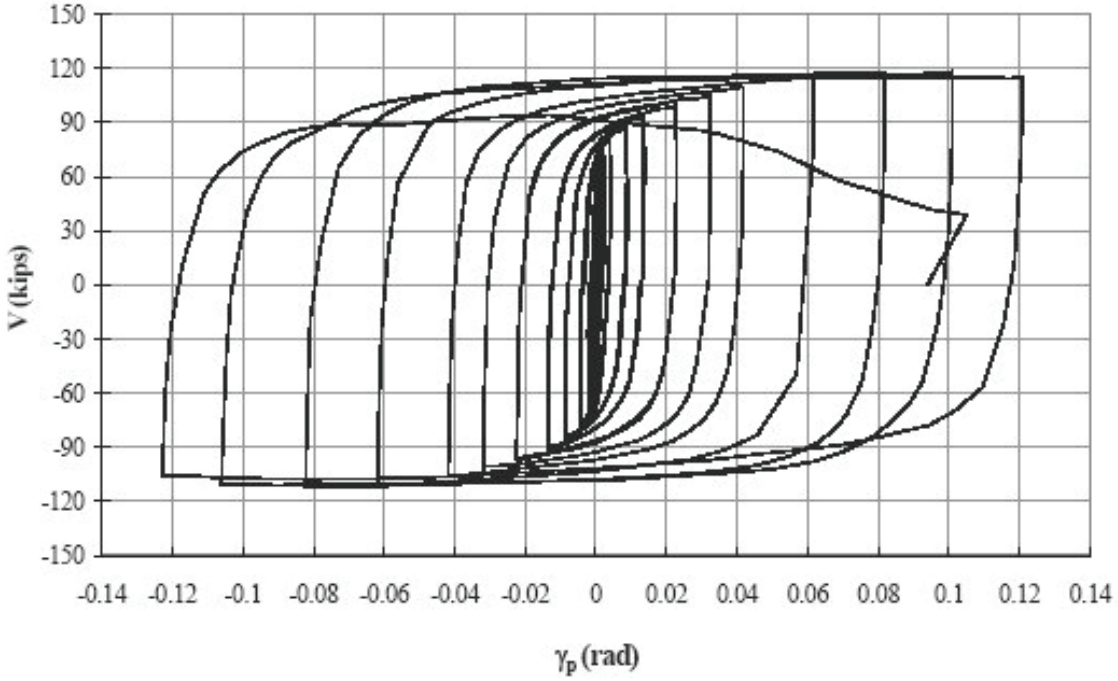

Figure C-50 Force-plastic rotation relationship for link 8 tested by Galvez (2004)

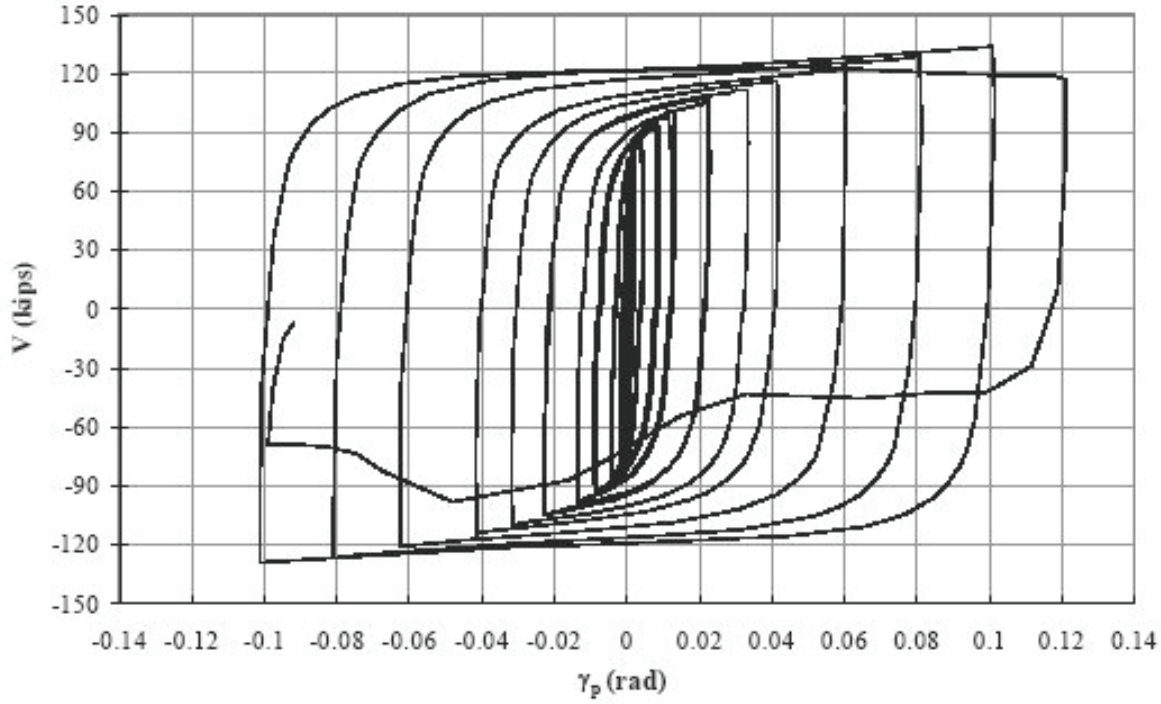

Figure C-51 Force-plastic rotation relationship for link 9 tested by Galvez (2004)

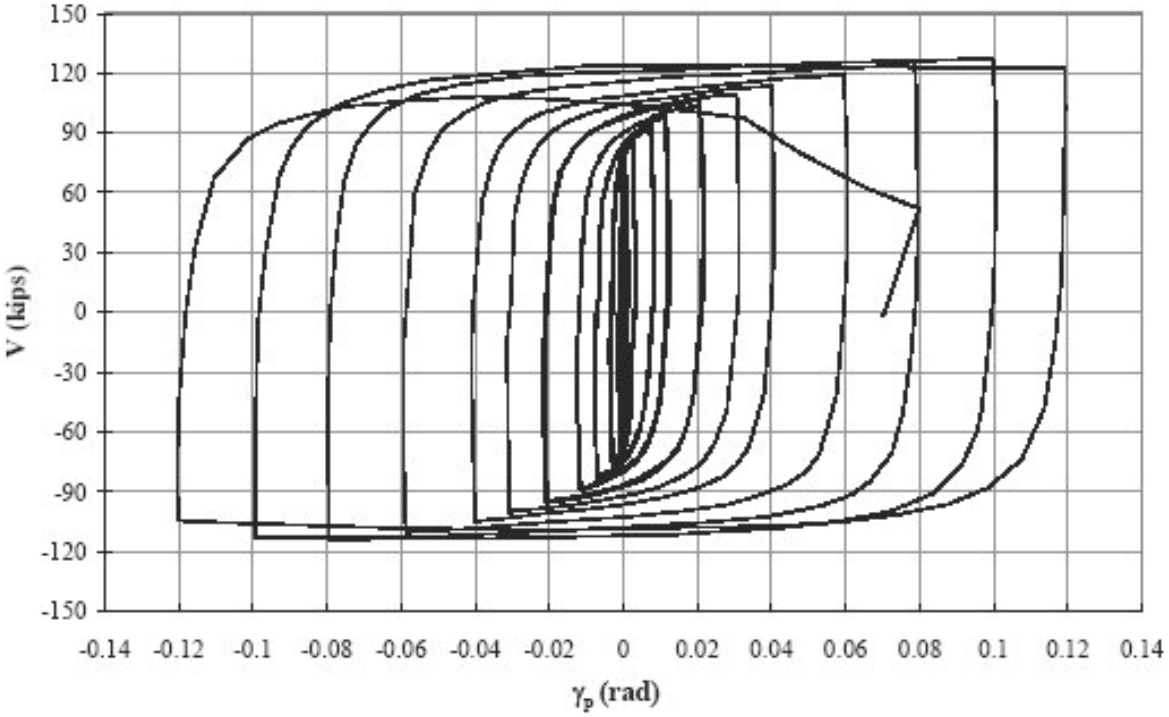

Figure C-52 Force-plastic rotation relationship for link 10 tested by Galvez (2004)

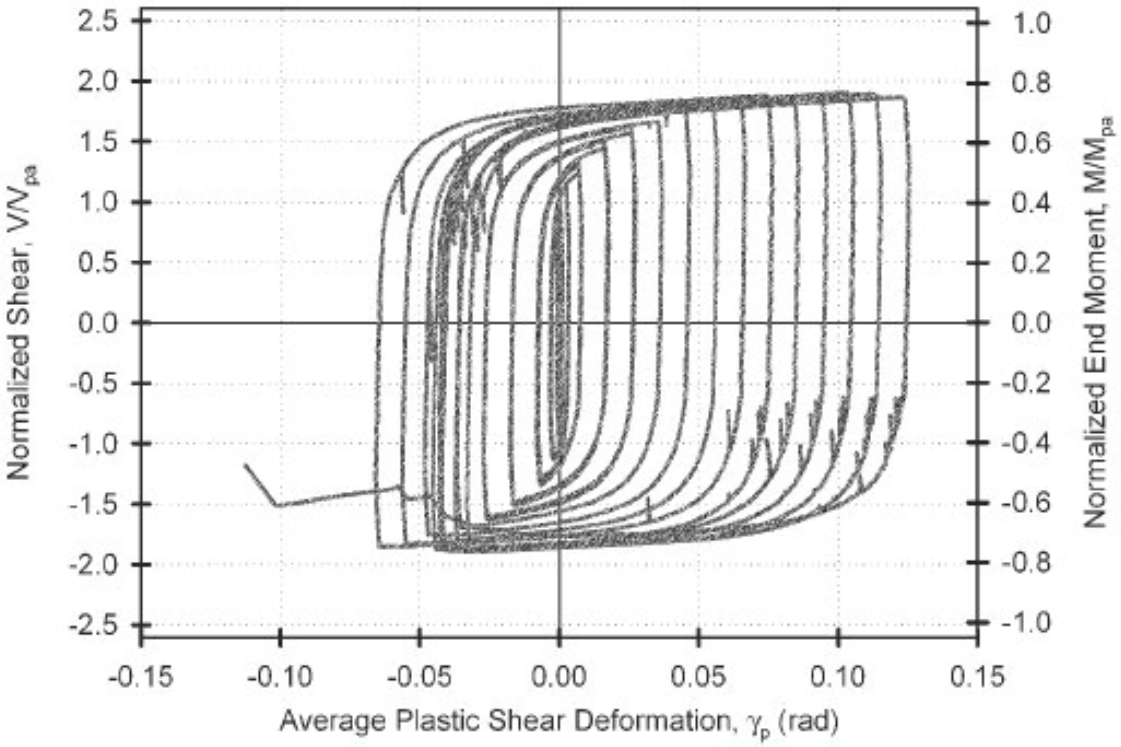

Figure C-53 Force-plastic rotation relationship for link C345a tested by Dusicka (2004)

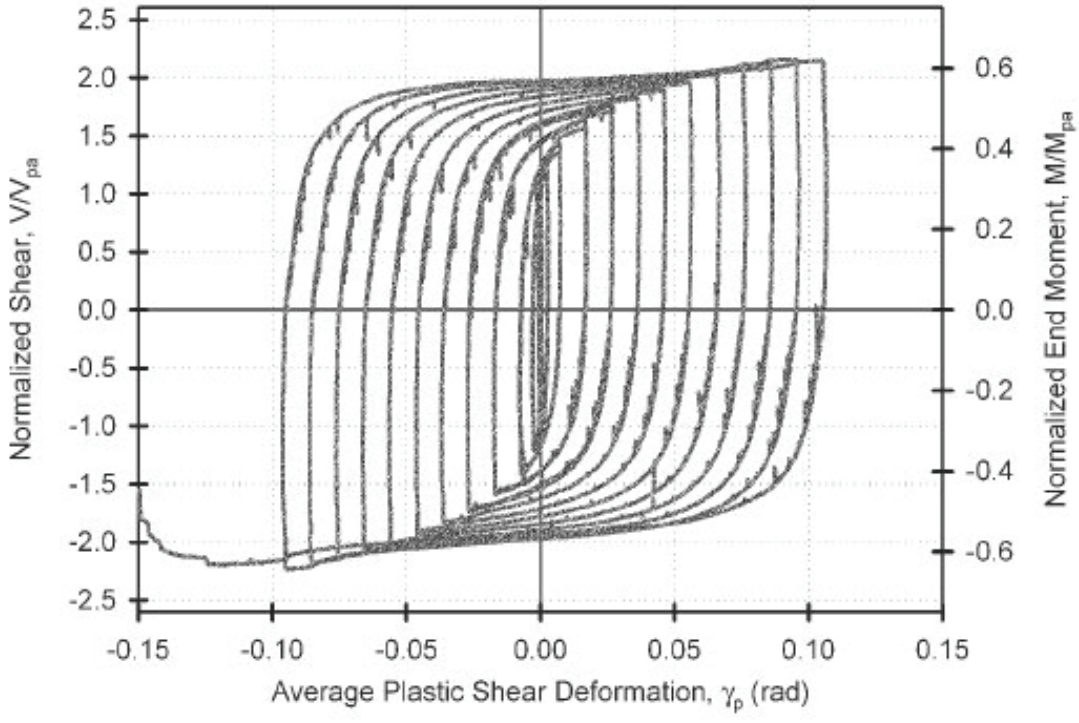

Figure C-54 Force-plastic rotation relationship for link C345b tested by Dusicka (2004)

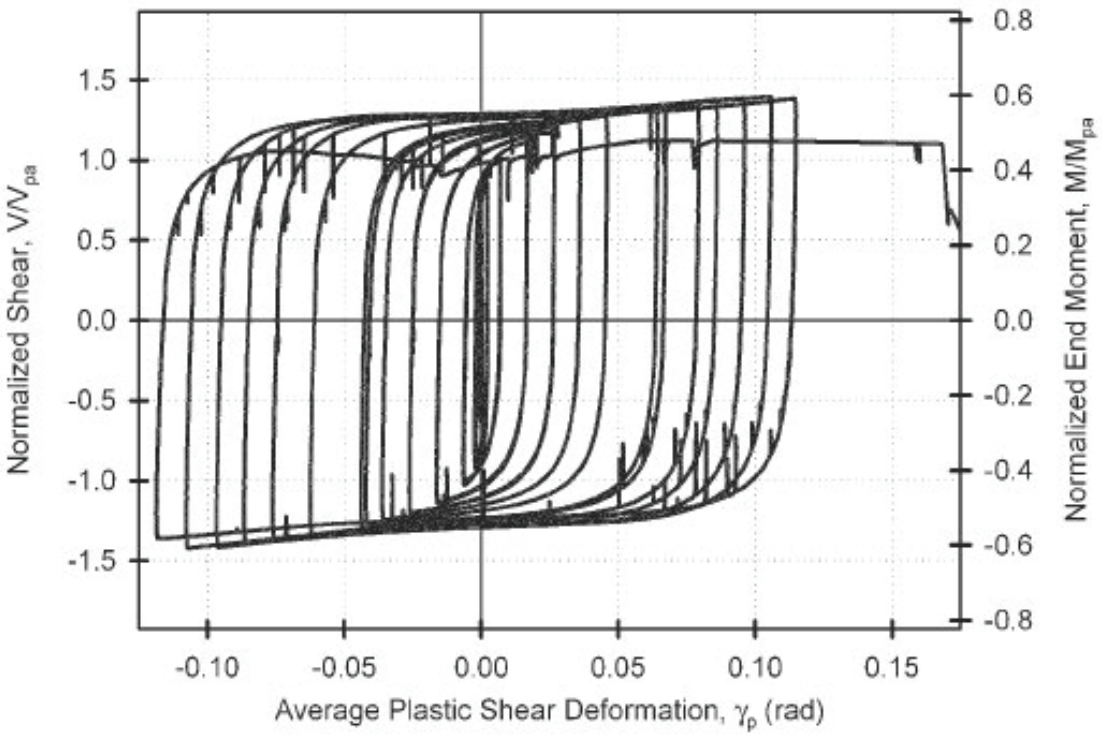

Figure C-55 Force-plastic rotation relationship for link H485 tested by Dusicka (2004)

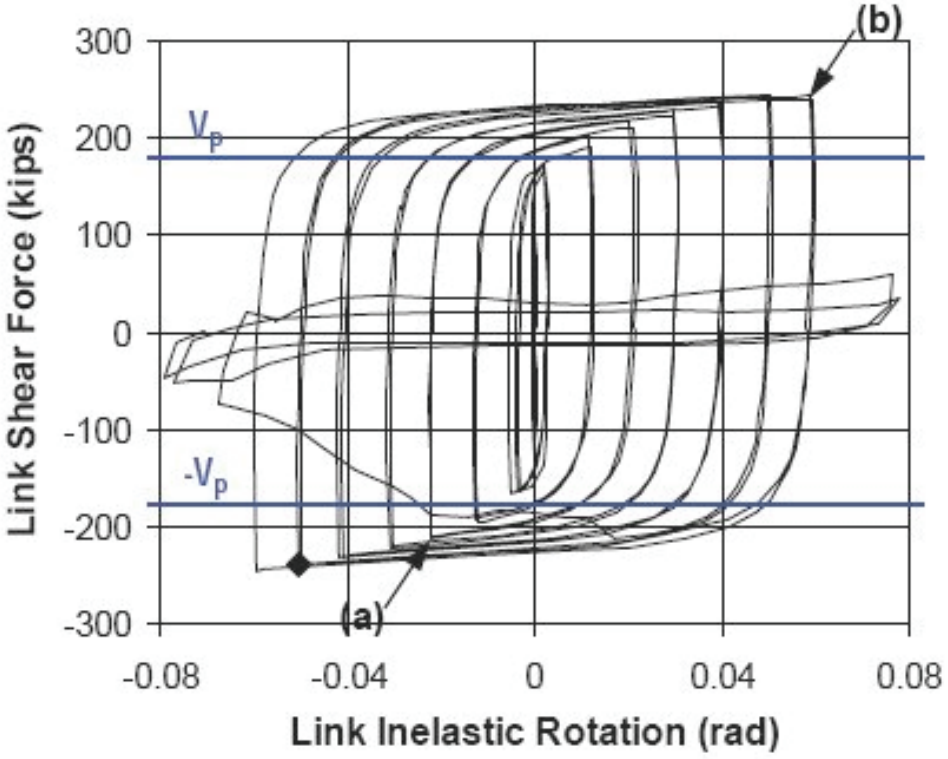

Figure C-56 Force-plastic rotation relationship for link FFS tested by Okazaki (2004)

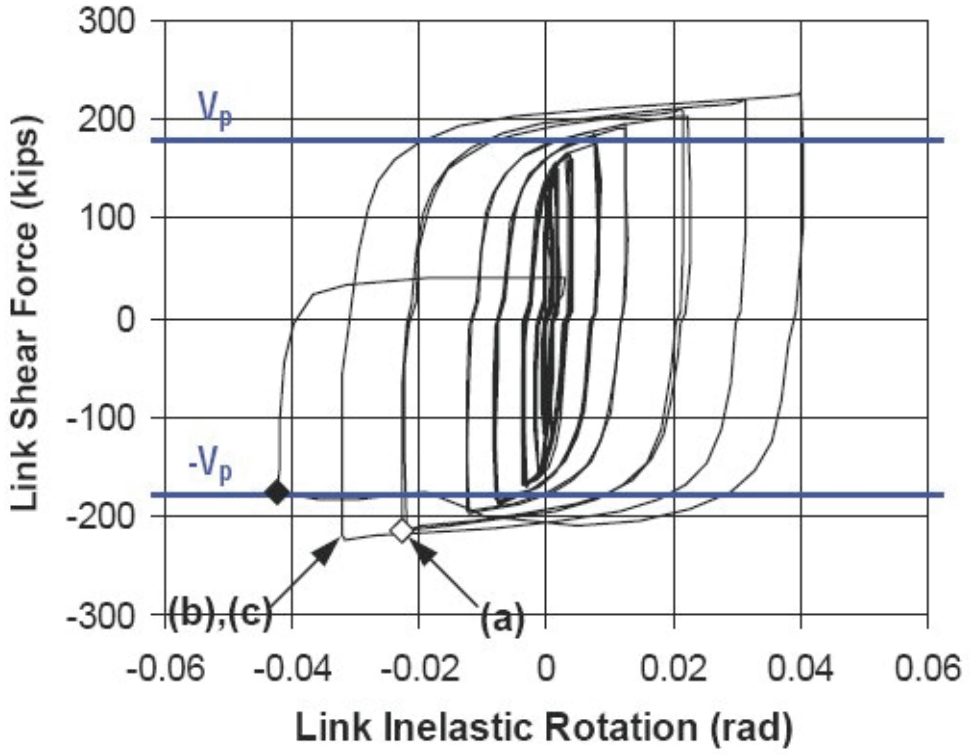

Figure C-57 Force-plastic rotation relationship for link FFS-RLP tested by Okazaki (2004)

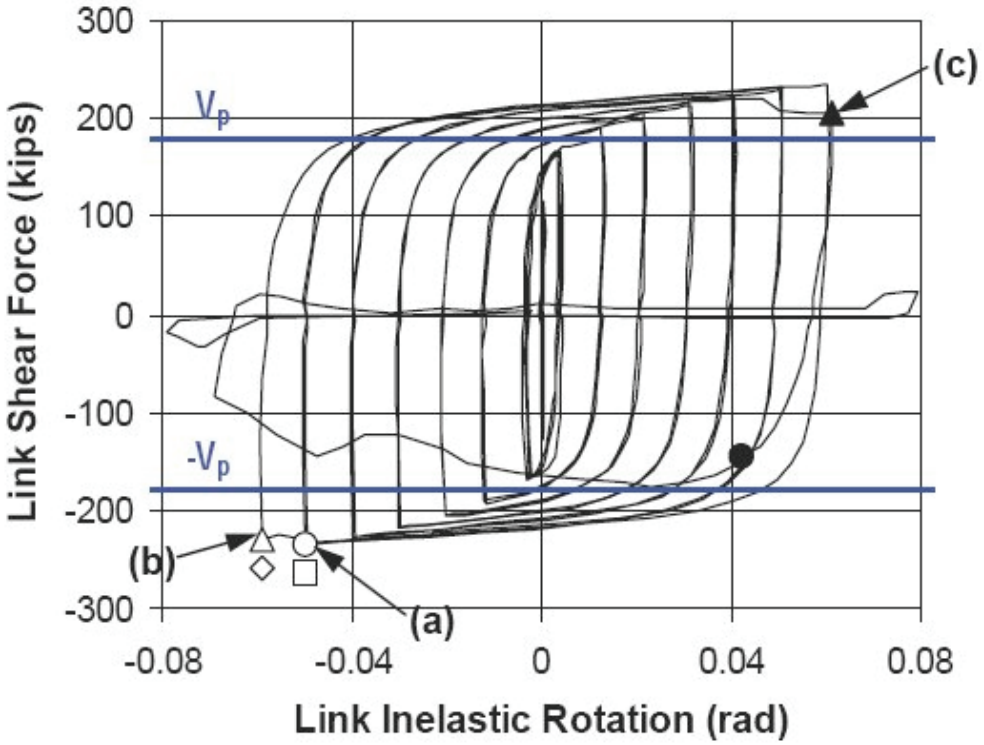

Figure C-58 Force-plastic rotation relationship for link MWS tested by Okazaki (2004)

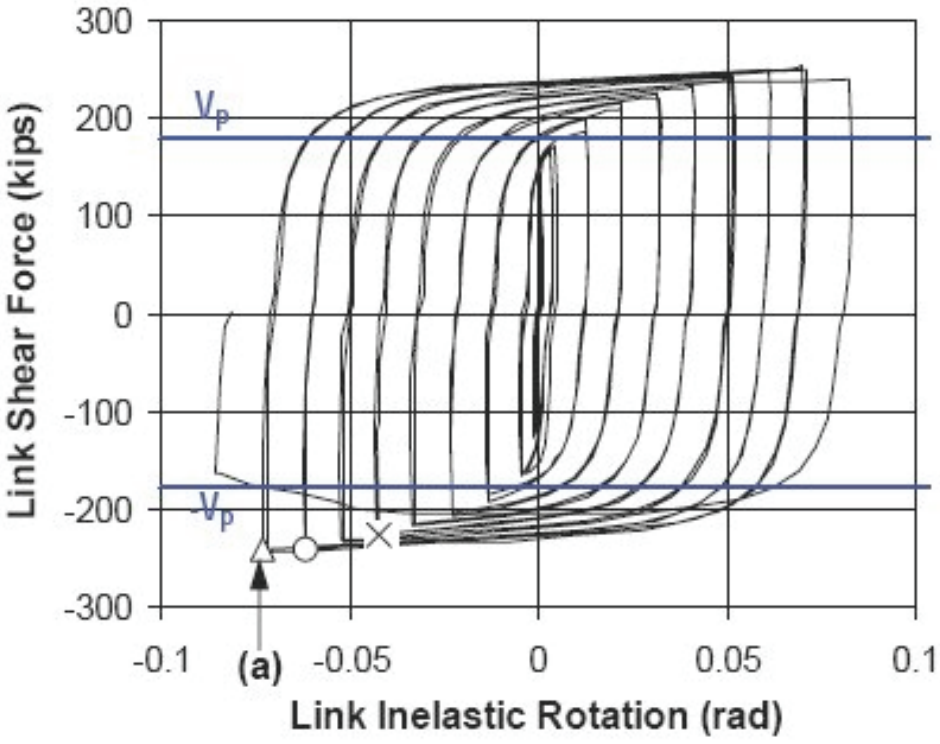

Figure C-59 Force-plastic rotation relationship for link NAS tested by Okazaki (2004)

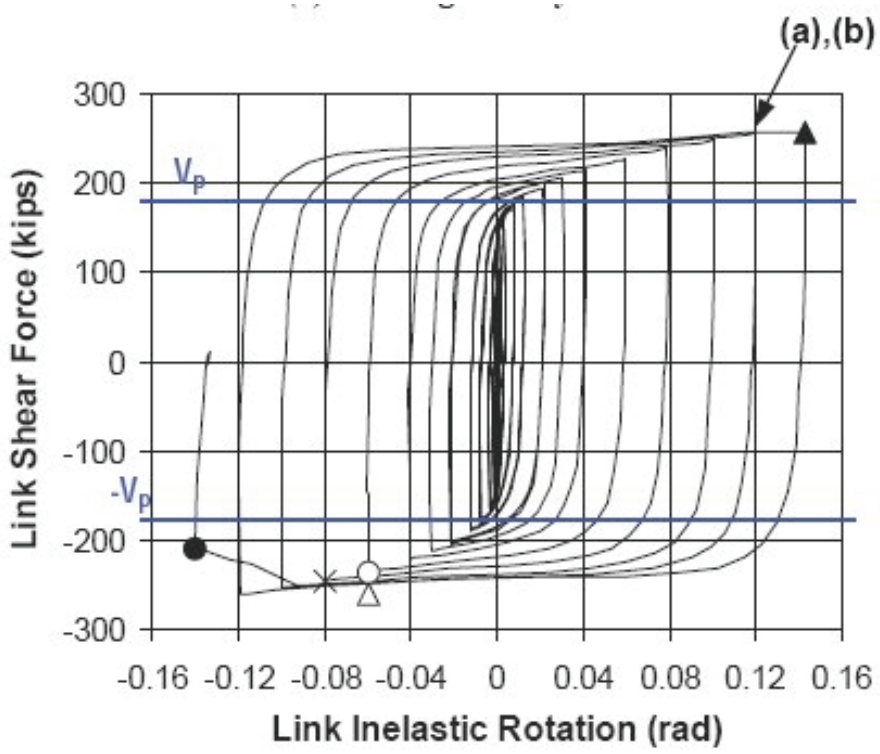

Figure C-60 Force-plastic rotation relationship for link NAS-RLP tested by Okazaki (2004)

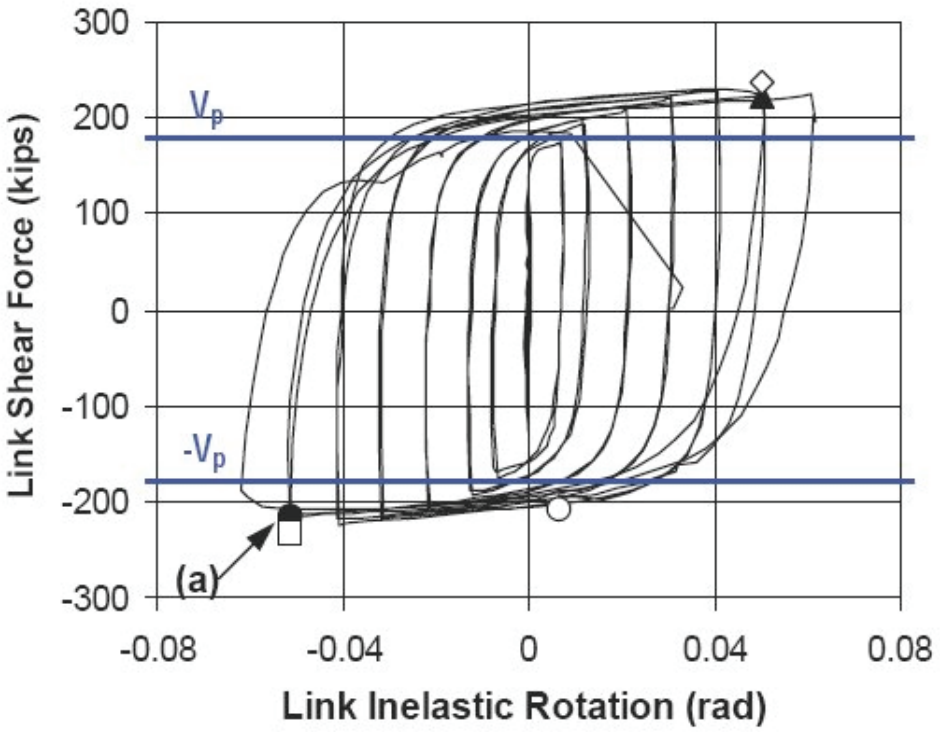

Figure C-61 Force-plastic rotation relationship for link PNS tested by Okazaki (2004)

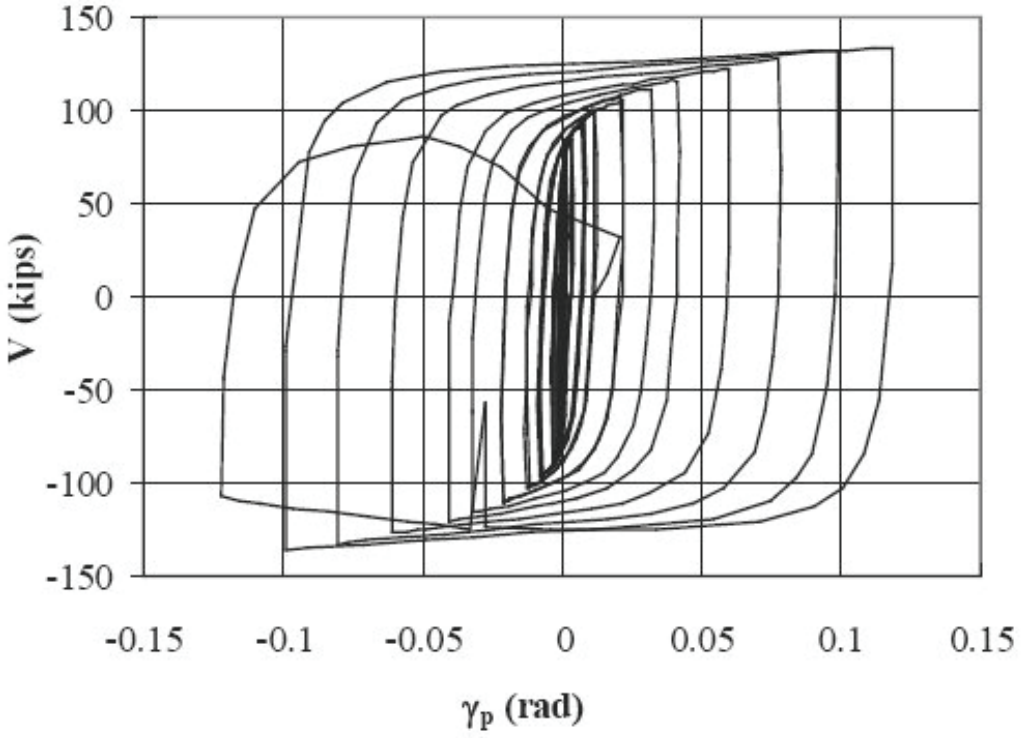

Figure C-62 Force-plastic rotation relationship for link 4A-RLP tested by Ryu (2005)

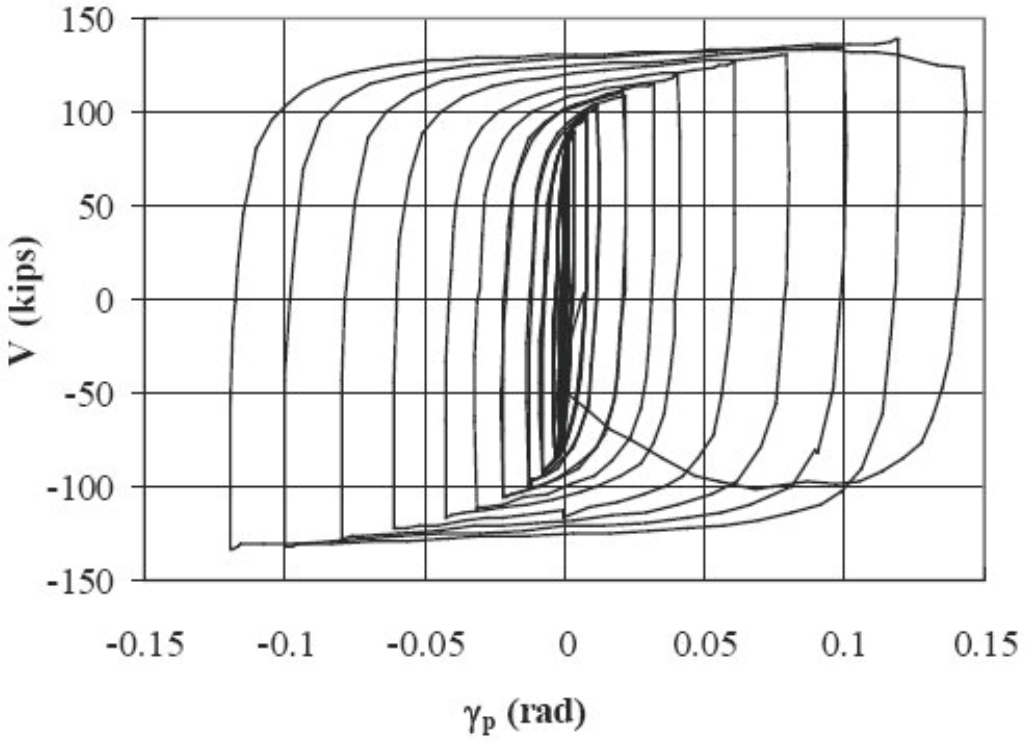

Figure C-63 Force-plastic rotation relationship for link 4C-RLP tested by Ryu (2005)

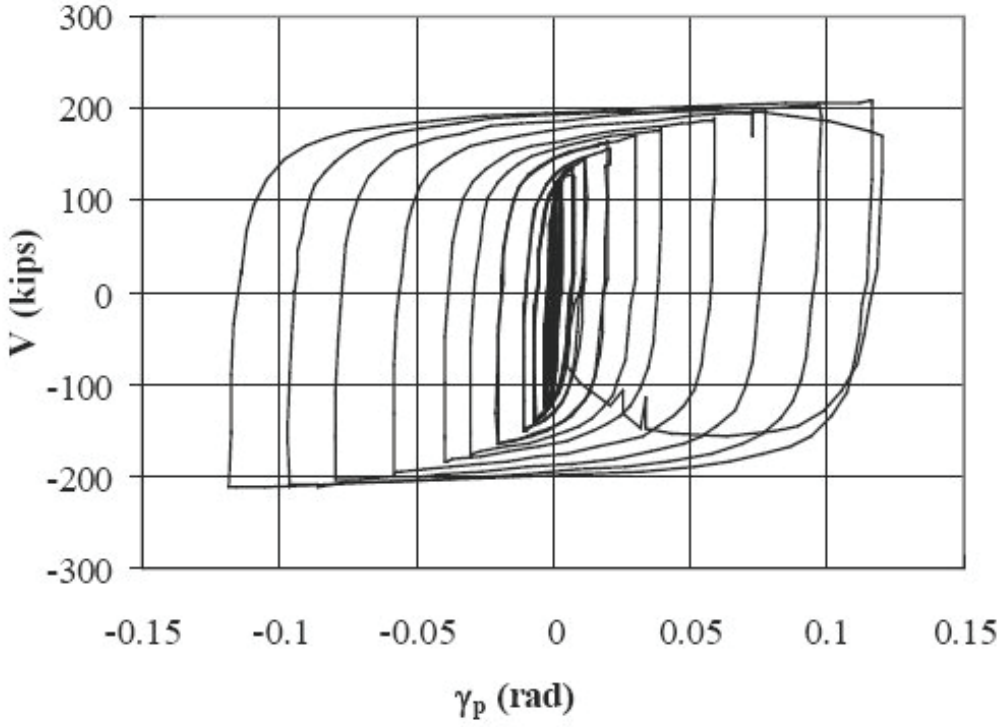

Figure C-64 Force-plastic rotation relationship for link 8-RLP tested by Ryu (2005)

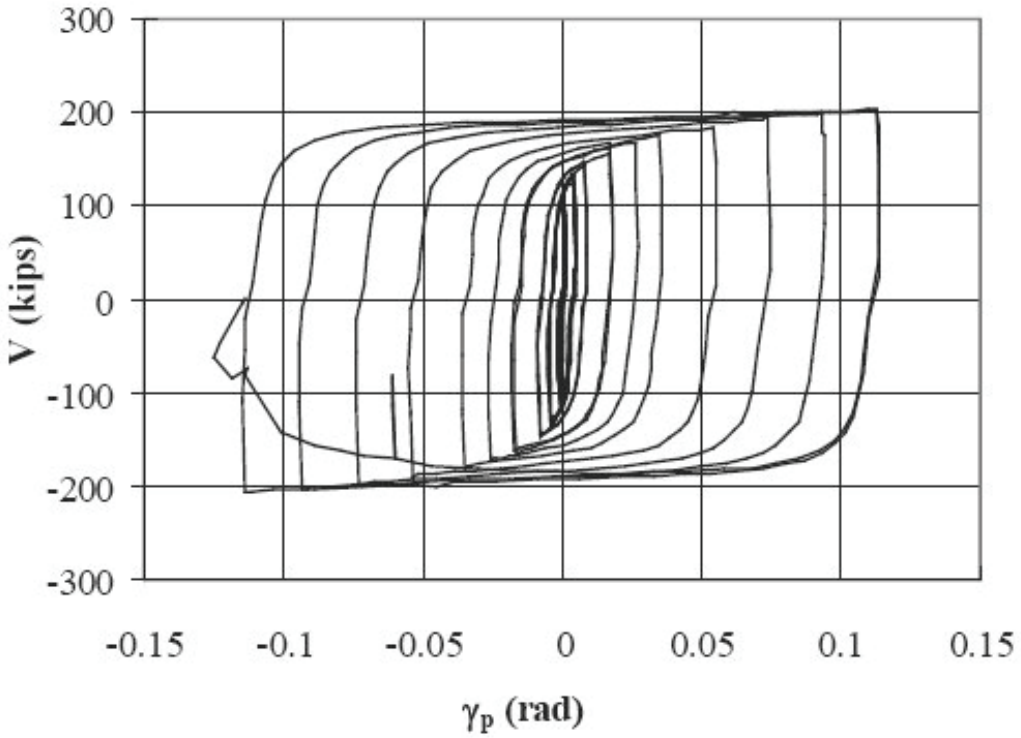

Figure C-65 Force-plastic rotation relationship for link 10-RLP tested by Ryu (2005)

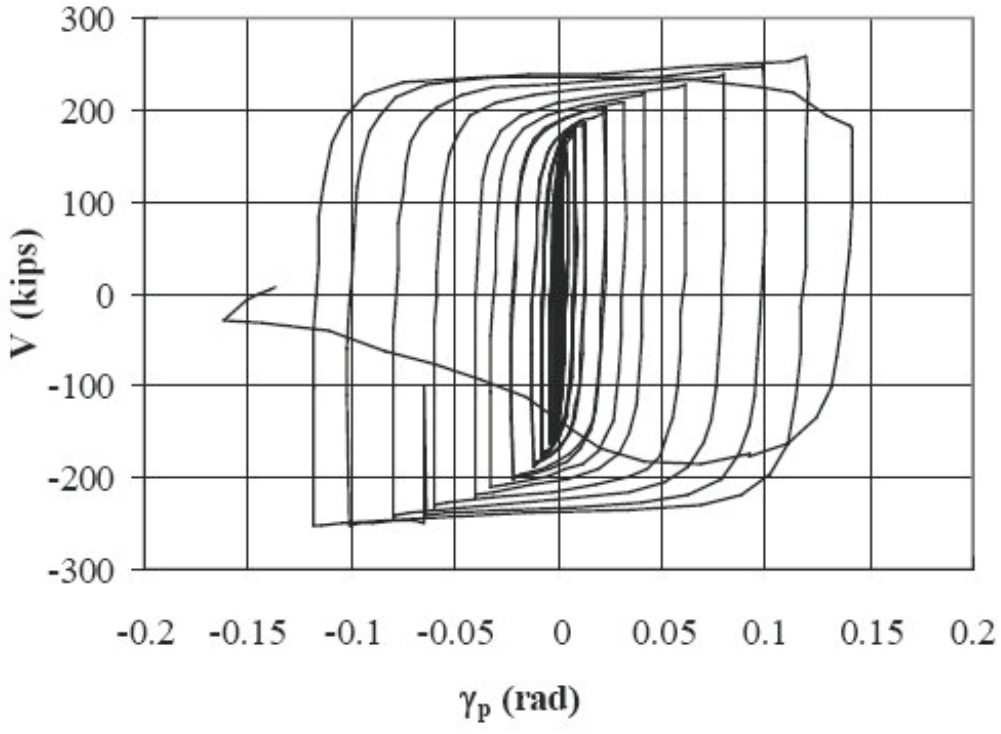

Figure C-66 Force-plastic rotation relationship for link 12-RLP tested by Ryu (2005)

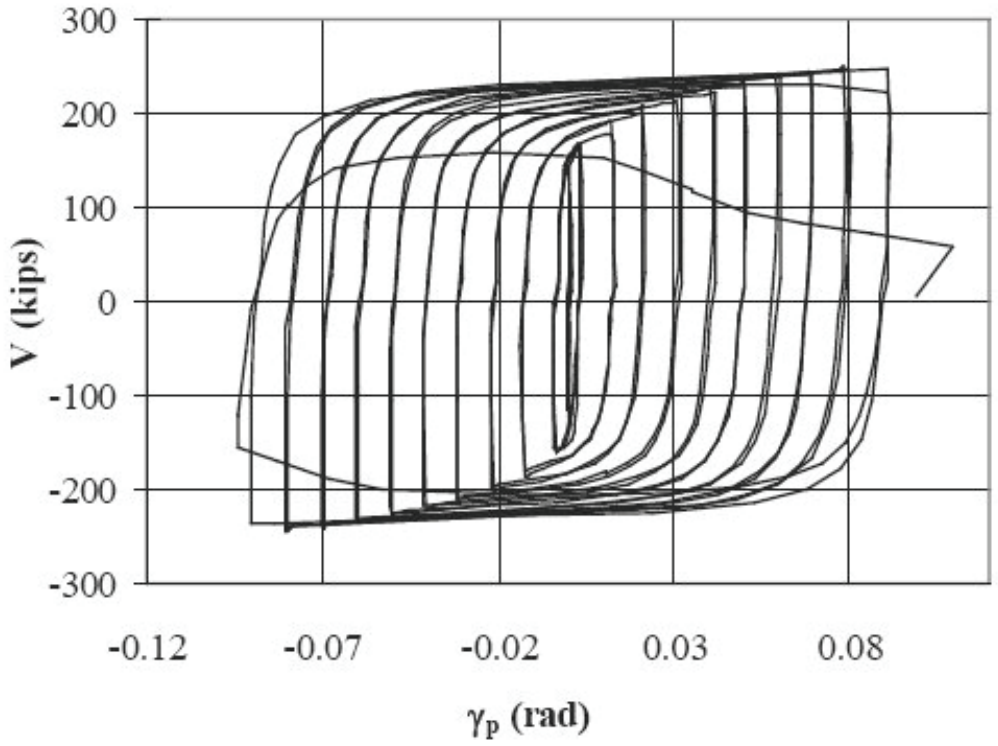

Figure C-67 Force-plastic rotation relationship for link 12-AISC tested by Ryu (2005)

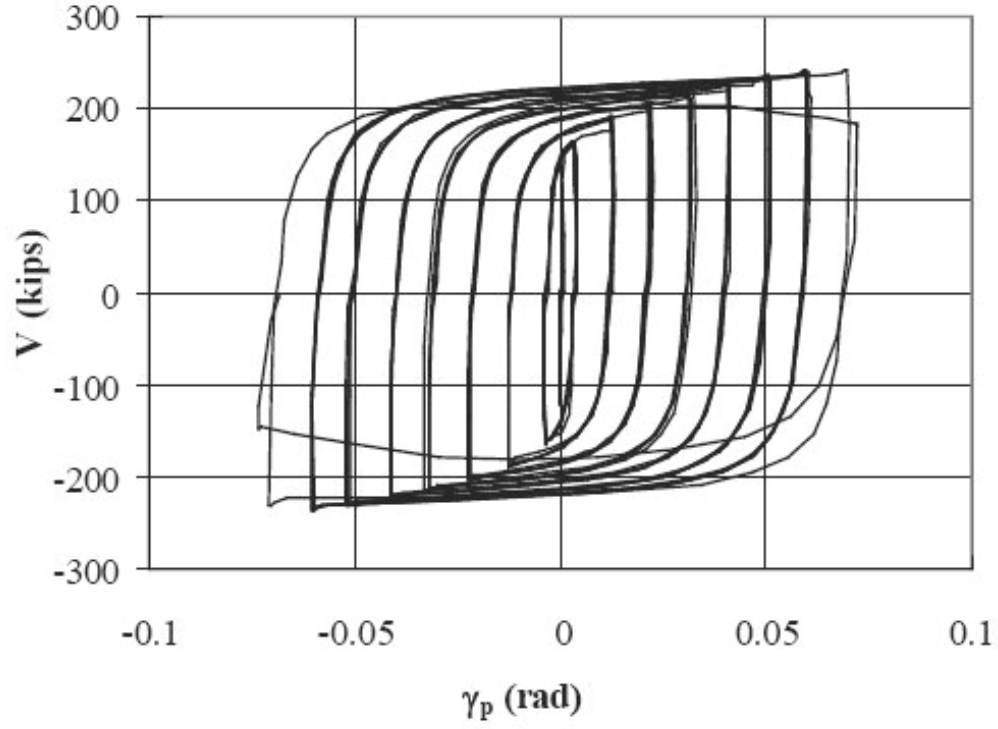

Figure C-68 Force-plastic rotation relationship for link 12-SEV tested by Ryu (2005)

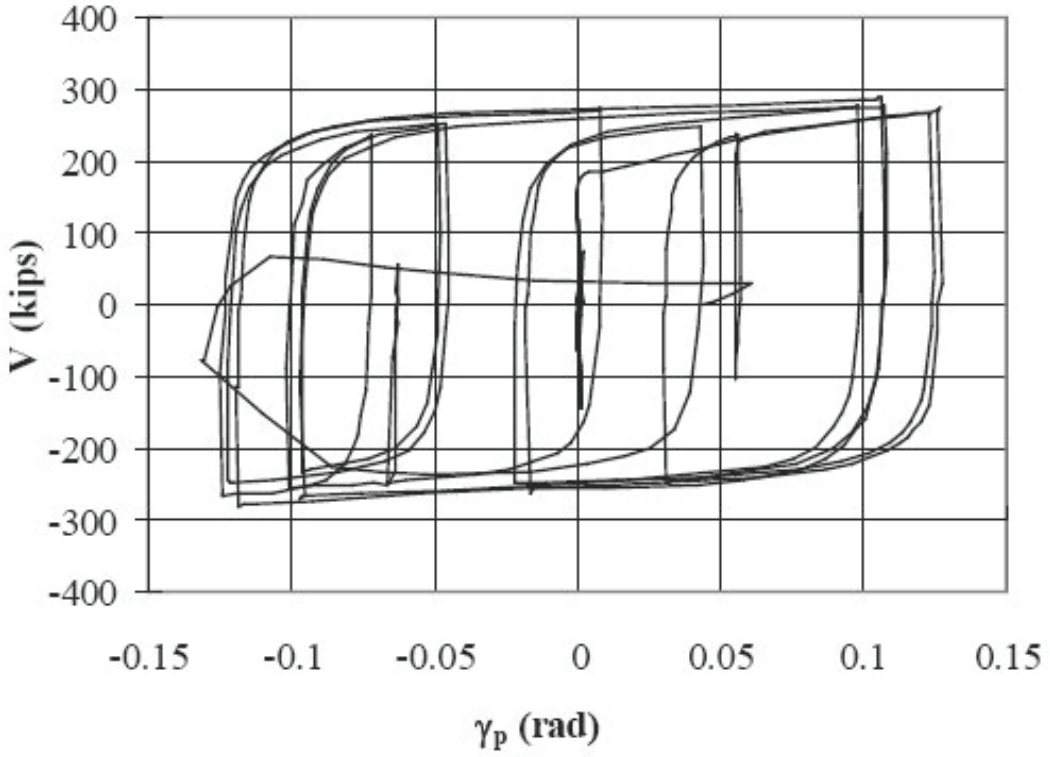

Figure C-69 Force-plastic rotation relationship for link 12-RAN tested by Ryu (2005)

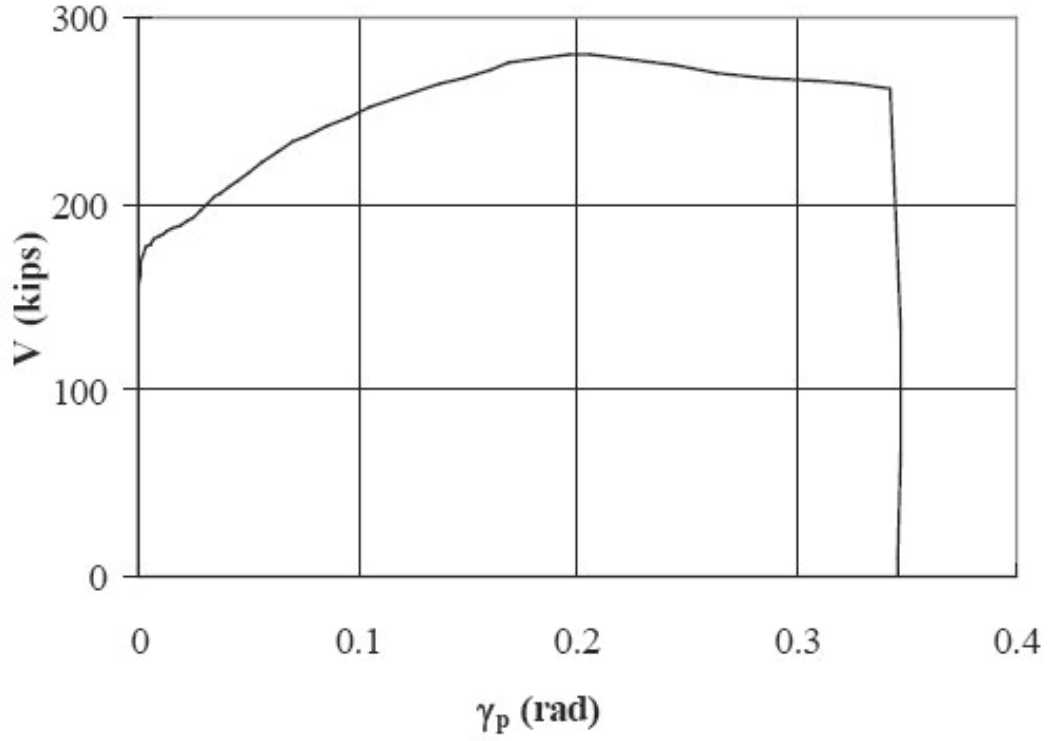

Figure C-70 Force-plastic rotation relationship for link 12-MON tested by Ryu (2005)

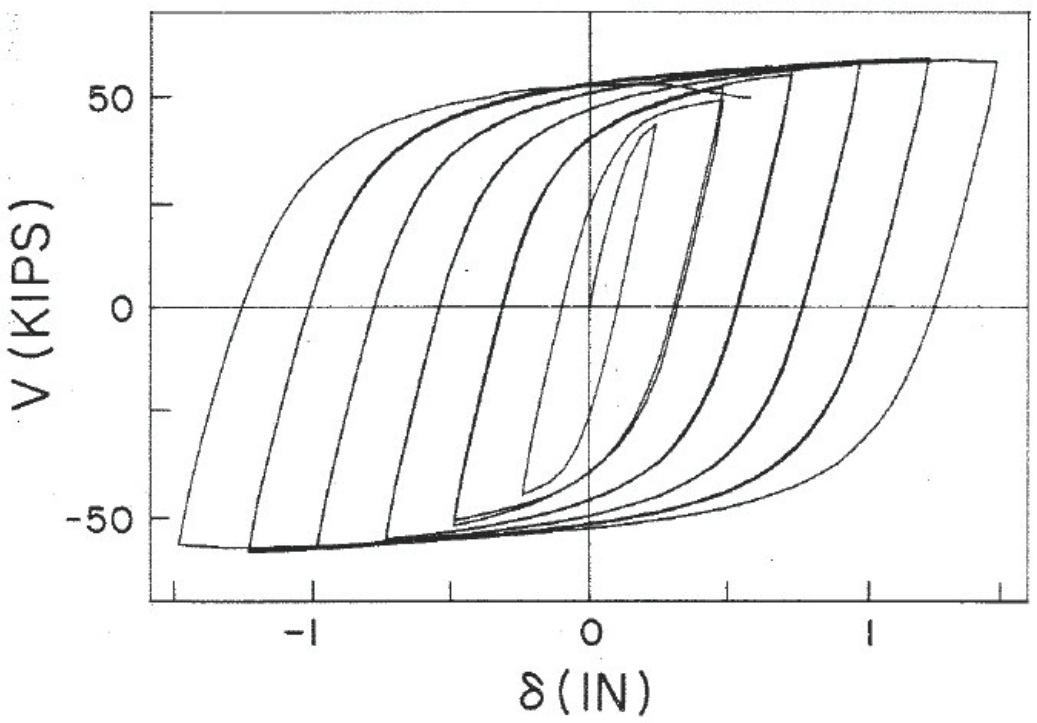

Figure C-71 Force-plastic rotation relationship for link 5 tested by Kasai and Popov (1986)

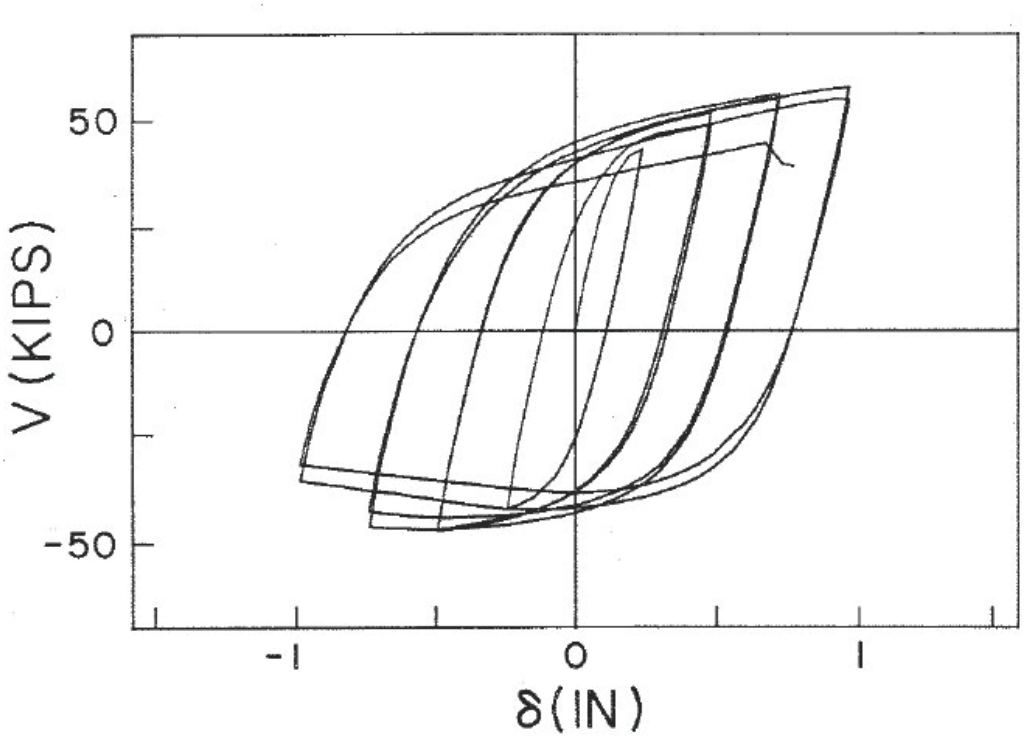

Figure C-72 Force-plastic rotation relationship for link 6 tested by Kasai and Popov (1986)

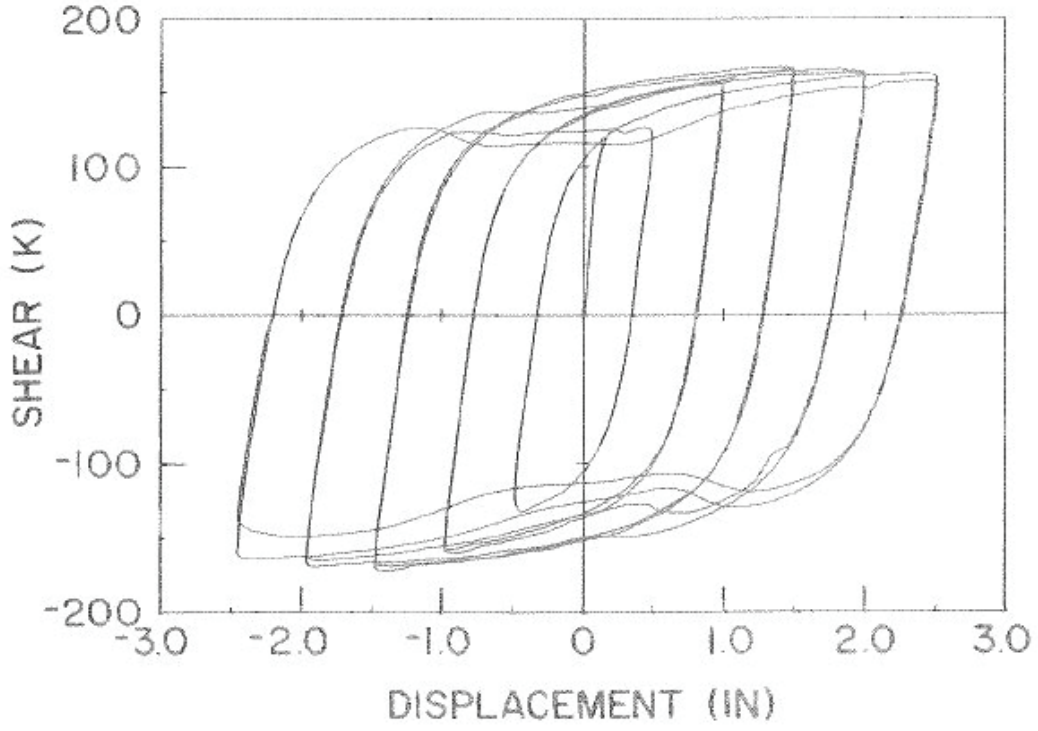

Figure C-73 Force-plastic rotation relationship for link 9 tested by Hjelmstad and Popov (1983)

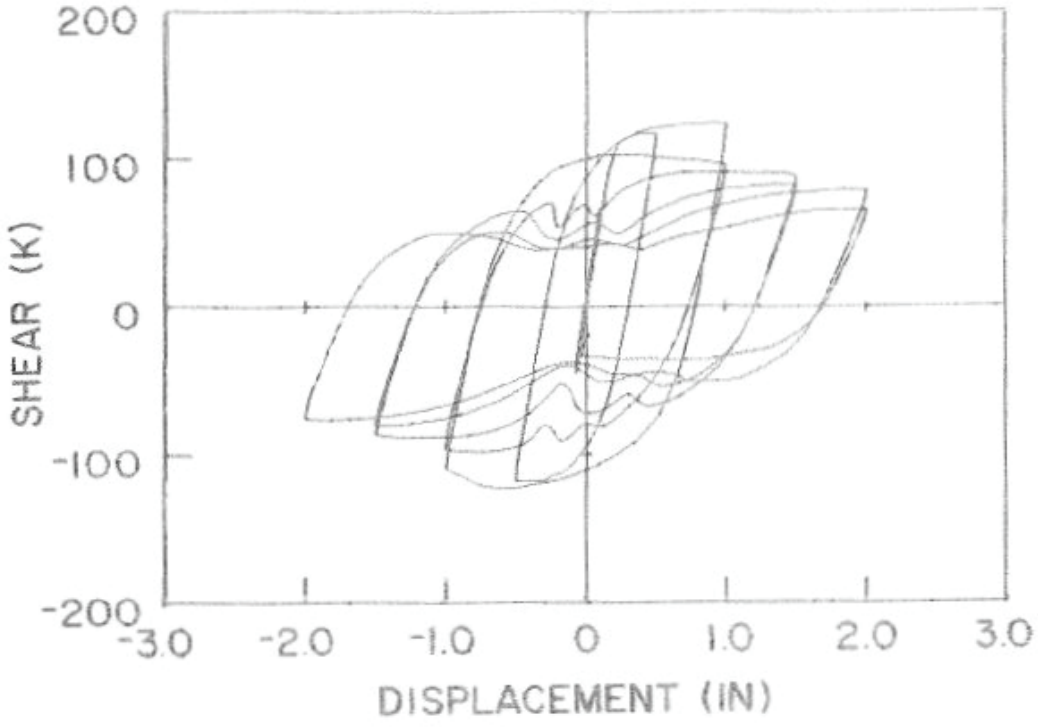

Figure C-74 Force-plastic rotation relationship for link 10 tested by Hjelmstad and Popov (1983)

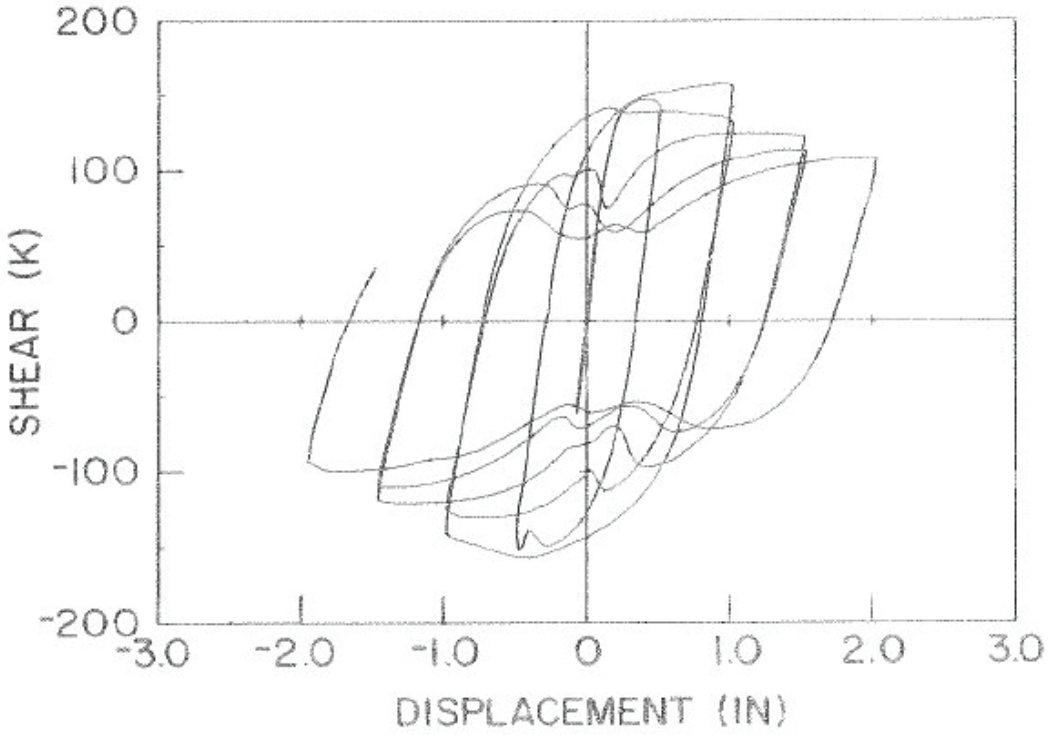

Figure C-75 Force-plastic rotation relationship for link 11 tested by Hjelmstad and Popov (1983)

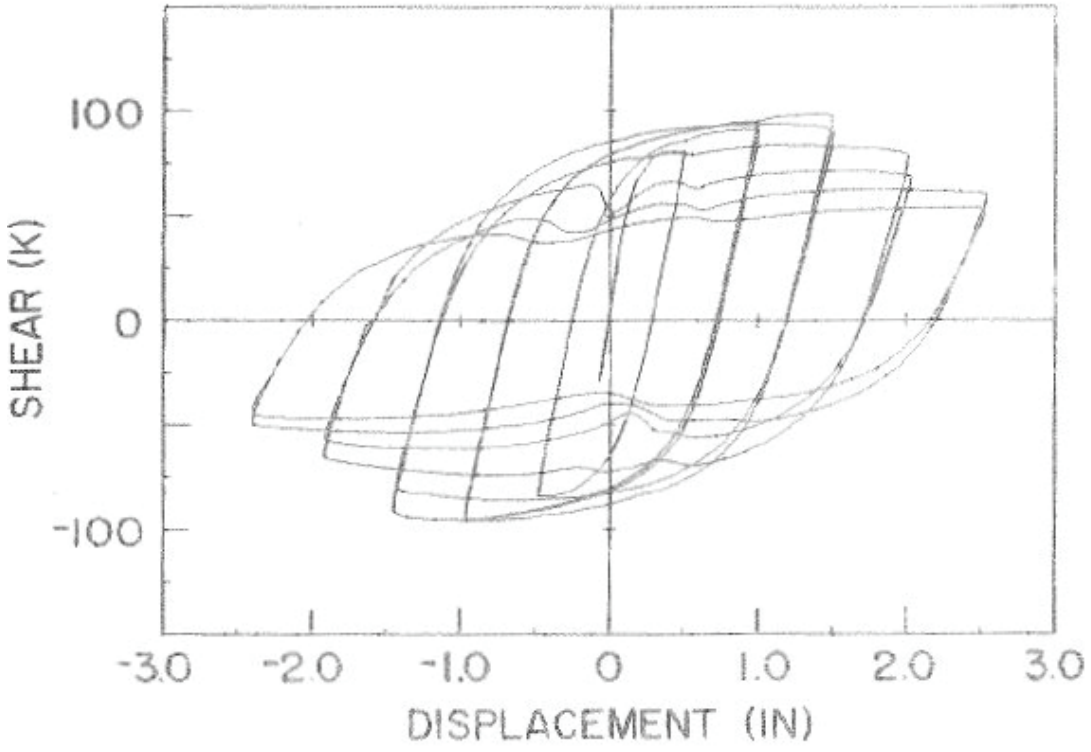

Figure C-76 Force-plastic rotation relationship for link 12 tested by Hjelmstad and Popov (1983)

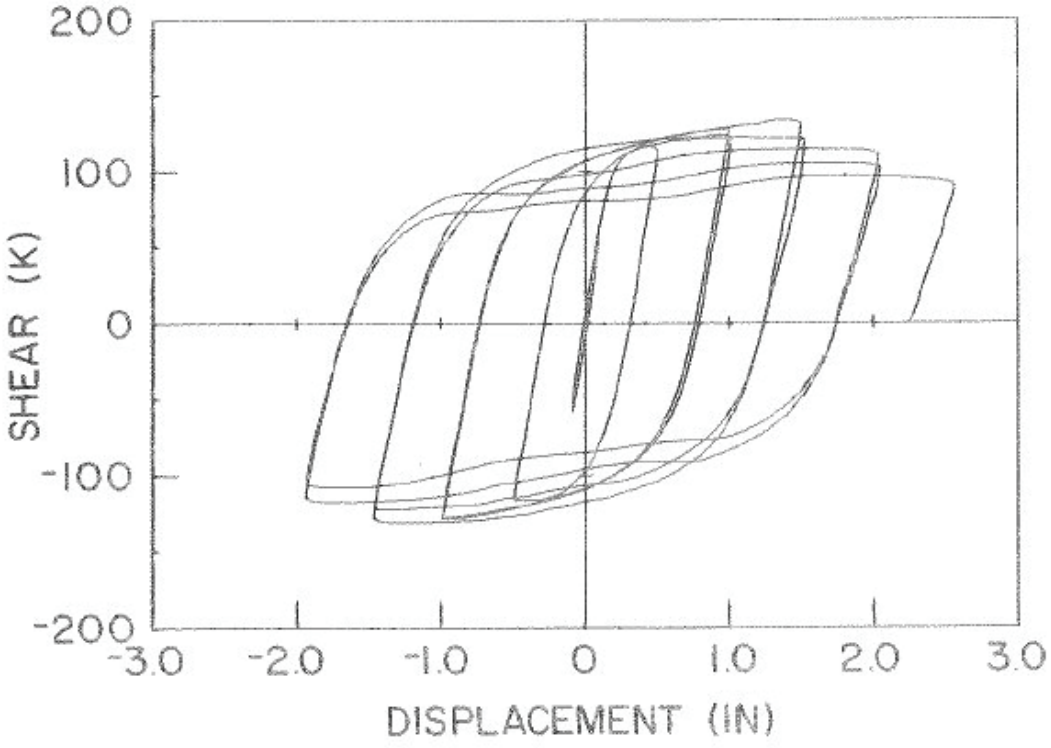

Figure C-77 Force-plastic rotation relationship for link 13 tested by Hjelmstad and Popov (1983)

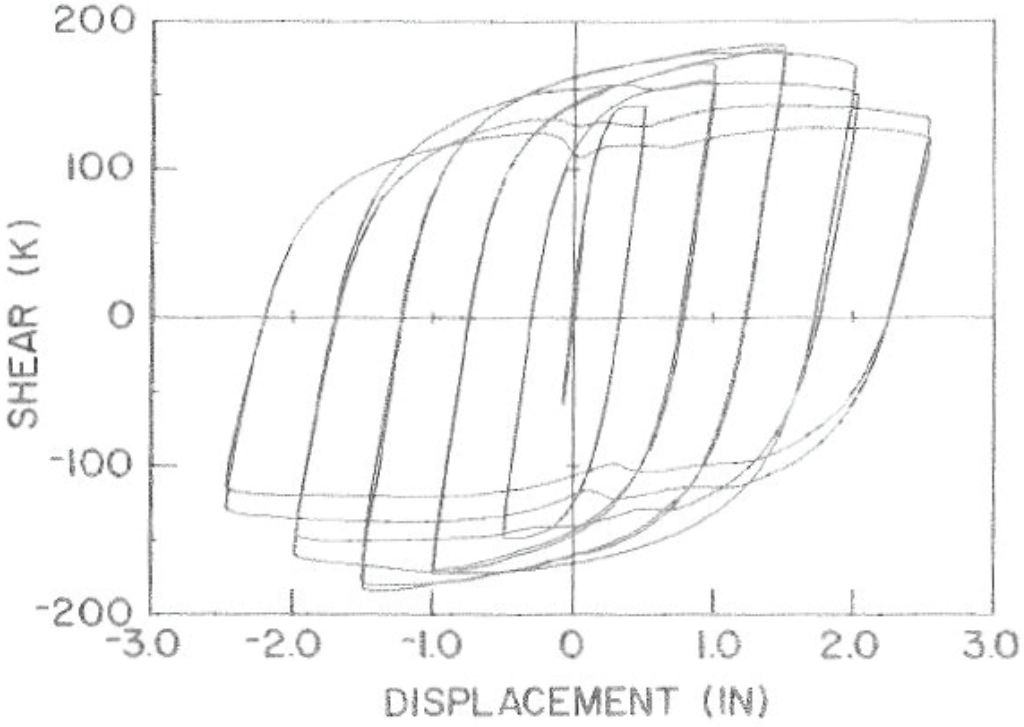

Figure C-78 Force-plastic rotation relationship for link 14 tested by Hjelmstad and Popov (1983)

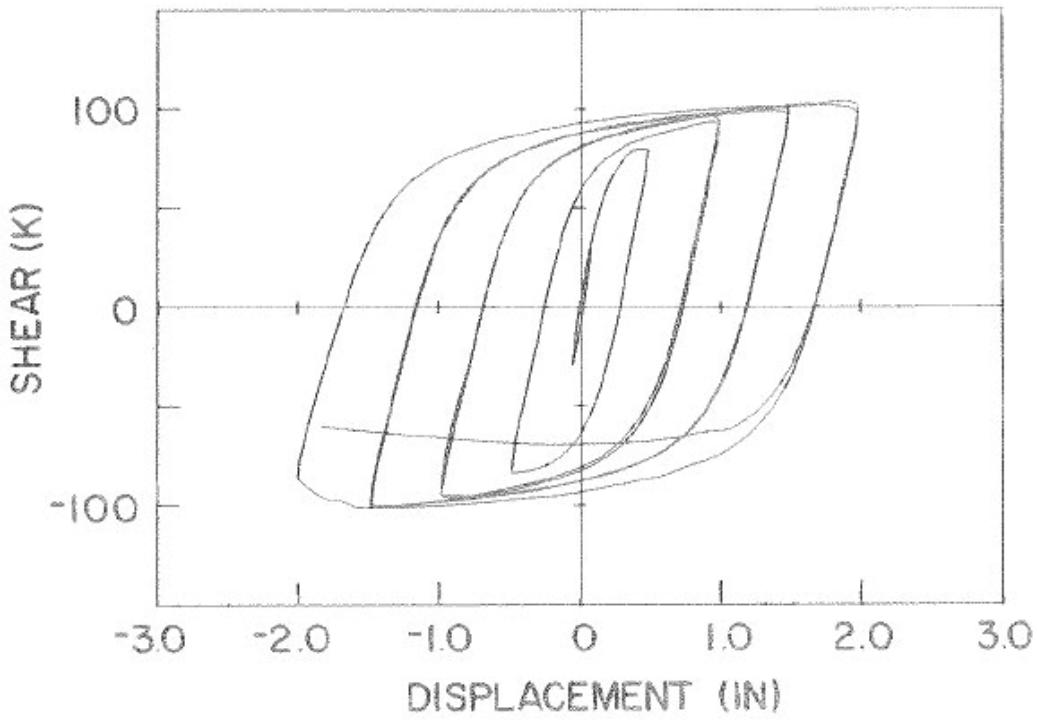

Figure C-79 Force-plastic rotation relationship for link 15 tested by Hjelmstad and Popov (1983)

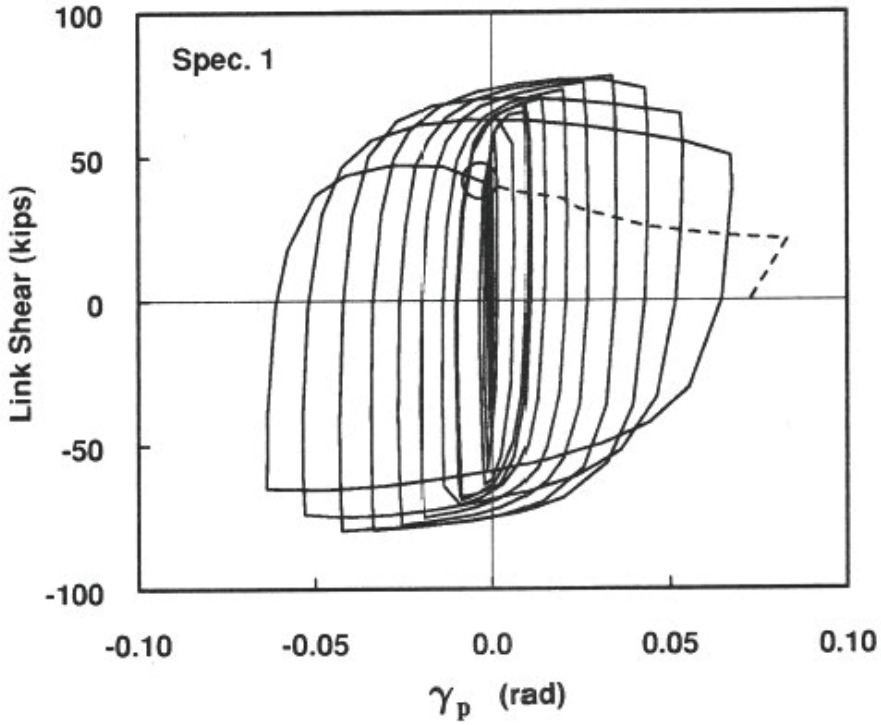

Figure C-80 Force-plastic rotation relationship for link 1 tested by Engelhardt and Popov (1989)

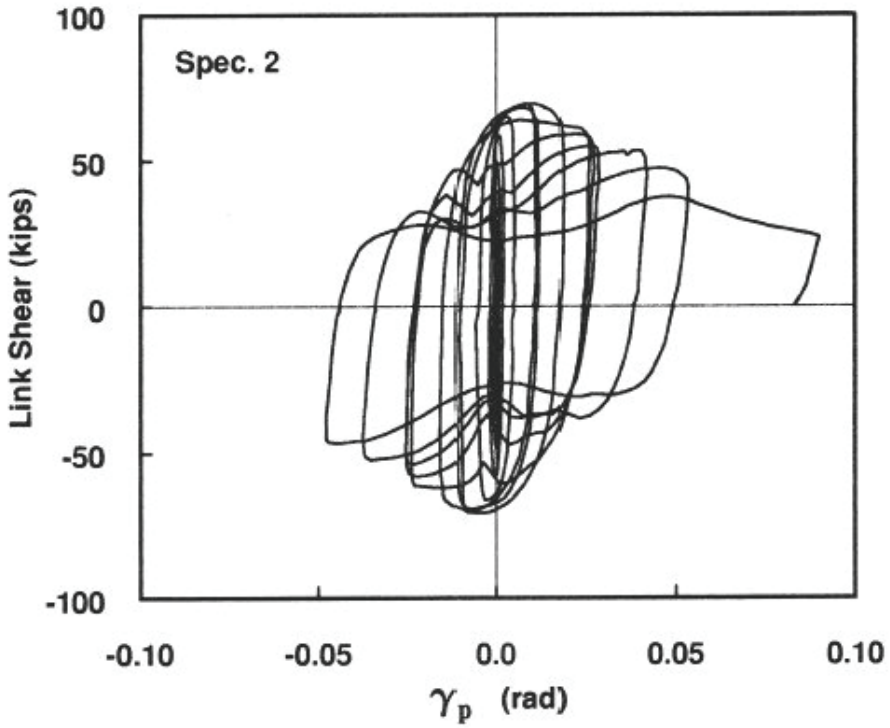

Figure C-81 Force-plastic rotation relationship for link 2 tested by Engelhardt and Popov (1989)

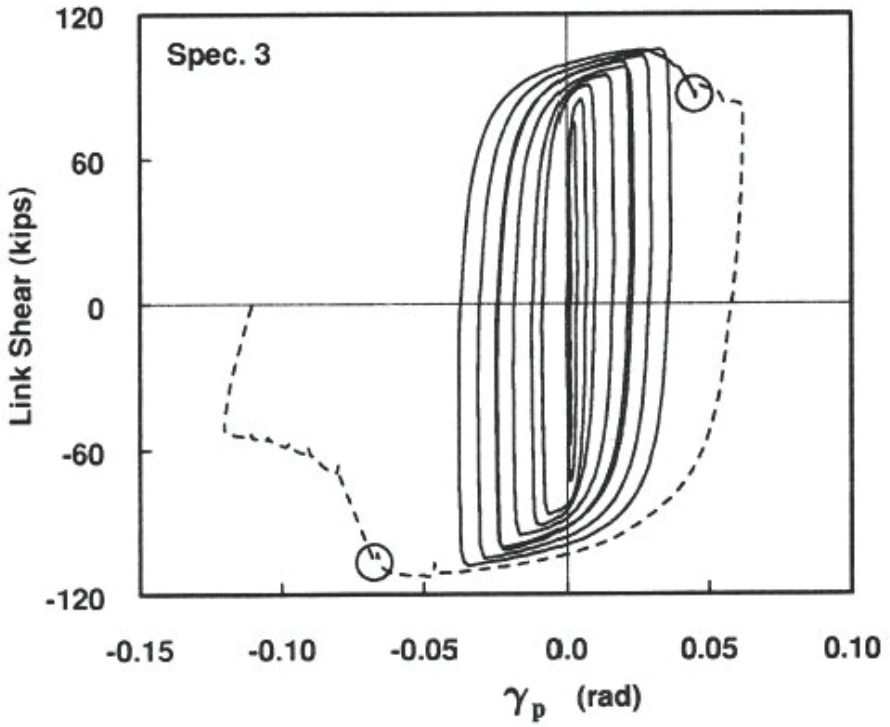

Figure C-82 Force-plastic rotation relationship for link 3 tested by Engelhardt and Popov (1989)

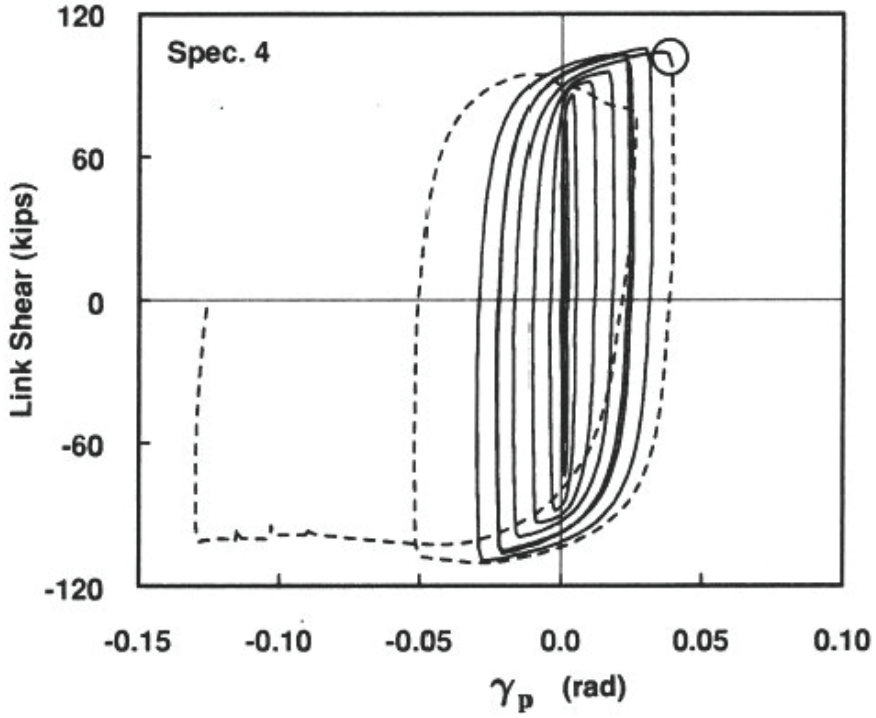

Figure C-83 Force-plastic rotation relationship for link 4 tested by Engelhardt and Popov (1989)

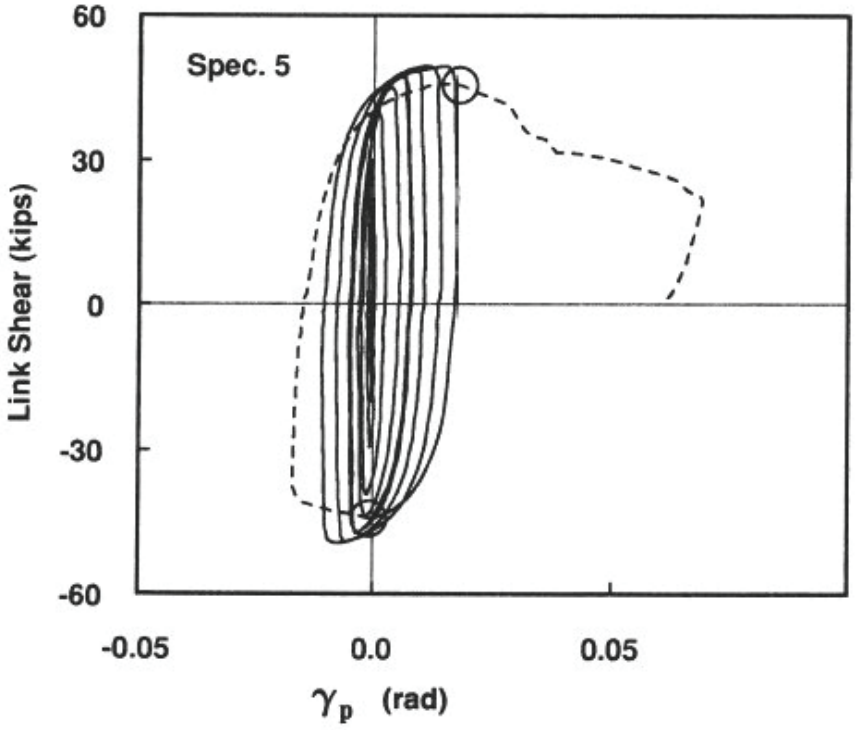

Figure C-84 Force-plastic rotation relationship for link 5 tested by Engelhardt and Popov (1989)

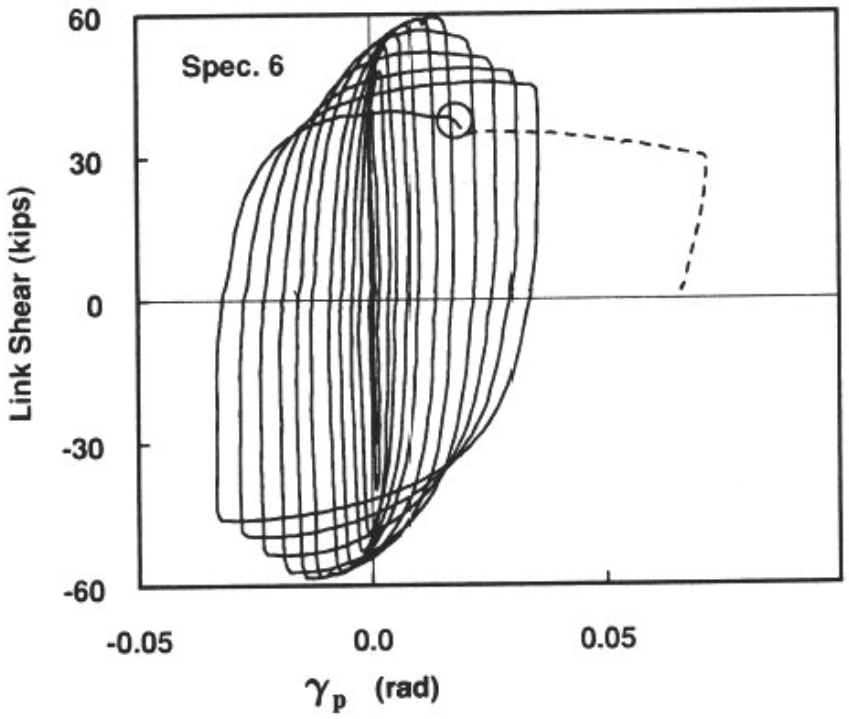

Figure C-85 Force-plastic rotation relationship for link 6 tested by Engelhardt and Popov (1989)

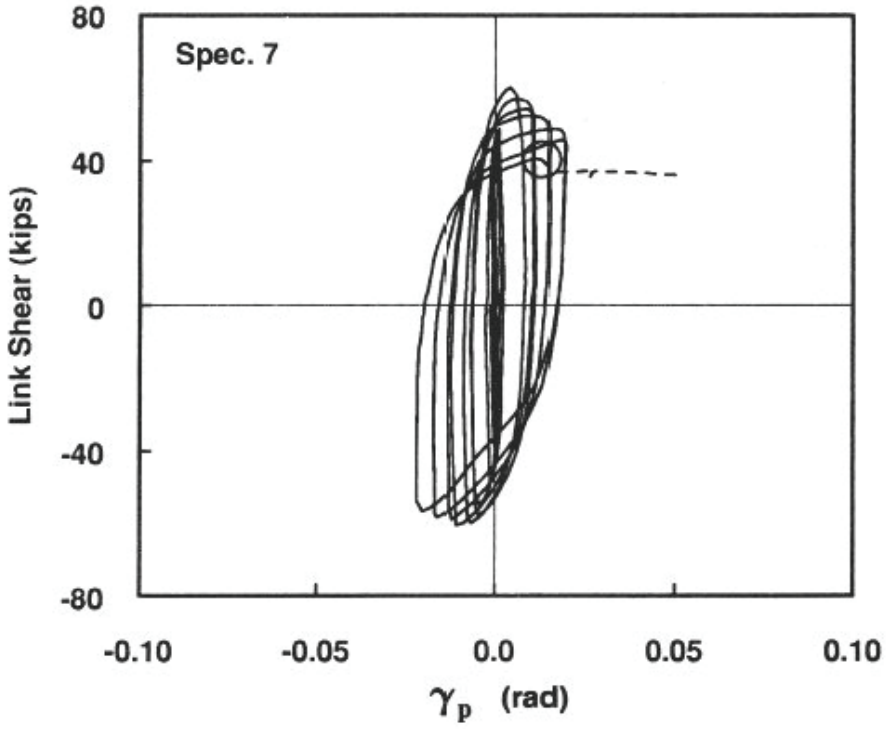

Figure C-86 Force-plastic rotation relationship for link 7 tested by Engelhardt and Popov (1989)

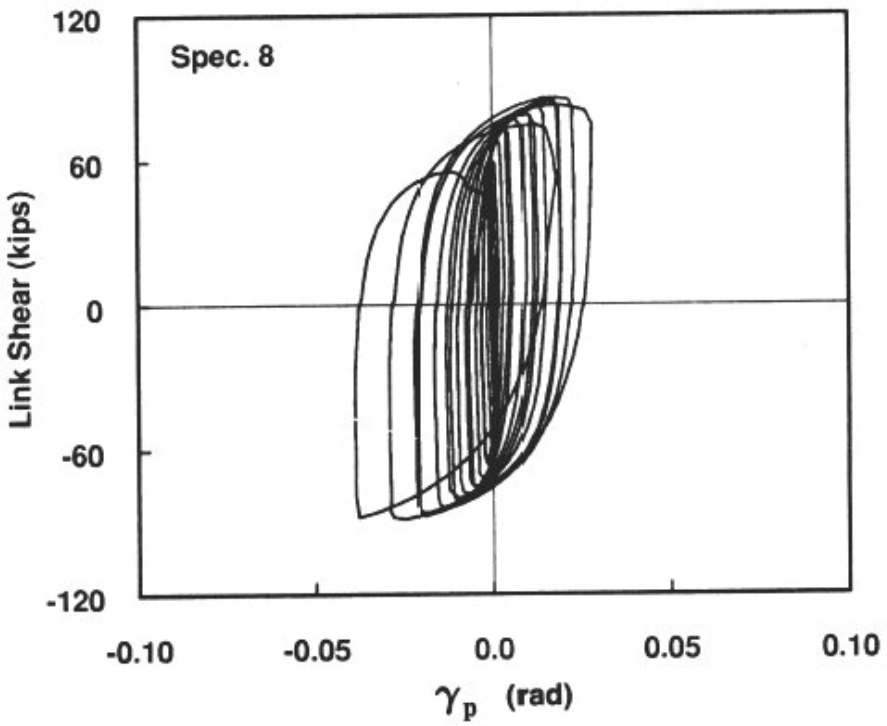

Figure C-87 Force-plastic rotation relationship for link 8 tested by Engelhardt and Popov (1989)

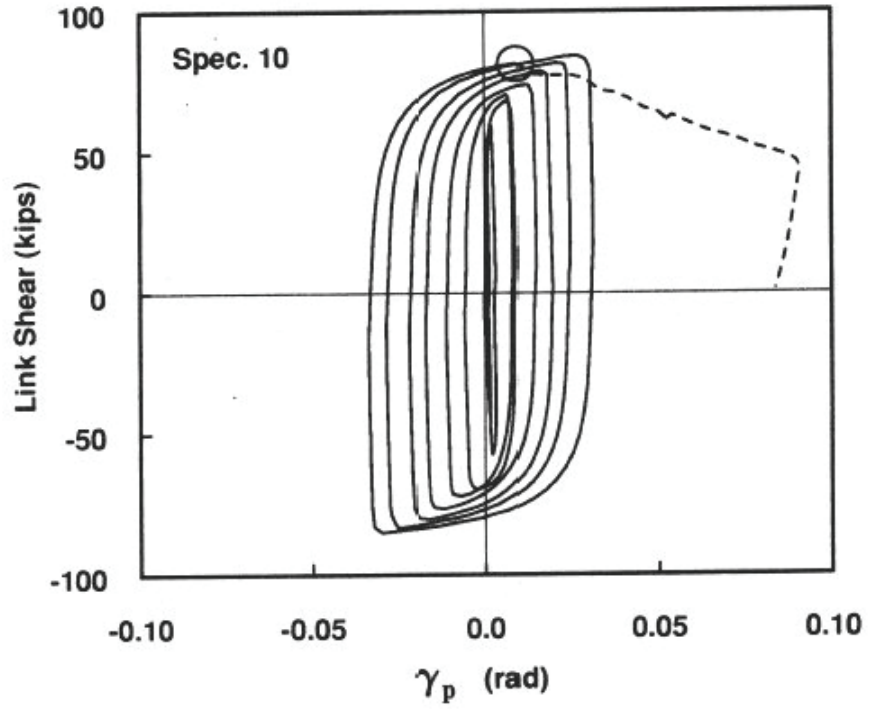

Figure C-88 Force-plastic rotation relationship for link 10 tested by Engelhardt and Popov (1989)

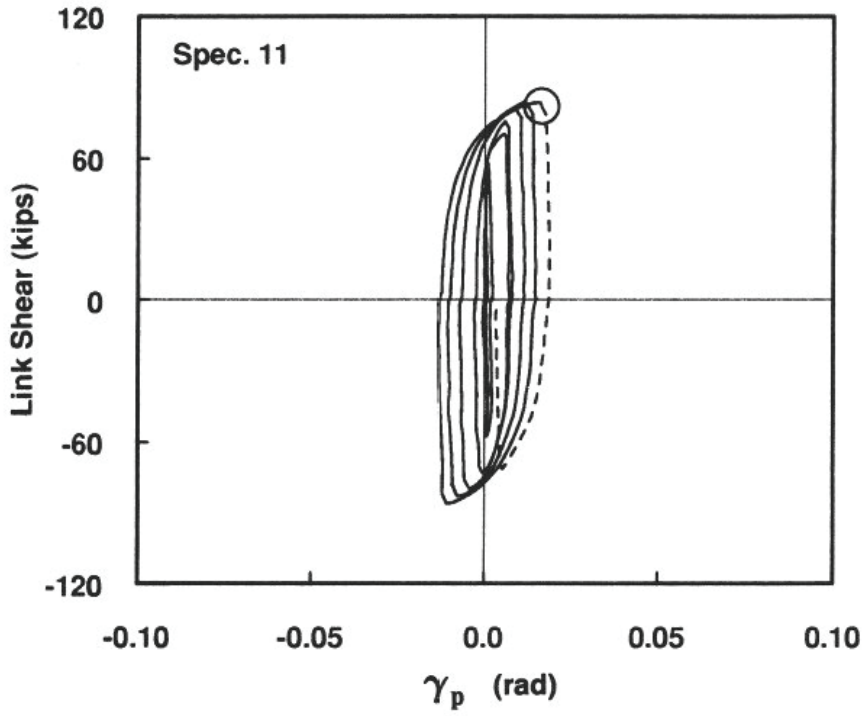

Figure C-89 Force-plastic rotation relationship for link 11 tested by Engelhardt and Popov (1989)

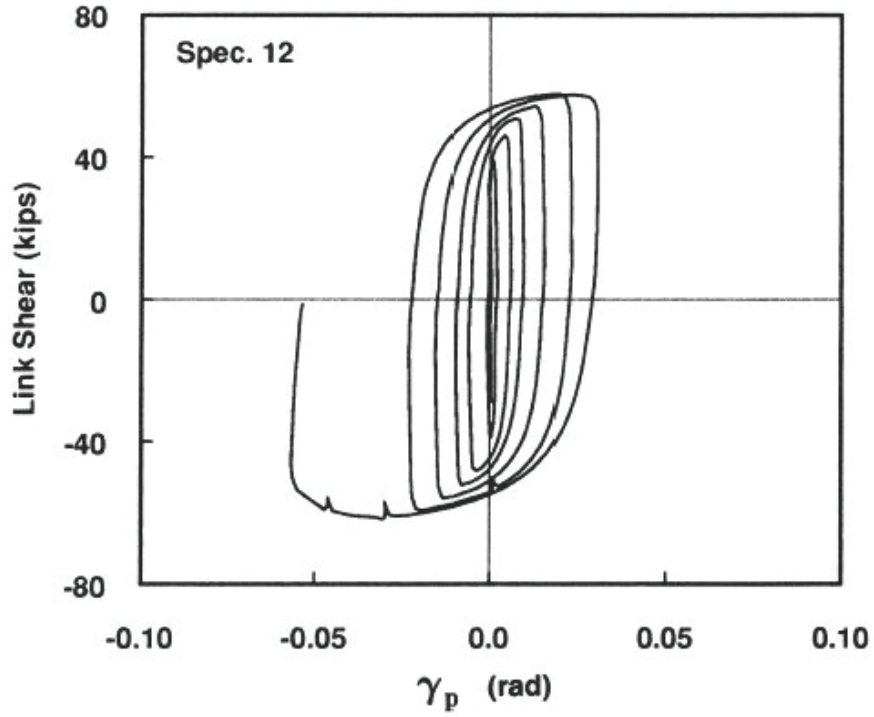

Figure C-90 Force-plastic rotation relationship for link 12 tested by Engelhardt and Popov (1989)

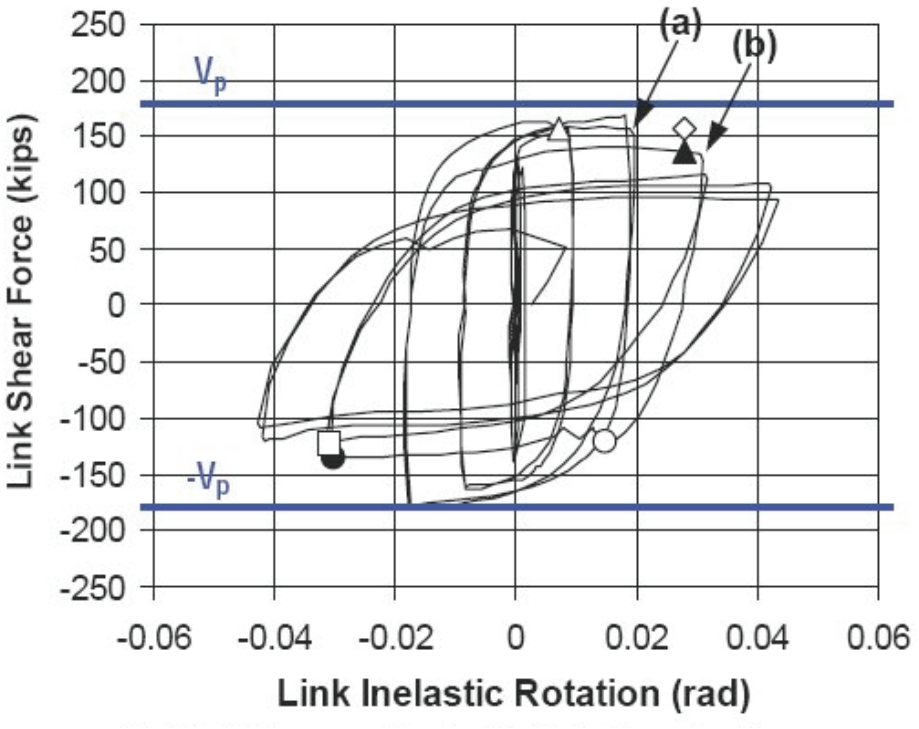

Figure C-91 Force-plastic rotation relationship for link PNI tested by Okazaki (2004)

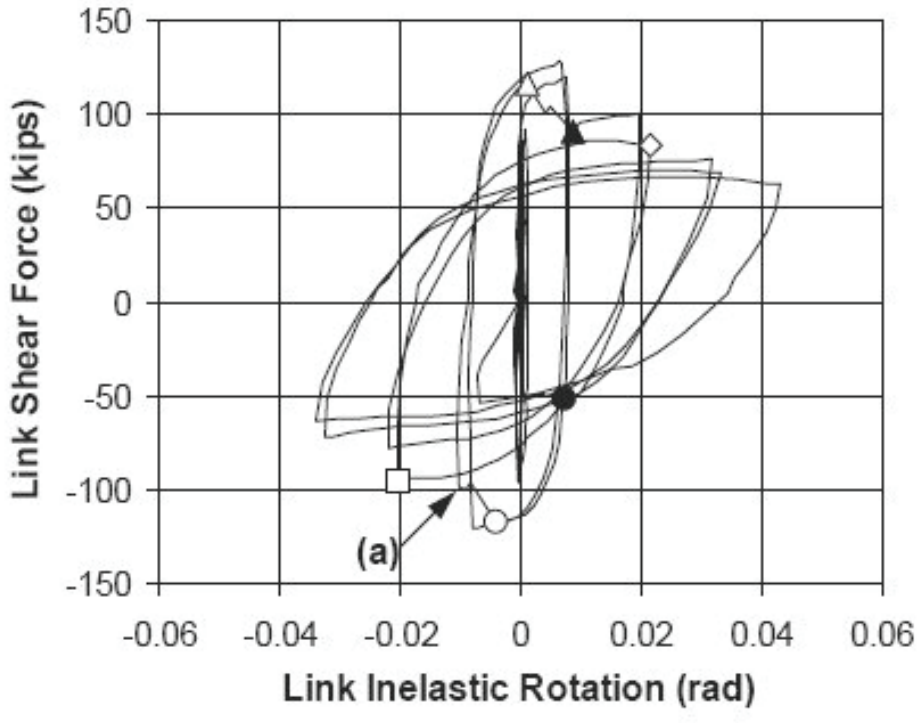

Figure C-92 Force-plastic rotation relationship for link PNM tested by Okazaki (2004)

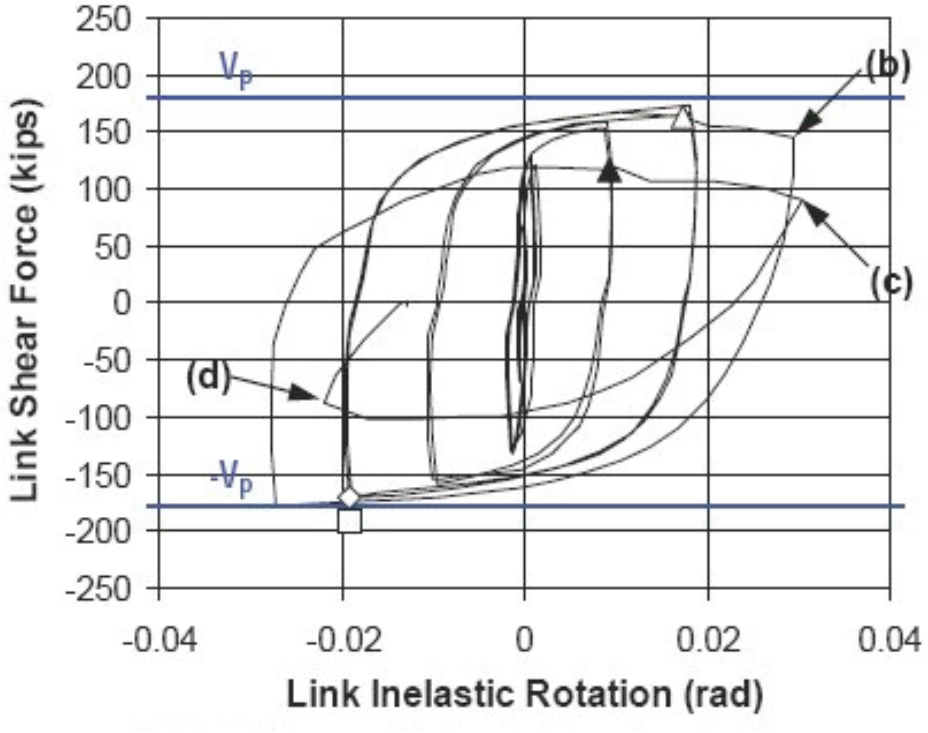

Figure C-93 Force-plastic rotation relationship for link MWI tested by Okazaki (2004)

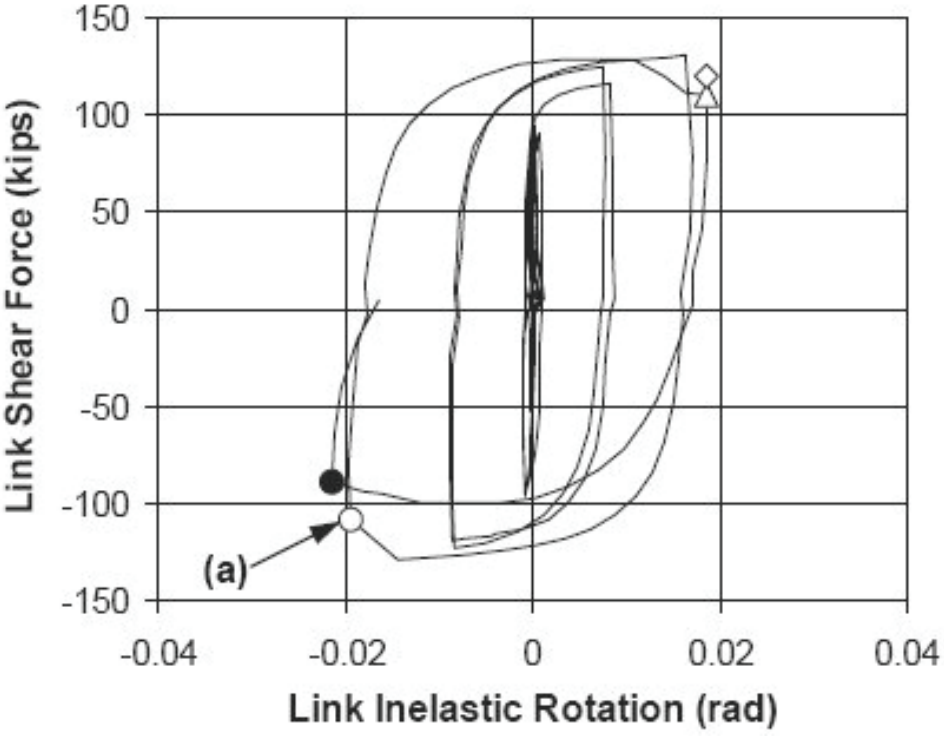

Figure C-94 Force-plastic rotation relationship for link MWM tested by Okazaki (2004)

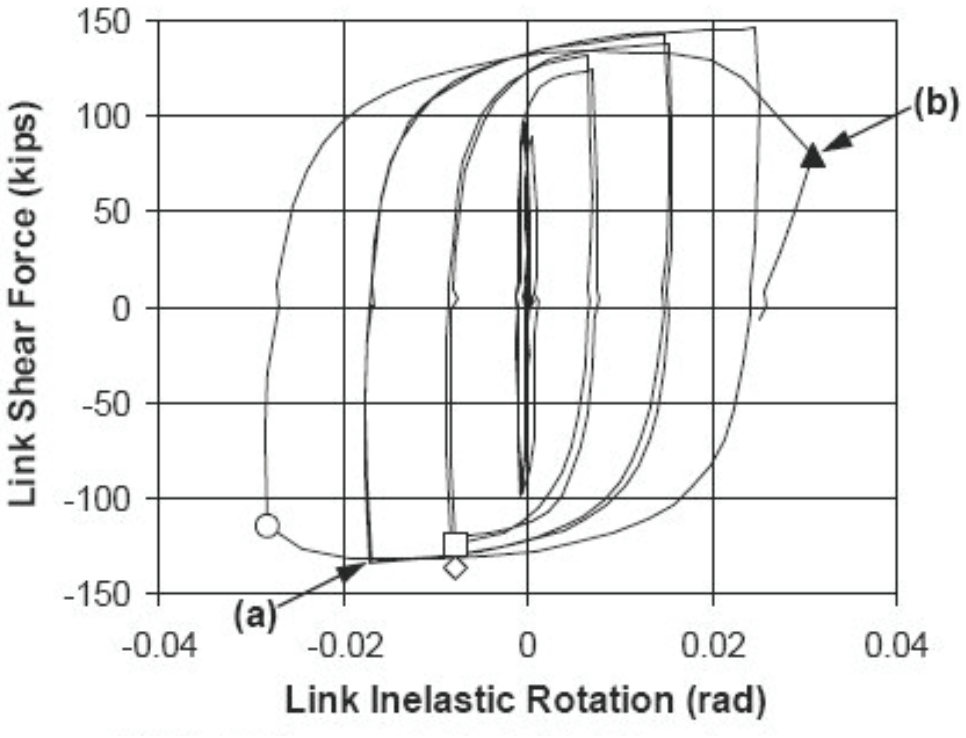

Figure C-95 Force-plastic rotation relationship for link FFI tested by Okazaki (2004)

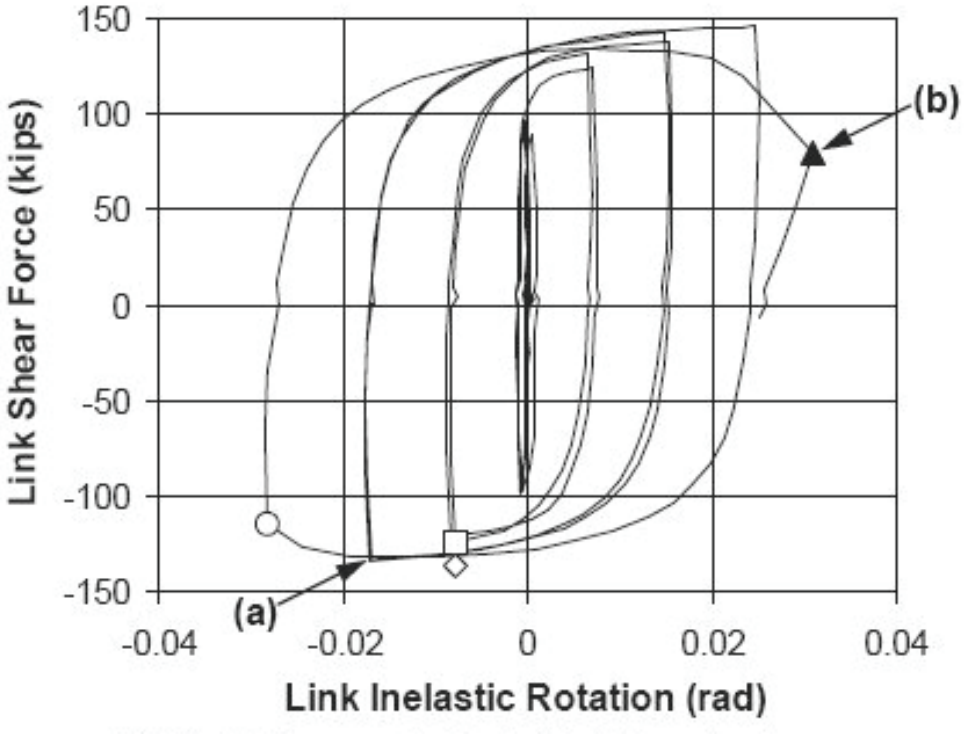

Figure C-96 Force-plastic rotation relationship for link FFM tested by Okazaki (2004)

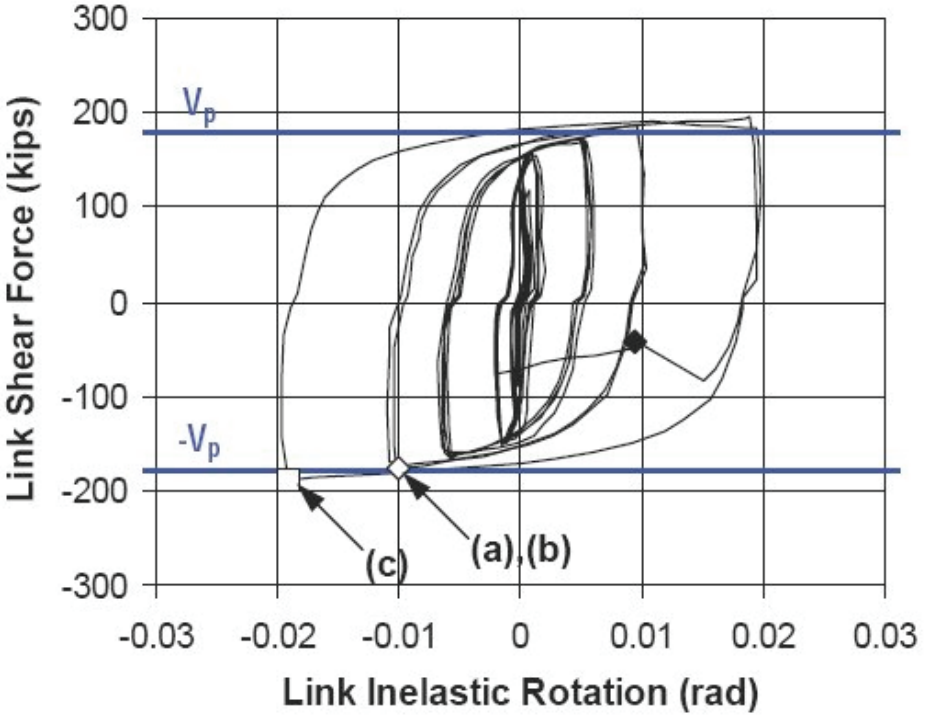

Figure C-97 Force-plastic rotation relationship for link FFSL-RLP tested by Okazaki (2004)

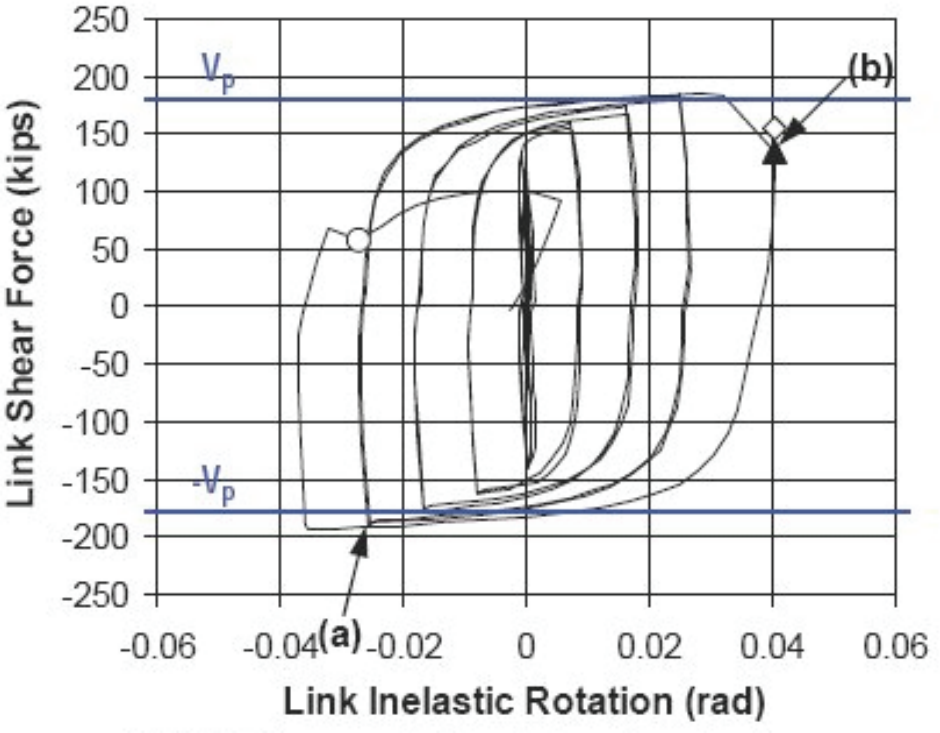

Figure C-98 Force-plastic rotation relationship for link NAI tested by Okazaki (2004)

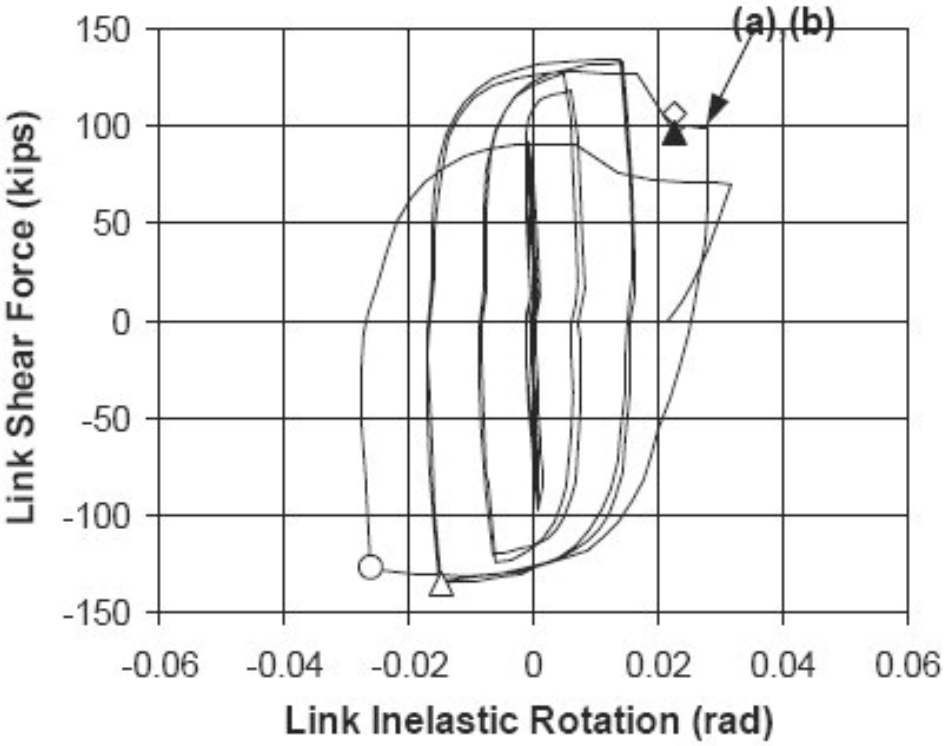

Figure C-99 Force-plastic rotation relationship for link NAM tested by Okazaki (2004)

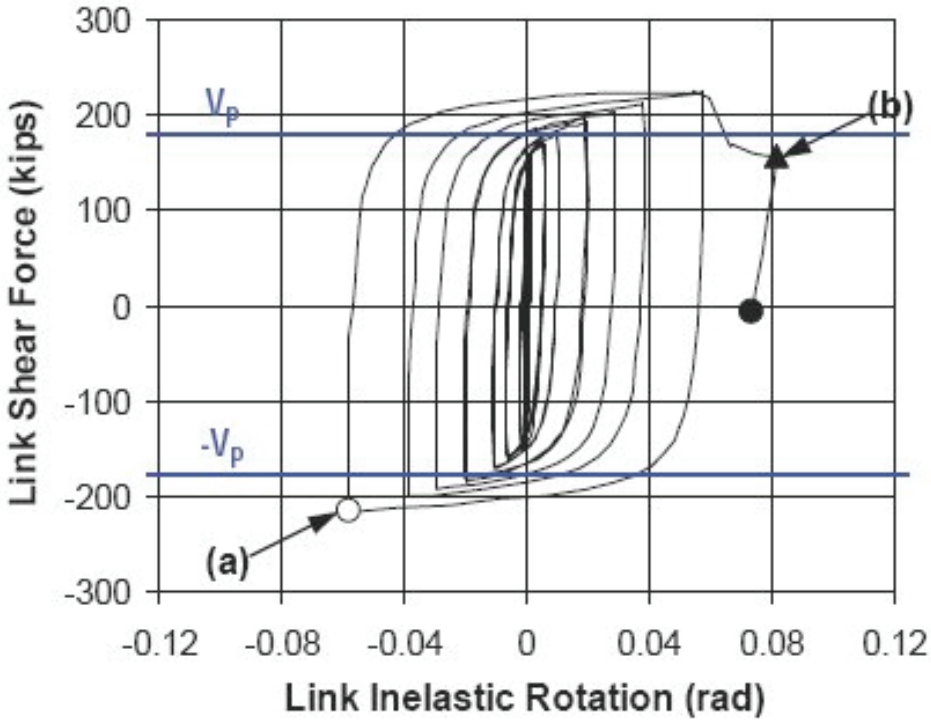

Figure C-100 Force-plastic rotation relationship for link NASL-RLP tested by Okazaki (2004)

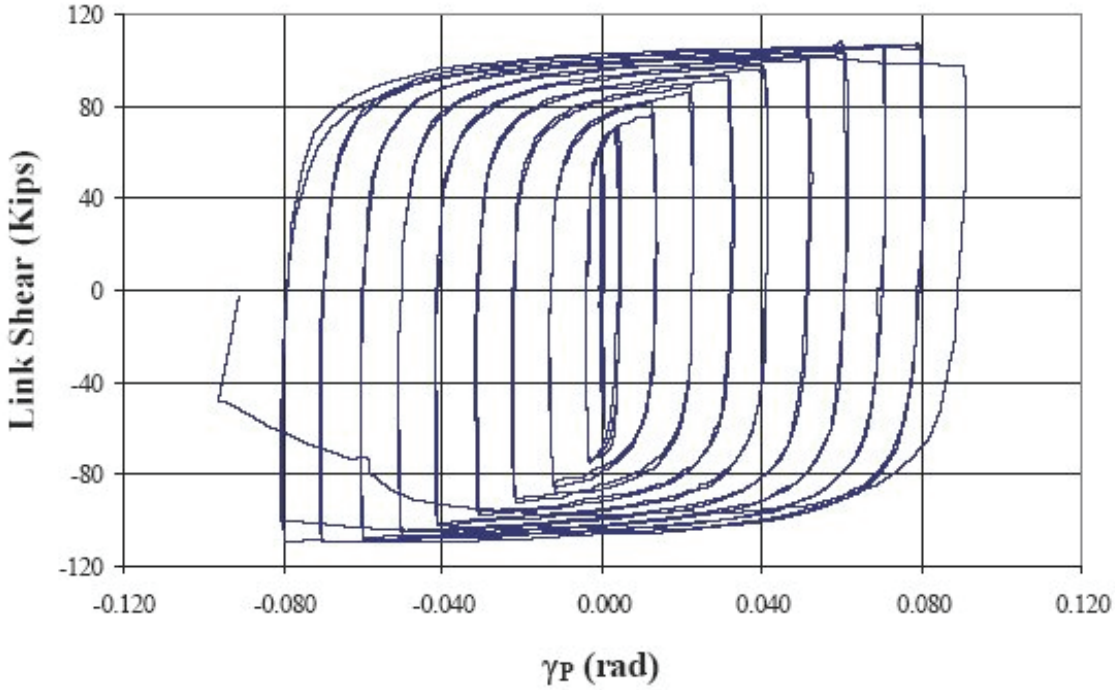

Figure C-101 Force-plastic rotation relationship for link 1c tested by Arce (2002)

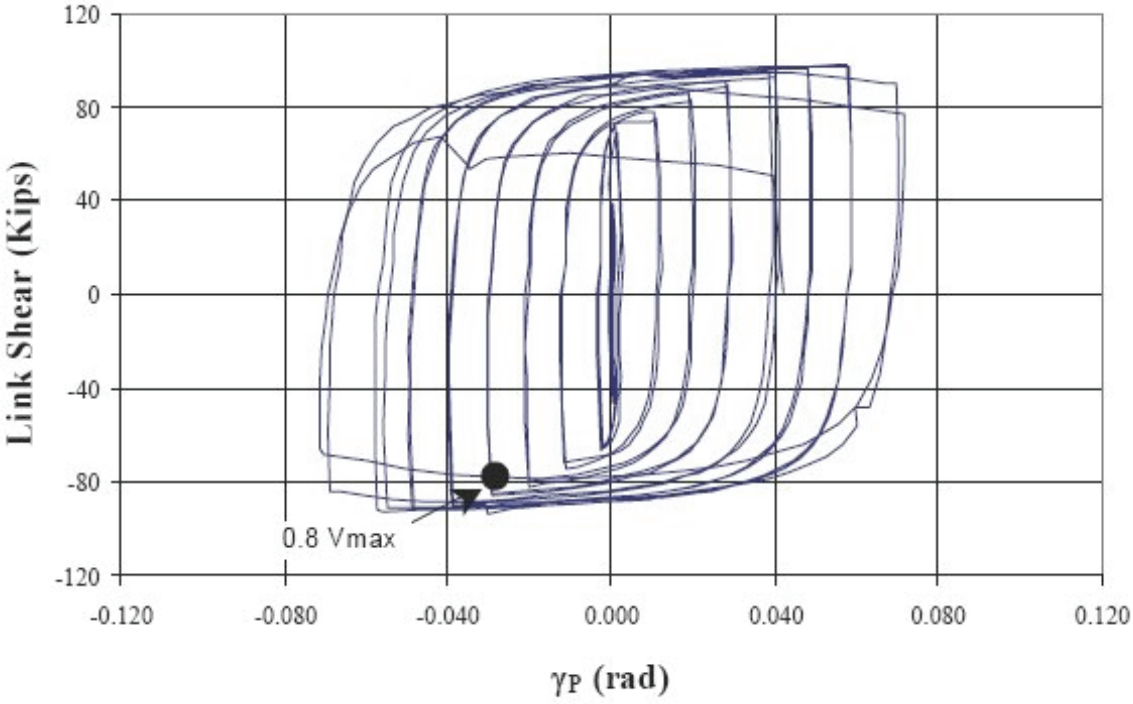

Figure C-102 Force-plastic rotation relationship for link 2 tested by Arce (2002)

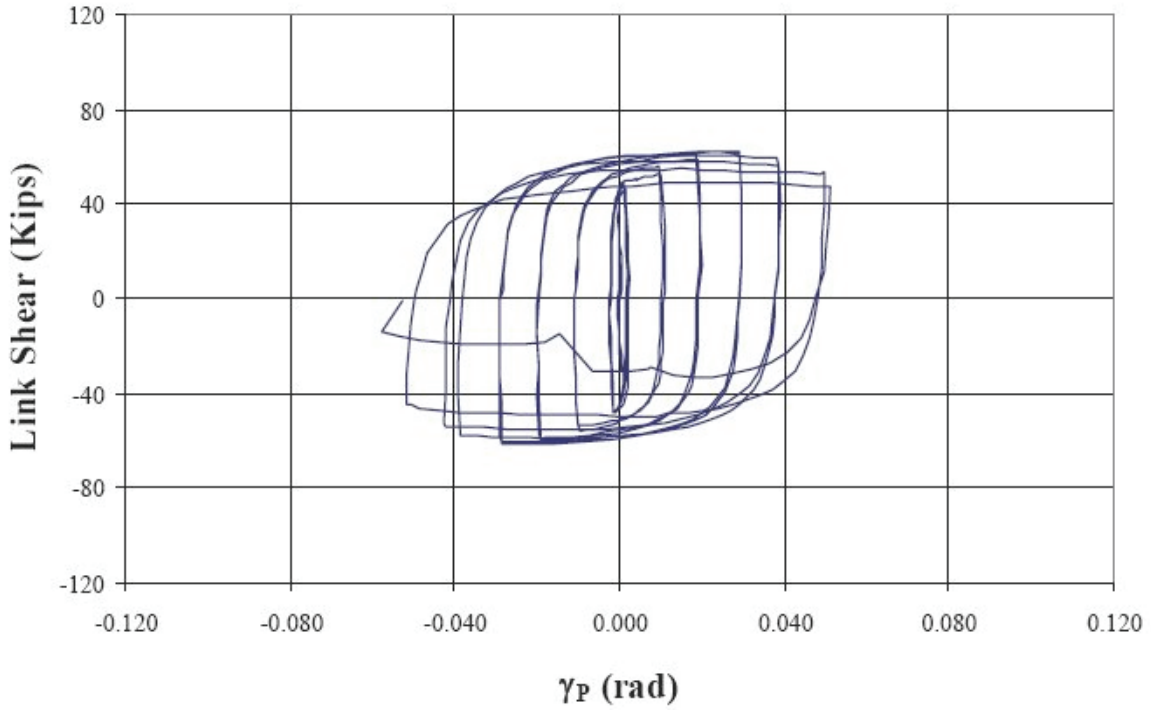

Figure C-103 Force-plastic rotation relationship for link 3 tested by Arce (2002)

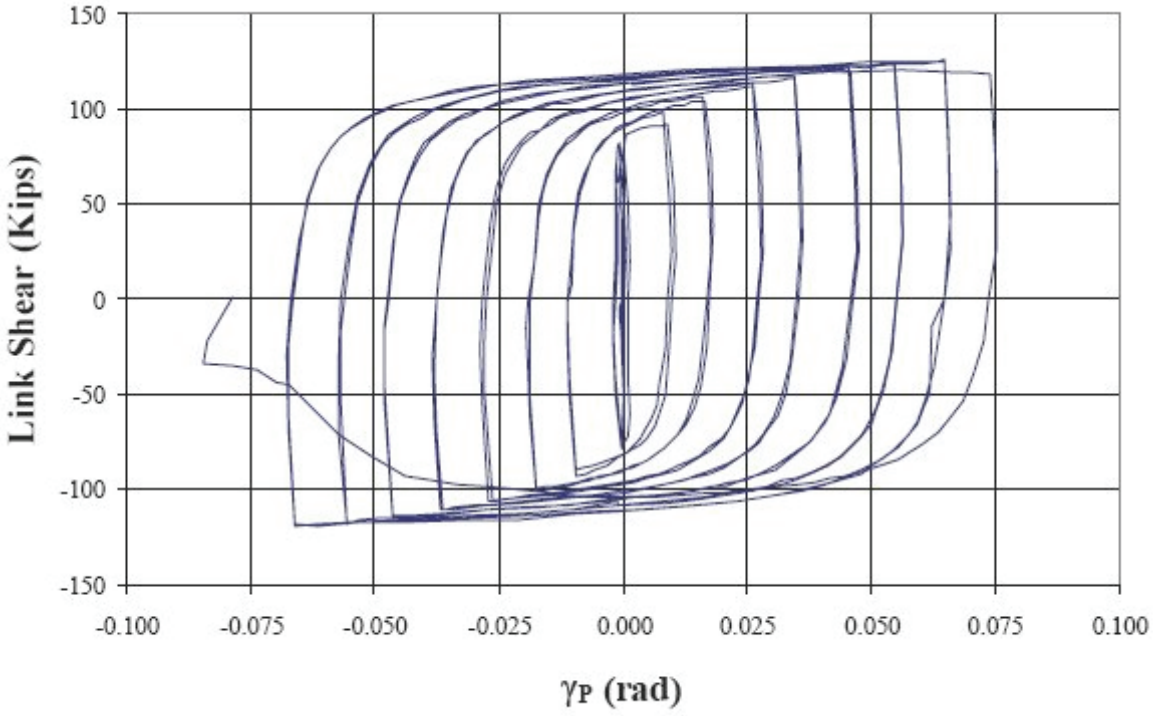

Figure C-104 Force-plastic rotation relationship for link 5 tested by Arce (2002)

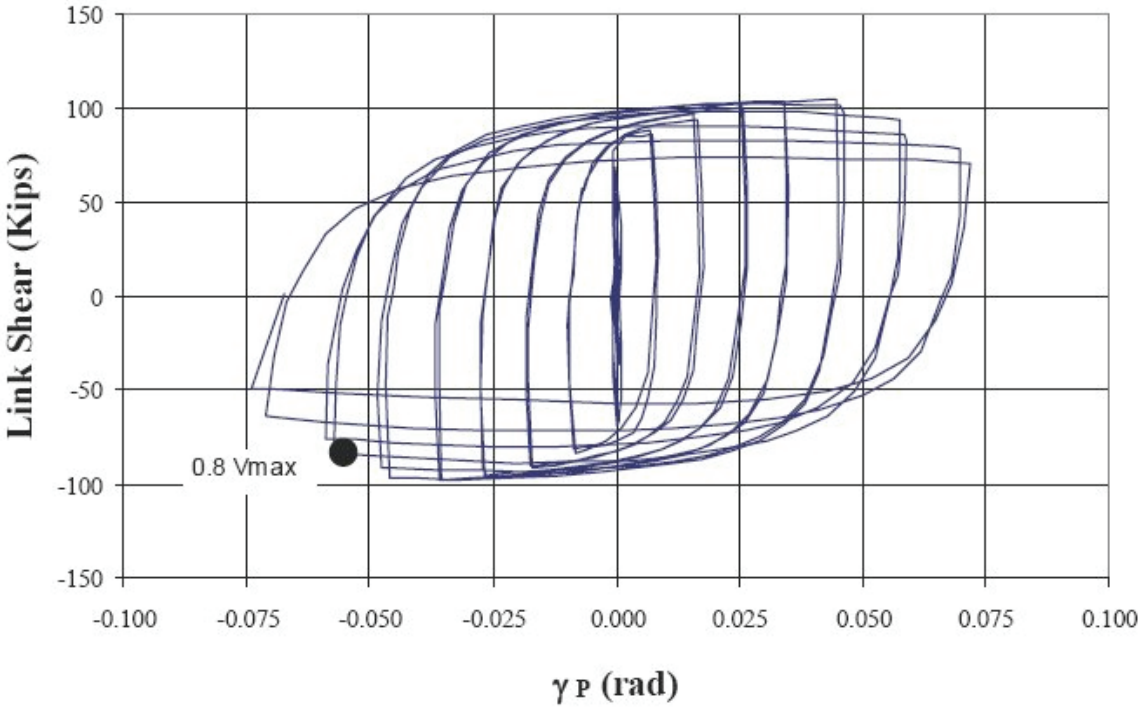

Figure C-105 Force-plastic rotation relationship for link 6b tested by Arce (2002)

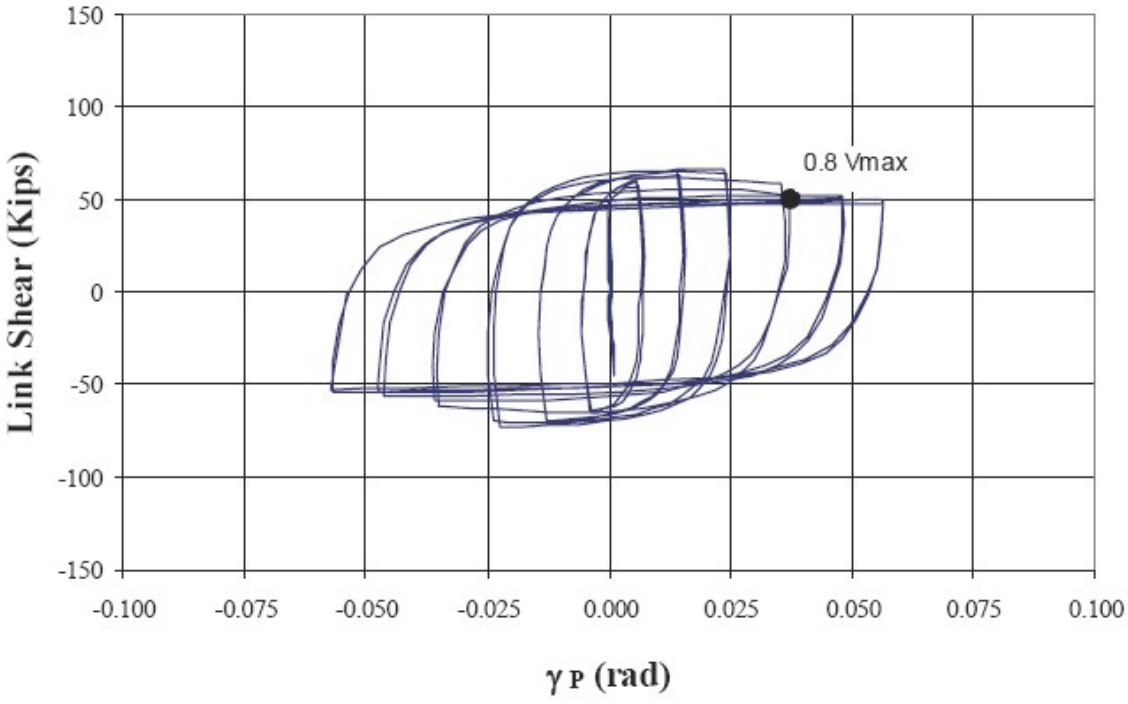

Figure C-106 Force-plastic rotation relationship for link 7 tested by Arce (2002)

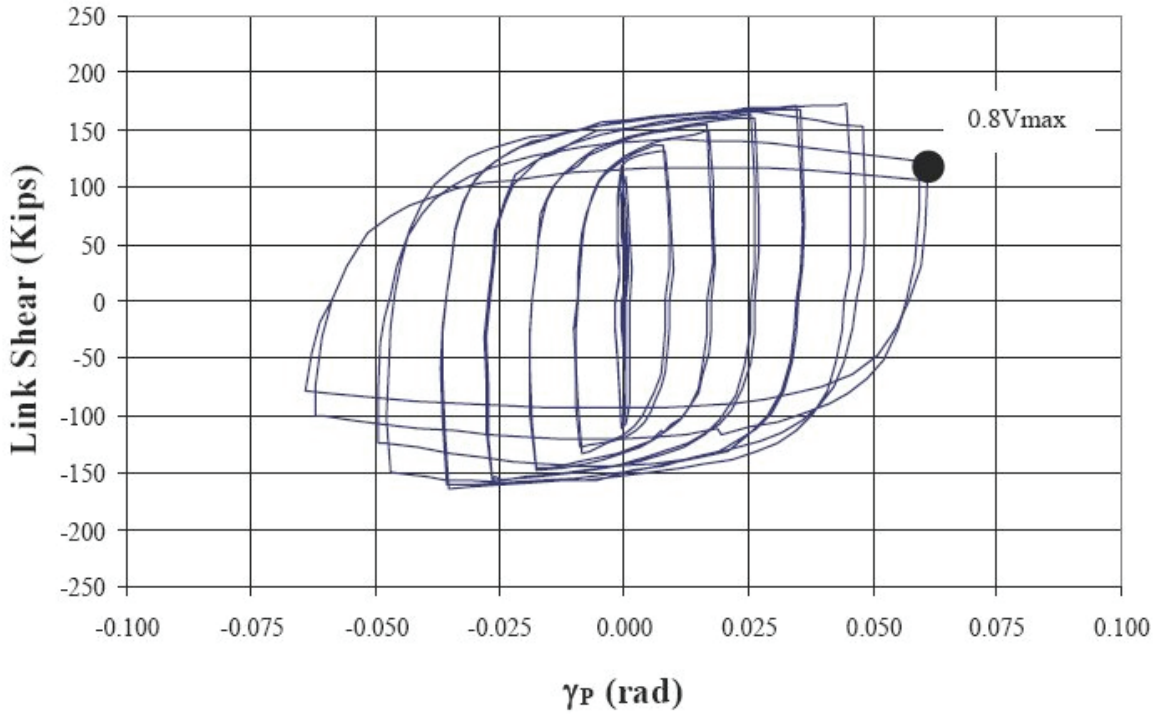

Figure C-107 Force-plastic rotation relationship for link 9 tested by Arce (2002)

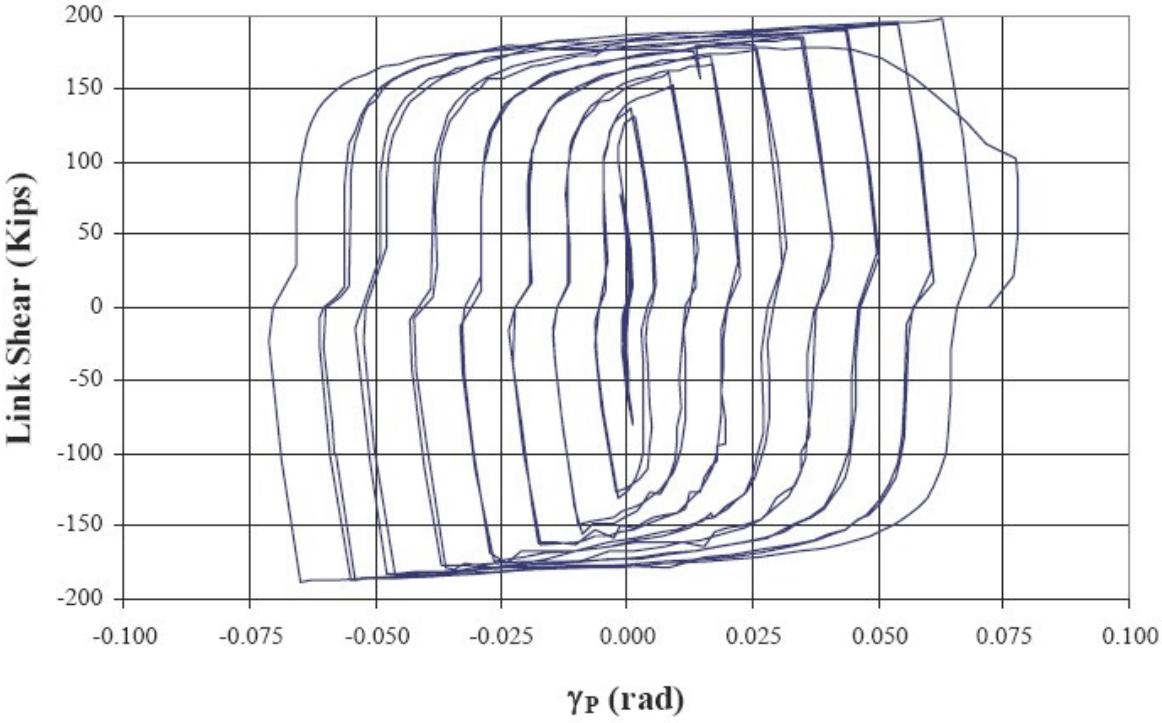

Figure C-108 Force-plastic rotation relationship for link 11 tested by Arce (2002)

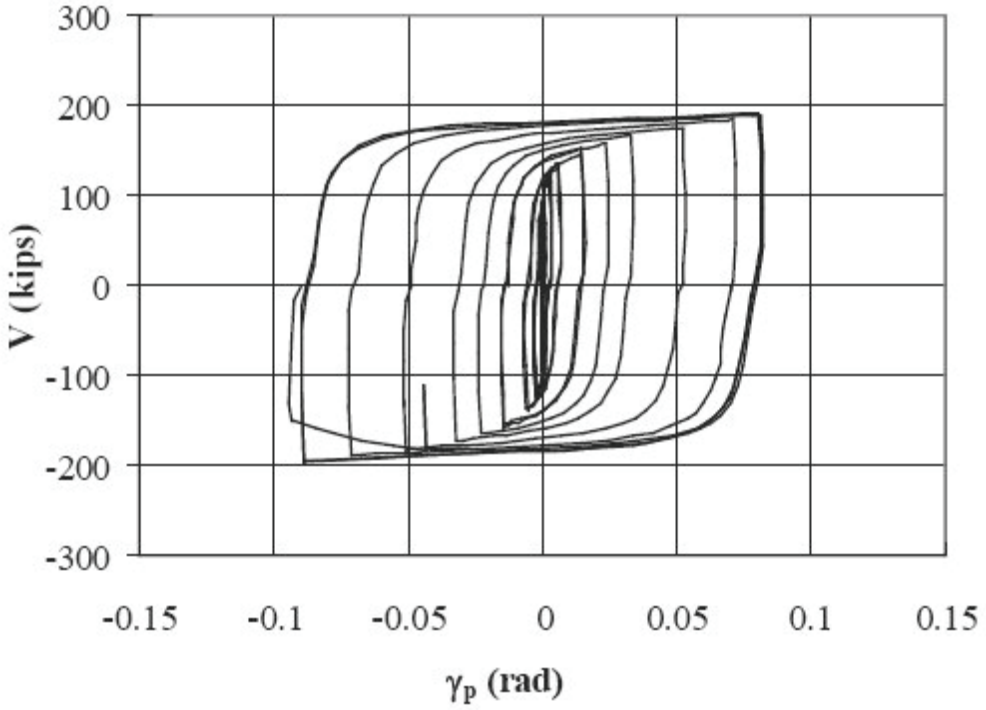

Figure C-109 Force-plastic rotation relationship for link 11-RLP tested by Ryu (2005)

Appendix D – Damage Photos

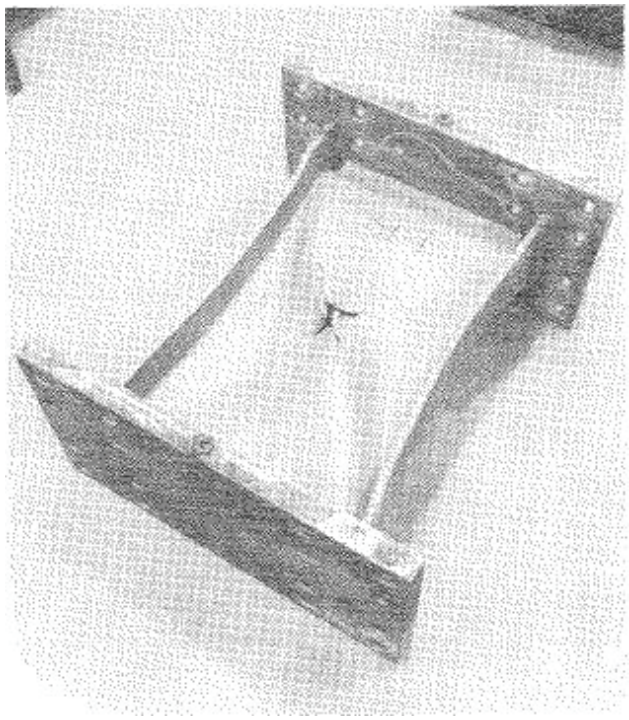

Figure D-1 Final condition of specimen 1 tested by Hjelmstad and Popov (1983)

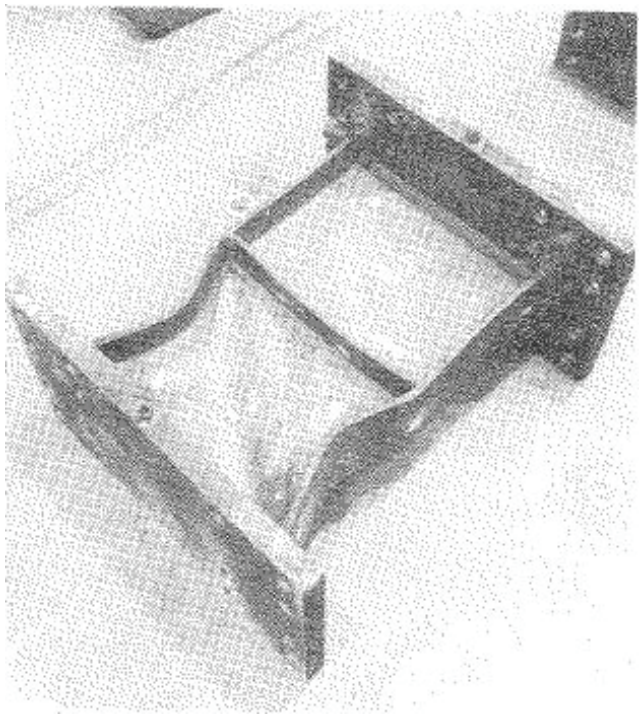

Figure D-2 Final condition of specimen 2 tested by Hjelmstad and Popov (1983)

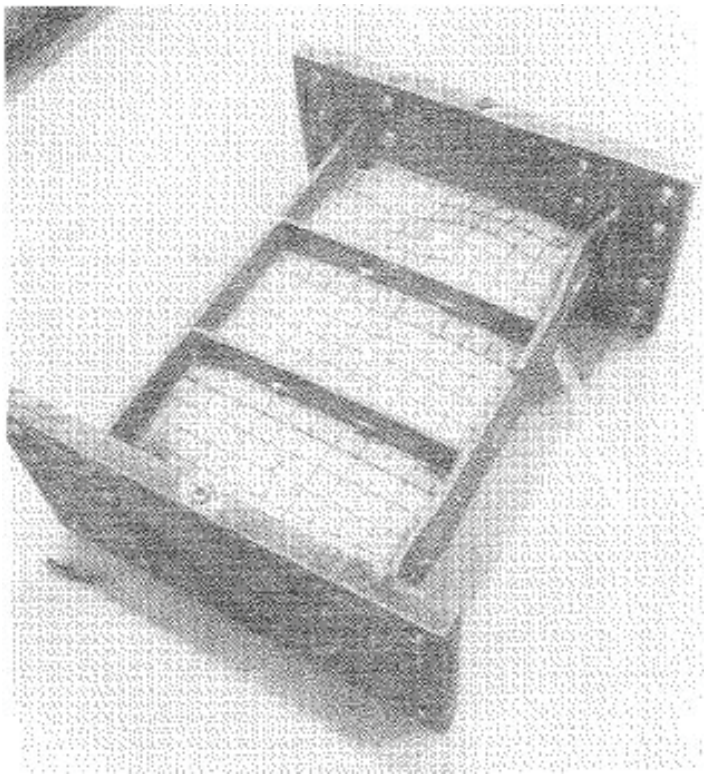

Figure D-3 Final condition of specimen 3 tested by Hjelmstad and Popov (1983)

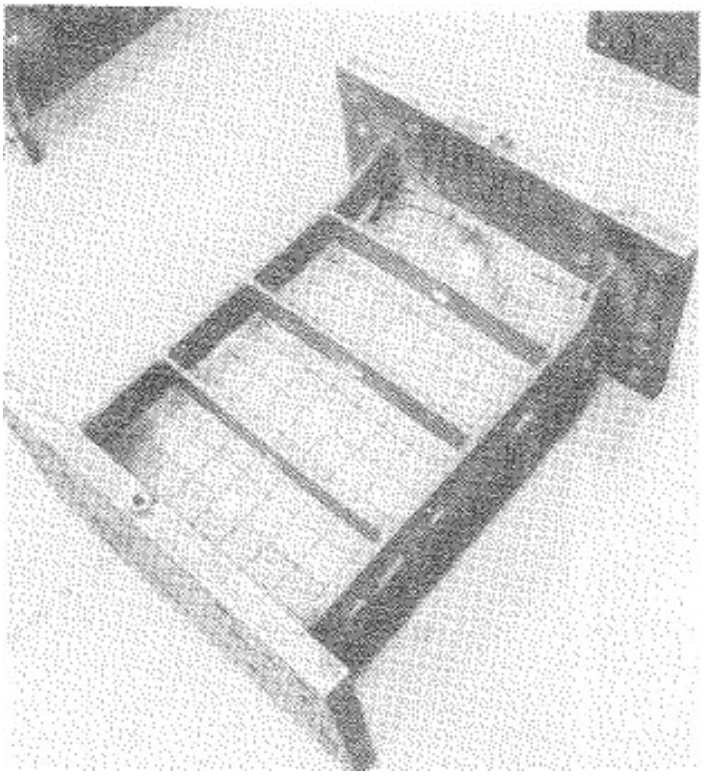

Figure D-4 Final condition of specimen 4 tested by Hjelmstad and Popov (1983)

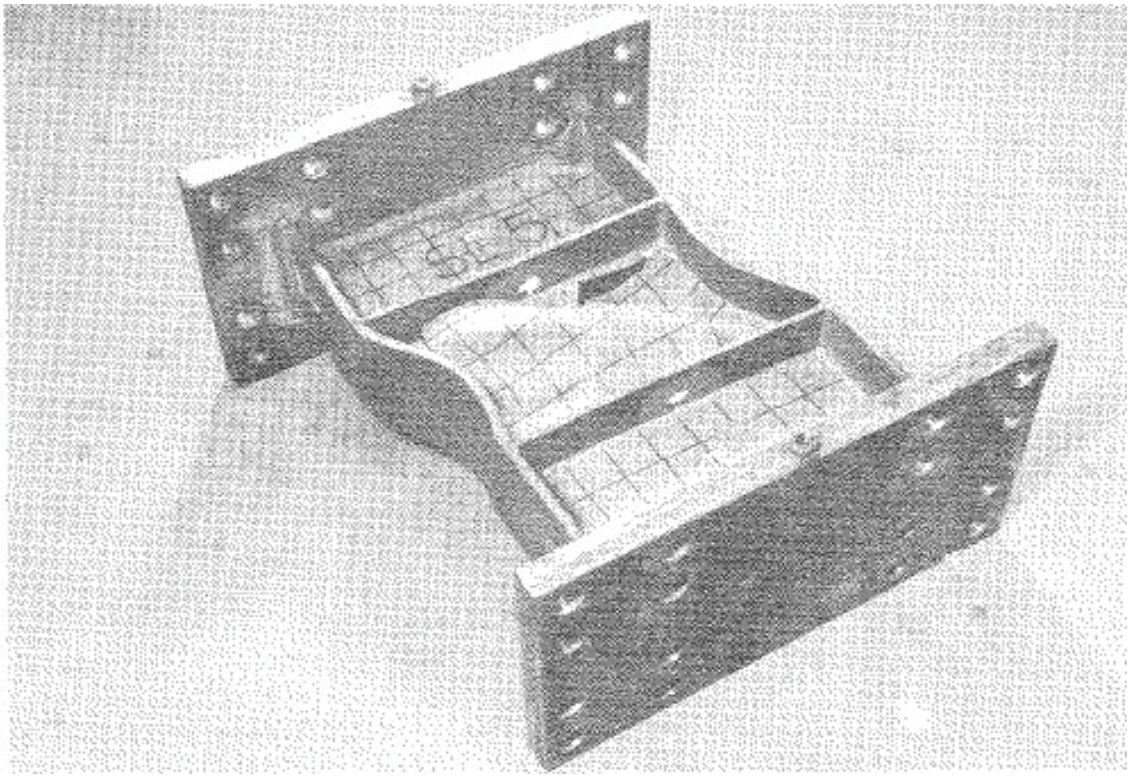

Figure D-5 Final condition of specimen 5 tested by Hjelmstad and Popov (1983)

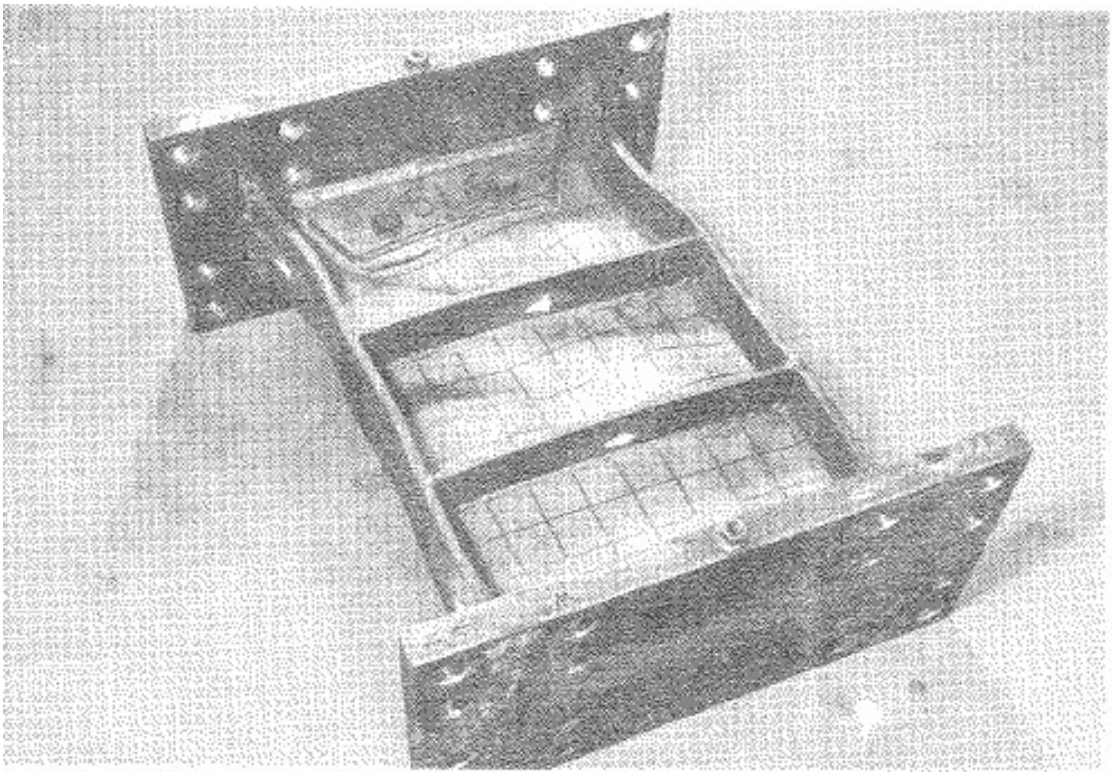

Figure D-6 Final condition of specimen 6 tested by Hjelmstad and Popov (1983)

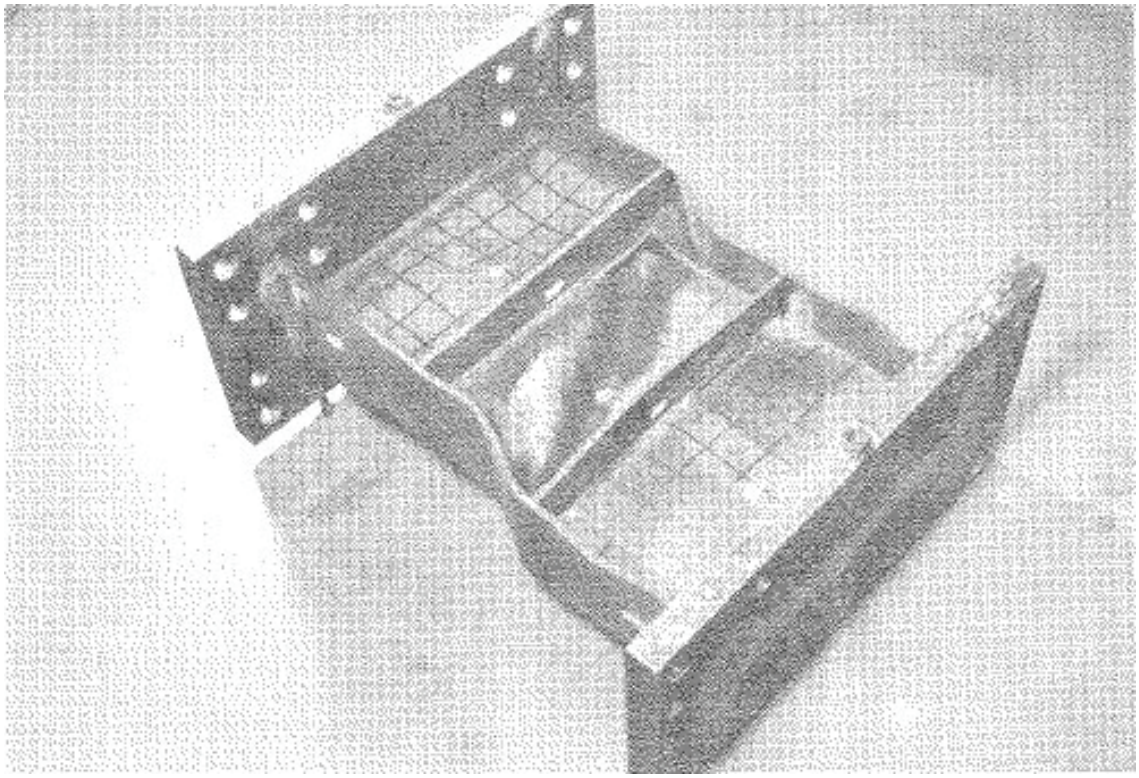

Figure D-7 Final condition of specimen 7 tested by Hjelmstad and Popov (1983)

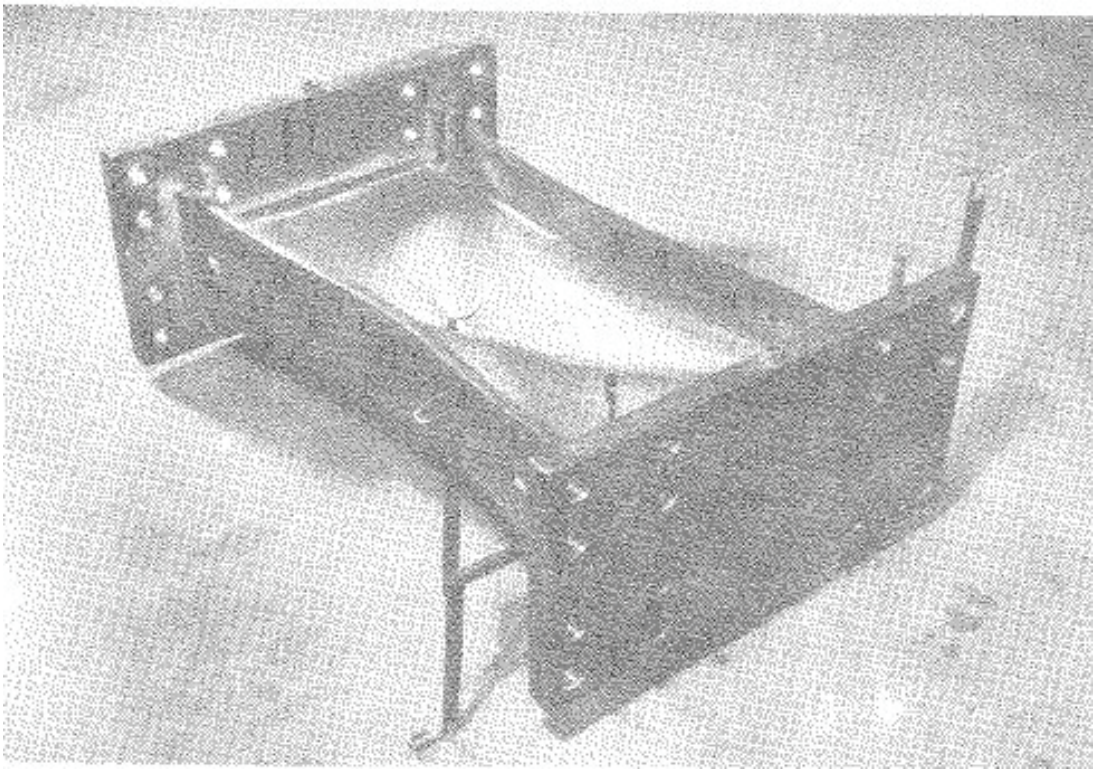

Figure D-8 Final condition of specimen 8 tested by Hjelmstad and Popov (1983)

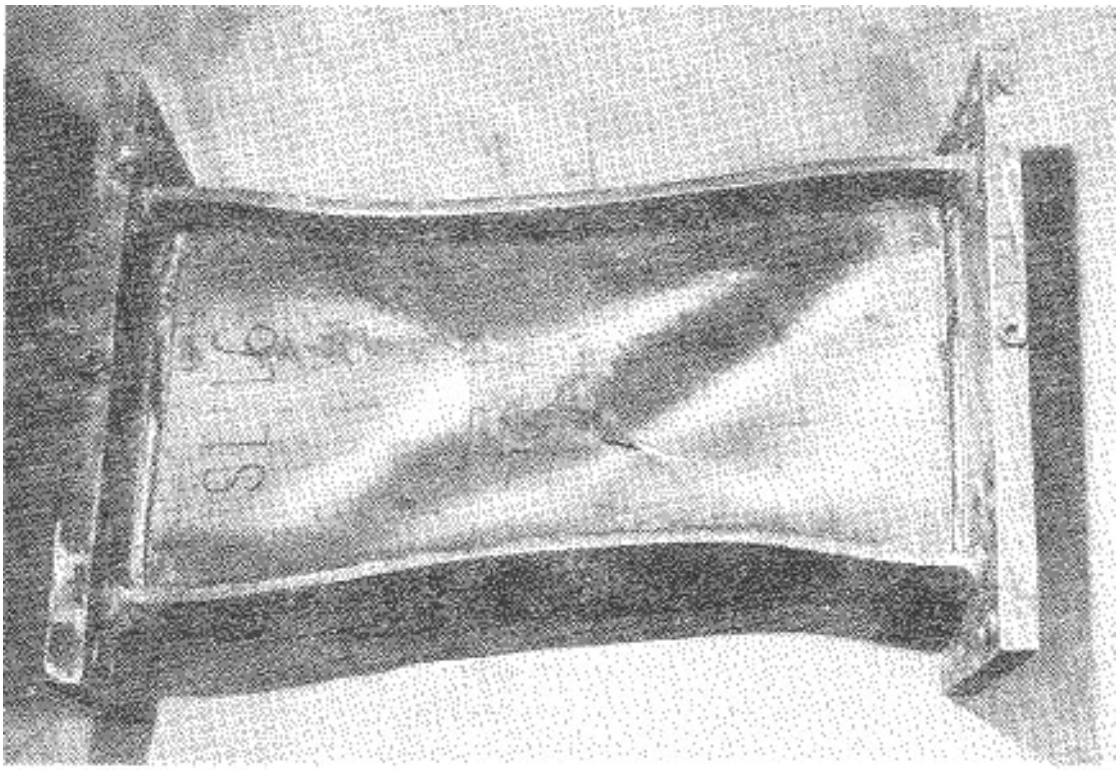

Figure D-9 Final condition of specimen 16 tested by Malley and Popov (1983)

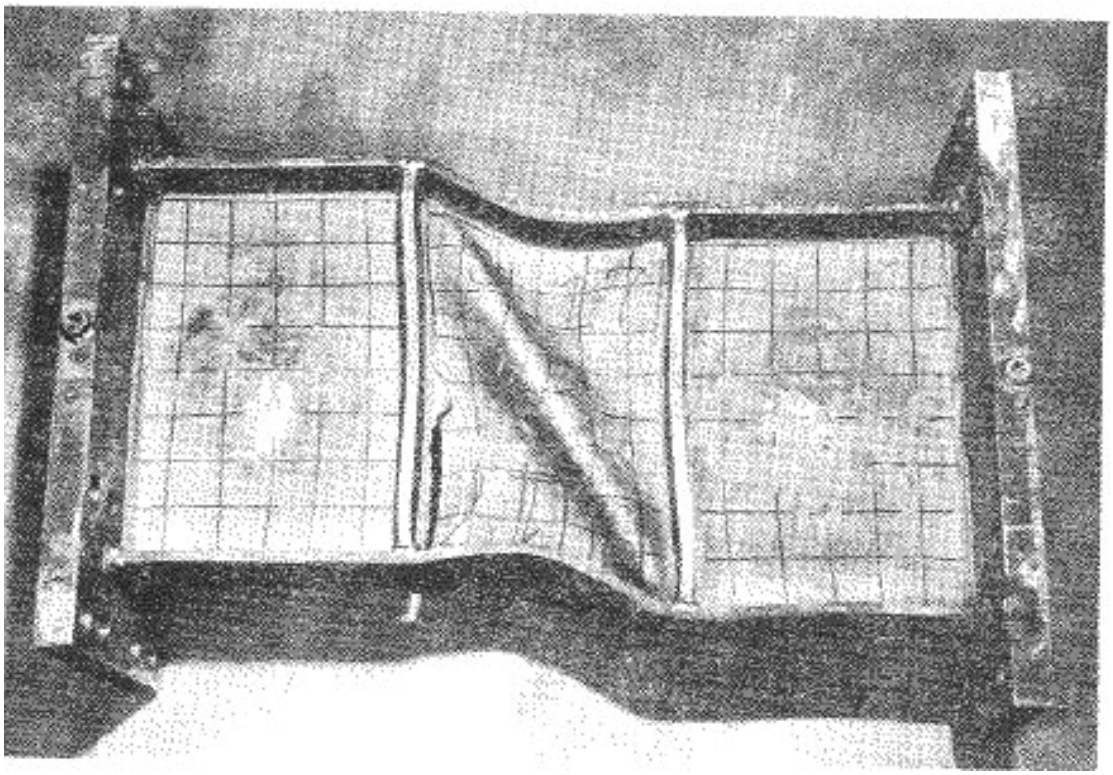

Figure D-10 Final condition of specimen 17 tested by Malley and Popov (1983)

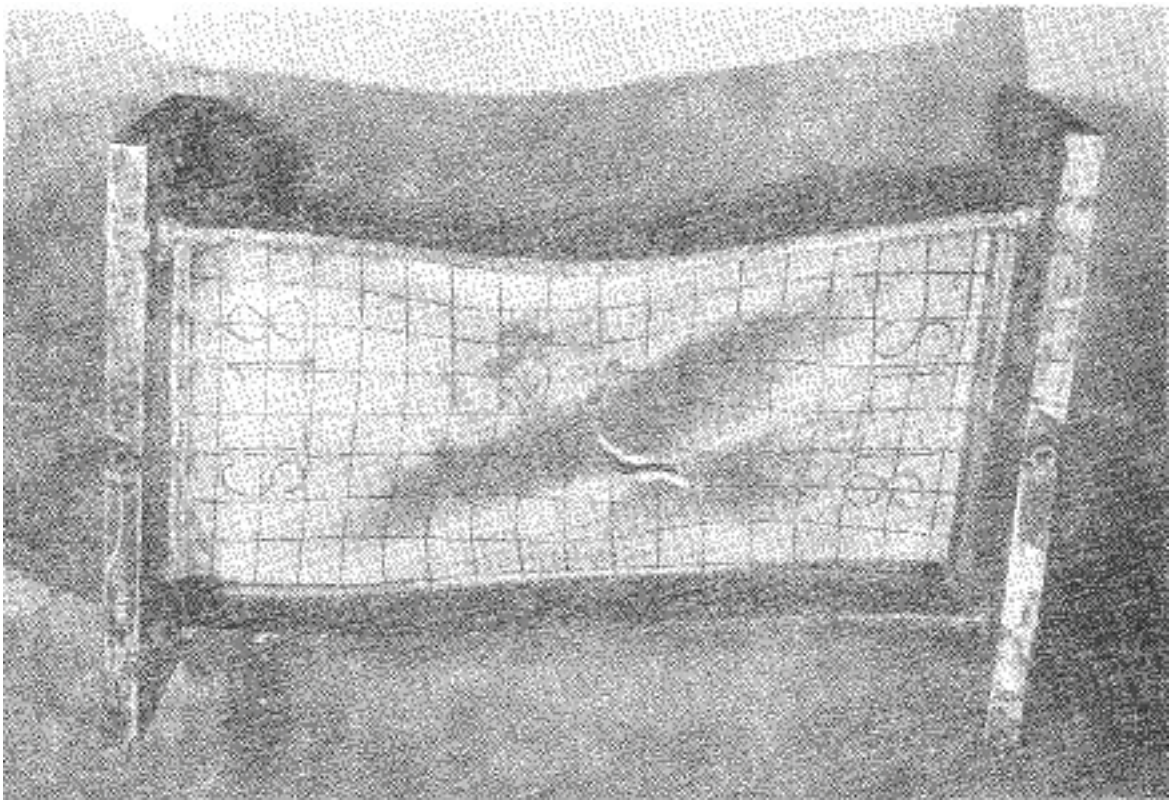

Figure D-11 Final condition of specimen 18 tested by Malley and Popov (1983)

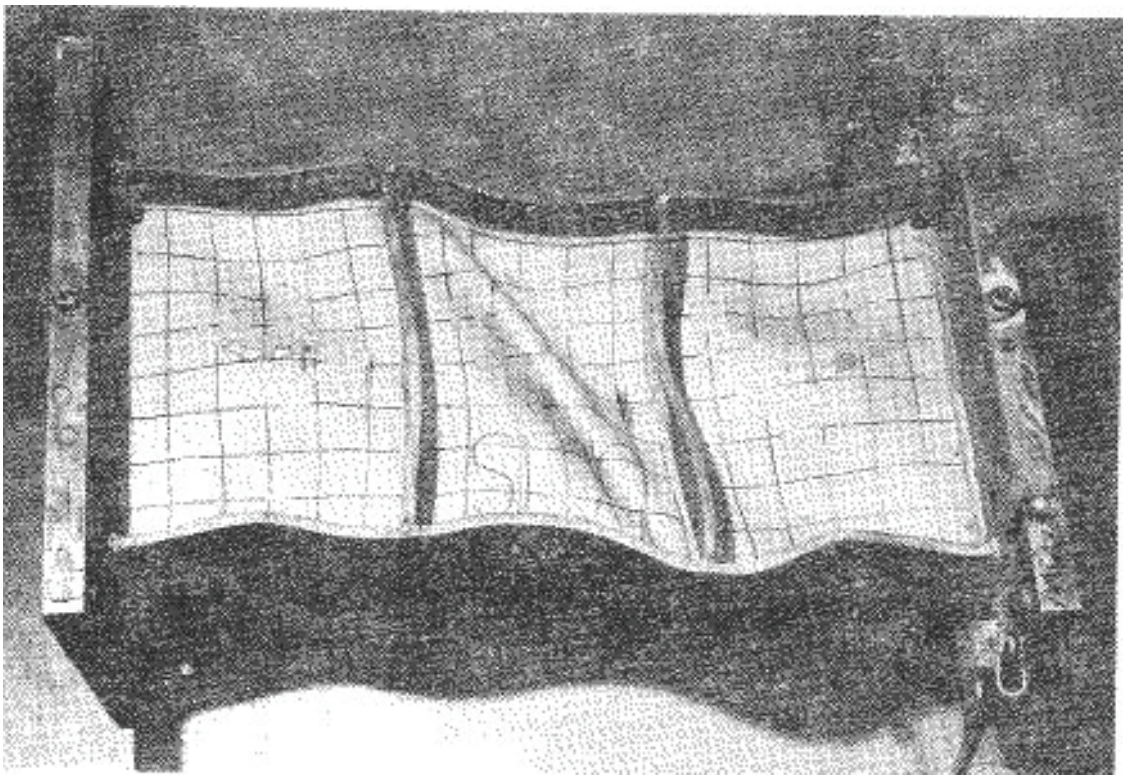

Figure D-12 Final condition of specimen 20 tested by Malley and Popov (1983)

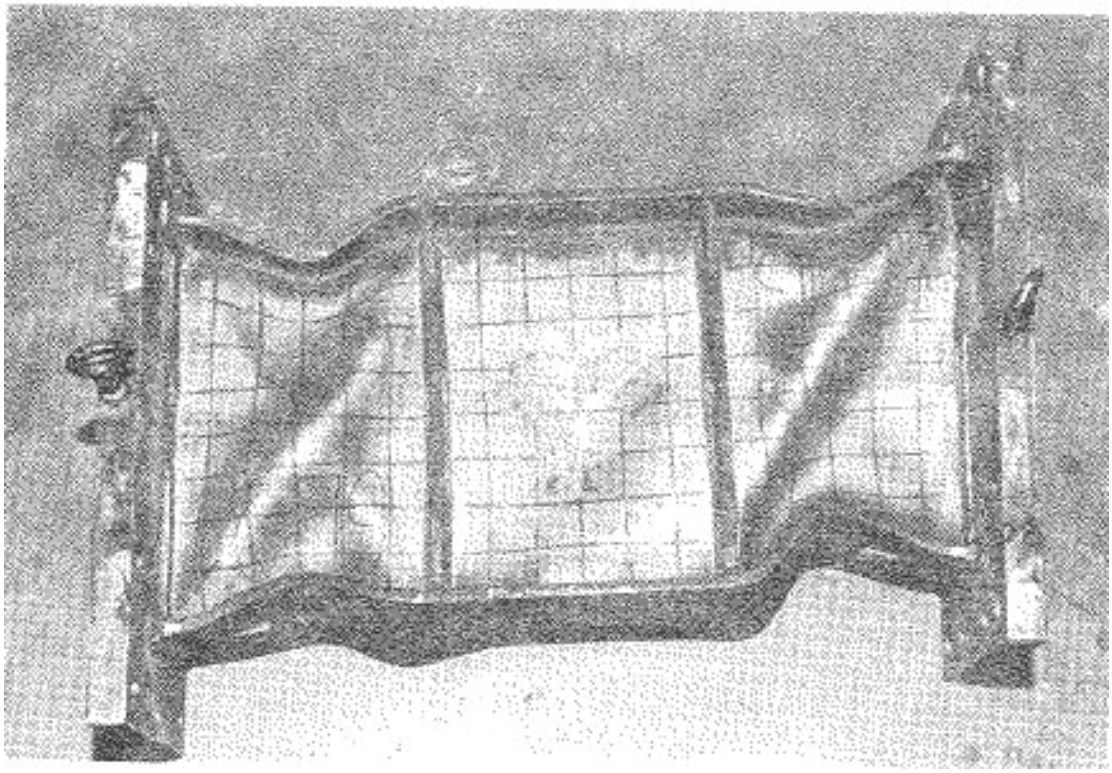

Figure D-13 Final condition of specimen 21 tested by Malley and Popov (1983)

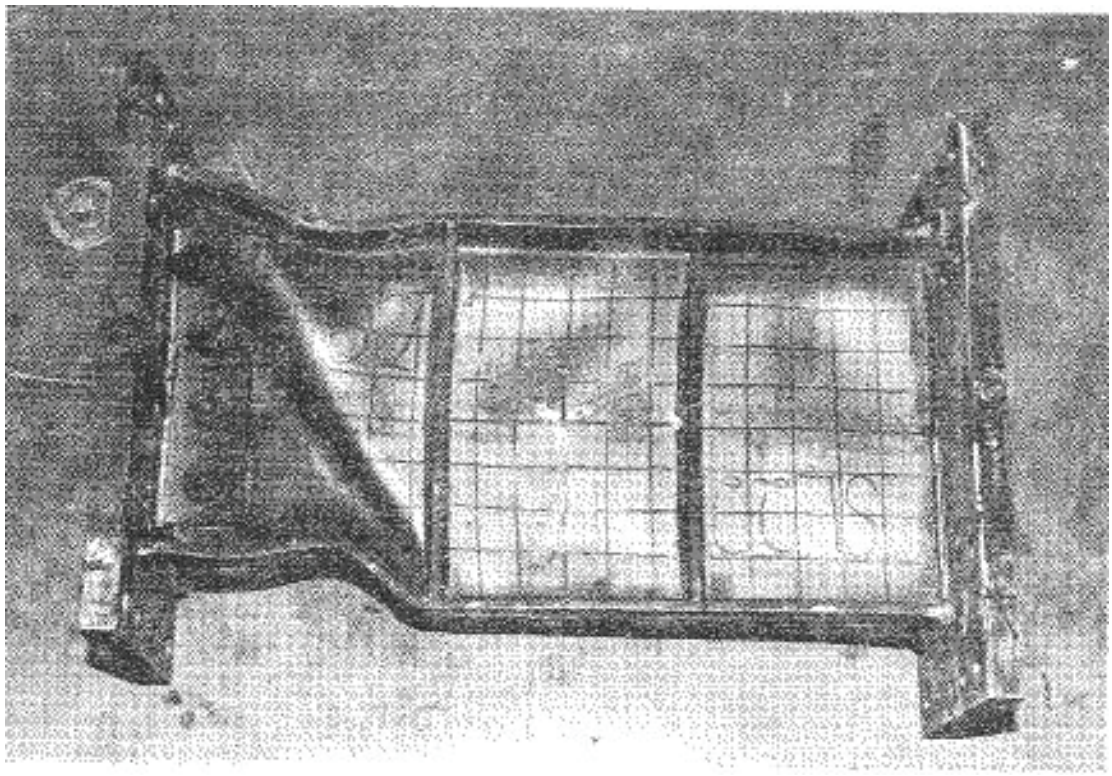

Figure D-14 Final condition of specimen 22 tested by Malley and Popov (1983)

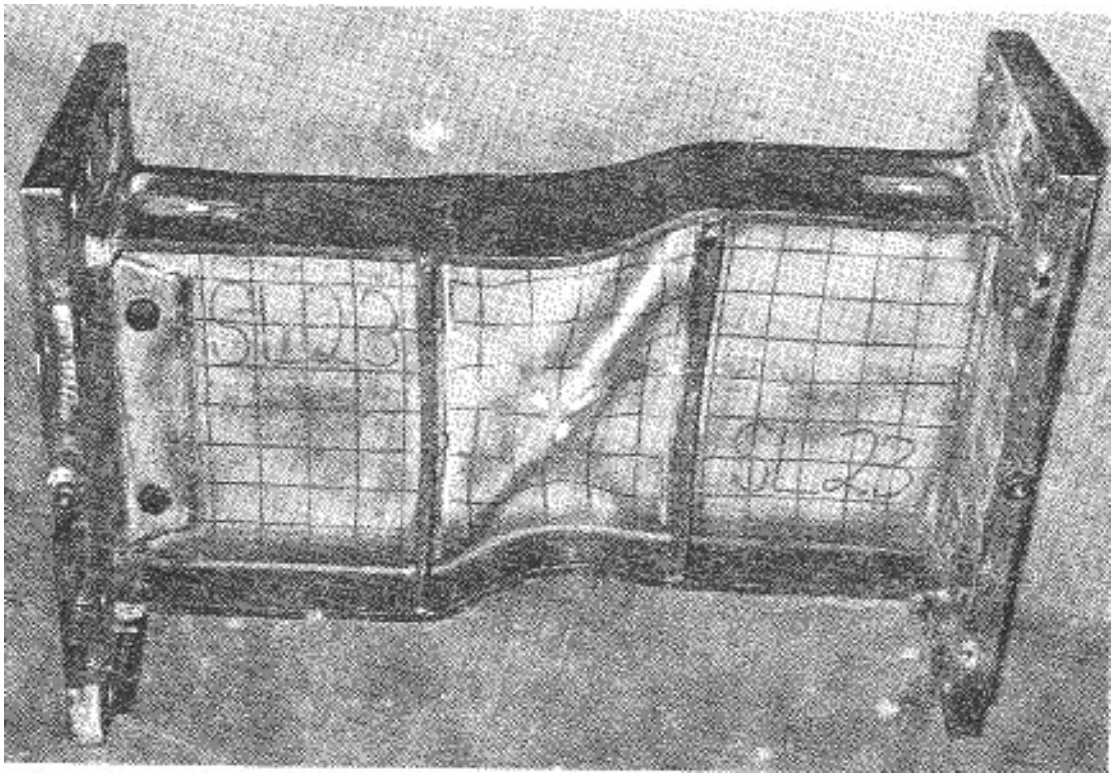

Figure D-15 Final condition of specimen 23 tested by Malley and Popov (1983)

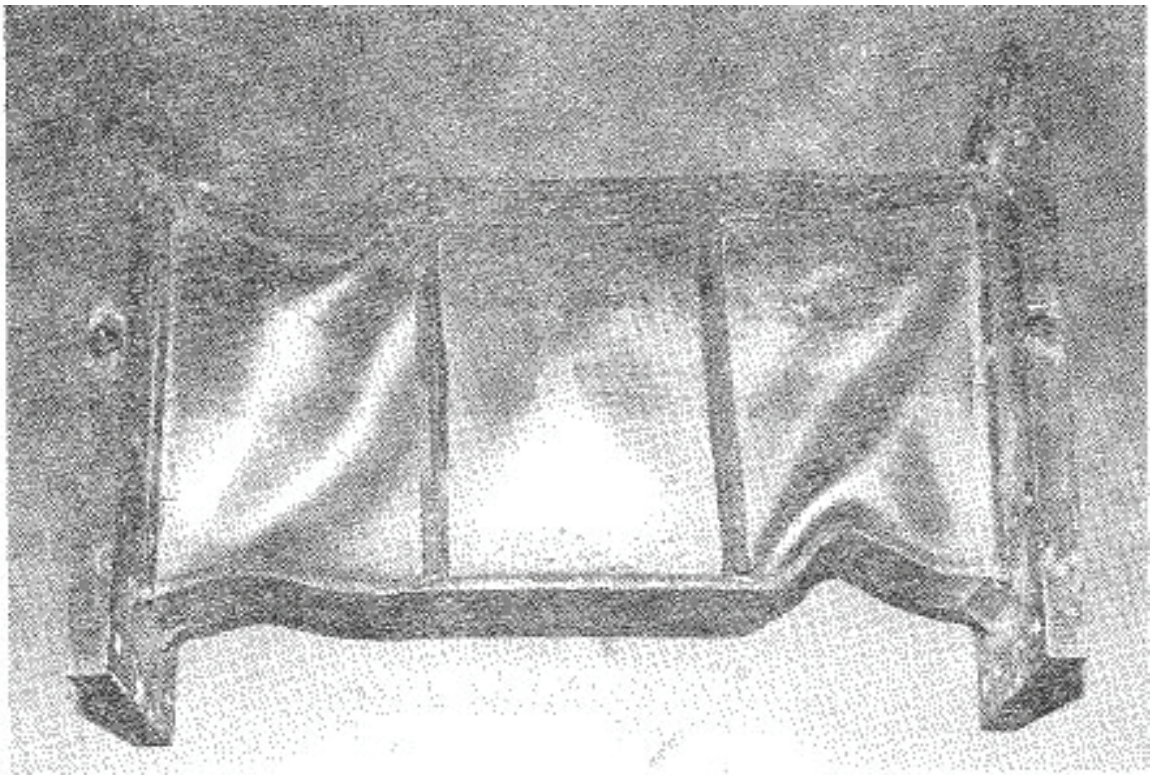

Figure D-16 Final condition of specimen 24 tested by Malley and Popov (1983)

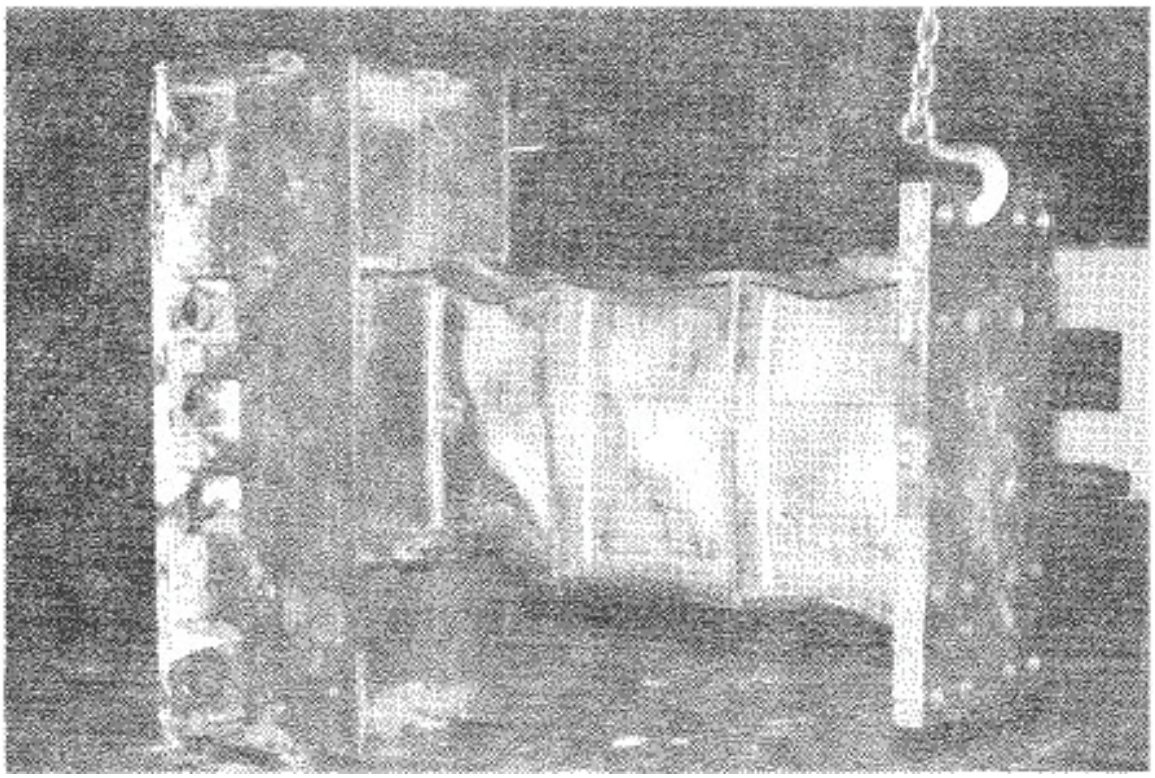

Figure D-17 Final condition of specimen 25 tested by Malley and Popov (1983)

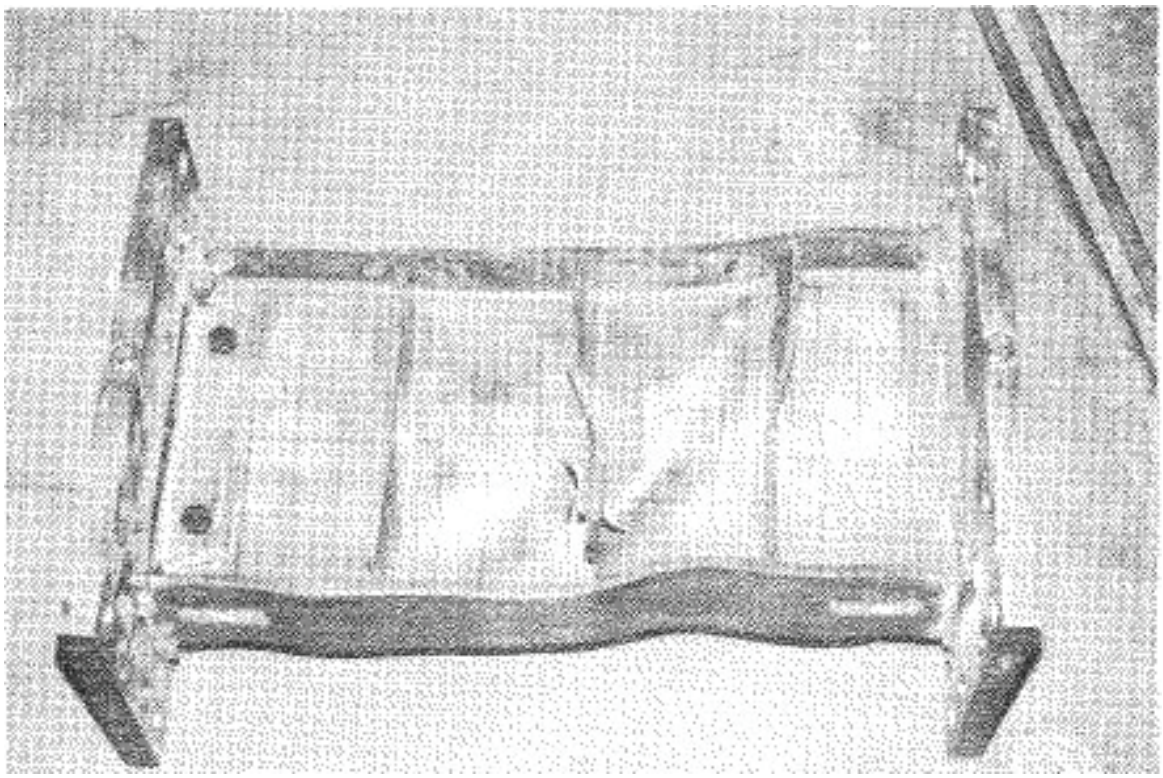

Figure D-18 Final condition of specimen 26 tested by Malley and Popov (1983)

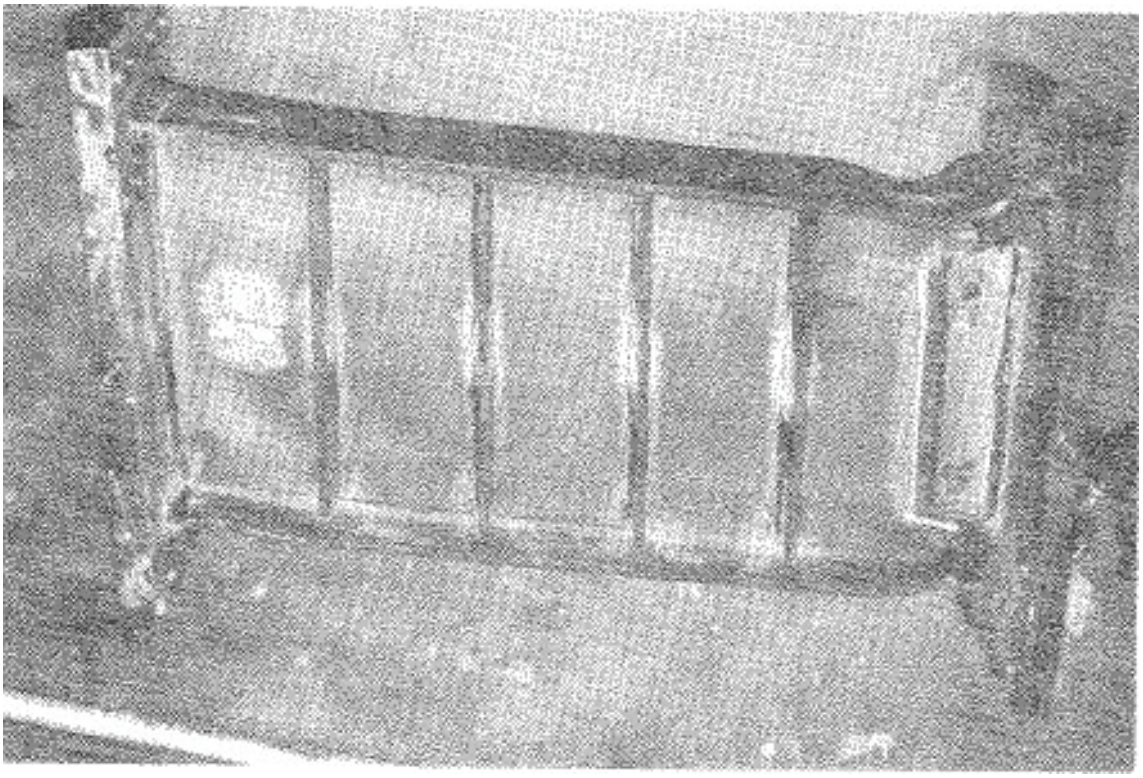

Figure D-19 Final condition of specimen 27 tested by Malley and Popov (1983)

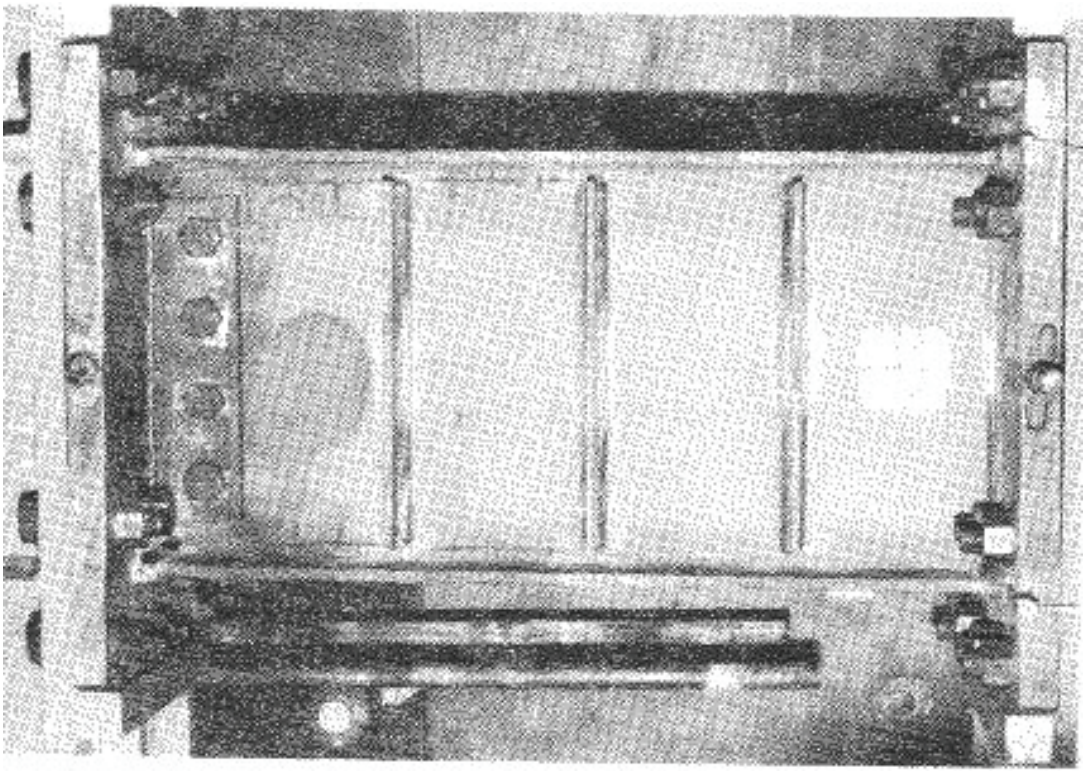

Figure D-20 Final condition of specimen 28 tested by Malley and Popov (1983)

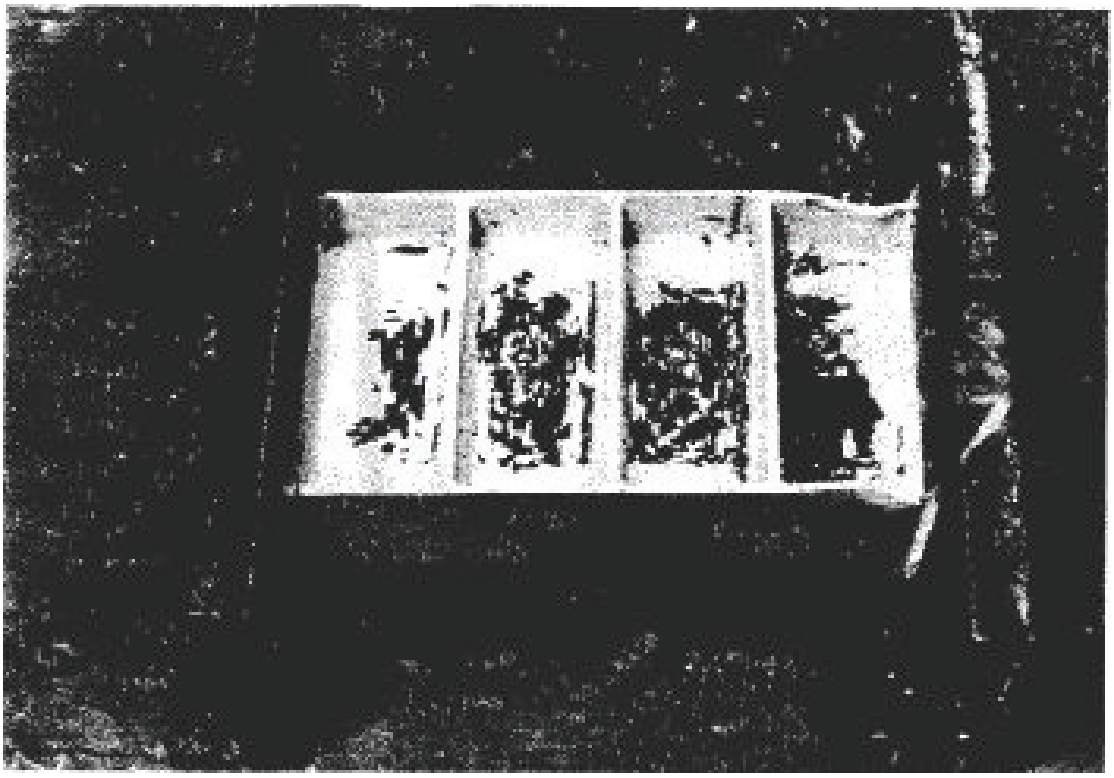

Figure D-21 Final condition of specimen 3 tested by Kasai and Popov (1986)

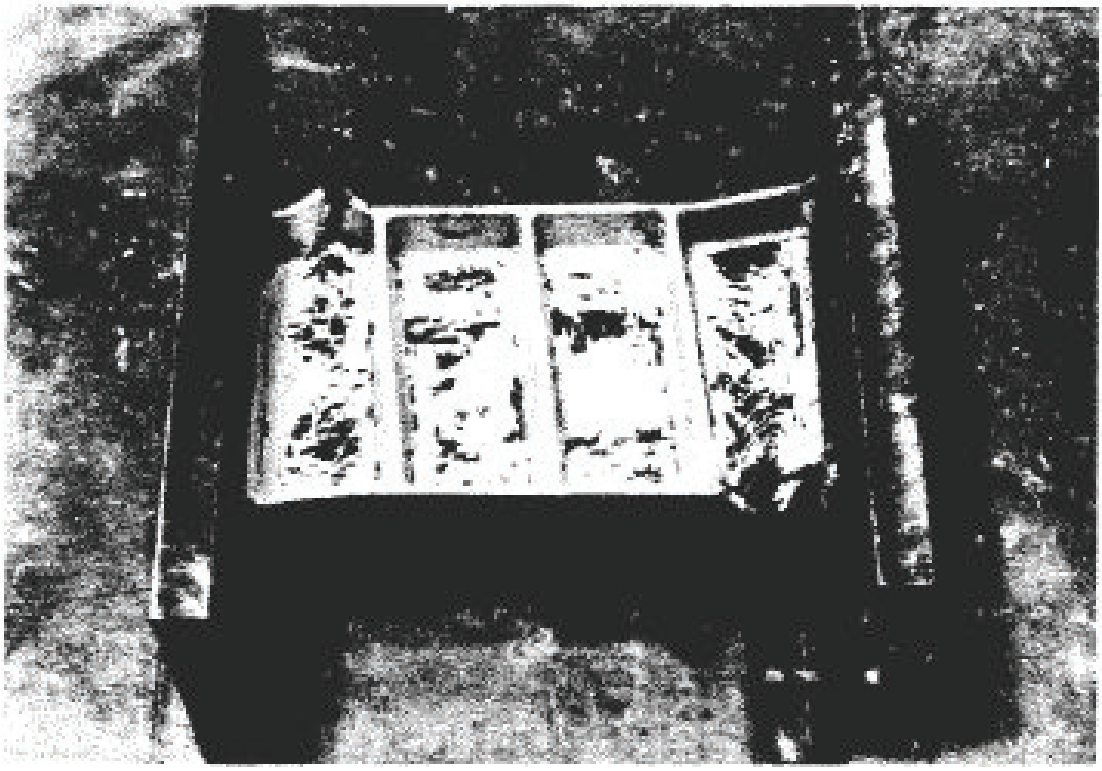

Figure D-22 Final condition of specimen 4 tested by Kasai and Popov (1986)

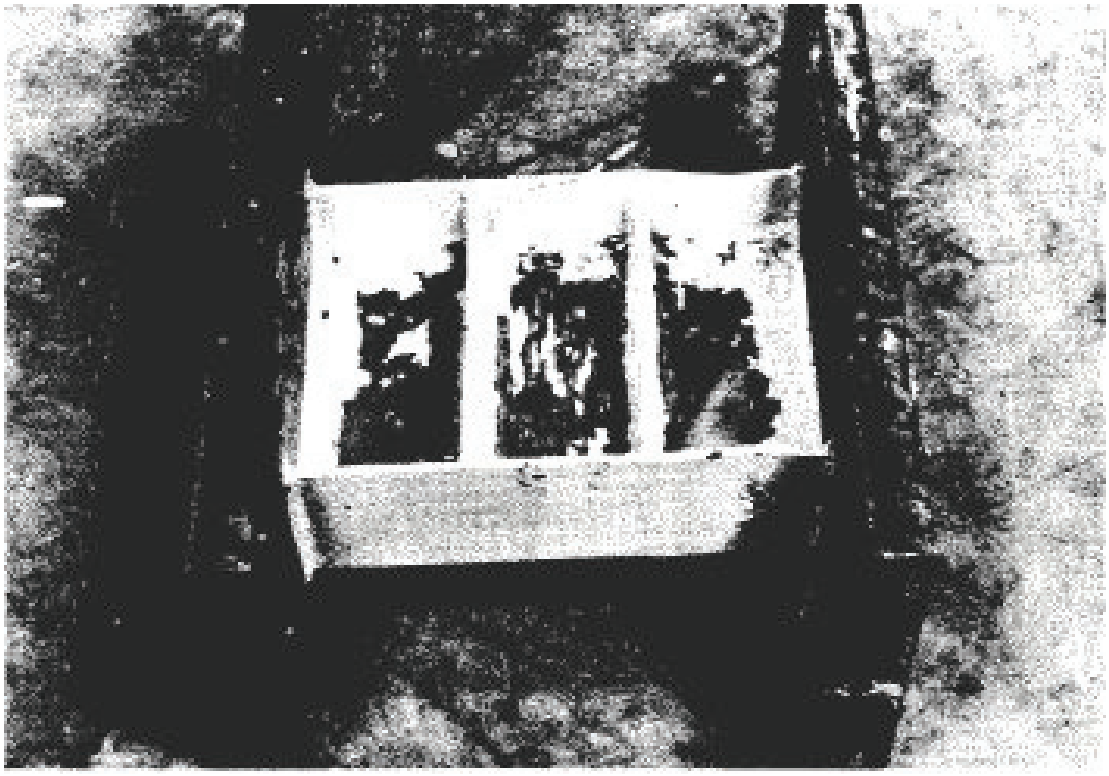

Figure D-23 Final condition of specimen 7 tested by Kasai and Popov (1986)

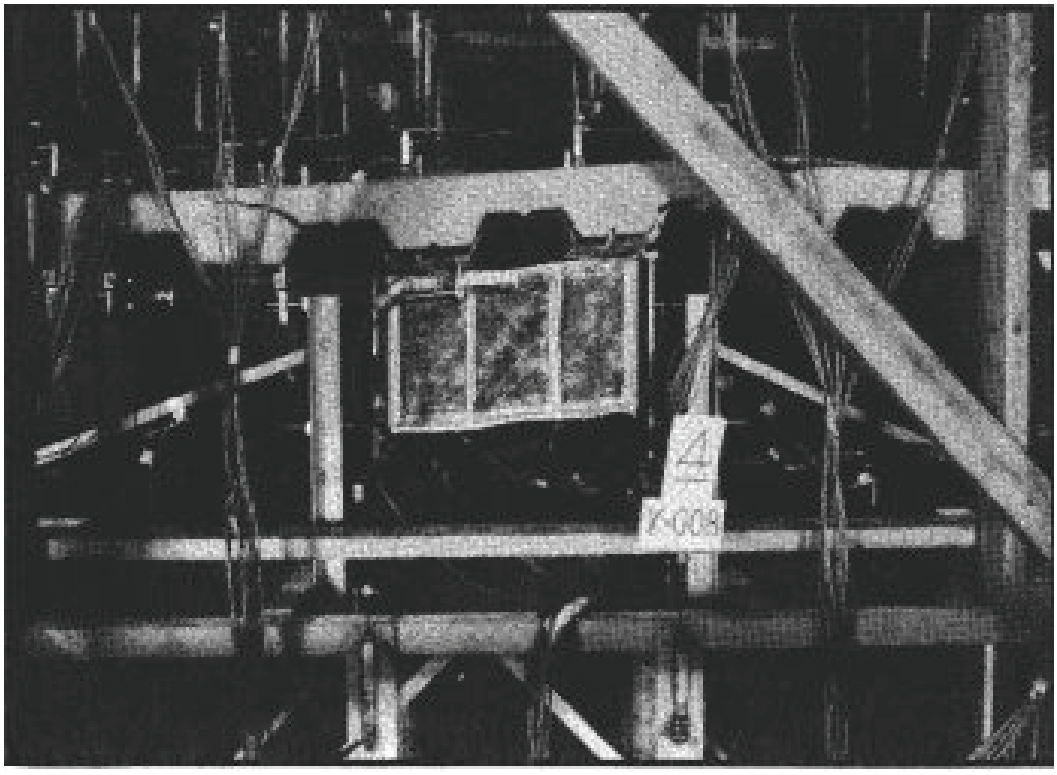

Figure D-24 Final condition of specimen A1 tested by Ricles and Popov (1987)

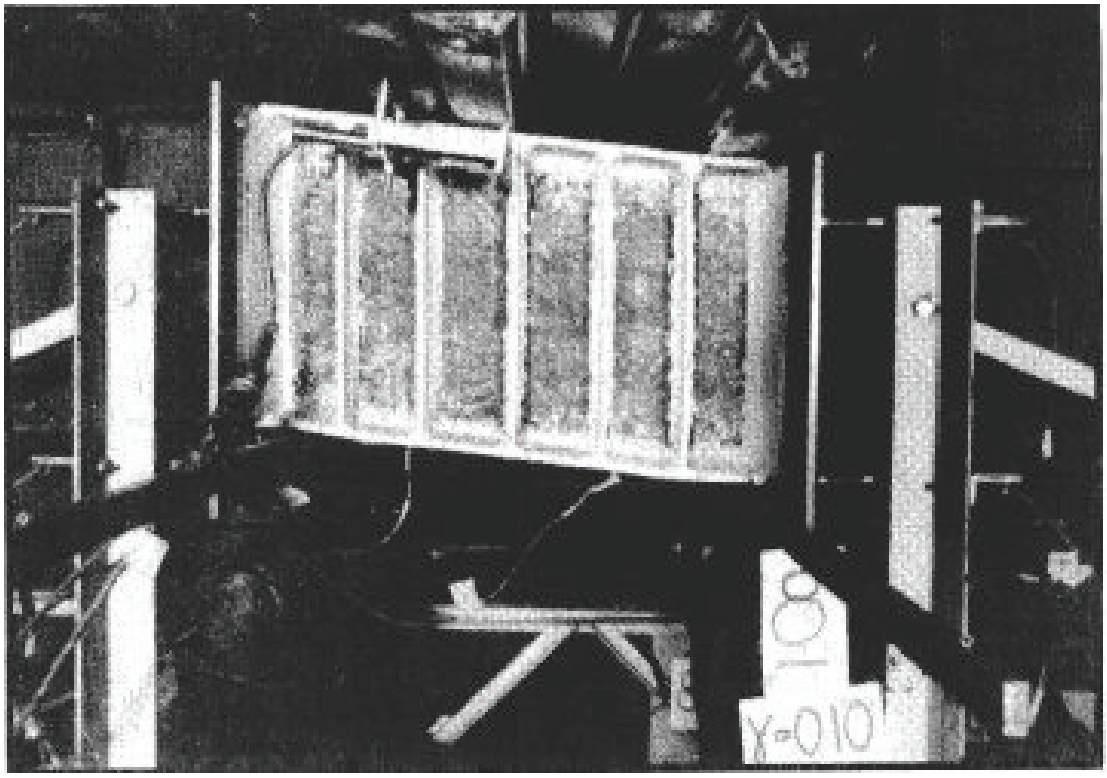

Figure D-25 Final condition of specimen A2 tested by Ricles and Popov (1987)

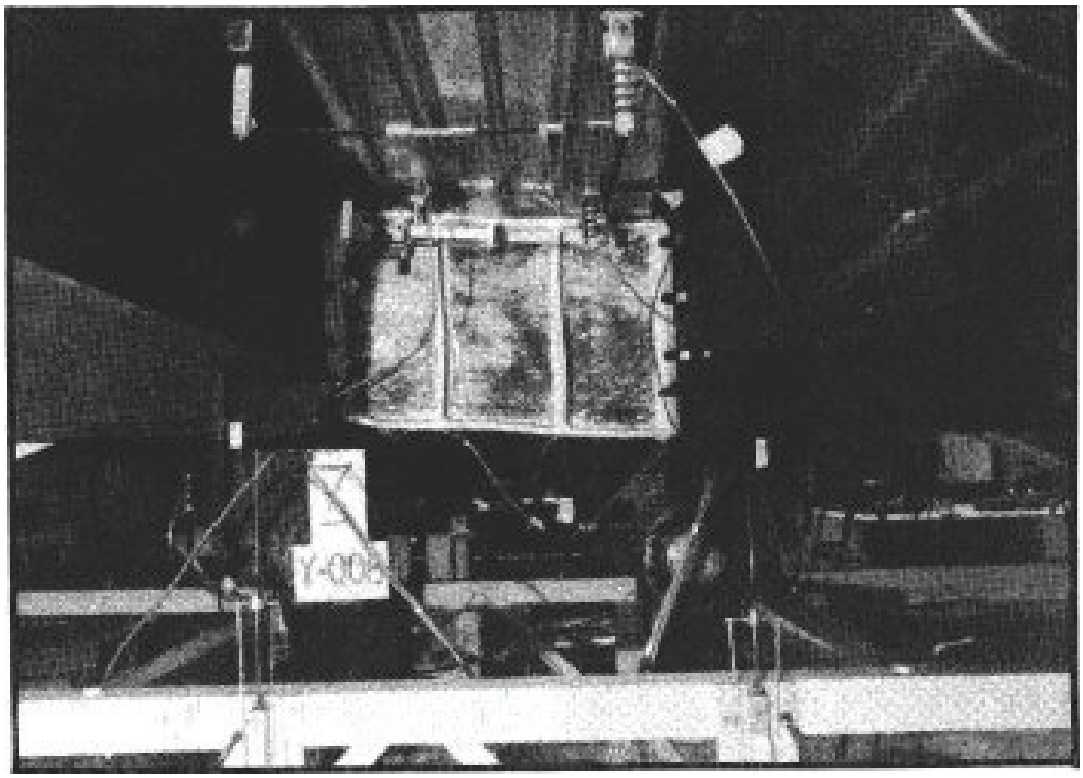

Figure D-26 Final condition of specimen B1 tested by Ricles and Popov (1987)

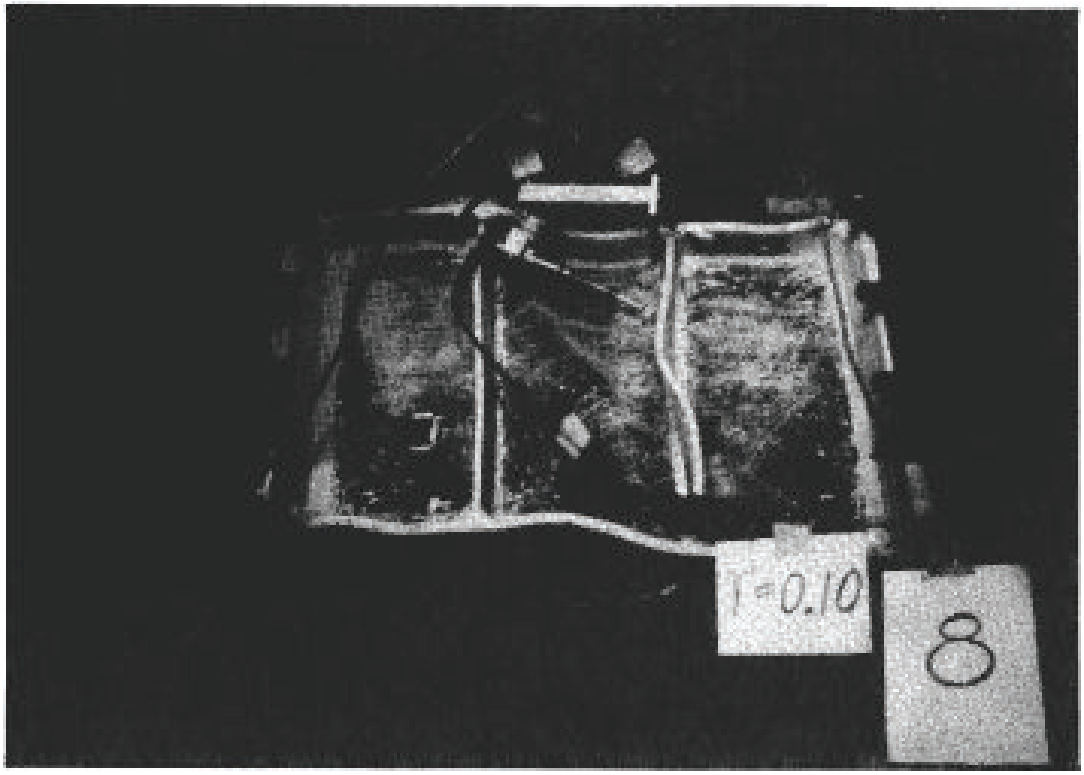

Figure D-27 Final condition of specimen B2 tested by Ricles and Popov (1987)

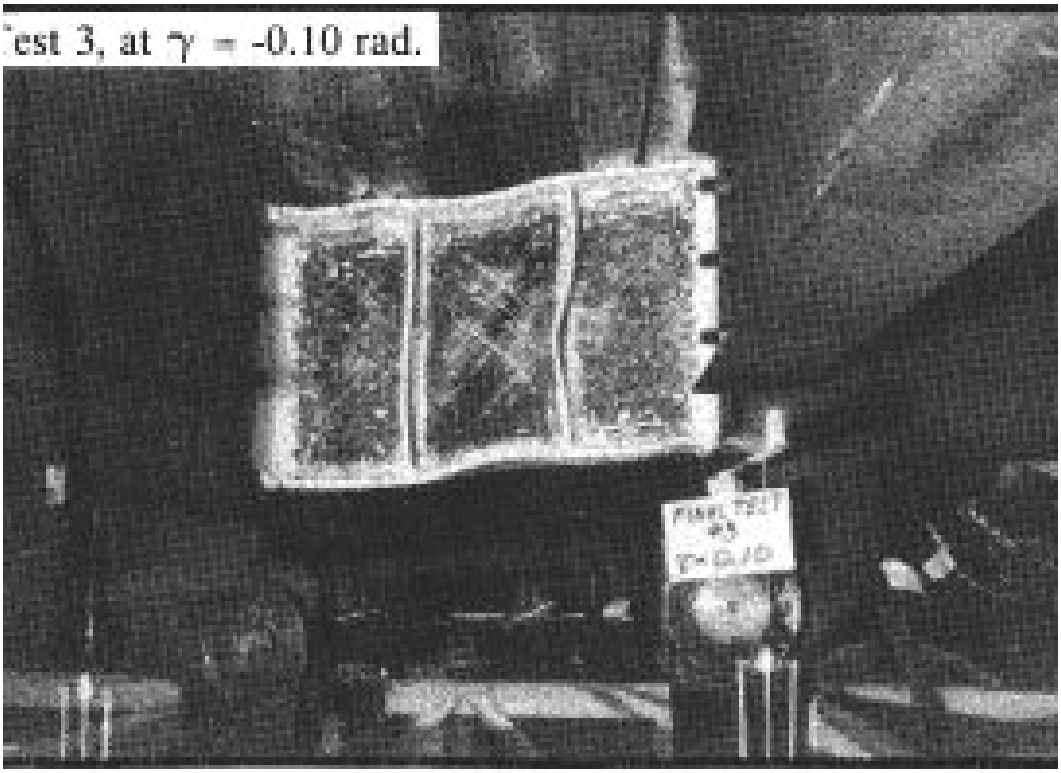

Figure D-28 Final condition of specimen C1 tested by Ricles and Popov (1987)

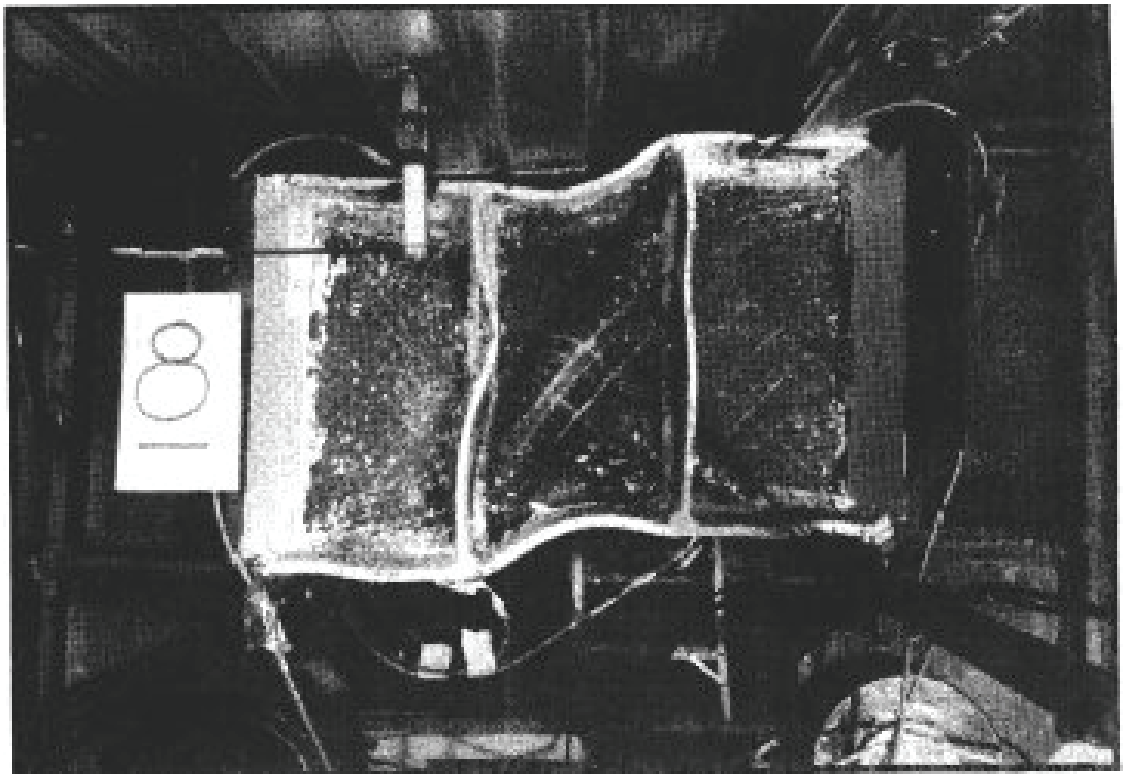

Figure D-29 Final condition of specimen C2 tested by Ricles and Popov (1987)

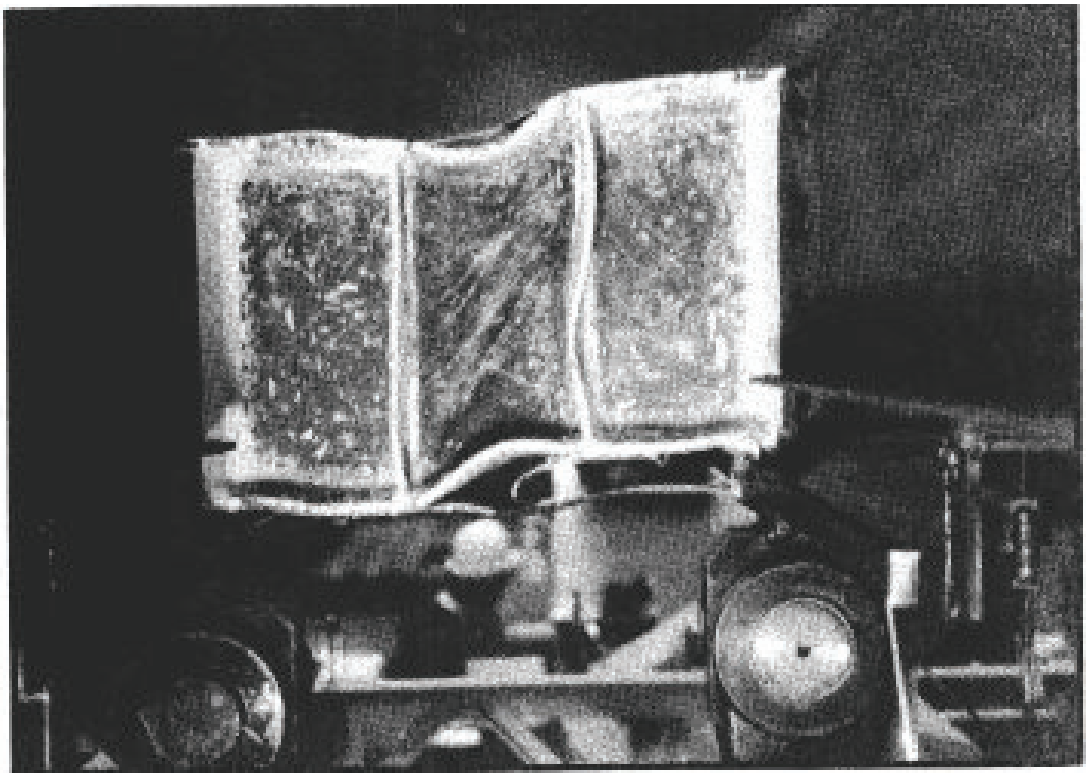

Figure D-30 Final condition of specimen D1 tested by Ricles and Popov (1987)

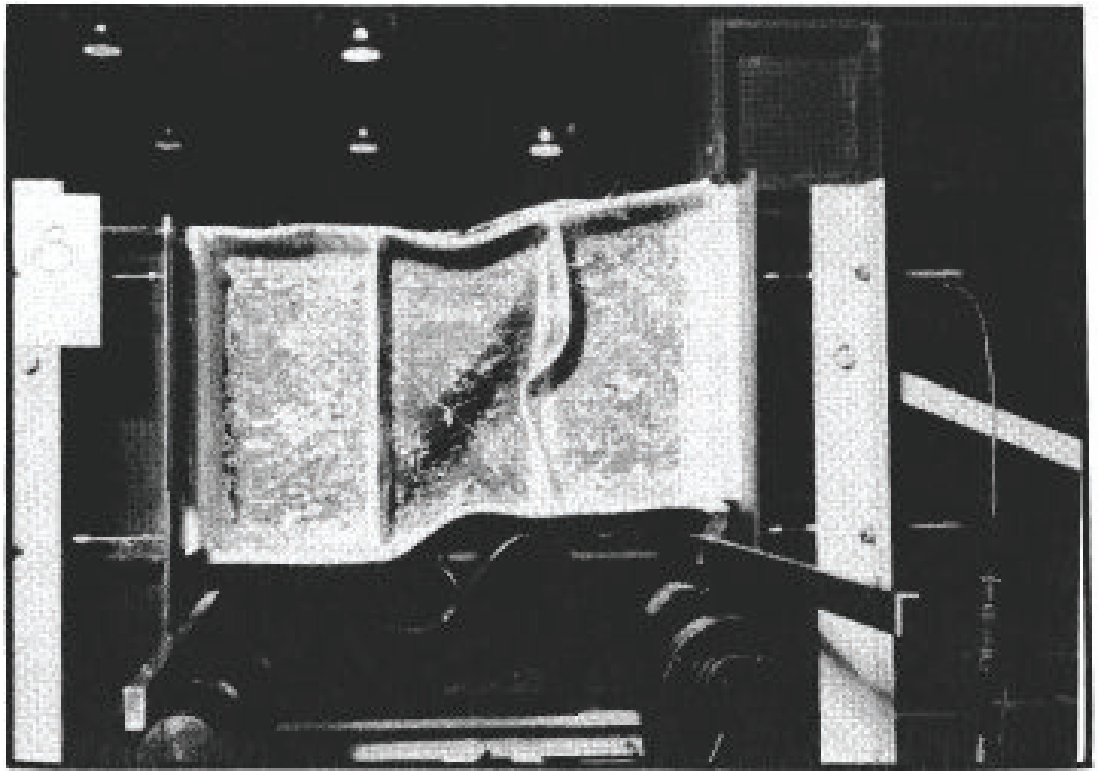

Figure D-31 Final condition of specimen D2 tested by Ricles and Popov (1987)

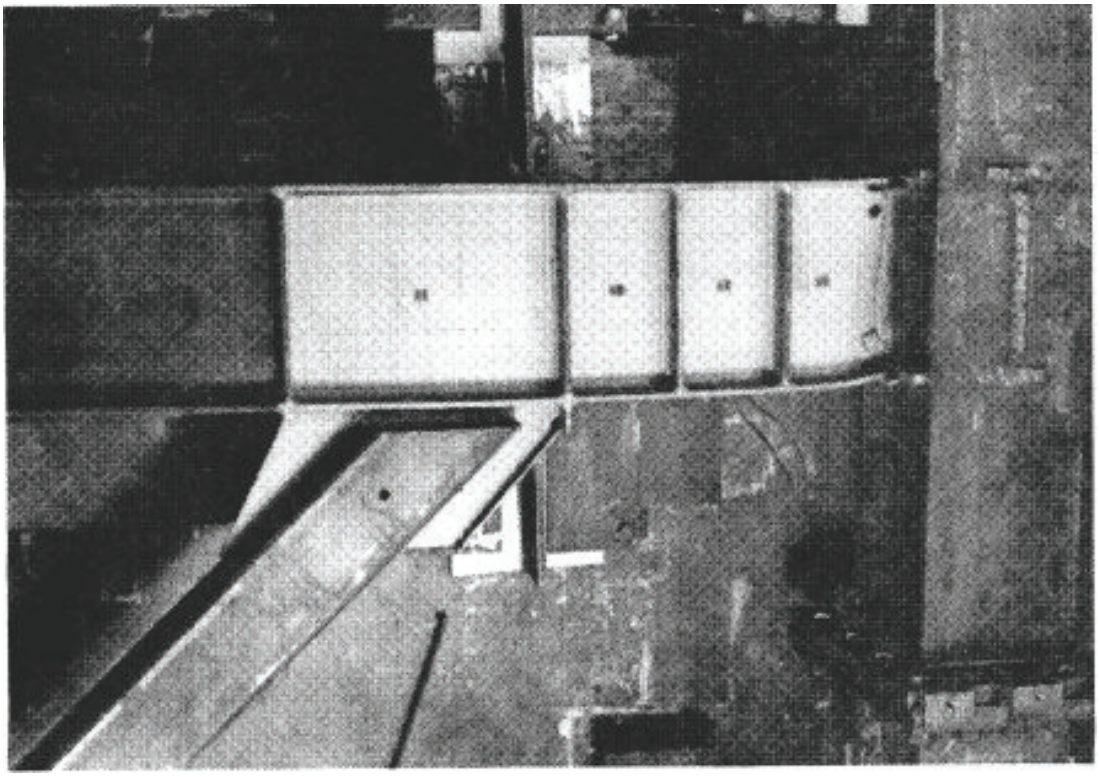

Figure D-32 Final condition of specimen 9 tested by Engelhardt and Popov (1989)

Figure D-33 Final condition of specimen PNS tested by Okazaki (2004)

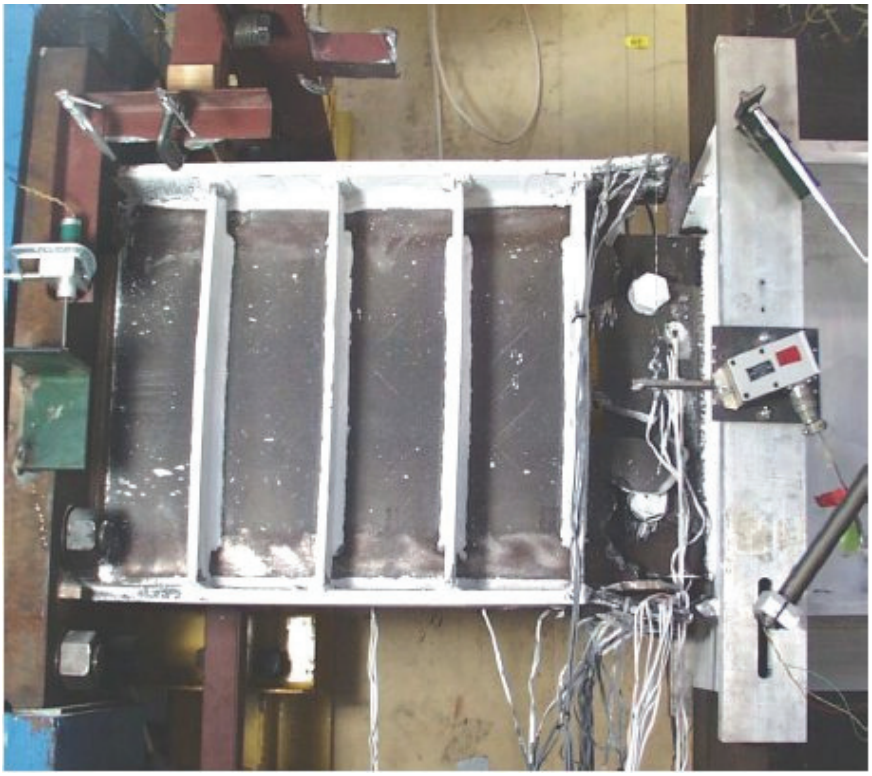

Figure D-34 Final condition of specimen MWS tested by Okazaki (2004)

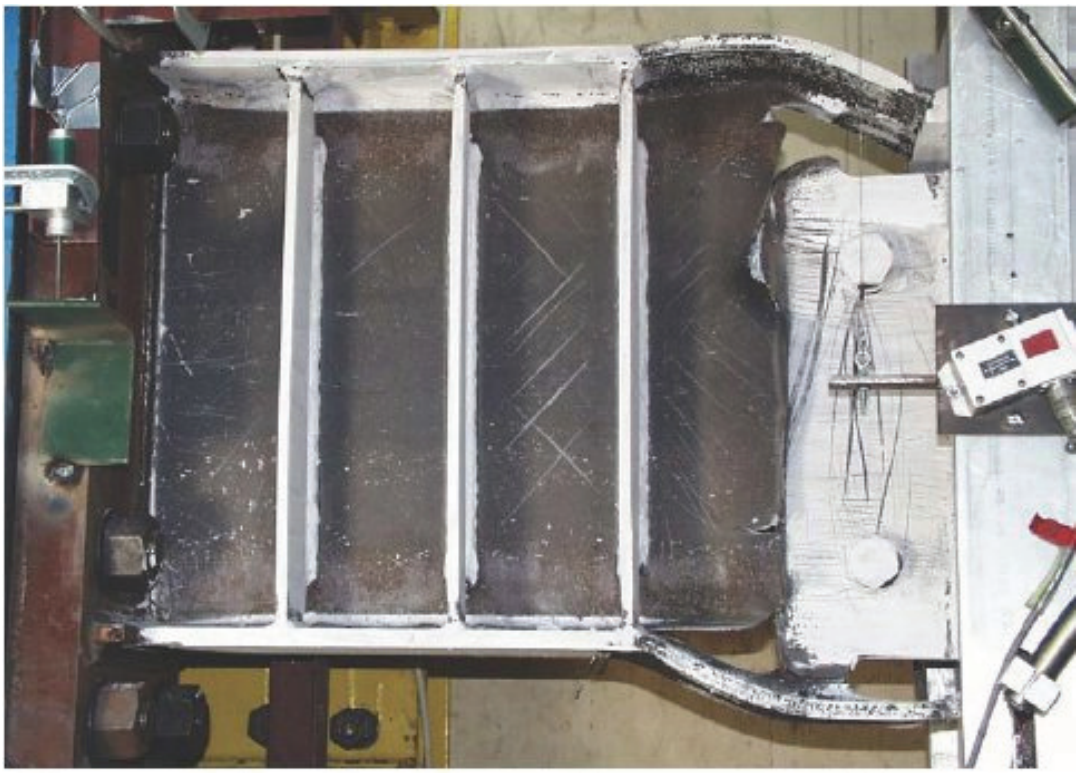

Figure D-35 Final condition of specimen FFS tested by Okazaki (2004)

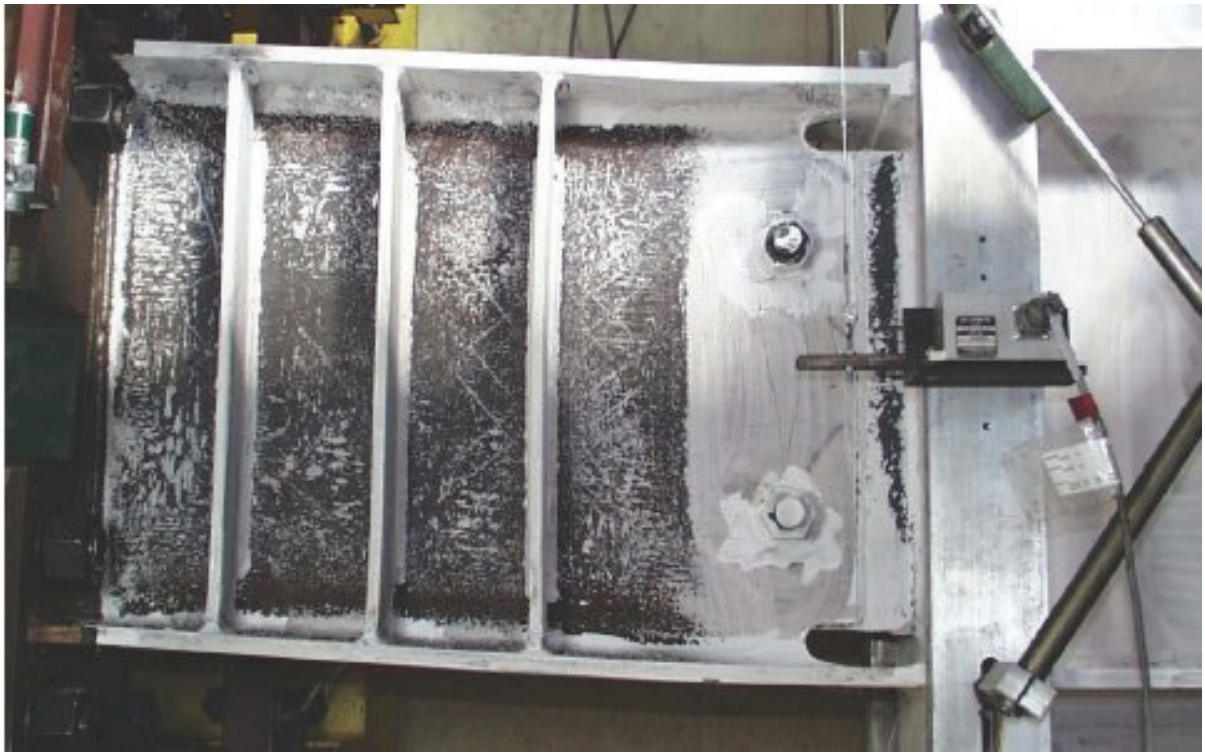

Figure D-36 Final condition of specimen FFS_RLP tested by Okazaki (2004)

Figure D-37 Final condition of specimen NAS tested by Okazaki (2004)

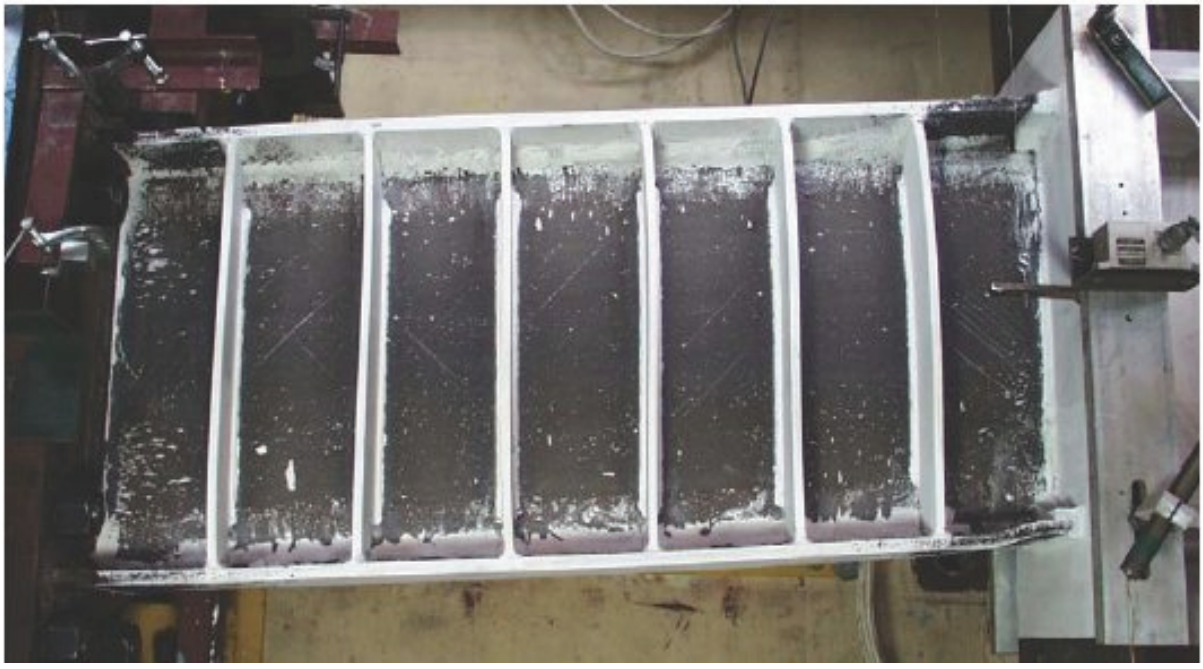

Figure D-38 Final condition of specimen NAS_RLP tested by Okazaki (2004)

Figure D-39 Final condition of specimen Type 1 tested by McDaniel et al. (2002)

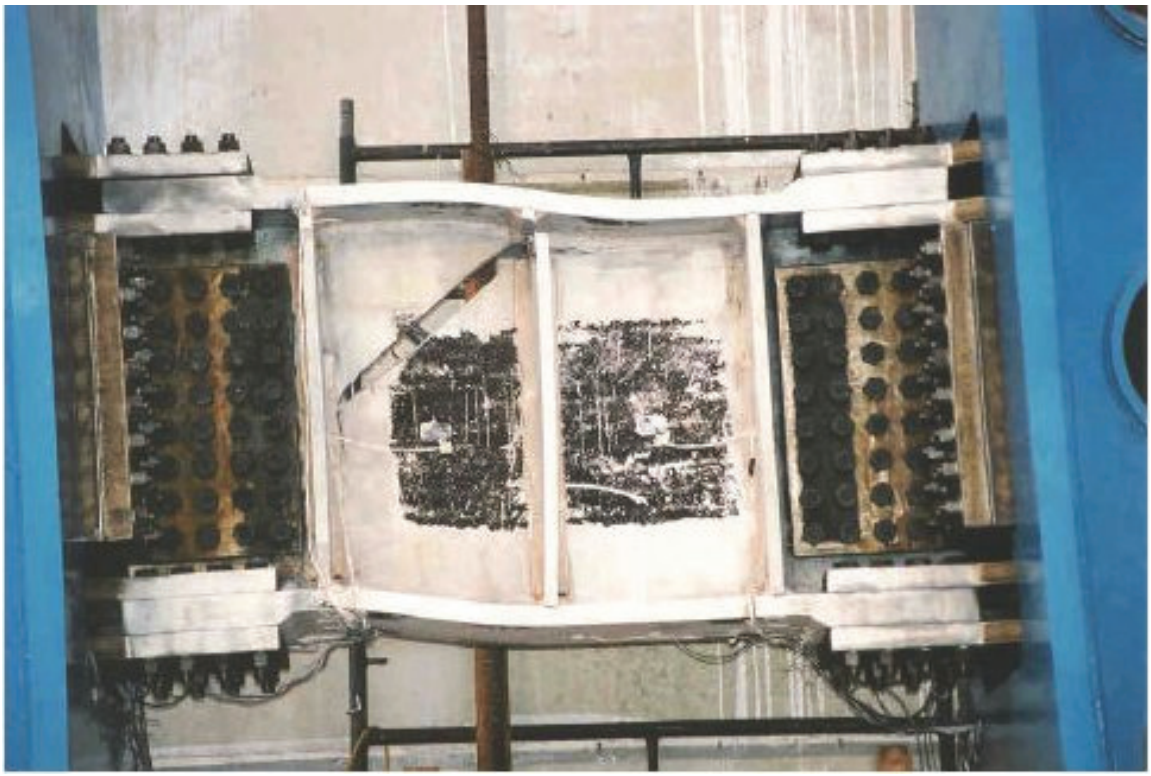

Figure D-40 Final condition of specimen Type 3 tested by McDaniel et al. (2002)

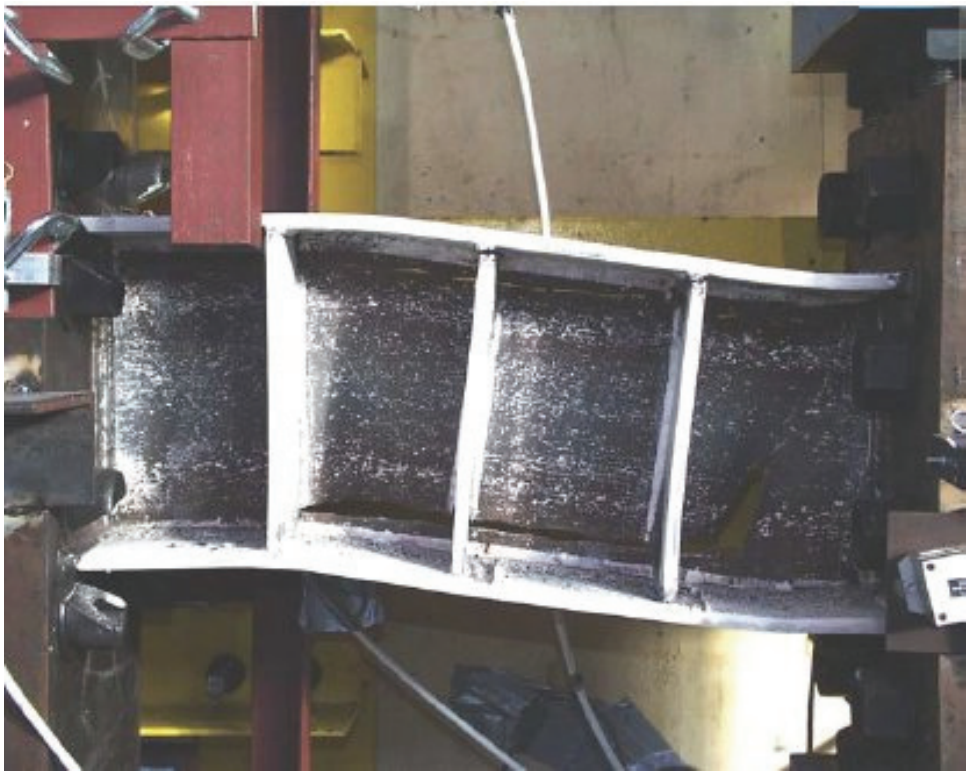

Figure D-41 Final condition of specimen 4a tested by Arce (2002)

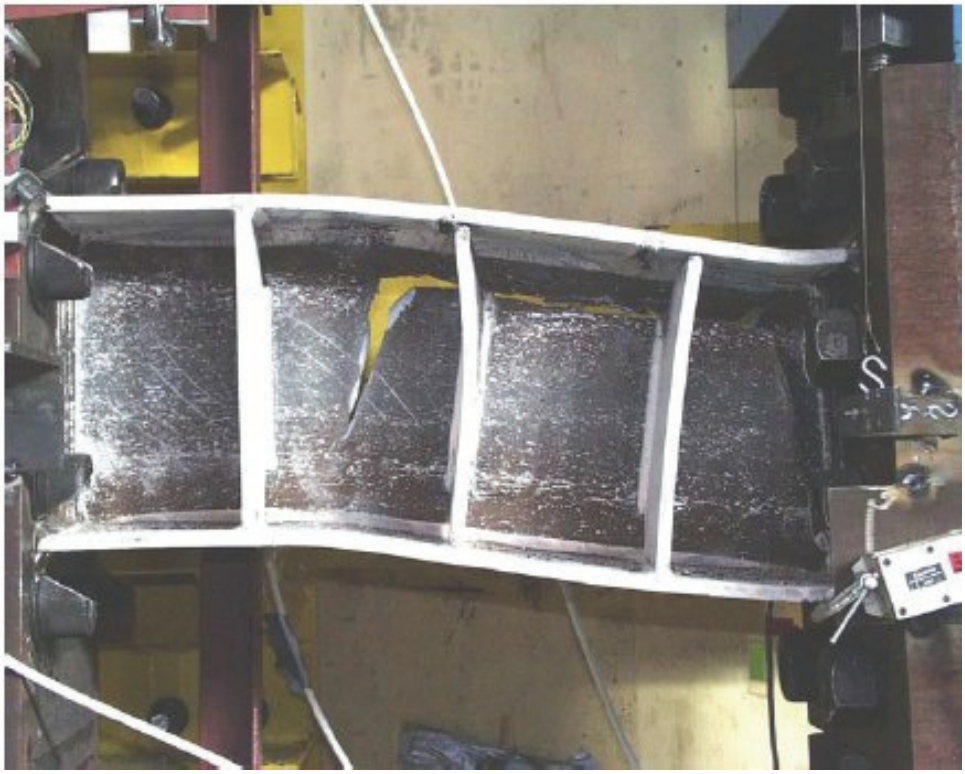

Figure D-42 Final condition of specimen 4b tested by Arce (2002)

Figure D-43 Final condition of specimen 4c tested by Arce (2002)

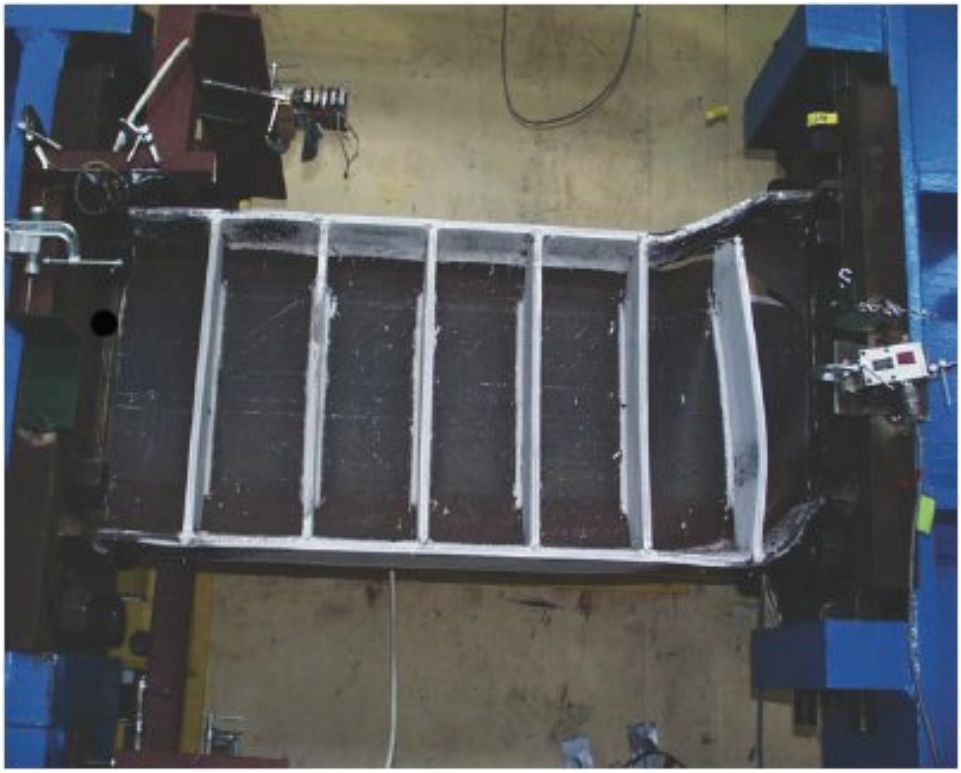

Figure D-44 Final condition of specimen 8 tested by Arce (2002)

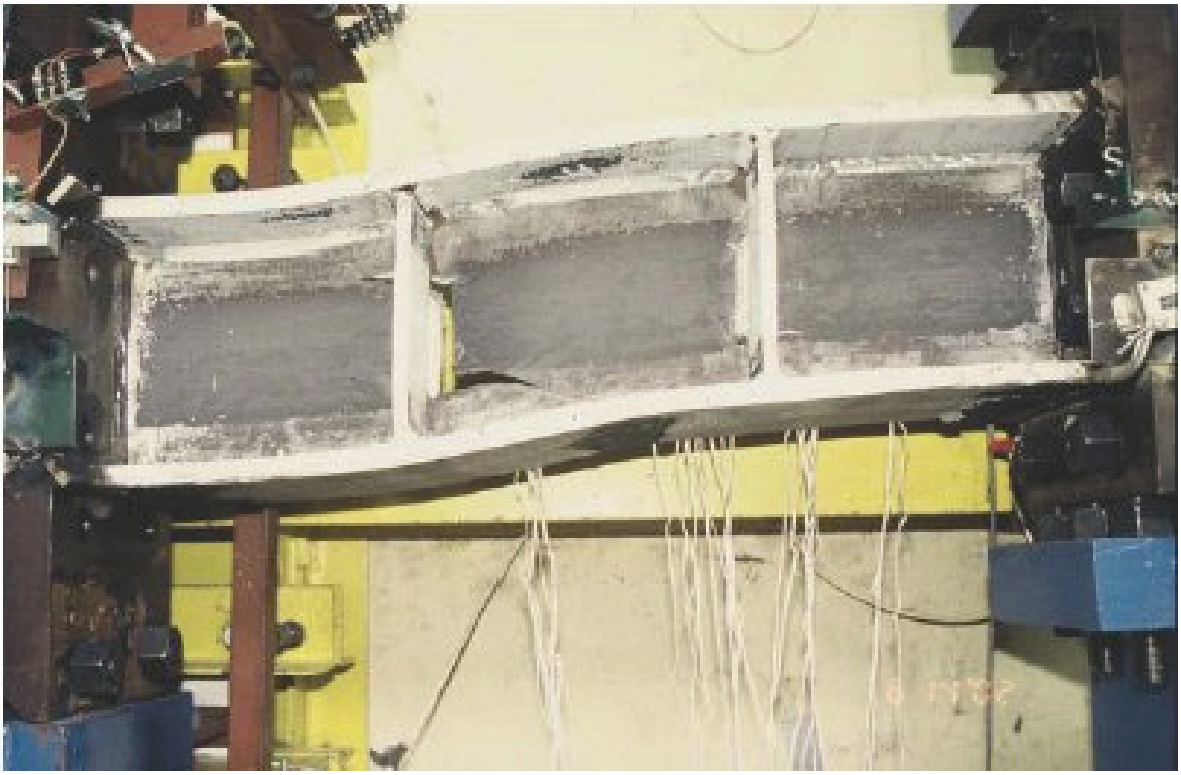

Figure D-45 Final condition of specimen 10 tested by Arce (2002)

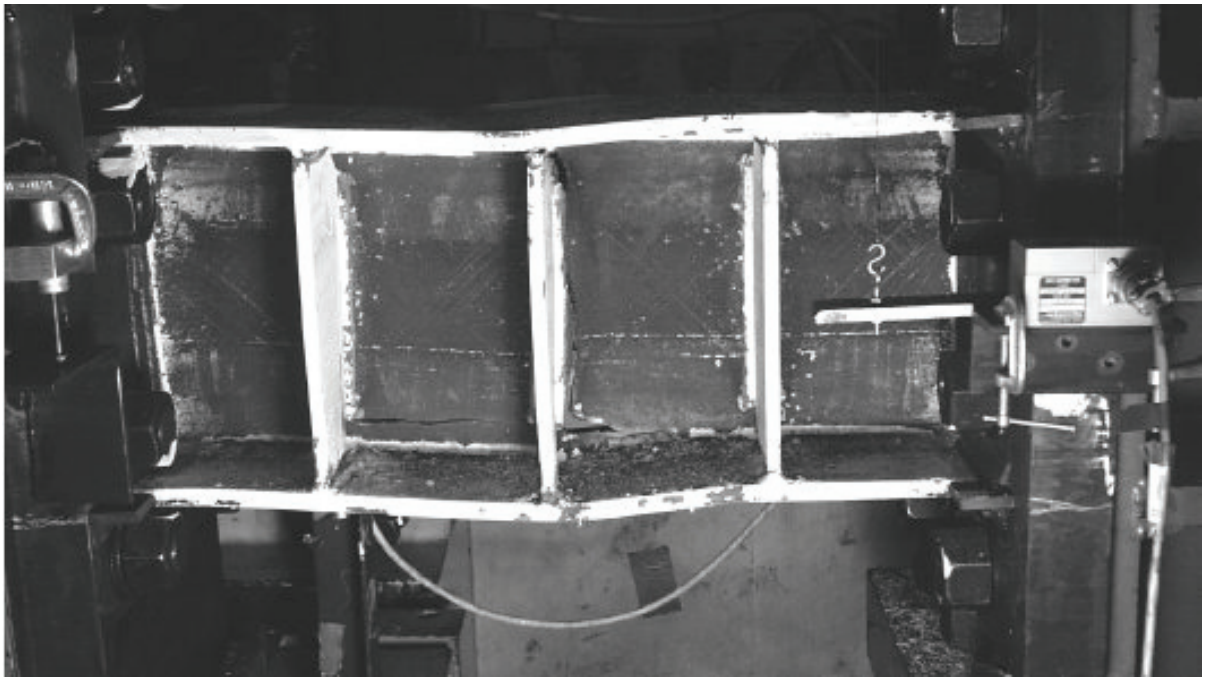

Figure D-46 Final condition of specimen 1 tested by Galvez (2004)

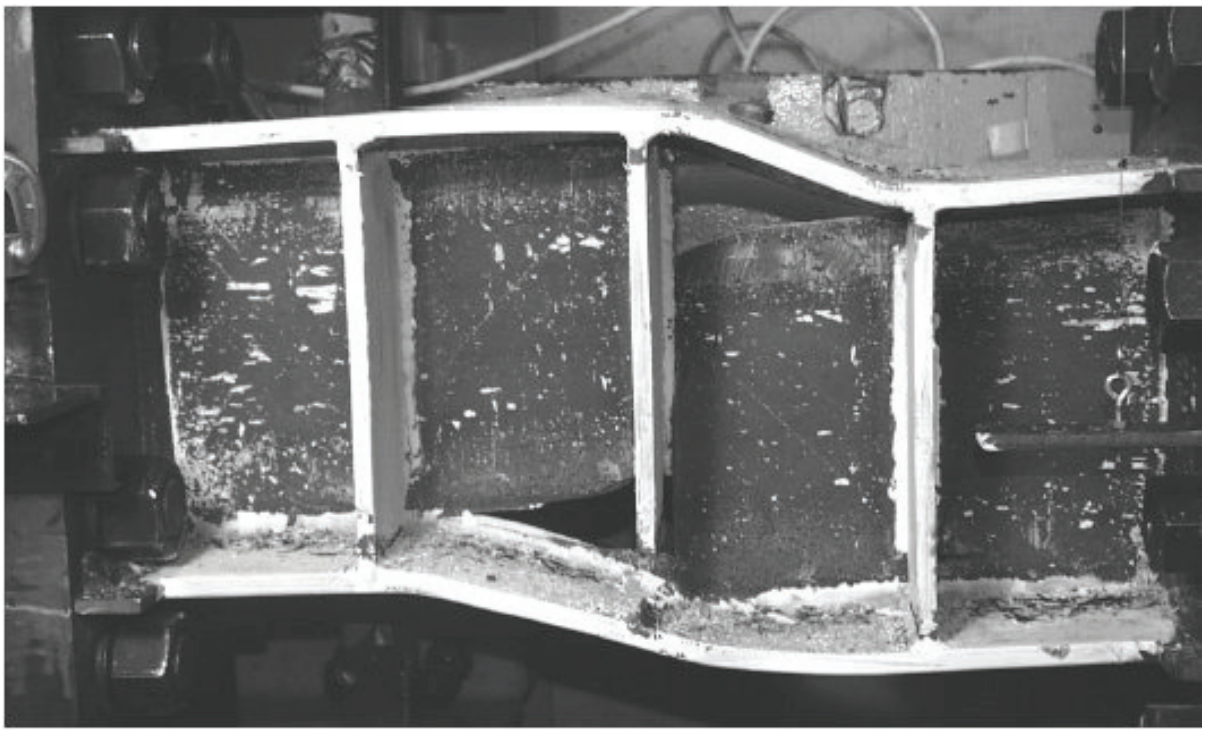

Figure D-47 Final condition of specimen 2 tested by Galvez (2004)

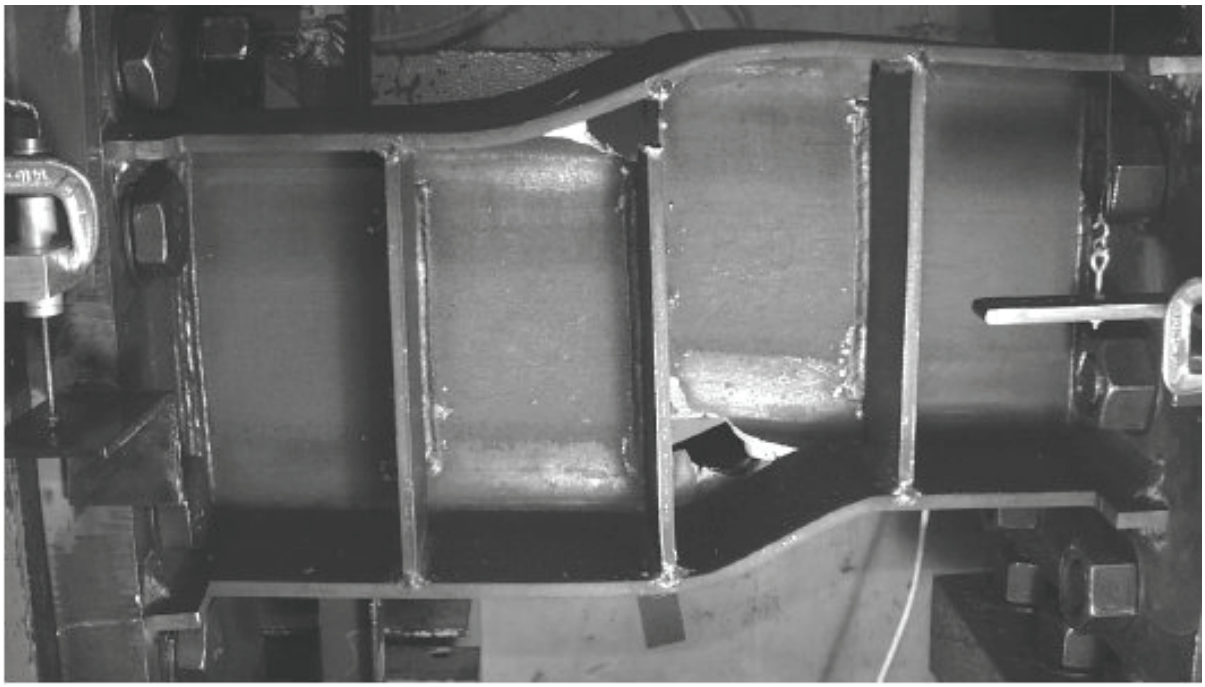

Figure D-48 Final condition of specimen 3 tested by Galvez (2004)

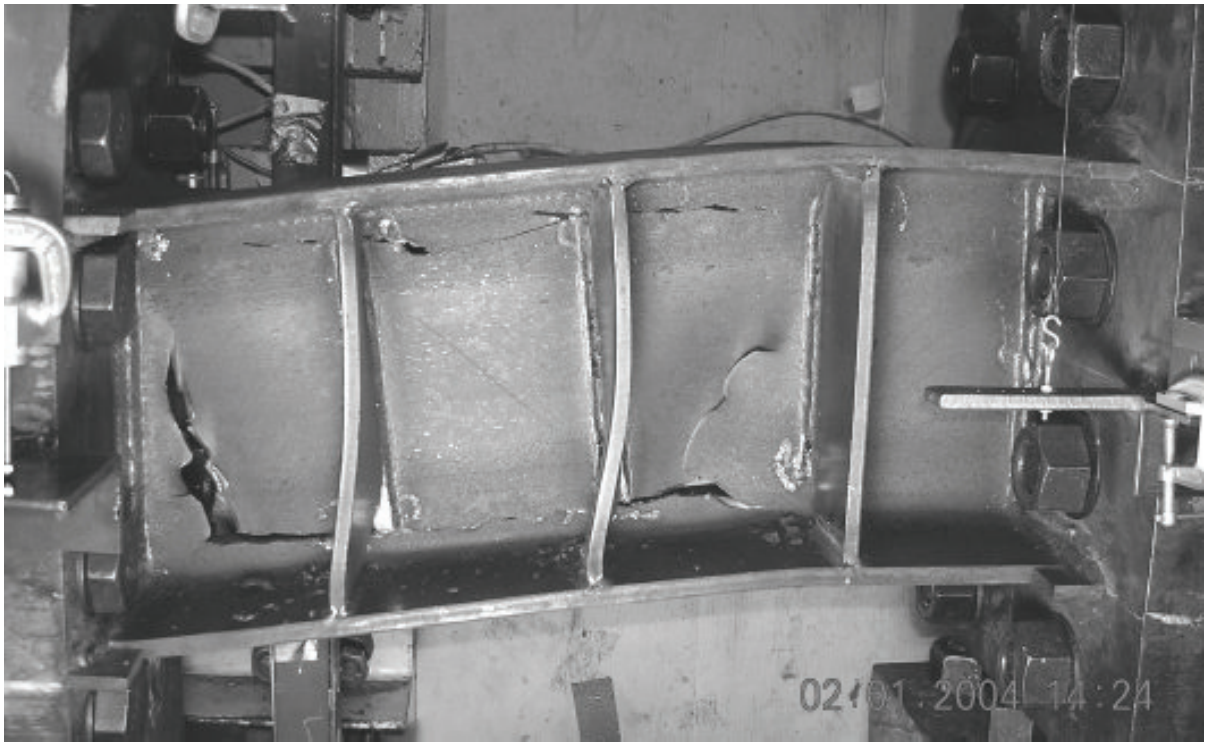

Figure D-49 Final condition of specimen 4 tested by Galvez (2004)

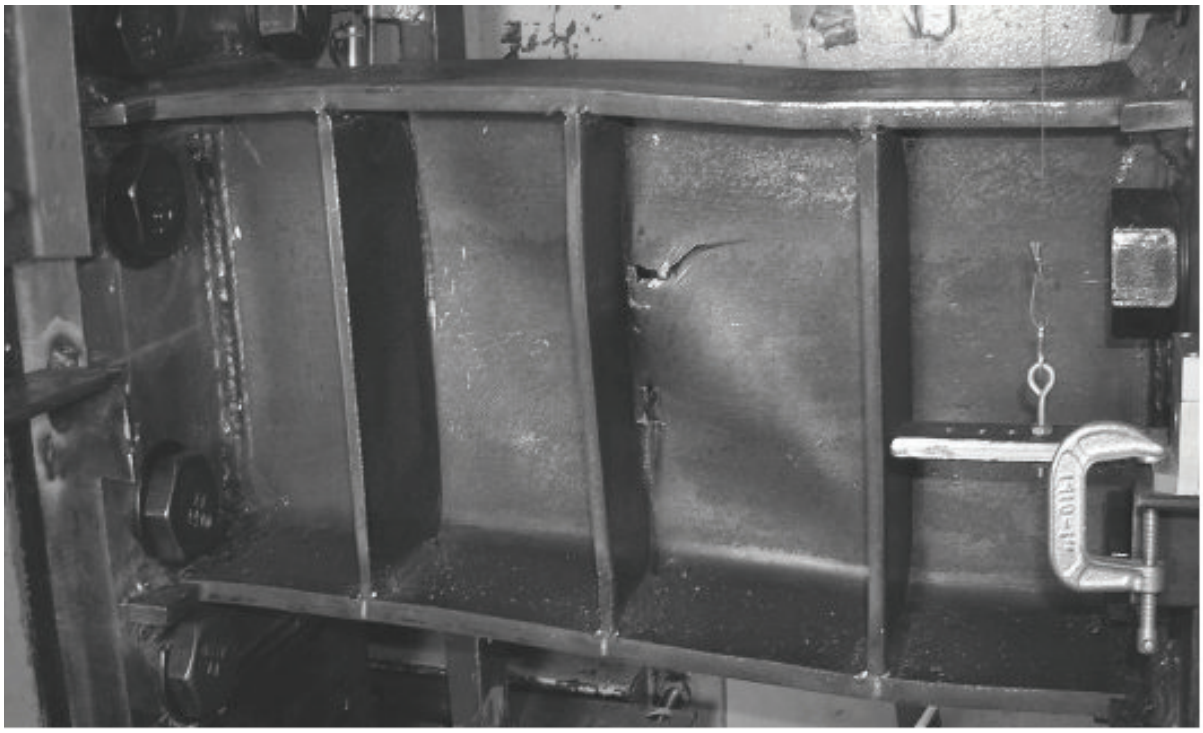

Figure D-50 Final condition of specimen 5 tested by Galvez (2004)

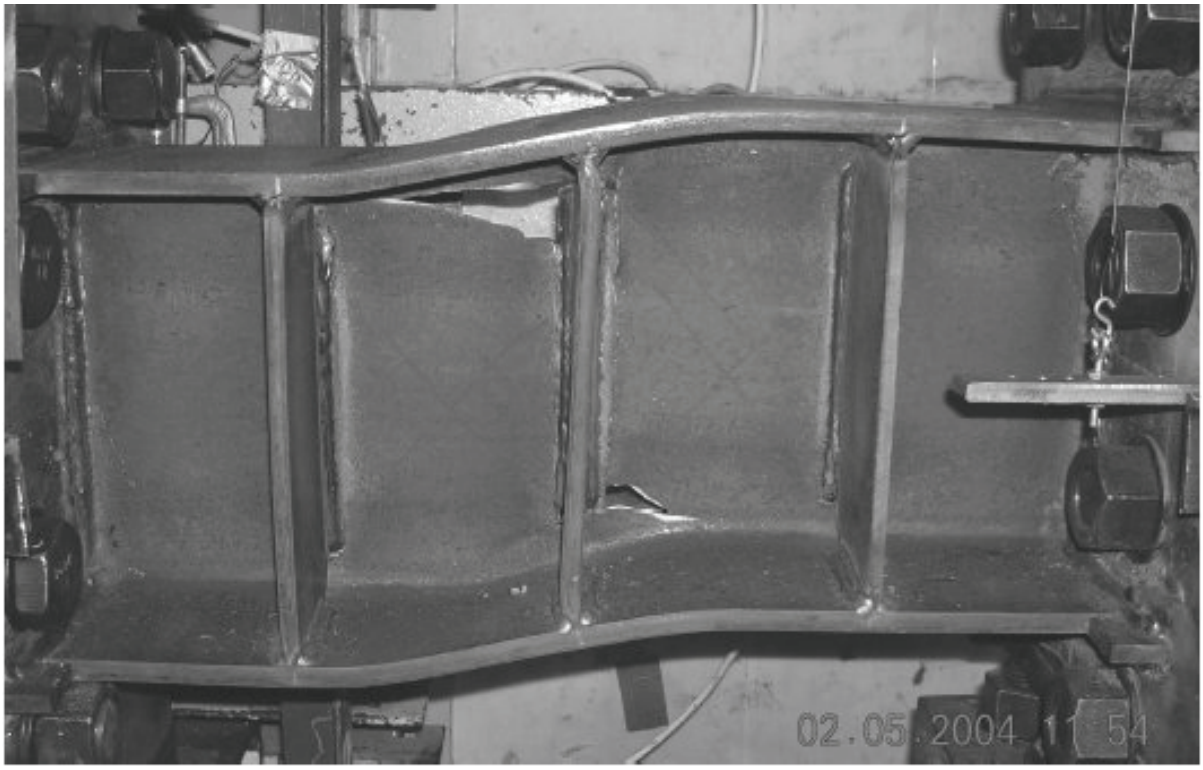

Figure D-51 Final condition of specimen 6 tested by Galvez (2004)

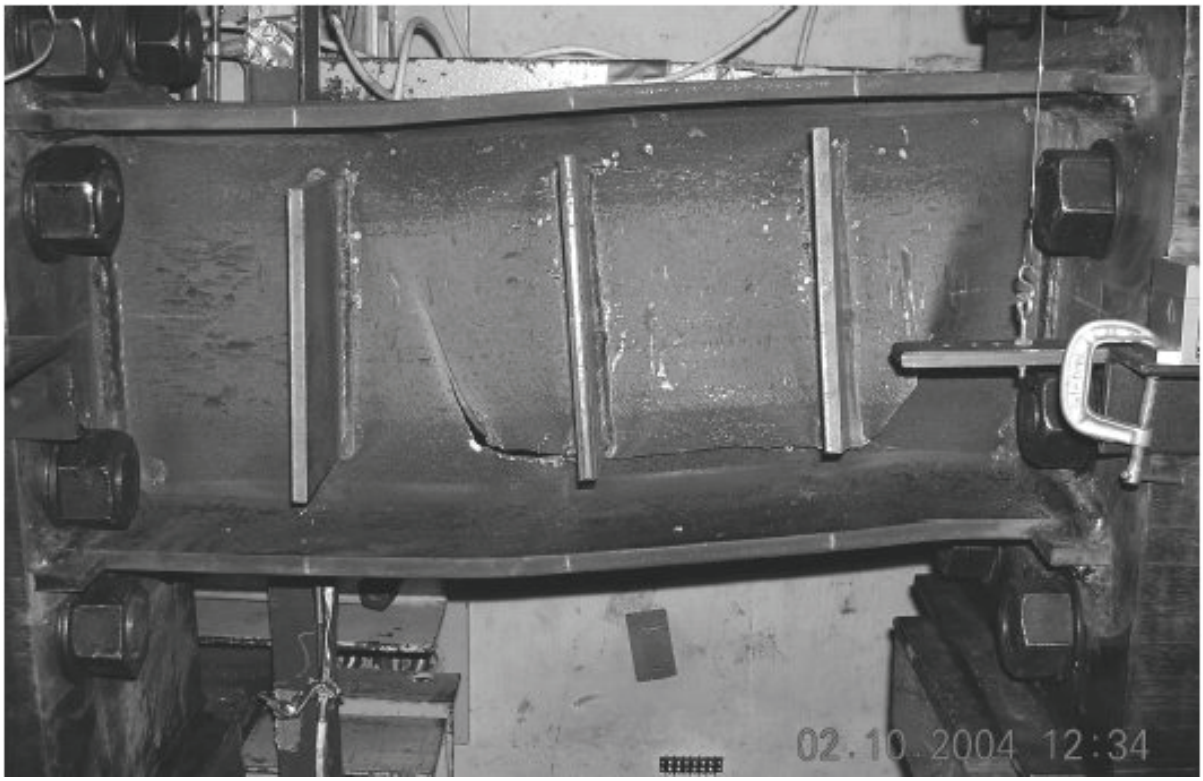

Figure D-52 Final condition of specimen 7 tested by Galvez (2004)

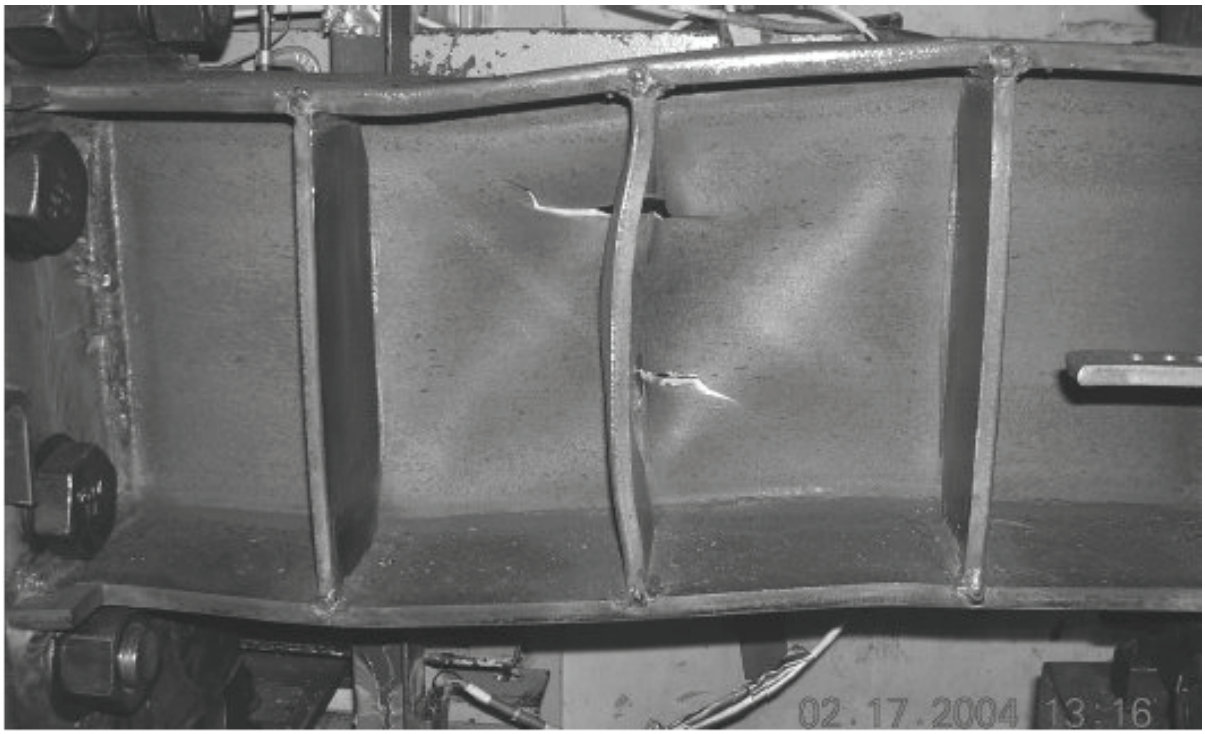

Figure D-53 Final condition of specimen 8 tested by Galvez (2004)

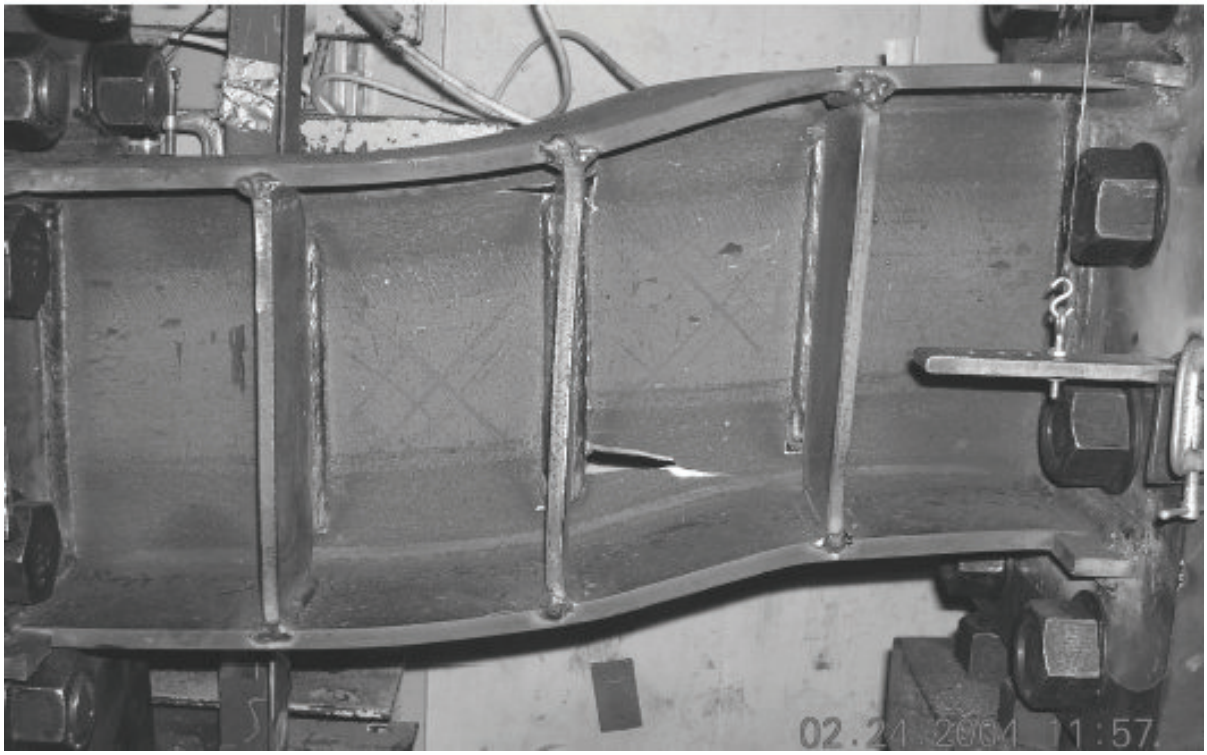

Figure D-54 Final condition of specimen 9 tested by Galvez (2004)

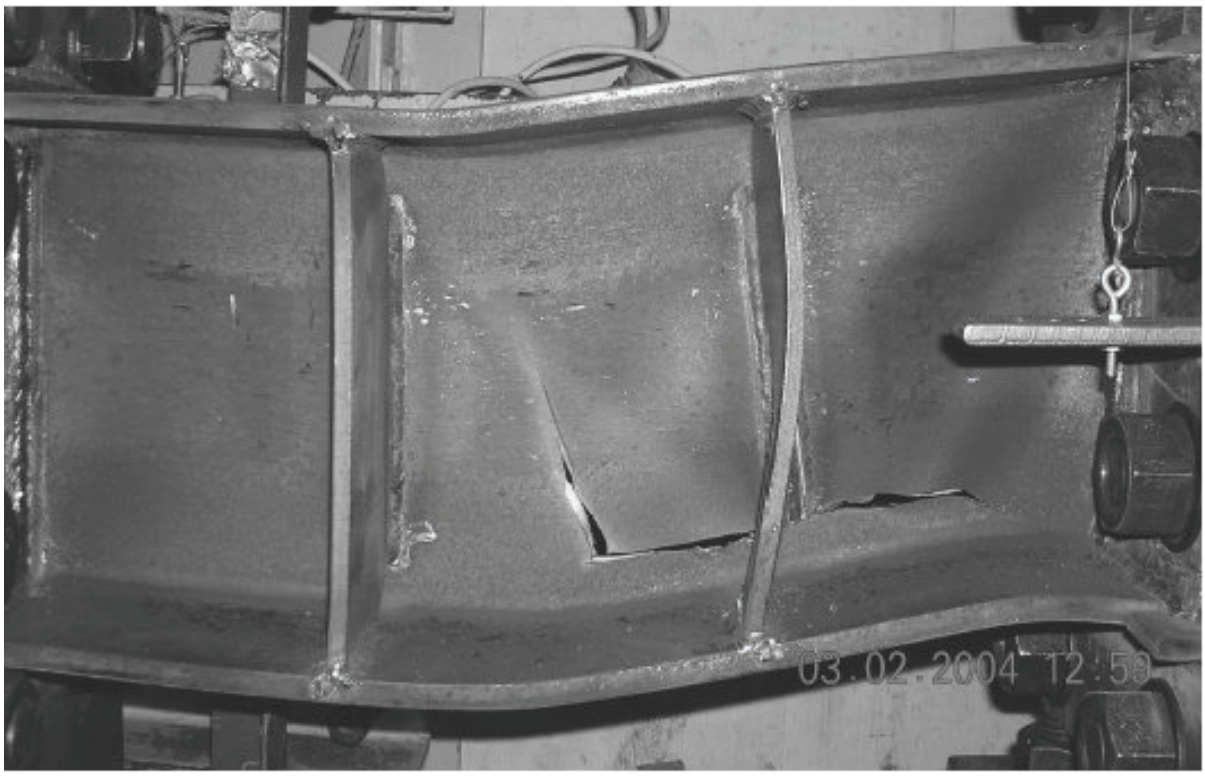

Figure D-55 Final condition of specimen 10 tested by Galvez (2004)

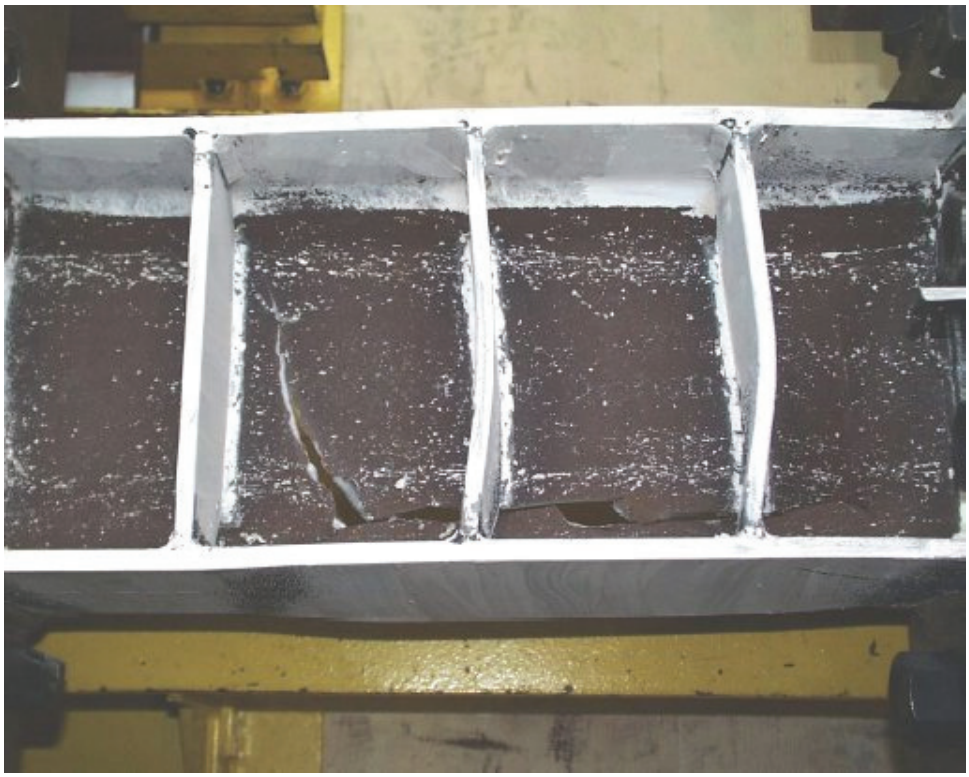

Figure D-56 Final condition of specimen 4A-RLP tested by Ryu (2005)

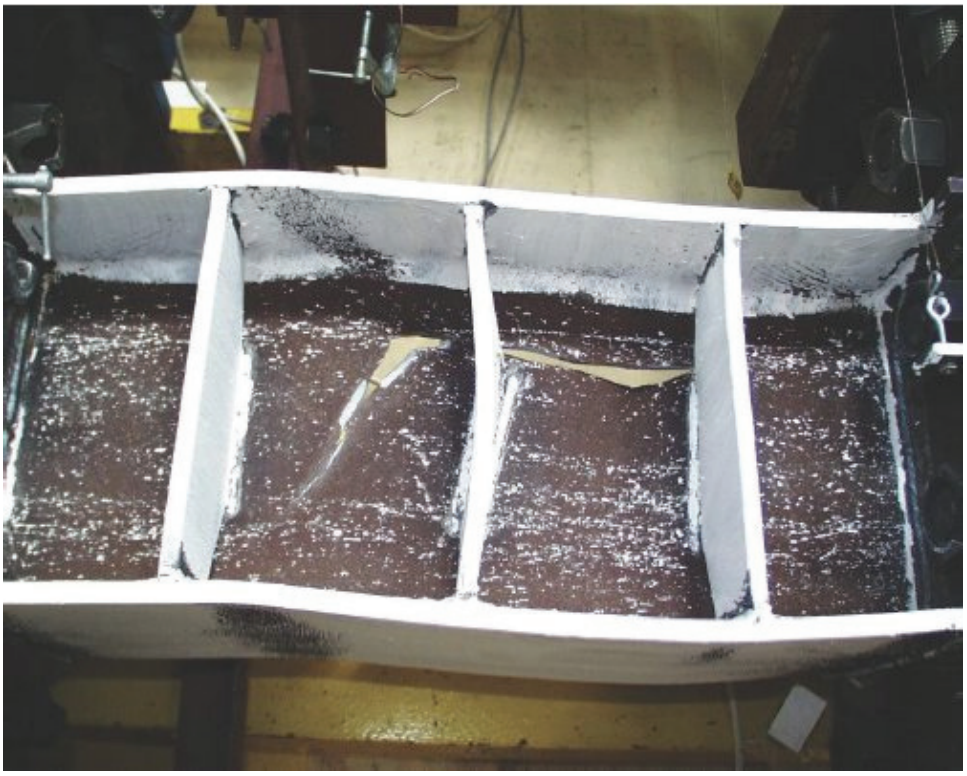

Figure D-57 Final condition of specimen 4C-RLP tested by Ryu (2005)

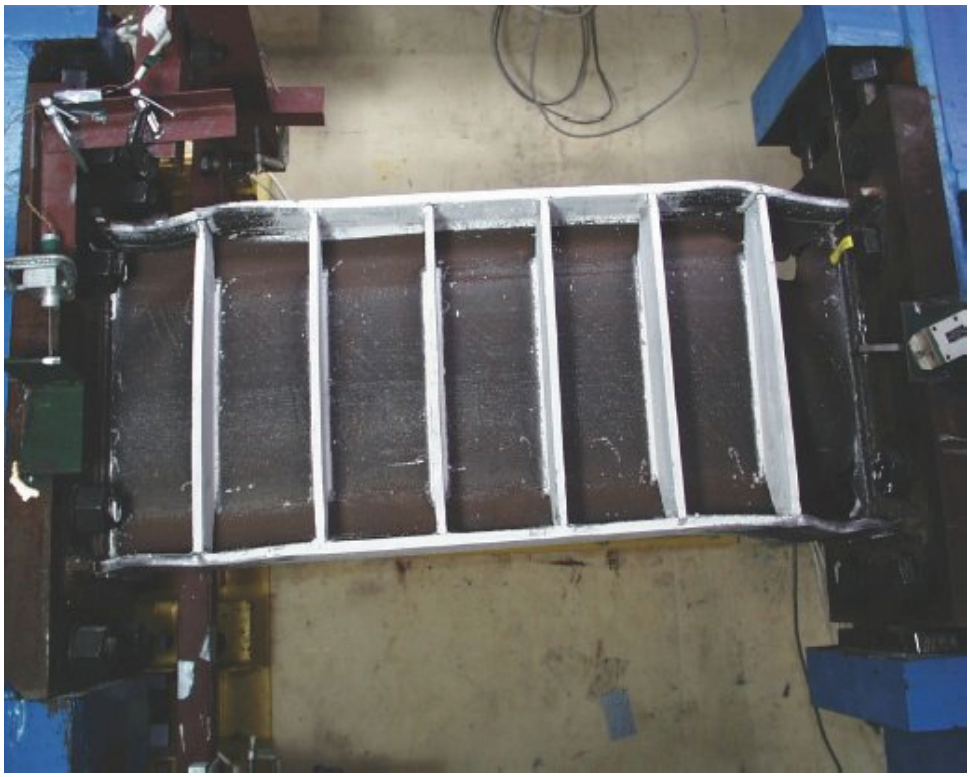

Figure D-58 Final condition of specimen 8-RLP tested by Ryu (2005)

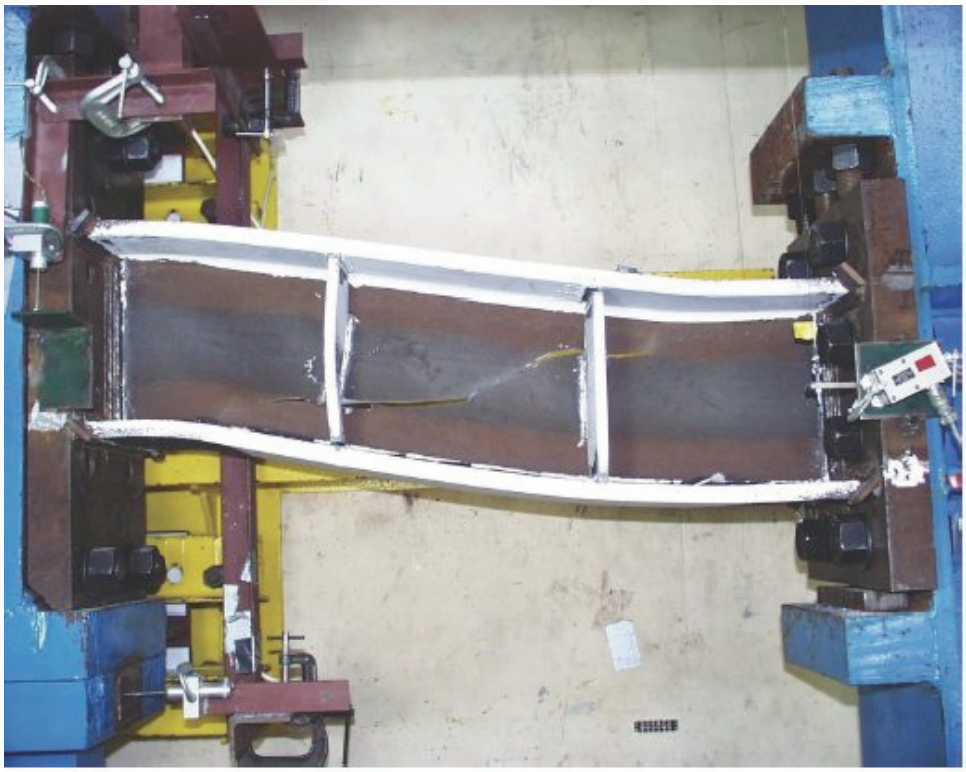

Figure D-59 Final condition of specimen 10-RLP tested by Ryu (2005)

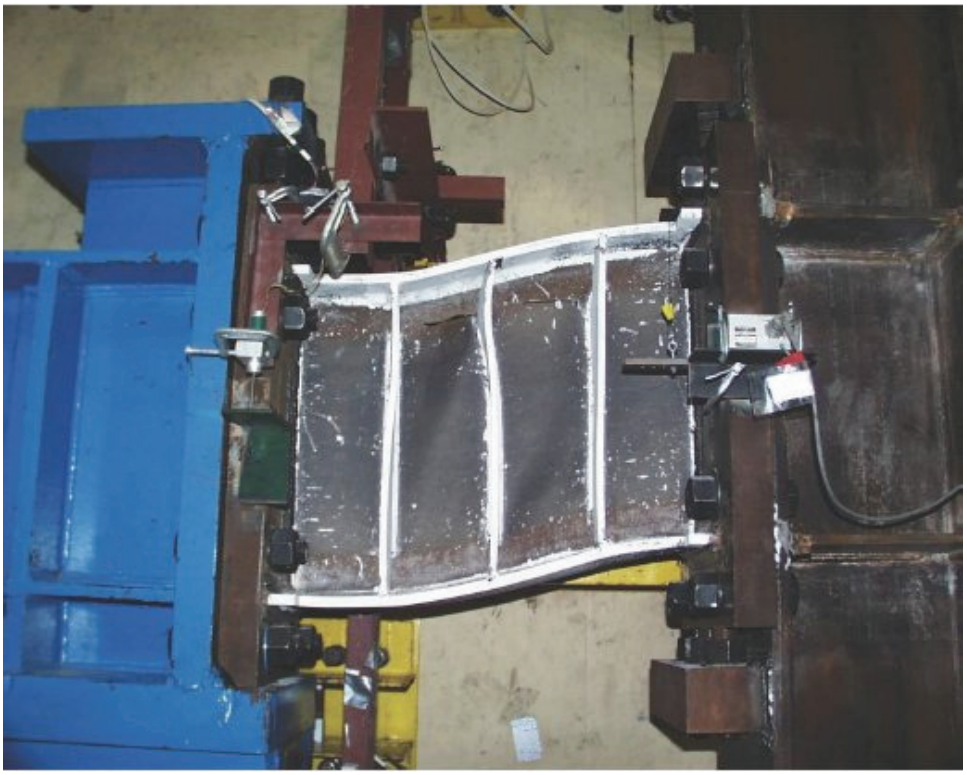

Figure D-60 Final condition of specimen 12-RLP tested by Ryu (2005)

Figure D-61 Final condition of specimen 12-AISC tested by Ryu (2005)

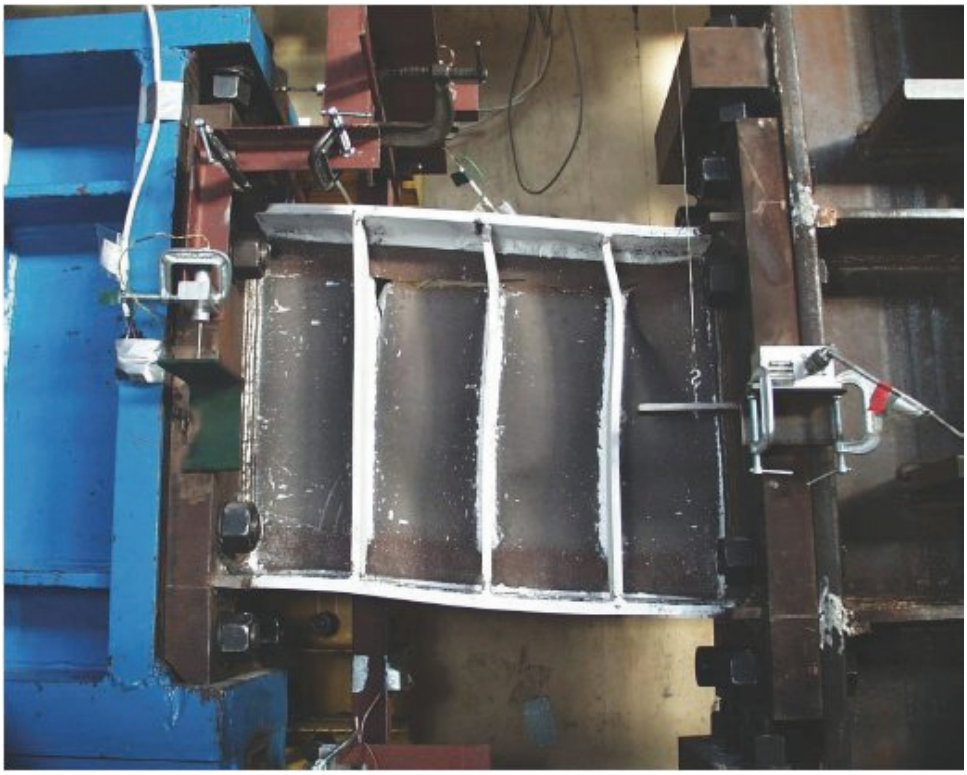

Figure D-62 Final condition of specimen 12-SEV tested by Ryu (2005)

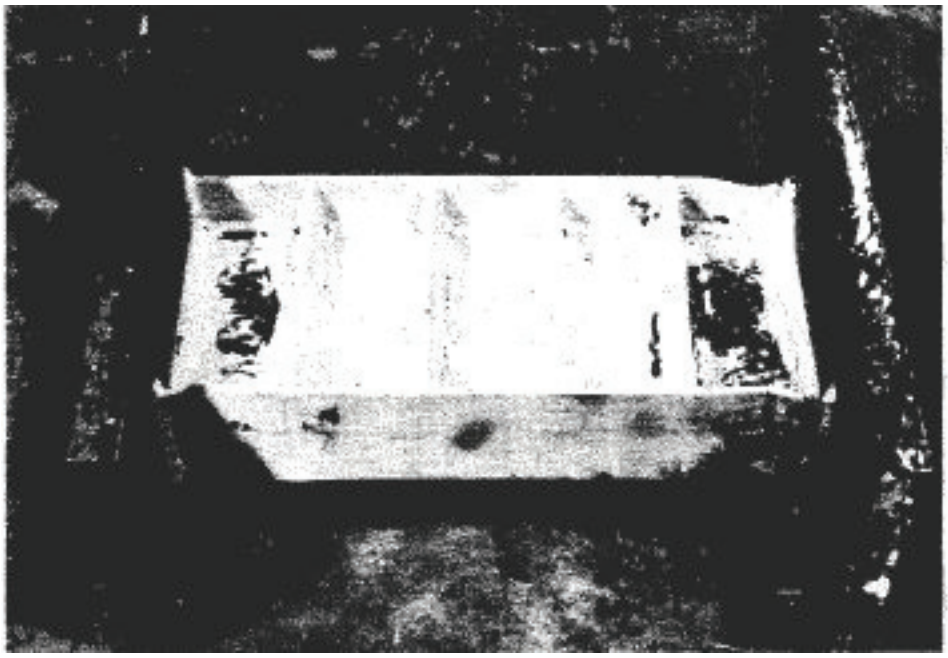

Figure D-63 Final condition of specimen 5 tested by Kasai and Popov (1986)

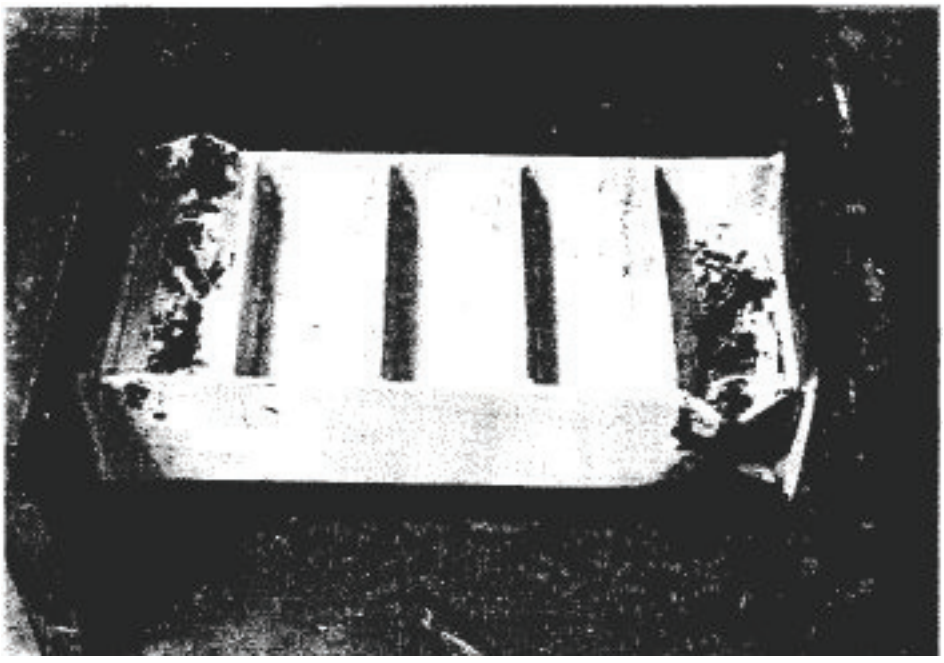

Figure D-64 Final condition of specimen 6 tested by Kasai and Popov (1986)

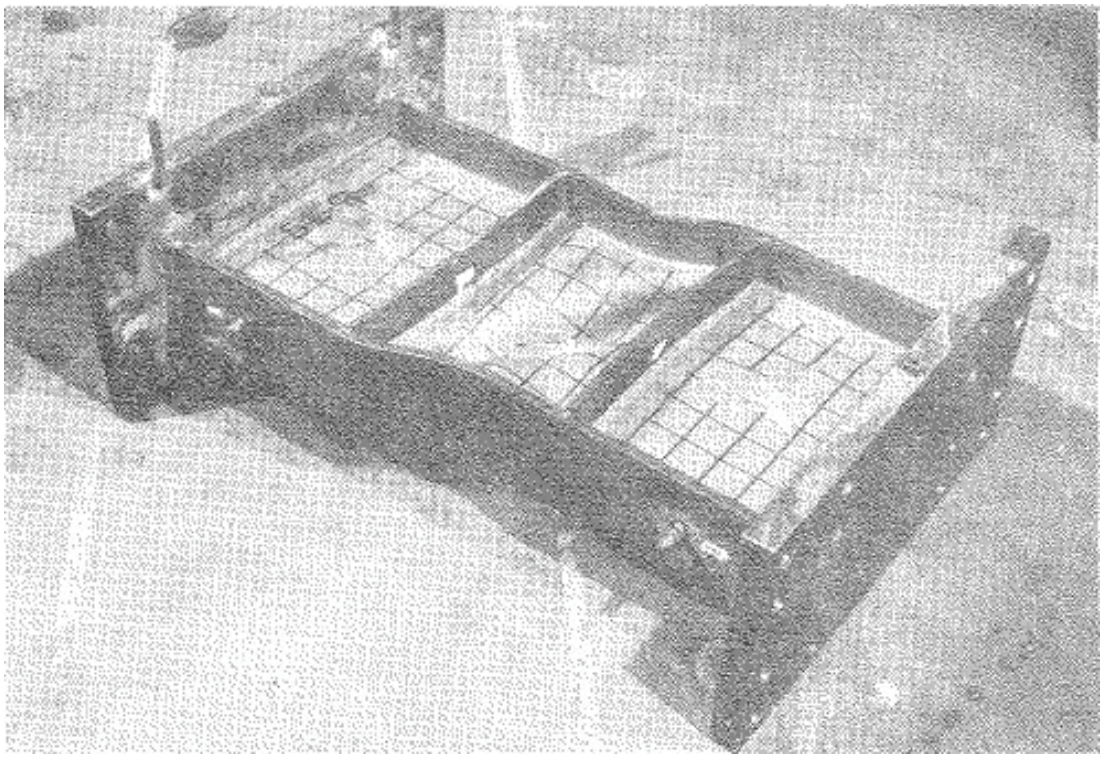

Figure D-65 Final condition of specimen 9 tested by Hjelmstad and Popov (1983)

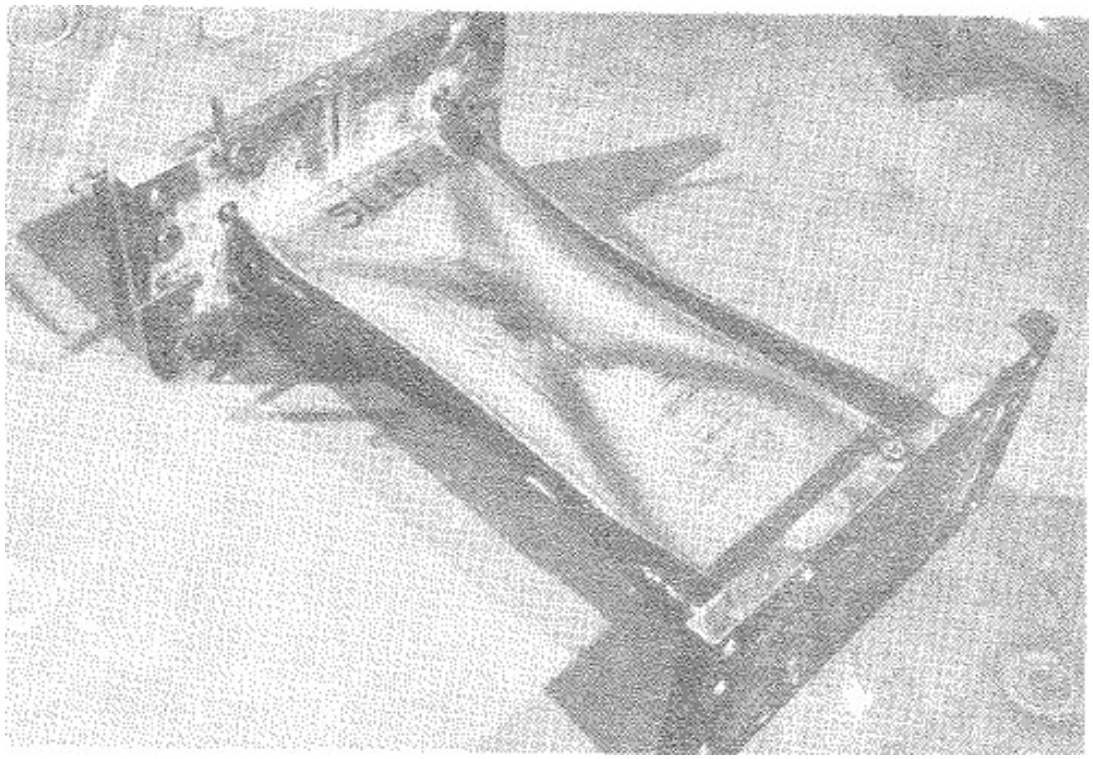

Figure D-66 Final condition of specimen 10 tested by Hjelmstad and Popov (1983)

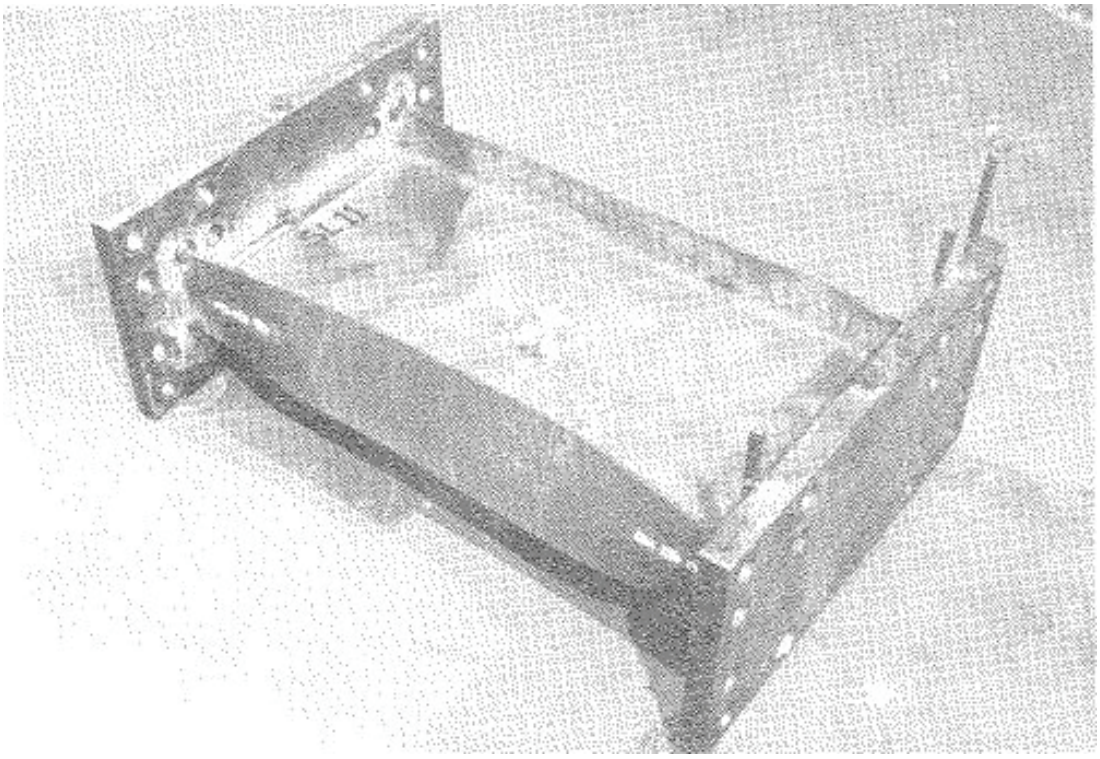

Figure D-67 Final condition of specimen 11 tested by Hjelmstad and Popov (1983)

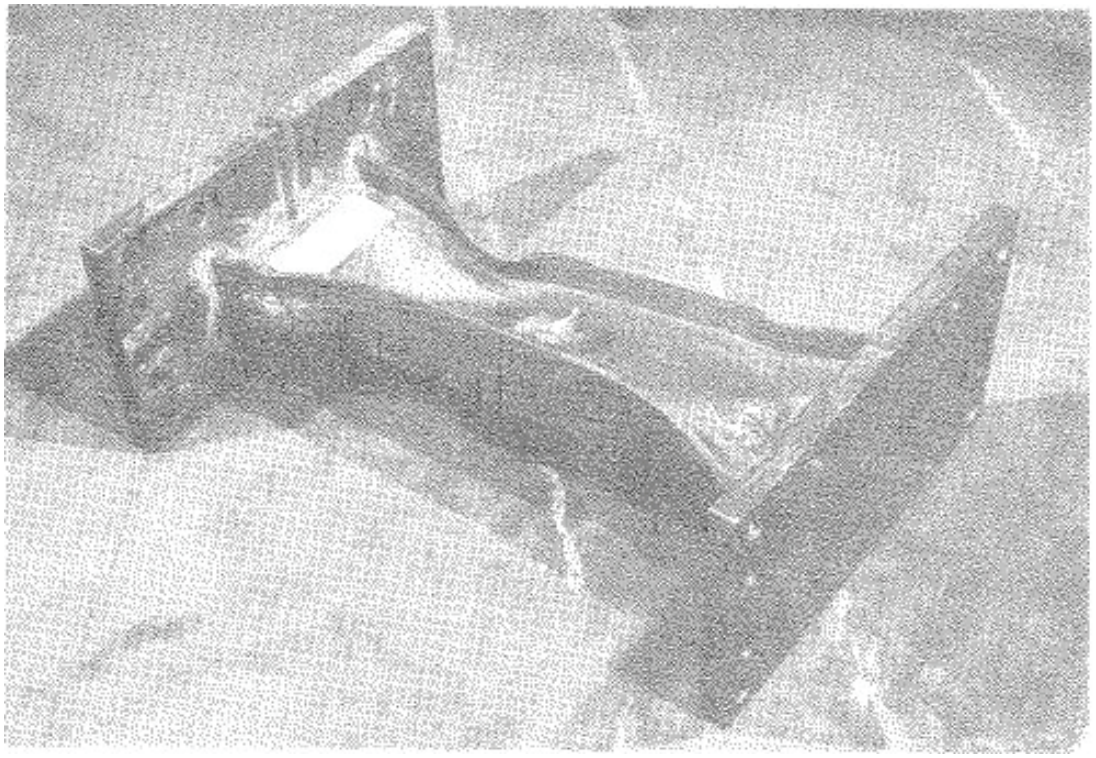

Figure D-68 Final condition of specimen 12 tested by Hjelmstad and Popov (1983)

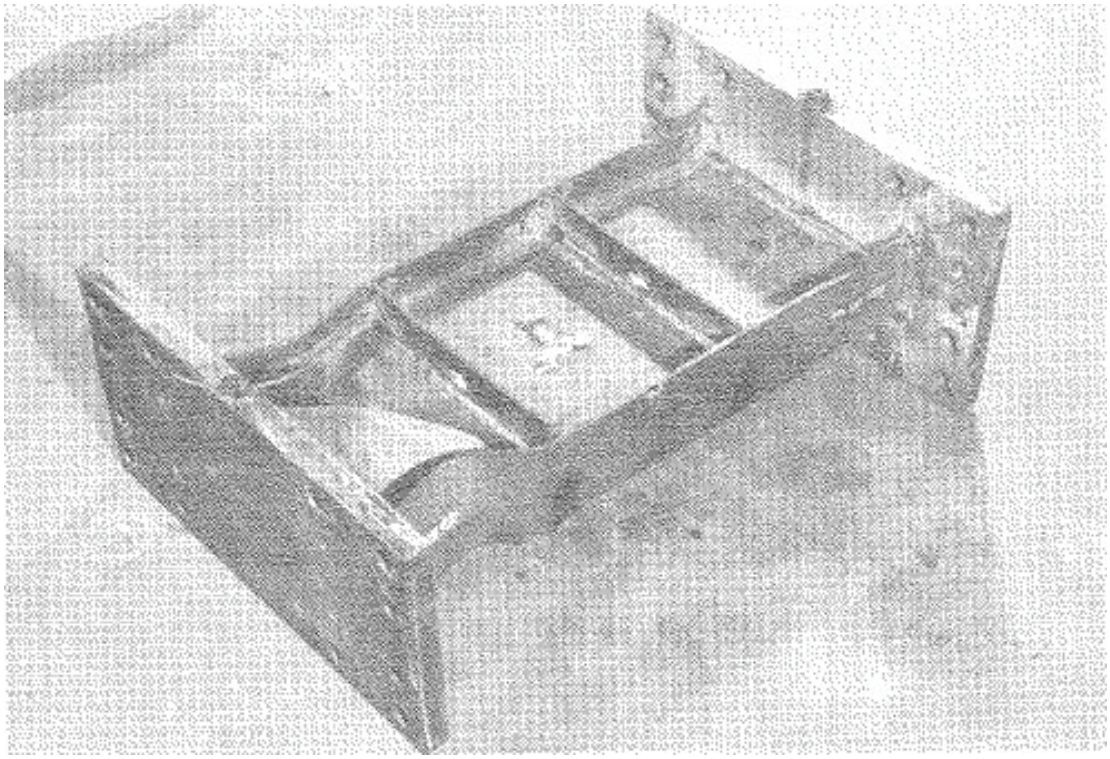

Figure D-69 Final condition of specimen 13 tested by Hjelmstad and Popov (1983)

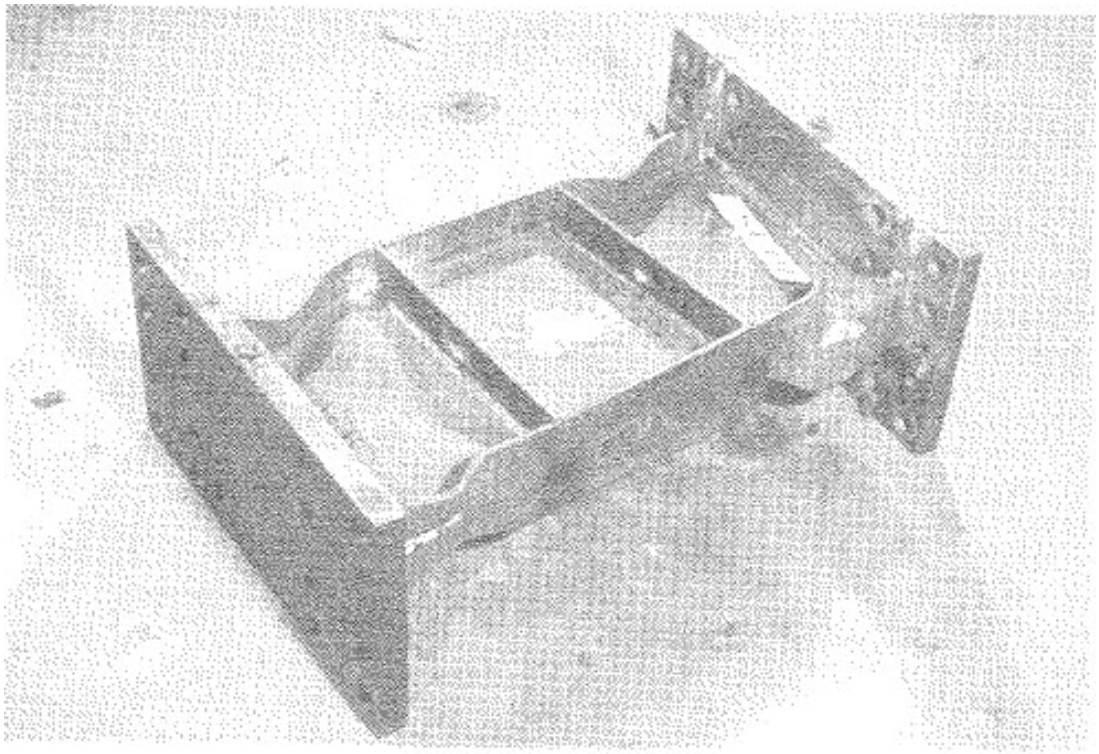

Figure D-70 Final condition of specimen 14 tested by Hjelmstad and Popov (1983)

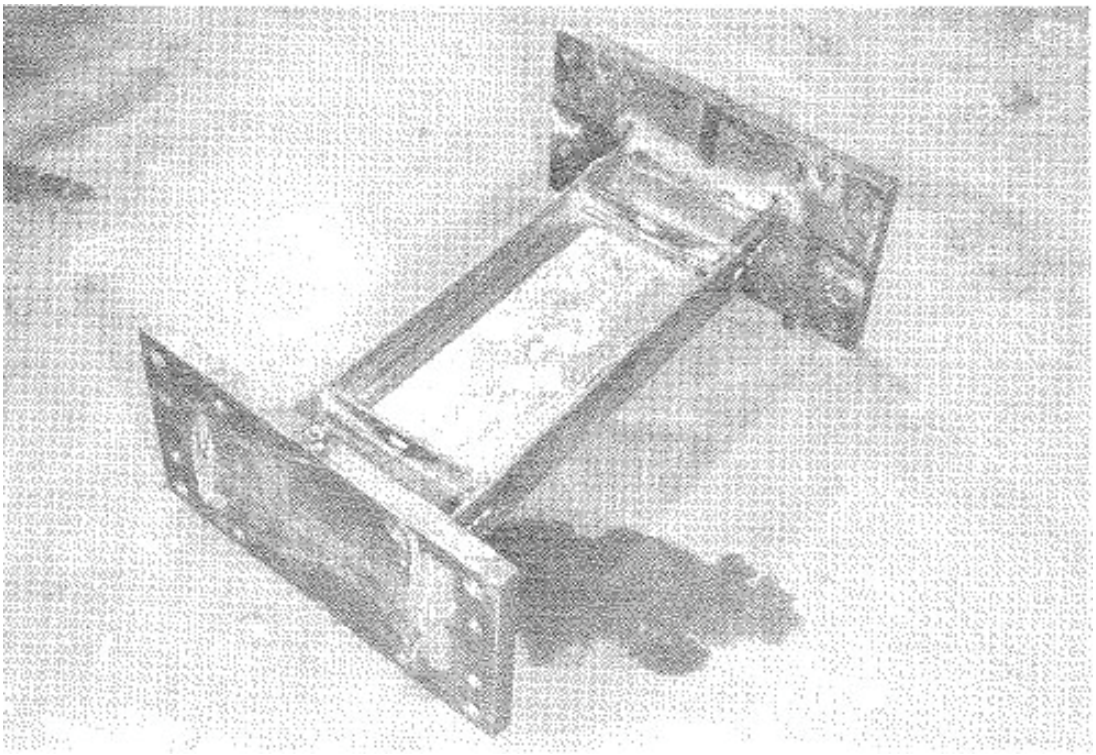

Figure D-71 Final condition of specimen 15 tested by Hjelmstad and Popov (1983)

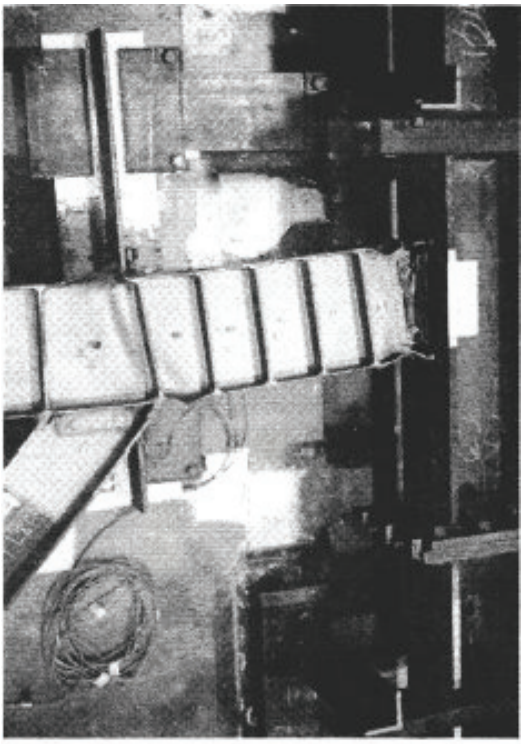

Figure D-72 Final condition of specimen 1 tested by Engelhardt and Popov (1989)

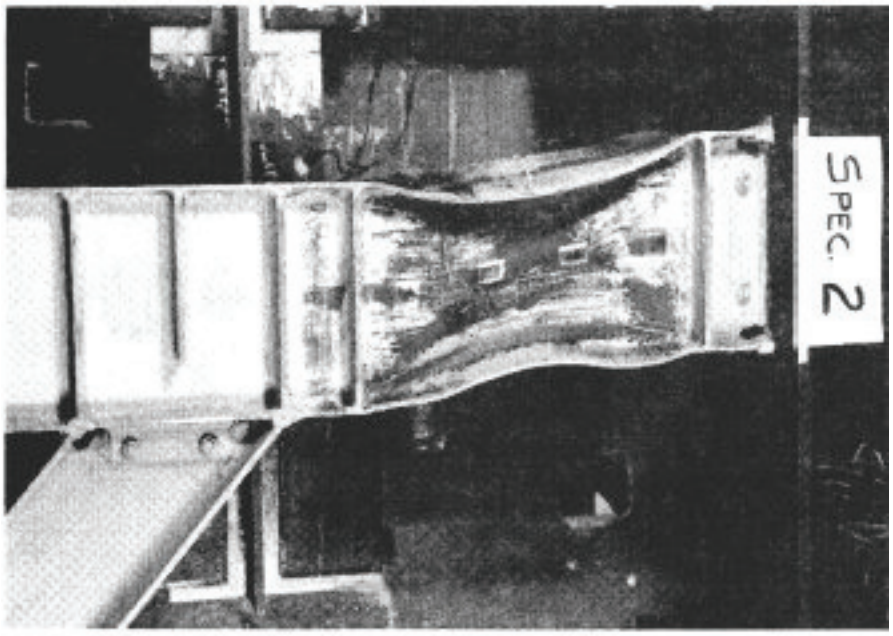

Figure D-73 Final condition of specimen 2 tested by Engelhardt and Popov (1989)

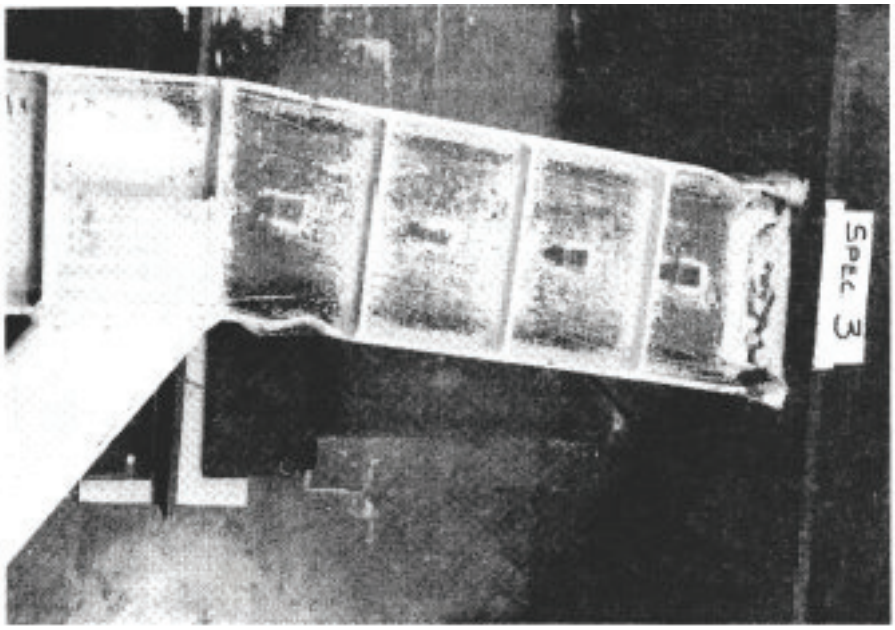

Figure D-74 Final condition of specimen 3 tested by Engelhardt and Popov (1989)

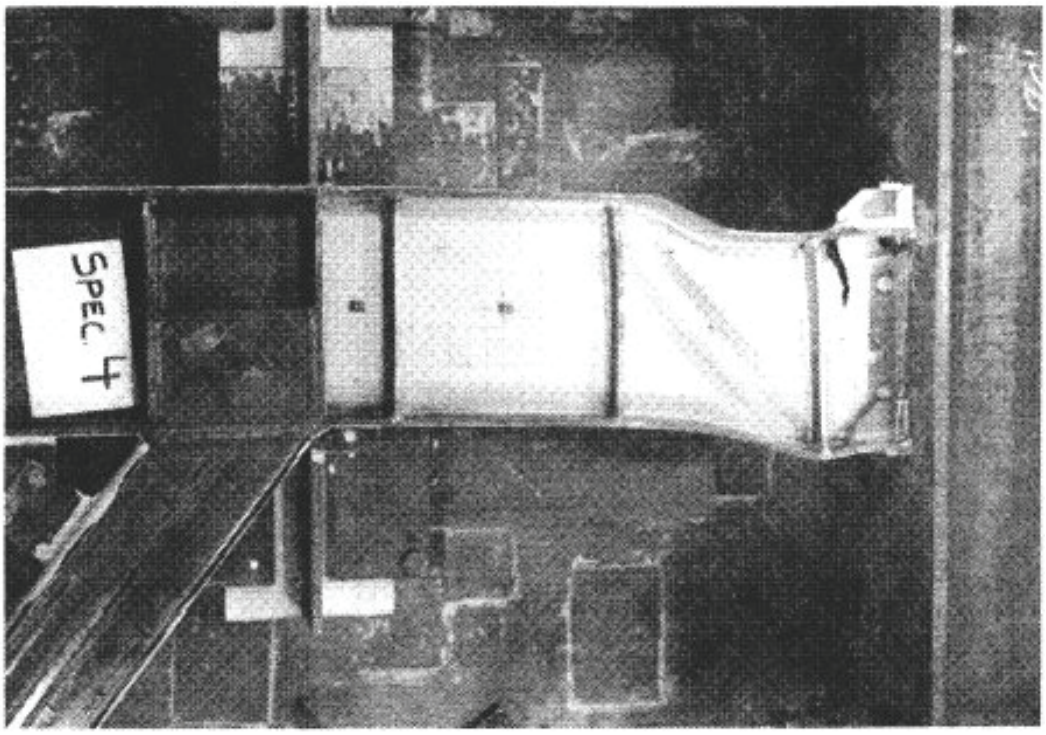

Figure D-75 Final condition of specimen 4 tested by Engelhardt and Popov (1989)

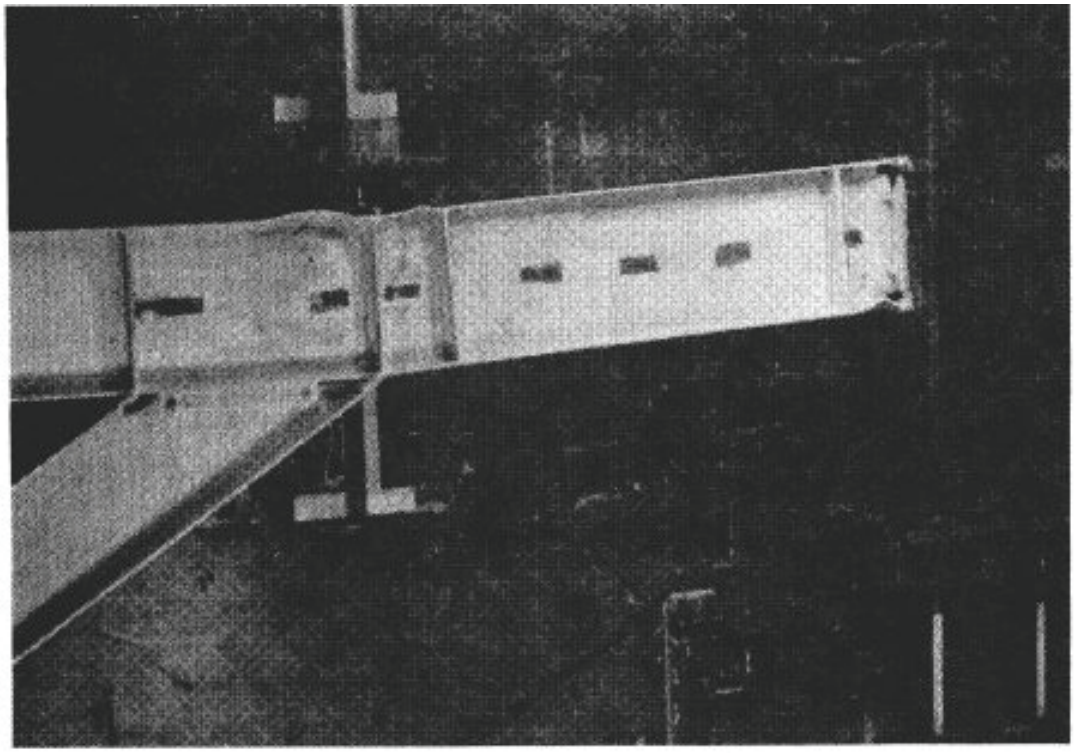

Figure D-76 Final condition of specimen 5 tested by Engelhardt and Popov (1989)

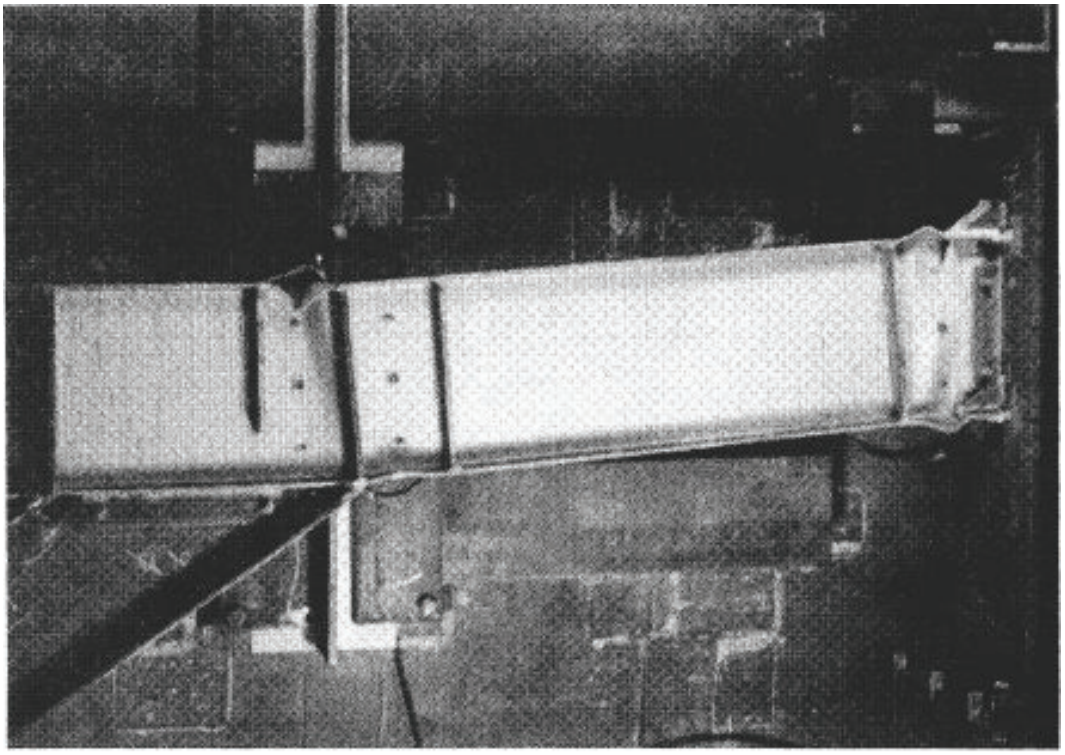

Figure D-77 Final condition of specimen 6 tested by Engelhardt and Popov (1989)

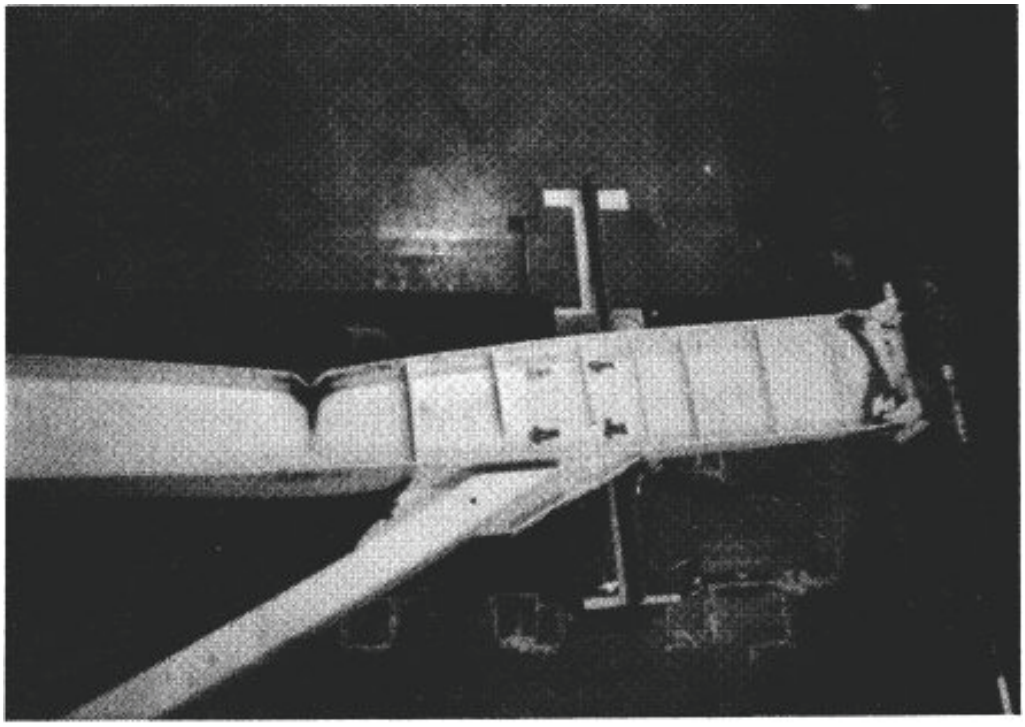

Figure D-78 Final condition of specimen 7 tested by Engelhardt and Popov (1989)

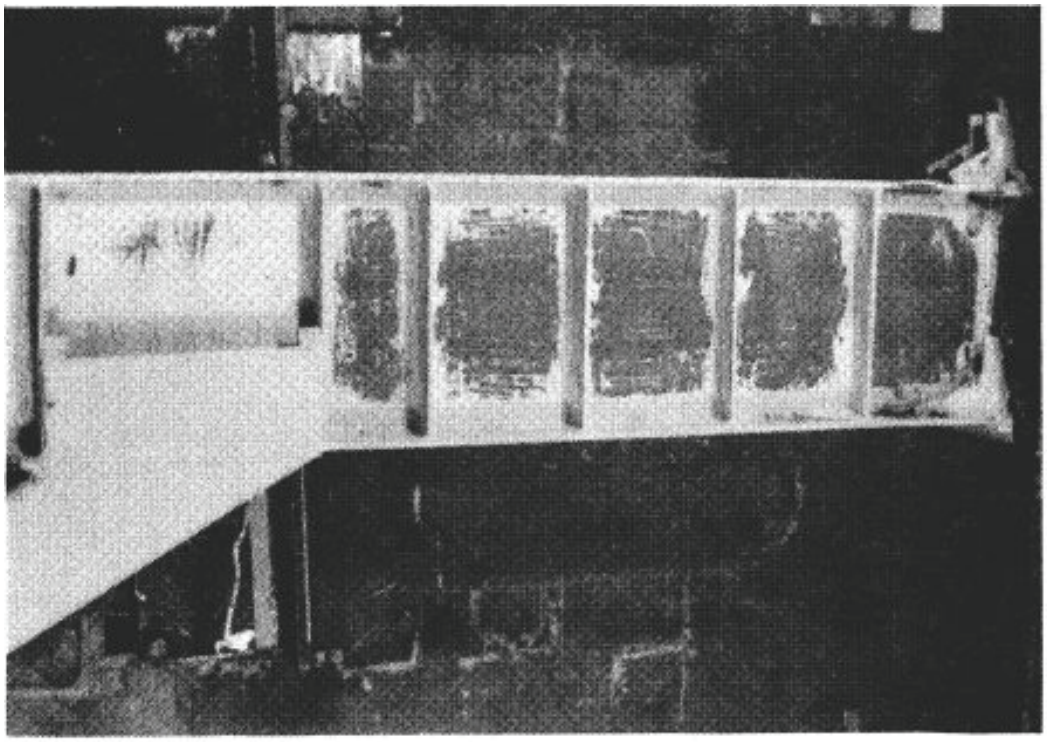

Figure D-79 Final condition of specimen 8 tested by Engelhardt and Popov (1989)

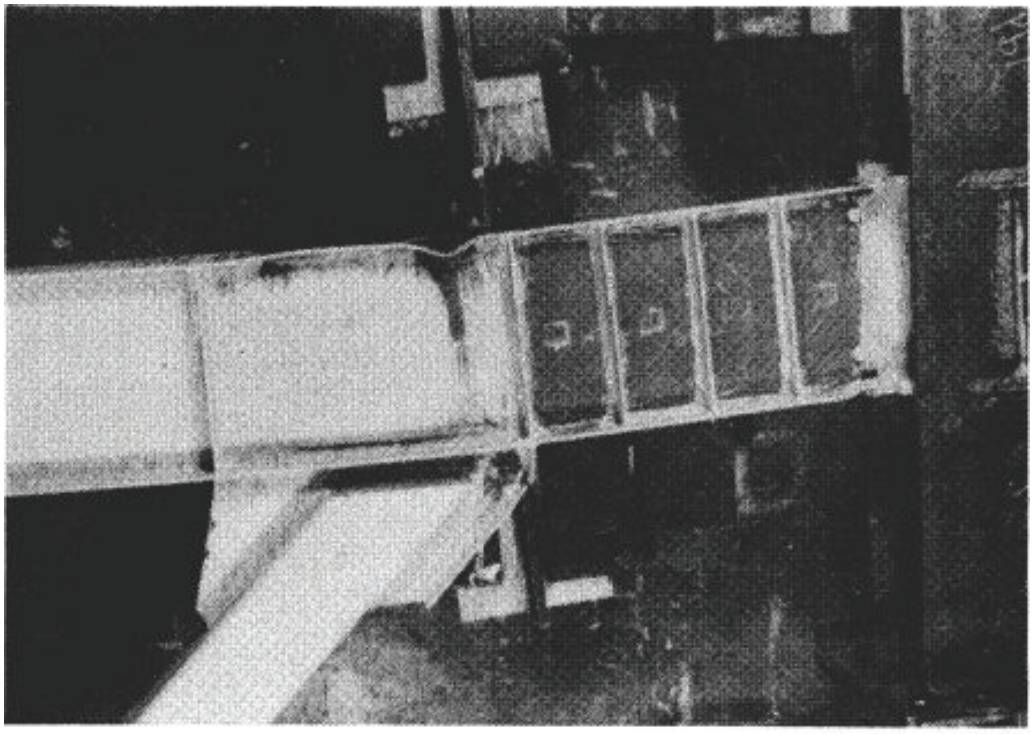

Figure D-80 Final condition of specimen 10 tested by Engelhardt and Popov (1989)

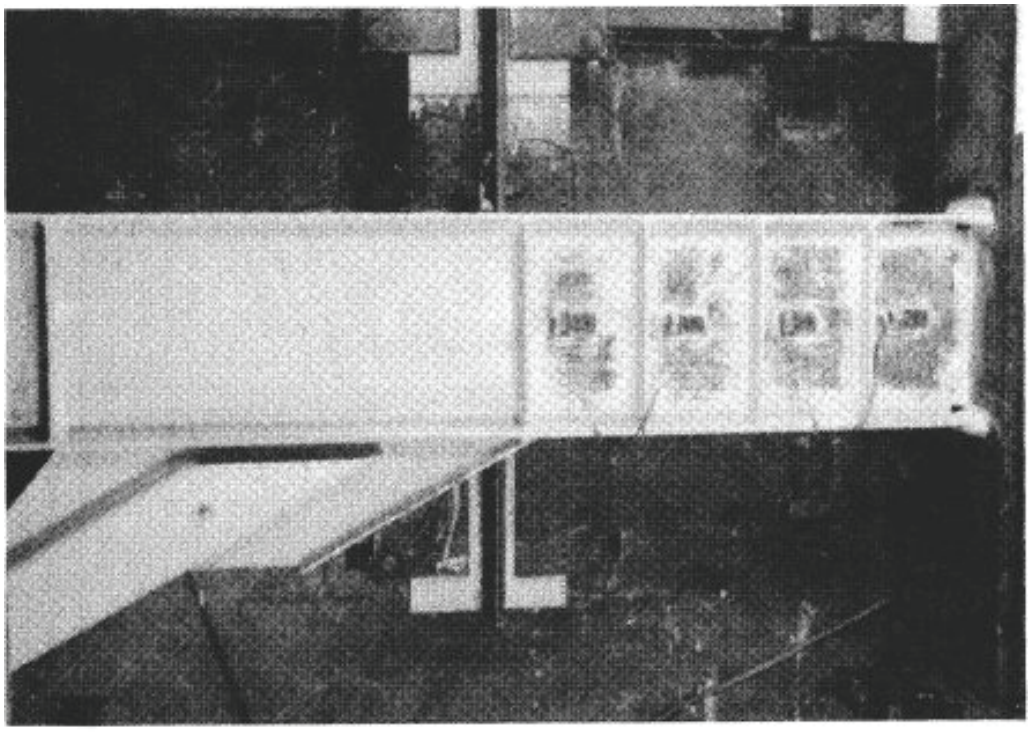

Figure D-81 Final condition of specimen 11 tested by Engelhardt and Popov (1989)

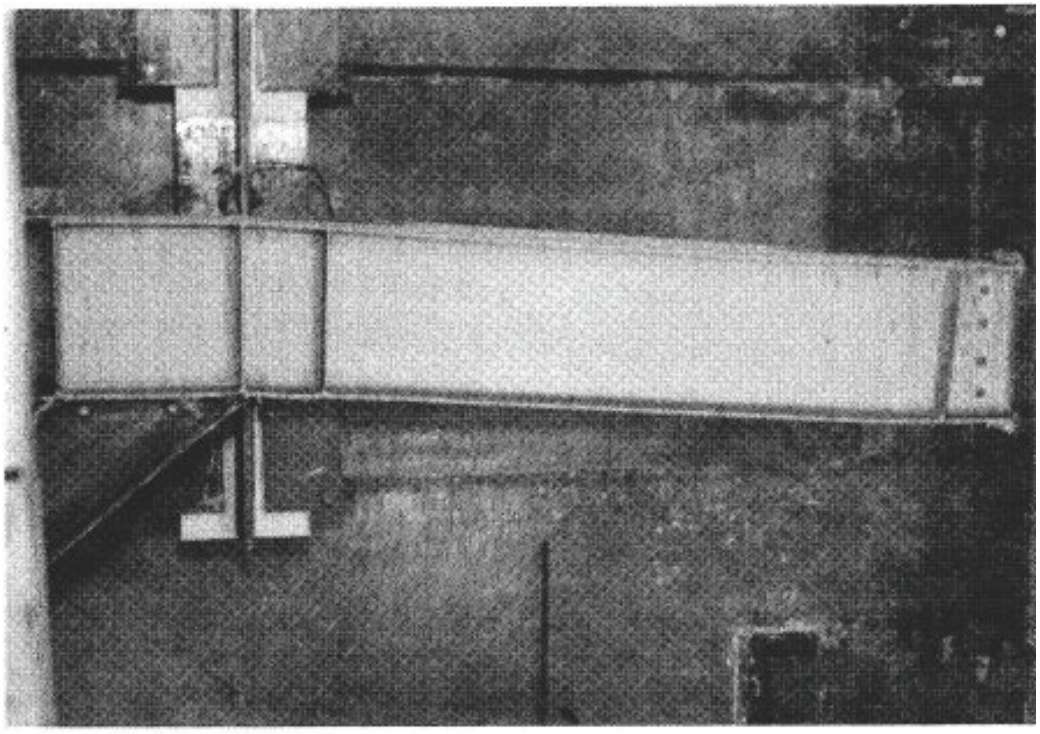

Figure D-82 Final condition of specimen 12 tested by Engelhardt and Popov (1989)

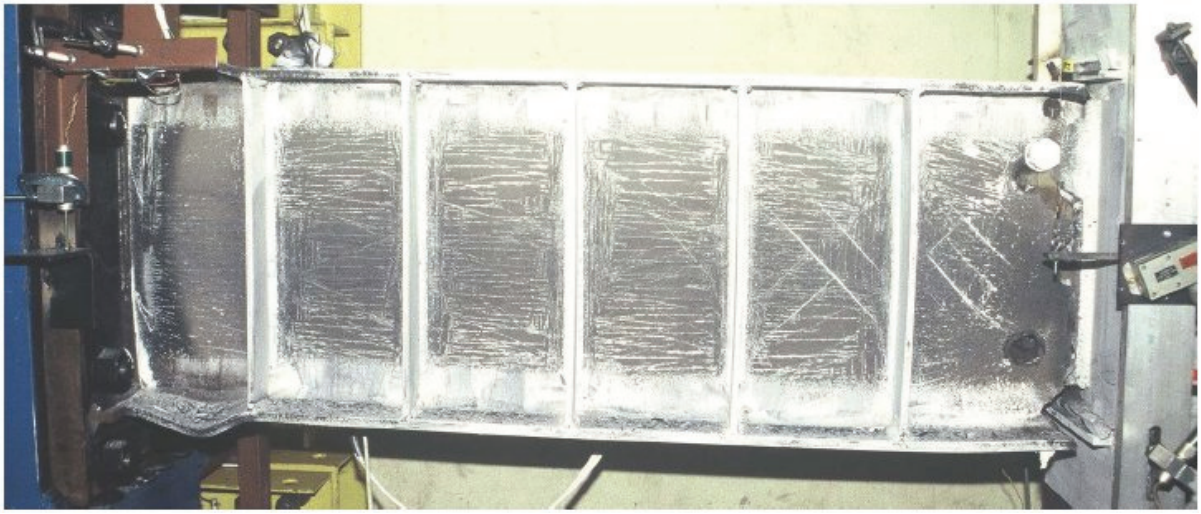

Figure D-83 Final condition of specimen PNI tested by Okazaki (2004)

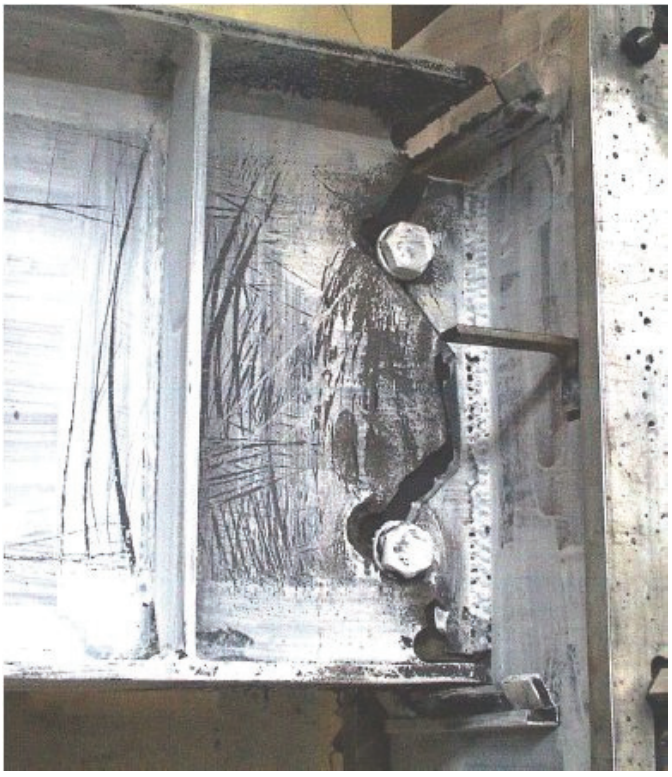

Figure D-84 Final condition of specimen PNM tested by Okazaki (2004)

Figure D-85 Final condition of specimen MWI tested by Okazaki (2004)

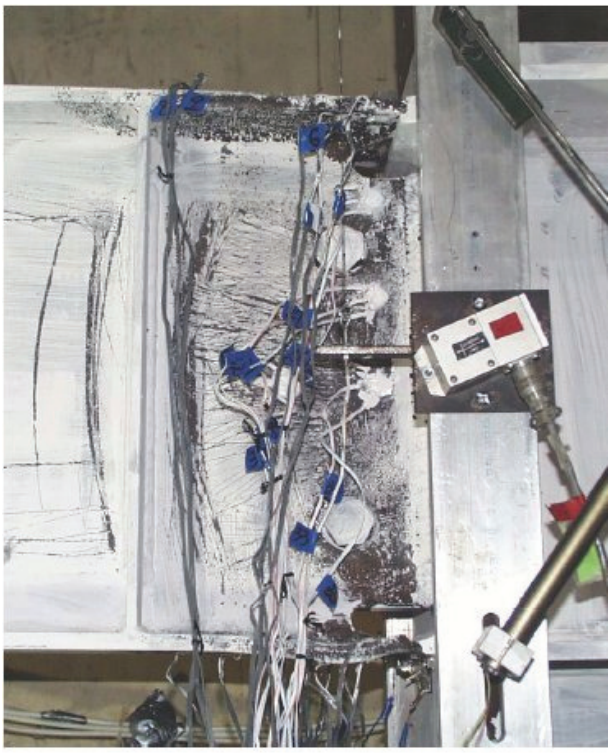

Figure D-86 Final condition of specimen MWM tested by Okazaki (2004)

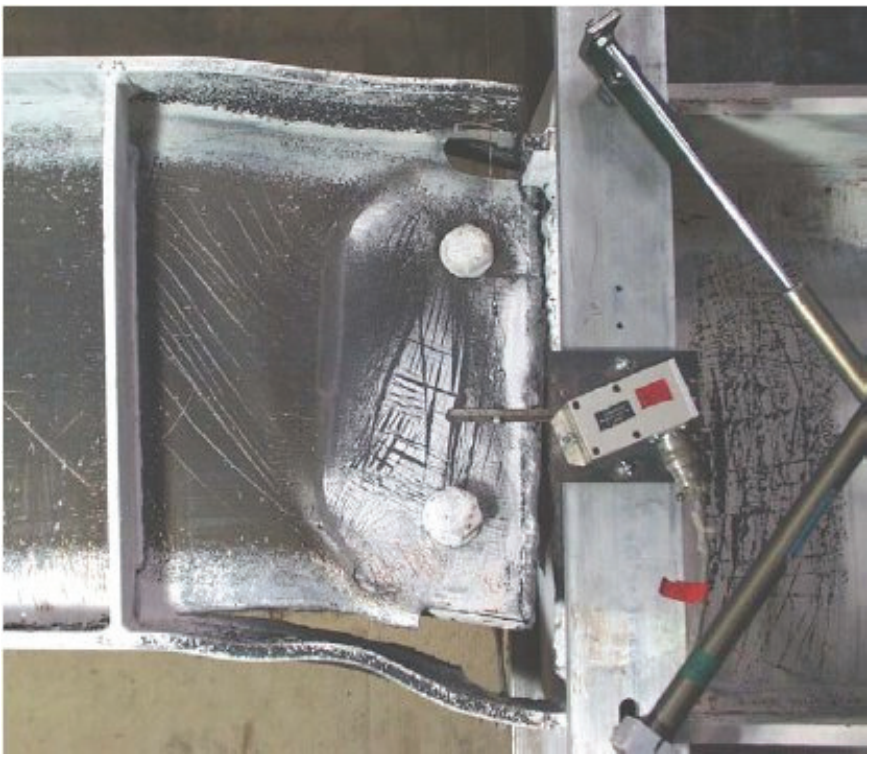

Figure D-87 Final condition of specimen FFI tested by Okazaki (2004)

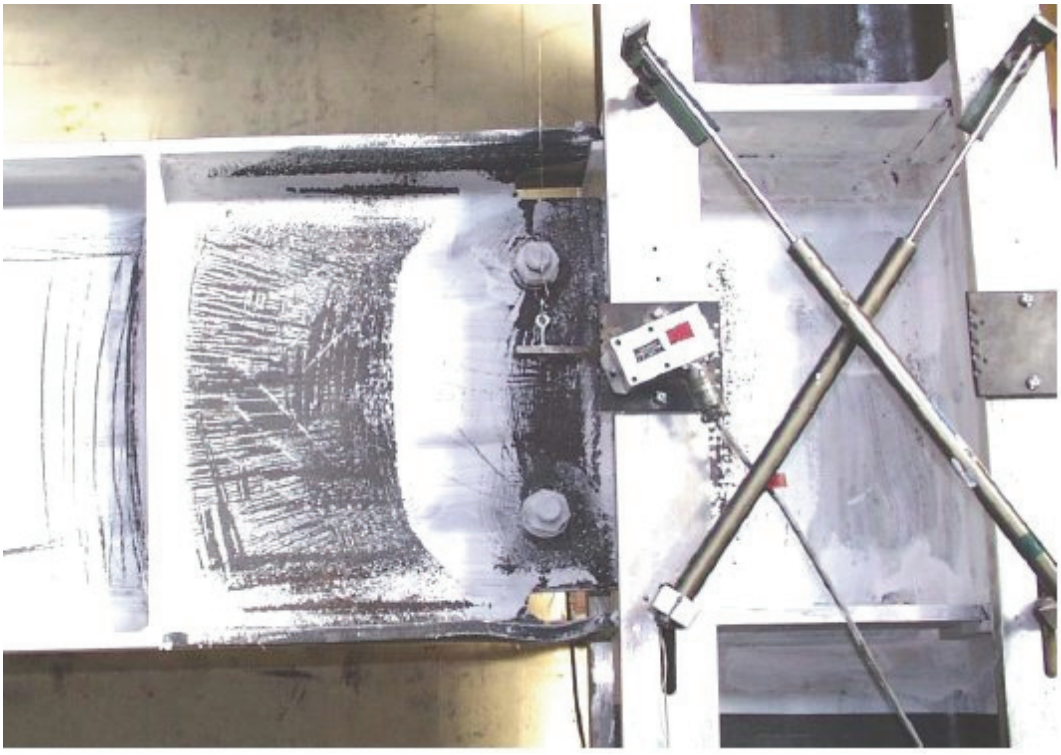

Figure D-88 Final condition of specimen FFM tested by Okazaki (2004)

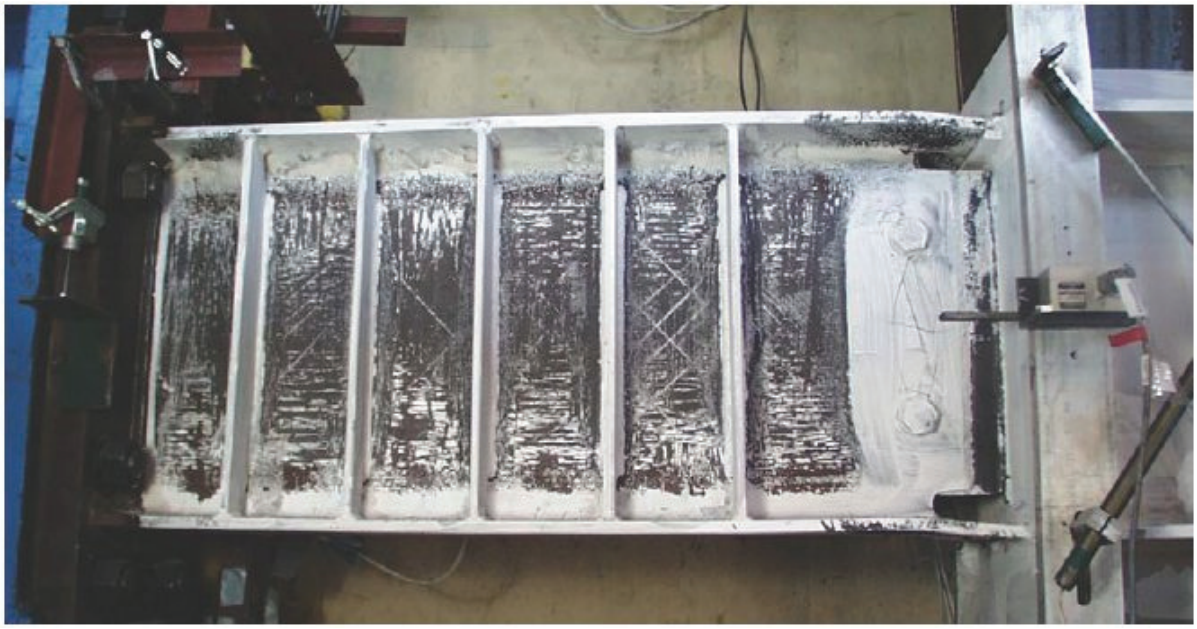

Figure D-89 Final condition of specimen FFSL-RLP tested by Okazaki (2004)

Figure D-90 Final condition of specimen NAI tested by Okazaki (2004)

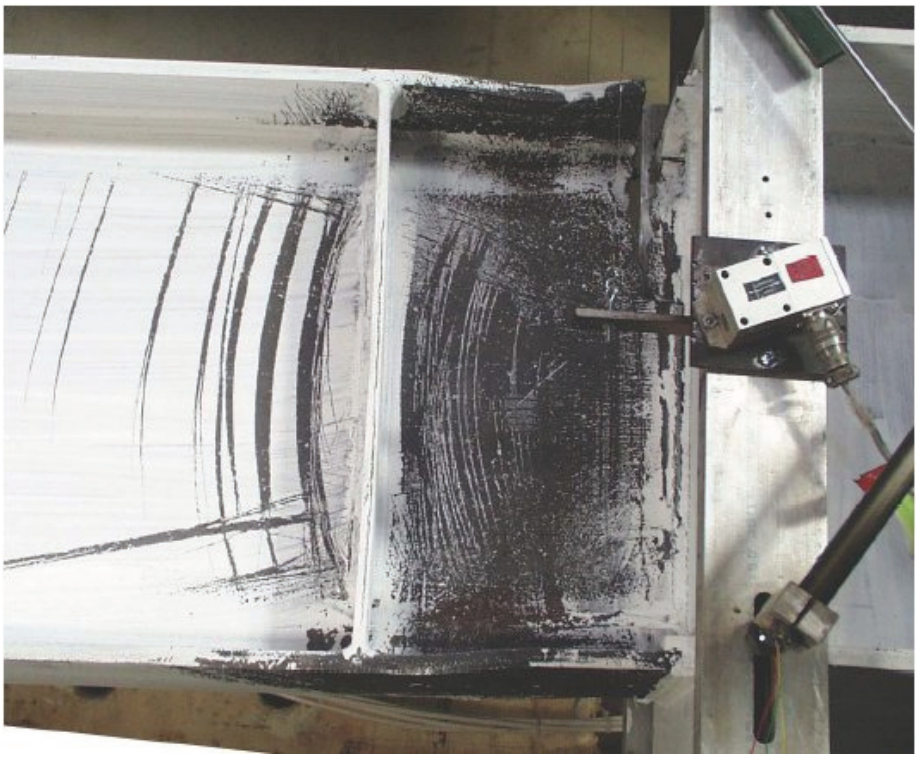

Figure D-91 Final condition of specimen NAM tested by Okazaki (2004)

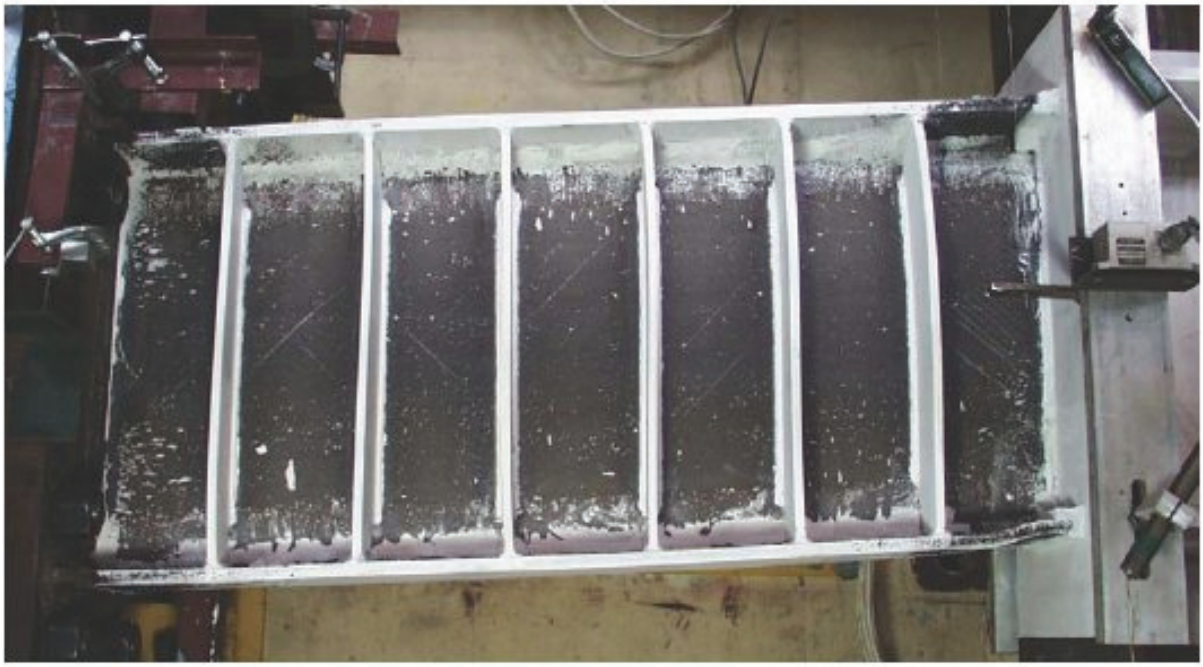

Figure D-92 Final condition of specimen NASL-RLP tested by Okazaki (2004)

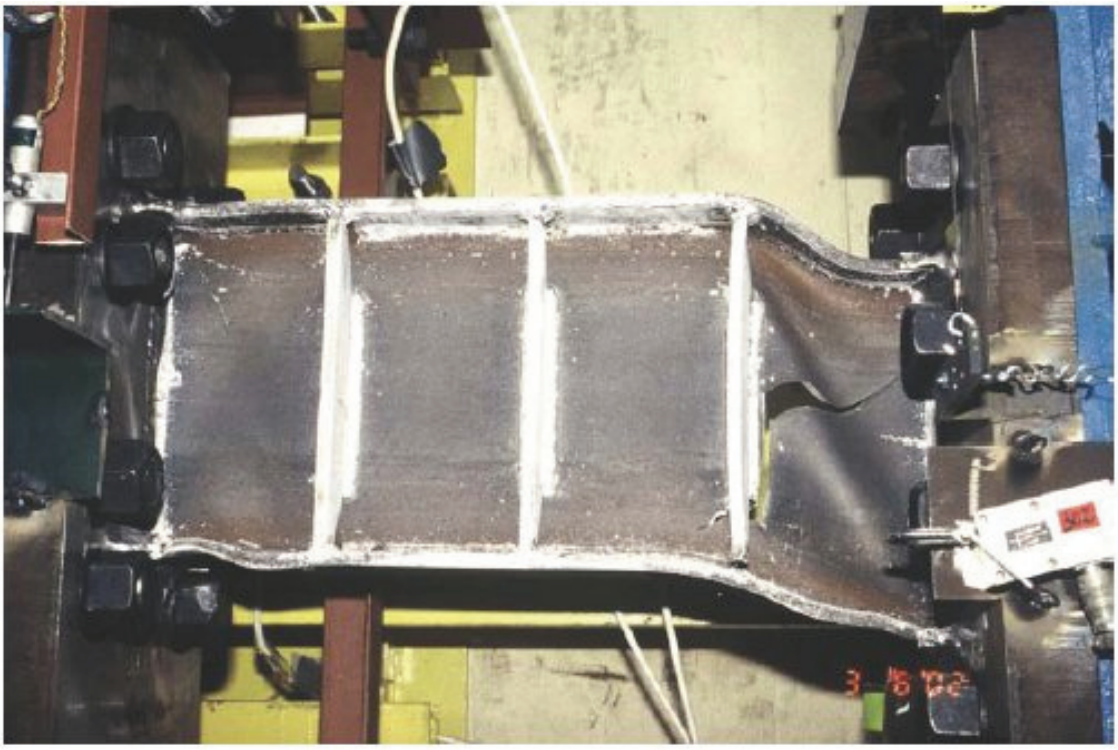

Figure D-93 Final condition of specimen 1c tested by Arce (2002)

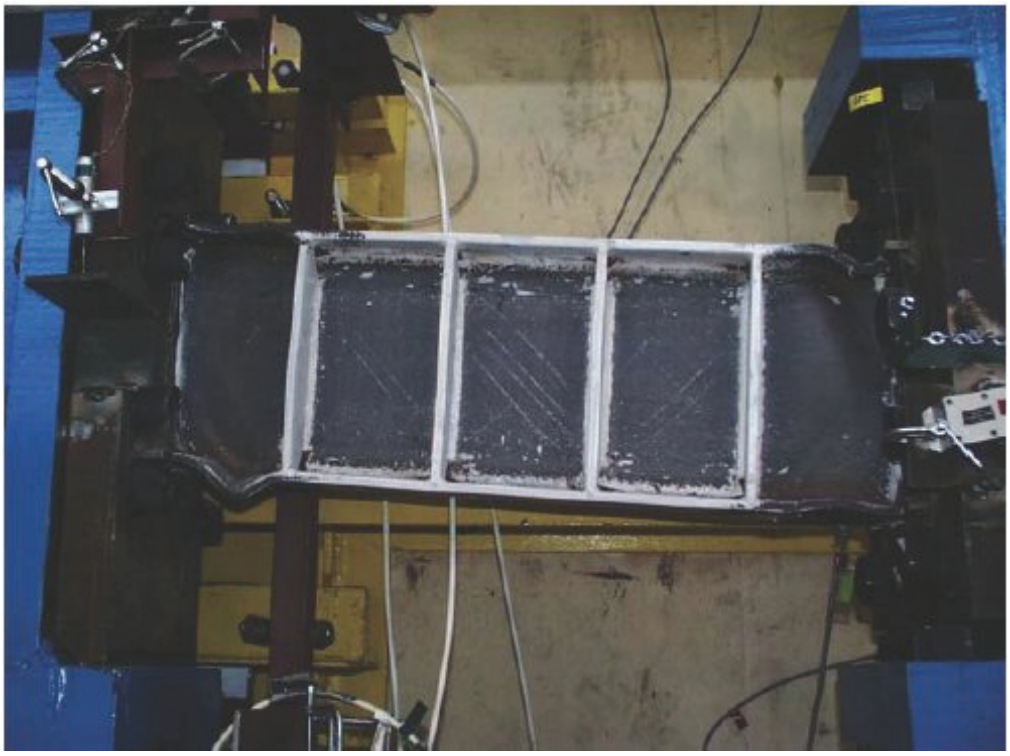

Figure D-94 Final condition of specimen 2 tested by Arce (2002)

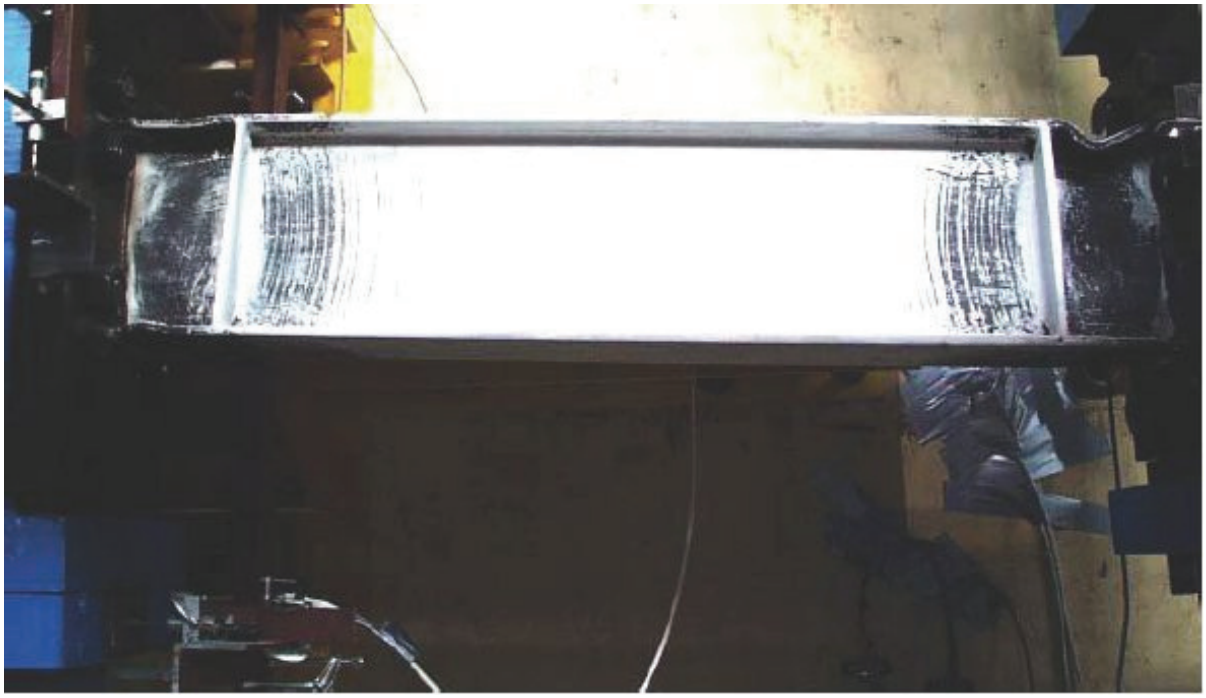

Figure D-95 Final condition of specimen 3 tested by Arce (2002)

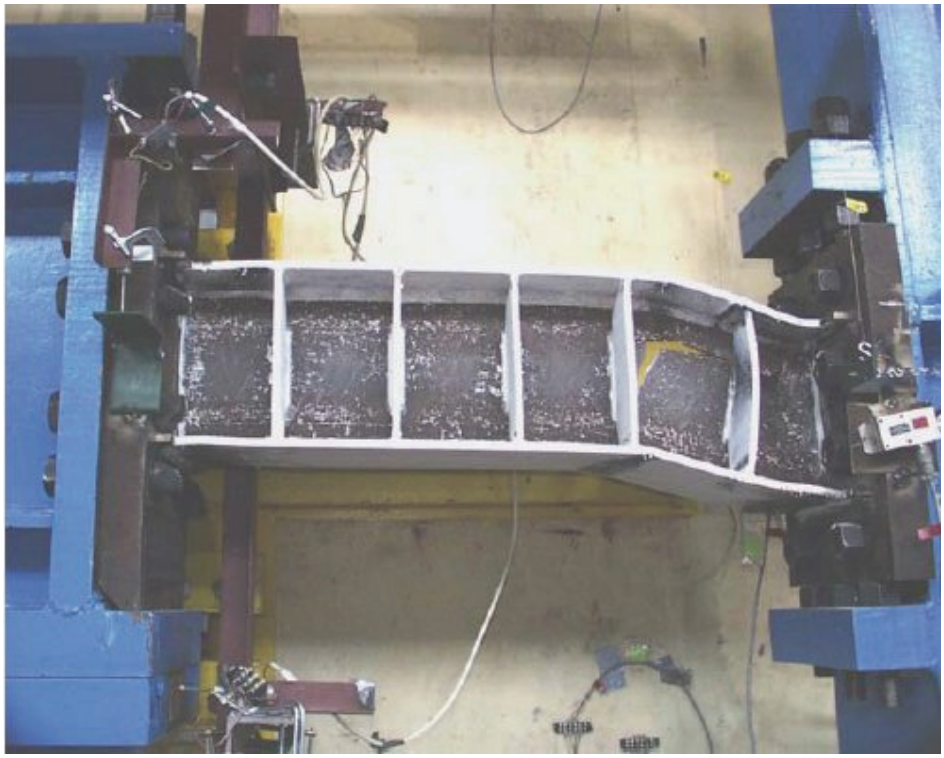

Figure D-96 Final condition of specimen 5 tested by Arce (2002)

Figure D-97 Final condition of specimen 6b tested by Arce (2002)

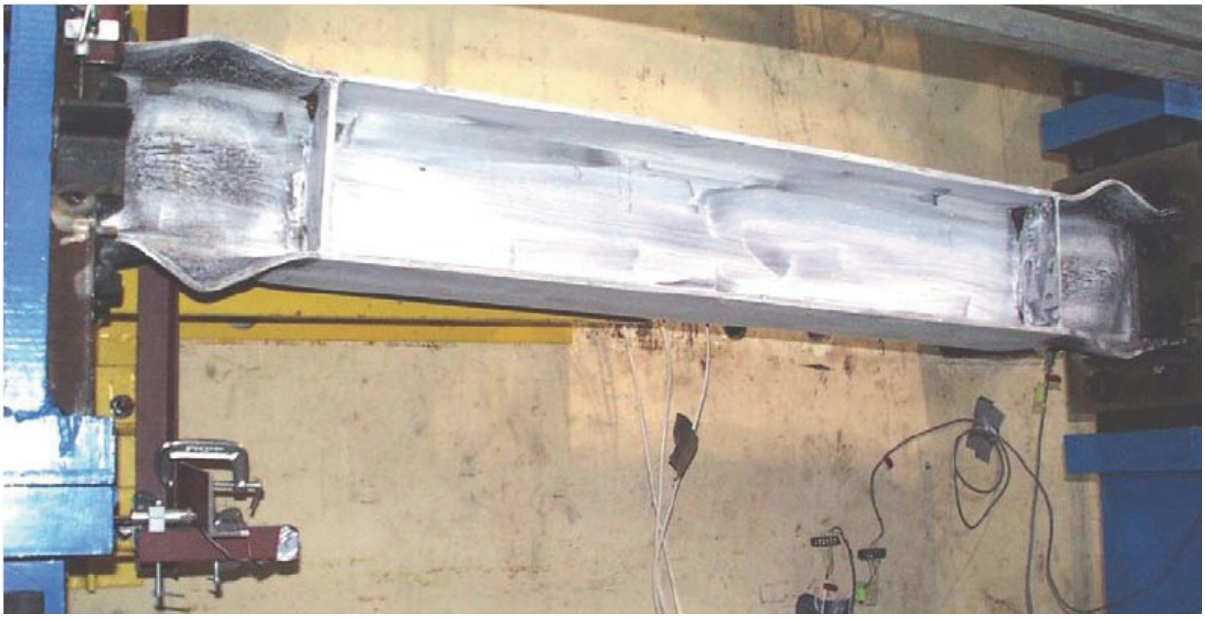

Figure D-98 Final condition of specimen 7 tested by Arce (2002)

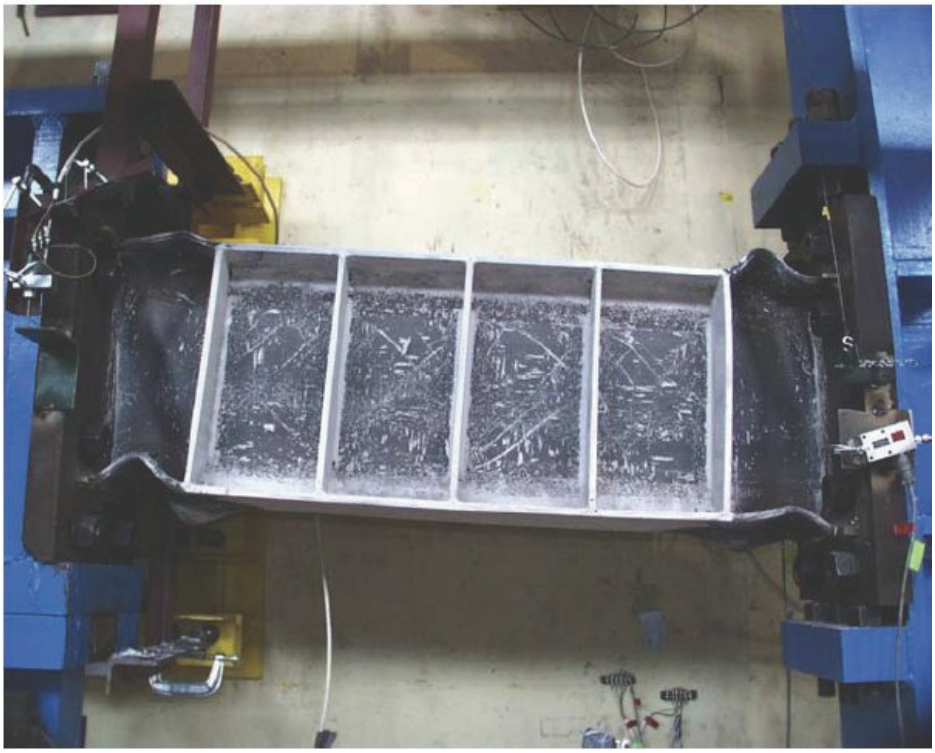

Figure D-99 Final condition of specimen 9 tested by Arce (2002)

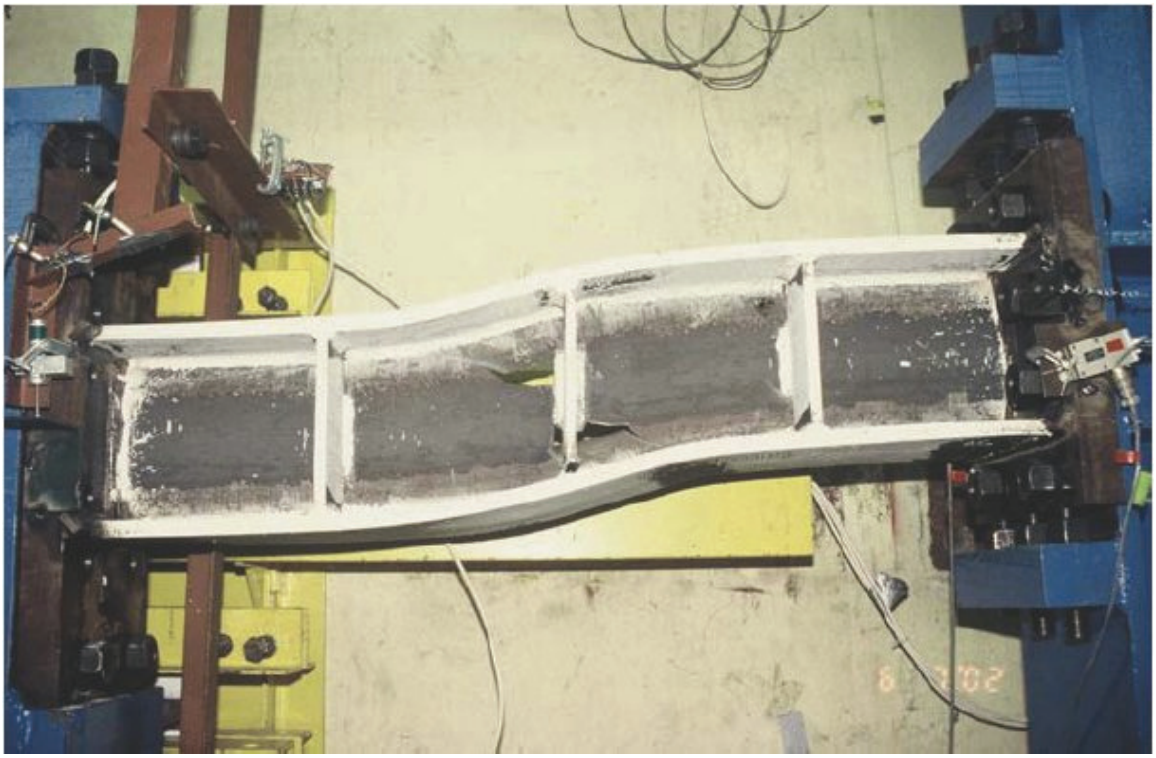

Figure D-100 Final condition of specimen 11 tested by Arce (2002)

Figure D-101 Final condition of specimen 11-RLP tested by Ryu (2005)a